THEORETICAL STUDIES OF CHEMICAL REACTION DYNAMICS

Thesis by

Stephen Jacob Klippenstein

In Partial Fulfillment of the Requirements
for the Degree of
Doctor of Philosophy

California Institute of Technology
Pasadena, California
1988

(Submitted May 12, 1988)

Acknowledgments

I would like to express my gratitude to my research advisor, Professor R. A. Marcus, for the time and insight which he has shared with me during my tenure here at Caltech. I have particularly appreciated the freedom he has given me to explore a variety of research topics within the area of reaction dynamics. The most important thing which he has taught me is the need for theory to stay in close contact with experiment.

I have very much enjoyed my interactions and collaborations with the past and present members of the Marcus group. In particular, I have greatly benefited from sharing an office with, first, Steven Lederman and then Walter Nadler. Also, my collaborations with Robert Cave, Vasil Babamov, Greg Voth, and Yong-Feng Zhang have been both enjoyable and fruitful. I have also benefited from my interactions with the other members of the Marcus group including Rafael Almeida, Hitoshi Sumi, and David Wardlaw. I have enjoyed my collaboration with Lutfur Khundkar and Professor A. H. Zewail which has given me some insight into picosecond photofragment spectroscopy. I would also like to acknowledge the Natural Sciences and Engineering Research Council of Canada for providing me with financial support in the form of a Postgraduate Scholarship from 1984 - 1987.

My deepest thanks must go to my parents, Jake and Mary Klippenstein, without whose help I would never have made it this far. I would like to thank them for their continual love and support and for encouraging me in my pursuit of higher learning. I would also like to thank them for giving me the freedom to pursue whatever I desired while at the same time encouraging me in everything I did. I am also grateful to the members of my family for taking the time to come and visit me here at Caltech.

Finally, I am extremely grateful to my wife, Gloria, for always encouraging me to continue working to the best of my ability. It was her love and devotion

which made it possible for me to endure the hardships of being a graduate student. I am particularly indebted to her for never complaining about my often long hours of study and for always helping out in whatever way she could. Most of all, I would like to thank Gloria, and her family (particularly my mother-in-law Maria Larios), for making my last four years here at Caltech very enjoyable.

Abstract

In this thesis theoretical models are developed and/or applied to the study of the dynamics of a variety of chemical reactions. First, a semiclassical model is developed to describe the effect of mutual orientation of the donor and acceptor on the rate of electron transfer between two large aromatic groups. The next reaction considered is that of gas phase H-atom transfer reactions. In this case a comparison is made of two previously developed approximations for the treatment of the particular case of H-atom transfer between two heavy particles.

The next topic involves the study of the rate of intramolecular vibrational redistribution of energy. First, an iterative procedure is developed for determining more and more accurate effective Hamiltonians for the description of the dynamics. The foundation of this method is the separation of the basis states into resonant and nonresonant sets followed by an adiabatic approximation for the dynamics of the off-resonant set. A second study involves the application of artificial intelligence techniques to the choice of a small set of basis states which are the states of greatest importance to the redistribution dynamics.

The remainder of the thesis is devoted to the study of those unimolecular dissociation/free radical recombination reactions which contain highly flexible transition states. For these reactions, a method for determining the quantum partition function for the transition state in terms of path integral ratios is developed and applied to the study of the thermally activated methyl radical recombination. Subsequently, a method is developed for determining the number of states, for the transition state, at a given energy and angular momentum. The basis of the method is the use of conventional Euler angle coordinates in the Monte Carlo evaluation of phase space integrals. This method is applied to the NCNO, CH_2CO, and H_2O_2 photodissociation processes. Also presented is a discussion of both the trend of the location of the transition state with increasing energy and the possible influence of excited potential energy surfaces.

Table of Contents

List of Tables and Figures

I. List of Tables

II. List of Figures

measured relative to the minimum of the HBr potential. $P_{02}(E)$ is denoted by —— , $P_{02}^{B}(E)$ by — — and $P_{02}^{B'}(E)$ by - - - .

Figure 2.6, P. 44: The probabilities P_{02} as a function of the total energy measured relative to the minimum of the HBr potential. $P_{02}(E)$ is denoted by —— , $P_{02}^{CS}(E)$ by — - — , $P_{02}^{CS'}(E)$ by — — and $P_{02}^{CS''}(E)$ by - - - .

Figure 3.1, P. 69: A schematic diagram of the four-state model system used in Sec. IV. Dotted lines denote the couplings between the zeroth-order states, and $|\varphi_1\rangle$ is the initial state.

Figure 3.2, P. 70: Initial state probability $P_1(t)$ for the model system shown in Fig. 3.1, with $\Delta = 337.7$, $V_1 = -43.9$ and $V_2 = -50.6$ cm^{-1}. The exact results are given by the solid line, the zeroth-order results by the long dashed line and the first-order results by the short dashed line.

Figure 3.3, P. 71: Initial state probability $P_1(t)$ for the model system shown in Fig. 3.1, with $\Delta = 150.0$, $V_1 = -43.9$ and $V_2 = -50.6$ cm^{-1}. The exact results are given by the solid line, the zeroth-order results by the long dashed line and the second-order results by the short dashed line.

Figure 3.4, P. 72: Initial state probability $P_1(t)$ for the second model system discussed in Sec. IV of the text. The exact results are given by the solid line, the zeroth-order results by the long dashed line and the first-order results by the short dashed line.

Figure 3.5, P. 73: "Corrected" initial state probability $P_1(t) \times f_R$ for the model system shown in Fig. 3.1, with $\Delta = 150.0$, $V_1 = -43.9$ and $V_2 = -50.6$ cm^{-1}. The exact results (with no correction factor) are given by the solid line, the zeroth-order results by the long dashed line and the second-order results by the short dashed line.

Figure 3.6, P. 74: "Corrected" initial state probability $P_1(t) \times f_R$ for the second model system discussed in Sec. IV of the text. The exact results (with no correction factor) are given by the solid line, the zeroth-order results by the long dashed line and the first-order results by the short dashed line.

Figure 4.1, P. 88: Example of a best incomplete paths search in which two levels of beam search are performed. The horizontal lines represent states and the dashed diagonal connecting lines represent non-zero couplings. The first number above each line is the number given to the basis state (according to the order in which it is found in the search), and the second number is the evaluation function for the path leading to that basis state.

Figure 4.2, P. 89: Comparison of the results for the excess energy in the left ligand plotted *vs* the time, with $\lambda = 0.1655$ (mass of Ge). The solid line (—) is the exact result, the dashed line (- - - -) is the AI result. E_L denotes the energy, and E_L^0 the zero-point energy, in the left ligand.

Figure 4.3, P. 90: As in Fig. 4.2 except $\lambda = 0.5$ (twice the mass of C).

Figure 7.1, P. 155: Schematic diagram of potential energy curves for typical unimolecular dissociation into two fragments. S denotes the lower singlet level and T denotes the upper triplet level. V(R) is the minimum potential energy for a given center of mass to center of mass separation distance R.

Figure 8.1, P. 178: Schematic potential energy diagram for the dissociation of NCNO into NC and NO, indicating singlet and triplet states.

Figure 8.2, P. 179: Plot of theoretically determined rate constants log k_{EJ} vs. energy for a variety of treatments of the T_1 triplet surface, and plot of the experimentally determined rate constants (plus signs). The circles denote RRKM calculations on the singlet surface only; boxes denote RRKM calculations including singlet and triplet surfaces with a degeneracy of three for the triplet.

Figure 8.3, P. 180: Plot of theoretically determined rate constants log k_{EJ} vs. energy for two different assumed parameters for the Varshni bonding potential, and a plot of the experimentally determined rate constants (plus signs). Also included is a calculation which uses $N_{EJ}(\infty)$. The circles denote RRKM calculations for an assumed potential with a β parameter of 0.48 Å^{-2}; boxes denote RRKM calculations for an assumed potential with a β parameter of 0.70 Å^{-2}.

INTRODUCTION

A chemical reaction process can only be termed completely understood when a theoretical model exists which accurately describes all of the experimentally observed quantities. The topic of this thesis is the development and application of models for the dynamics of a few specific chemical processes. In particular, theoretical studies of electron transfer reactions, gas phase H-atom transfer reactions, the dynamics of intramolecular vibrational redistribution of energy, and unimolecular dissociation reactions are presented.

Electron transfer reactions are important steps in biological processes.[1,2] In biological electron transfer reactions (e.g., photosynthetic reaction centers) the donor and acceptor moieties are often fixed with respect to each other. As a result, studies on the dependence of the rate of electron transfer on the distance separating the donor and acceptor and also on their mutual orientation are of interest. Recent experimental studies have examined this distance and orientation dependence through the chemical synthesis of a set of rigid molecules having different bridging groups linking the donor and acceptor.[3] The first chapter of this thesis deals with the theoretical description of the orientation dependence of the rate of electron transfer between two large aromatic molecules. A semiclassical method for determining approximate wavefunctions corresponding to the lowest unoccupied and highest occupied molecular orbitals of porphyrin-like molecules is developed in Chapter 1. The model used was developed by Siders, Cave, and Marcus,[4,5] and is based on the use of oblate spheroidal potential wells to describe the interaction between the electron which is transferred and the donor and acceptor subgroups. From the resulting one-electron wavefunctions the electronic matrix element H_{BA}, which contains most of the orientation dependence for a nonadiabatic electron transfer, is calculated through Gauss-Legendre quadrature. The semiclassical calculations of H_{BA} give good agreement (within the spheroidal model) with quantum calculations,[4] while requiring much less computer time and may be applied to the study of specific, experimentally determined, orientation

dependences of the electron transfer rate.

There have been numerous theoretical studies recently on the dynamics of light-atom exchange between two heavy particles.[6] Comparisons of the results from the different methods are of use in evaluating the validity of any approximations involved. Chapter 2 of this thesis examines two approximate treatments[7,8] for the particular case of H-atom transfers, both of which involve a two-state approximation. One of the treatments[7] is based on a partial exponentiation of the distorted wave Born approximation[9] formula for the two-state reactive transition probability. The other treatment[8] is based on the Crothers-Stückelberg[10] expression for the two-state reactive transition probability. A comparison of the Boltzmann-averaged reactive transition probabilities for these two different approximate treatments with the exact two-state result shows that for energies of chemical interest the distorted wave treatment is considerably more accurate.

Unimolecular dissociation reactions have been of interest to chemical physicists for many years. One standard theory, RRKM theory[11], for describing the rate of unimolecular dissociation reactions is based on statistical and transition state theory approximations. One factor of importance in unimolecular dissociation reactions is the dynamics of the distribution of energy among the vibrational and rotational states of the molecule. RRKM theory assumes that this energy rapidly becomes statistically distributed among the available states. Experiments have shown that this is indeed a valid assumption for thermally activated dissociation processes. However, when laser induced dissociation processes are considered, the time scale for the redistribution of energy and the dissociation time-scale are not necessarily well separated. A necessary condition for the development of a "laser selective chemistry"[12] where lasers are used to control dissociation processes is that the dissociation time-scale be shorter than the redistribution time-scale.

The high density of states for polyatomic molecules at typical energies of interest causes difficulties in the theoretical study of the energy redistribution

process. Because of this high density of states, the number of basis states in some reasonable energy range is much too large to be feasibly handled computationally. Thus, one method for decreasing the difficulty of the theoretical study of this problem is to find some way to consider only a part of all the basis states. Chapters 3 and 4 present two such methods for reducing the number of basis states which have to be expliclitly included when calculating the time-evolution of an initially prepared nonstationary rovibrational state. In particular, in Chapter 3 a previously developed adiabatic elimination scheme[13] for the theoretical treatment of intramolecular vibrational dynamics is generalized. The adiabatic elimination scheme discussed here is motivated by[13] the partitioning of the basis states into a set which is resonant in energy and/or strongly coupled and another set which is nonresonant and/or weakly coupled. The time dynamics of the nonresonant states may then be expected to adiabatically follow that of the resonant states. As a result, the nonresonant states may be adiabatically eliminated to given an effective Hamiltonian for the dynamics of the resonant states. The generalization presented in Chapter 3 involves the determination of an iterative scheme for determining higher-order effective Hamiltonians.

In Chapter 4 an alternative approach is presented for the problem of the large number of basis states involved in the description of intramolecular vibrational distribution (IVR) problems. In this chapter an artificial intelligence method[14] is presented for use in the IVR problem. This method is based on choosing only those basis states which will have a significant effect on the dynamics. This is done by searching through the "tree" formed by the coupling of the basis states to each other, and assigning an importance function to each of the basis states encountered in the search. Only those basis states with a high importance function are then retained for later use in determining the dynamics. The importance function used is motivated by perturbation theory considerations. Application of this method to a model eleven-coordinate IVR problem[15a] is also presented there. Further application of this method to the study of the intramolecular dynamics

of highly excited CH overtone states in benzene is currently being considered.[15b]

Recent experimental studies[16,17] have probed the energy and angular momentum dependence of unimolecular reaction rates and product state distributions for dissociation reactions in which there is no barrier to dissociation. The last four chapters of the thesis focus on the calculation of unimolecular reaction rates for these dissociation reactions which have a highly flexible transition state. Statistical theories have been found to provide a ground description of many unimolecular dissociation reactions. In particular, two statistical theories commonly being used at present are RRKM theory[11] and phase space theory (PST).[18] In the standard implementation of RRKM theory the hindered rotational modes of the separating fragments at the transition state are treated as quantum vibrators whereas in PST they are treated as quantum free rotors.

A common requirement of statistical theories for dissociation reactions is the need to evaluate the amount of phase space available for the two separating fragments as a function of energy, angular momentum and separation distance. Recently, Wardlaw and Marcus[19] have developed and applied a method for performing the phase space integral while treating the hindered rotational modes as classical hindered rotors and the vibrational modes quantum mechanically. This classical treatment of the hindered rotational motion raises the question of the possibility for quantum corrections. In Chapter 5 the cumulative effect of quantum mechanics on the hindered rotational modes is studied for the methyl radical recombination reaction. This is done by calculating various partition function ratios through the Monte Carlo evaluation[20] of Feynman path-integral[21] expressions. The result of this study is that at least for the particular reaction and conditions there is a negligible quantum effect for the hindered rotational modes.

An alternative method for treating the hindered rotational modes is presented in Chapter 6 of the thesis and further expounded in Chapter 7. This method gives equivalent results to the action-angle coordinate based method of Ref. 19, but is based instead on the use of conventional Euler angle coordinates[22]

and their conjugate momenta. In both of these treatments the reaction coordinate is implicitly assumed to be the separation distance. They are also both based on the approximate separation of the modes into the "conserved" vibrational modes which have little change in going from reactants to products and the remaining transitional modes which include the free and hindered rotations. The conserved modes are then treated as quantum oscillators while the rotational modes are treated as classical motion on a given potential energy surface. The final result is an integral expression for the number of states for a given energy and angular momentum which can be evaluated through Monte Carlo integration.[20] The integration method suggested here also differs from that of Ref. 19. Also presented in Chapter 6 is a comparison of the results of the present method and of that of Ref. 19 for the methyl radical recombination reaction.

In Chapter 6 formulae are presented for the specific case of two nonlinear fragments. The corresponding formalism for all combinations of atomic, linear, and nonlinear fragments is presented in Chapter 7. It has been observed in several calculations[23] that as the total energy E increases, the separation between the two fragments at the transition states decreases. This point is also discussed in Chapter 7 along with a discussion of the role of repulsive potential energy curves and the role of two minima in the plot of the number of states versus separation distance.

A detailed application of the formalism presented in Chapters 6 and 7 is given in Chapter 8 where theoretical results for the dissociation of NCNO into NC and NO are compared to the corresponding experimental results[16]. The calculations given there indicate that the present implementation of RRKM theory together with a dynamical assumption about motion after the transition state gives product vibrational distributions that are in better agreement with the experimental determined distributions than are those of PST. Also the present implementation of RRKM theory aids in the understanding of the possible role of the upper triplet state by indicating that for a simple model triplet surface the

contribution of the triplet state is much less in terms of RRKM than in terms of PST. The rate constants determined from PST and the present implementation of RRKM are quite similar (when only the singlet state is included) for excess energies up to about 1000 cm^{-1}. The results also indicate the desirability of obtaining accurate *ab initio* potential energy surfaces for the hindered rotational modes.

The dissociation of CH_2CO into CH_2 and CO is another reaction which has received considerable experimental attention recently.[24] In Chapter 9 further results are briefly presented for the dissociation of CH_2CO into the CH_2 and CO radicals. The results for the CH_2CO dissociation indicate a greater difference from PST than did those for the NCNO dissociation. Also, these results reemphasize the need for more accurate potential energy surfaces for the hindered rotational modes.

An alternative model, labelled the statistical adiabatic channel model, has been proposed by Quack and Troe[25] for treating the hindered rotational motions of the separation fragments. This method is based on the exponential interpolation of energy levels from reactant to product. In the appendix a brief comparison is given of the present implementation of RRKM theory and the statistical adiabatic channel model[25] of Quack and Troe for the dissociation of H_2O_2 into 2OH radicals.

REFERENCES

[1] S. G. Boxer, Biochim. Biophys. Acta **726**, 265 (1983).

[2] R. A. Marcus and N. Sutin, Biochim. Biophys. Acta **811**, 265 (1985).

[3] D. Heiler, G. McLendon, and P. Rogalskyj, J. Am. Chem. Soc. **109**, 604 (1987); R. J. Harrison, B. Pearce, G. S. Beddard, J. A. Cowan and J. K. M. Sanders, Chem. Phys. **116**, 429 (1987); B. Leyland, A. Joran, P. Felker, J. Hopfield, A. Zewail and P. B. Dervan, J. Phys. Chem. **89**, 5571 (1985); M. R. Wasielewski, M. P. Niemczyk, W. A. Svec and E. B. Pewitt, J. Am. Chem. Soc. **107**, 1080, 5562 (1985).

[4] P. Siders, R. J. Cave, and R. A. Marcus, J. Chem. Phys. **81**, 5613 (1984).

[5] R. J. Cave, P. Siders, and R. A. Marcus, J. Phys. Chem. **90**, 1436 (1986).

[6] A. Persky and M. Broida, Chem. Phys. **114**, 85 (1987); A. Persky and H. Kornweitz, Chem. Phys. Lett. **142**, 37 (1987); P. L. Gertitschke, J. Manz, J. Romelt and H. H. R. Schor, J. Chem. Phys. **83**, 208 (1985); E. Pollak, M. Baer, N. Abu-Salbi, and D. J. Kouri, Chem. Phys. **99**, 15 (1985); A. Ohsaki and H. Nakamura, Chem. Phys. Lett. **142**, 37 (1987).

[7] V. K. Babamov, V. Lopez, and R. A. Marcus, Chem. Phys. Lett. **101**, 507 (1983).

[8] H. Nakamura, J. Phys. Chem. **88**, 4812 (1984); **89**, 5862 (1985).

[9] E.g., see M. S. Child, *Molecular Collision Theory* (Academic, New York, 1974).

[10] A. Bárány and D. S. F. Crothers, Phys. Scr. **23**, 1096 (1981).

[11] R. A. Marcus and O. K. Rice, J. Phys. Colloid Chem. **55**, 894 (1951); R. A. Marcus, J. Chem. Phys. **20**, 359 (1952); **43**, 2658 (1965); **52**, 1018 (1970).

[12] E.g., see Adv. Chem. Phys. **47**, (1981).

[13] G. A. Voth and R. A. Marcus, J. Chem. Phys. **82**, 2254 (1985).

[14] P. H. Winston, *Artificial Intelligence* (Addison-Wesley, Reading, 1984).

[15a] S. M. Lederman and R. A. Marcus, J. Chem. Phys. *in press*; S. M. Lederman, V. Lopez, V. Fairen, G. A. Voth, and R. A. Marcus, J. Chem. Phys.

to be submitted.

[15b] Y. F. Zhang, S. J. Klippenstein and R. A. Marcus, *work in progress.*

[16] L. R. Khundkar, J. L. Knee, and A. H. Zewail, J. Chem. Phys. **87**, 77 (1987).

[17] C. X. W. Qian, M. Noble, I. Nadler, H. Reisler, and C. Wittig, J. Chem. Phys. **83**, 5573 (1985), and references cited therein.

[18] P. Pechukas and J. C. Light, J. Chem. Phys. **42**, 3281 (1965); P. Pechukas, R. Rankin, and J. C. Light, J. Chem. Phys. **44**, 794 (1965); C. Klotz, J. Phys. Chem. **75**, 1526 (1971); W. Chesnavich and M. Bowers, J. Chem. Phys. **66**, 2306 (1977).

[19] D. M. Wardlaw, and R. A. Marcus, Chem. Phys. Lett. **110**, 230 (1984); D. M. Wardlaw and R. A. Marcus, J. Chem. Phys. **83**, 3462 (1985); D. M. Wardlaw and R. A. Marcus, J. Phys. Chem. **90**, 5383 (1986); D. M. Wardlaw and R. A. Marcus, Adv. Chem. Phys. **70**, 231 (1988).

[20] J. P. Valleau and S. G. Whittington, in *Statistical Mechanics*, edited by B. J. Berne (Plenum, New York, 1977), p. 137; J. P. Valleaus and S. G. Whittington, *ibid.*, p. 169.

[21] R. P. Feynman and A. R. Hibbs, *Quantum Mechanics and Path Integrals* (McGraw-Hill, New York, 1965).

[22] H. Goldstein, *Classical Mechanics*, 2nd ed. (Addison-Wesley, Reading, 1980).

[23] S. N. Rai and D. G. Truhlar, J. Chem. Phys. **79**, 6046 (1983); W. L. Hase, Chem. Phys. Lett. **139**, 389 (1987); M. Quack and J. Troe, Ber. Bunsenges Phys. Chem. **81**, 329 (1977); G. Smith and D. M. Golden, Int. J. Chem. Kinet. **10**, 489 (1978); S. W. Benson, Can. J. Chem. **61**, 881 (1983).

[24] I.-C. Chen, W. H. Green, Jr., and C. B. Moore, preprint, and references cited therein; A. J. Hoffman, L. R. Khundkar, and A. H. Zewail, work in progress.

[25] M. Quack and J. Troe, Ber. Bunsenges. Phys. Chem. **78**, 240 (1974); *ibid.* **79**, 170 (1975); J. Troe, J. Chem. Phys. **75**, 226 (1981).

Chapter 1: A Semiclassical Model for Orientation Effects in Electron Transfer Reactions

[The text of this chapter appeared in: R. J. Cave, S. J. Klippenstein, and R. A. Marcus, J. Chem. Phys. **84**, 3089 (1986).]

A semiclassical model for orientation effects in electron transfer reactions

Robert J. Cave, Stephen J. Klippenstein, and R. A. Marcus
Arthur Amos Noyes Laboratory of Chemical Physics, California Institute of Technology,[*] *Pasadena, California 91125*

(Received 26 August 1985; accepted 12 December 1985)

An approximate solution to the single-particle Schrödinger equation with an oblate spheroidal potential well of finite depth is presented. The electronic matrix element H_{BA} for thermal electron transfer is calculated using these wave functions, and is compared with values of H_{BA} obtained using the exact solution of the same Schrödinger equation. The present method yields accurate results for H_{BA}, within the oblate spheroidal potential well model, and is useful for examining the orientational effects of the two centers on the rate of electron transfer.

I. INTRODUCTION

Increased understanding of biological redox systems has led to the need for detailed information regarding the effects of mutual orientation and separation distance on the rate of electron transfer. The nonspherical structure of many biological redox components, such as hemes, chlorophyll *a* and *b*, and quinones leads one to expect that the mutual orientation of redox partners can significantly affect the rate of electron transfer.

Examples of systems for which orientational effects are expected include electron transfers involving cytochrome *c* as well as various components in photosynthetic reaction centers. It will be recalled that cytochrome *c* is a complex in which a heme lies in a crevice created by a surrounding protein and is bonded to the protein by thioether bridges.[1] It is believed that electron transfers to and from the heme occur predominantly near the opening of the crevice to the solution.

Several previous studies have attempted to qualitatively assess orientational effects using simplified models.[2] Recently, Siders *et al.*[3] developed a model for examining orientation effects in transfers between large, aromatic molecules, where the high lying electrons are delocalized, and have applied[4] it to several systems of current experimental interest. The basis of the model is the calculation of single-site, one-electron wave functions of oblate-spheroidal wells having constant potentials. These wave functions are then used to calculate the electron-transfer matrix element, the predominant distance dependent quantity in theories of nonadiabatic electron transfer.

In the present paper two simple approximations to this model are introduced. The resulting approximate model is computationally much faster, conceptually simpler, and will be seen to yield accurate results for H_{BA}, within the original model. The paper is organized as follows. The exact model and the form of the electron-transfer matrix element are outlined in Sec. II. The exact wave functions for the original model[3] are described in Sec. III and the two additional approximations are introduced in Sec. IV. The calculation of H_{BA} and the energy quantization for the approximate wave functions are briefly discussed there. The exact and approximate results for the wave function and the electron-transfer matrix element are compared and discussed in Sec. V, with concluding remarks made in Sec. VI.

II. THE THEORETICAL MODEL

The present model[3] is intended to describe electron transfer between two fixed sites, *A* and *B*. In the zeroth-order problem *A* and *B* do not interact and only the transferable electron is considered explicitly, i.e., each electronic wave function is a one-electron wave function. The states localized at sites *A* and *B* are labeled Ψ^A and Ψ^B, respectively. The model has been designed to assess orientational effects, at various distances, in electron transfer between large aromatic systems and it is thus assumed that the transferable electron is delocalized over the aromatic ring system.

Each isolated site is modeled as an oblate spheroid of constant negative potential inside the well and zero potential outside the well. Thus, in oblate spheroidal coordinates[5] (ξ,η,φ) the potential V is a constant, $-V_0$, inside the well $(\xi<\xi_0)$, and another constant $(V=0)$ outside,[3] and is depicted in Fig. 1. The molecule is taken to lie in the *xy* plane of the spheroid; *a* (in Fig. 1) is chosen as an approximate in-plane radius of the molecule, and *b* is chosen to yield a reasonable thickness for the electronic orbital of interest. The usual Cartesian coordinates are readily defined in terms of these coordinates [Eq. (2) of Ref. 3].

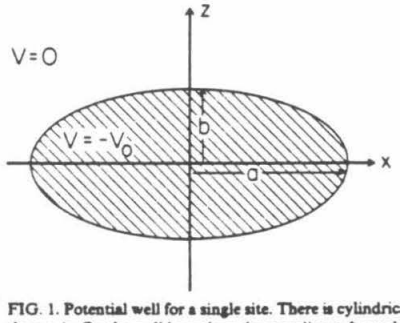

FIG. 1. Potential well for a single site. There is cylindrical symmetry about the *z* axis. On the well boundary the coordinate ξ equals ξ_0.

[*] Contribution No. 7267

 0021-9606/86/063089-10$02.10

The single-site one-electron Schrödinger equation may be written as

$$(\nabla^2 + k^2)\Psi = 0, \tag{1}$$

where k^2 equals $2\mu(E + V_0)/\hbar^2 \equiv k_i^2$ inside the well and $2\mu E/\hbar^2 \equiv k_0^2$ outside. A choice of V_0 yields a specific value of an orbital's energy E upon quantization.

The rate of nonadiabatic electron transfer between two such localized fixed states $A \rightarrow B$ may be written as[6–8]

$$k_{A\rightarrow B} = \frac{2\pi}{\hbar} |T_{BA}|^2 (\mathrm{FC}), \tag{2}$$

where (FC) is a Franck–Condon sum, discussed in detail elsewhere, e.g., Refs. 8–10. T_{BA} is the electronic matrix element which, in the present model, was expressed in terms of H_{BA}, H_{AA}, and S_{AB} as

$$T_{BA} = (H_{BA} - S_{AB}H_{AA})/(1 - |S_{AB}|^2), \tag{3a}$$

$$H_{BA} = \int \Psi^{B*} V^B \Psi^A \, d\tau, \quad H_{AA} = \int \Psi^{A*} V^B \Psi^A \, d\tau, \tag{3b}$$

$$S_{AB} = \int \Psi^{A*} \Psi^B \, d\tau, \tag{3c}$$

where V^B is the potential of the transferable electron for the isolated site B. T_{BA} is the primary distance and orientation dependent quantity in the expression for $k_{A\rightarrow B}$. T_{BA} was found[3] to agree with H_{BA} when H_{BA} was nonzero to within 3% for states similar to those examined here, when the wells were in contact and the agreement improved with increasing separation distance. Furthermore, the zeros of T_{BA} and H_{BA} were within 2° of one another (for a specific state examined).[4] Since the evaluation of T_{BA} requires considerably more computational time, only H_{BA} is calculated here.

The present model was developed to obtain approximate expressions for Ψ^A and Ψ^B and thereby to significantly simplify the calculation of H_{BA}. To facilitate the description of the two approximations introduced below, the calculation of the exact wave function is outlined briefly first.

III. THE EXACT SINGLE-WELL EIGENFUNCTIONS

In the oblate spheroidal coordinate system, Eq. (1) is separable.[5] Therefore, assuming that $\Psi \equiv \Psi_{mn}(\xi,\eta,\varphi) = R_{mn}(\xi)S_{mn}(\eta)\Phi_m(\varphi)$ one obtains the separated equations[5]

$$\frac{d^2\Phi_m}{d\varphi^2} + m^2\Phi_m = 0, \tag{4a}$$

$$\frac{d}{d\eta}\left[(1-\eta^2)\frac{dS^i_{mn}}{d\eta}\right] + \left\{\frac{d^2}{4}\eta^2 k_i^2 - \frac{m^2}{1-\eta^2} + \lambda^i_{mn}\right\} S^i_{mn} = 0, \tag{4b}$$

$$\frac{d}{d\xi}\left[(1+\xi^2)\frac{dR^i_{mn}}{d\xi}\right] + \left\{\frac{d^2}{4}\xi^2 k_i^2 + \frac{m^2}{1+\xi^2} - \lambda^i_{mn}\right\} R^i_{mn} = 0, \tag{4c}$$

where $d = 2\sqrt{a^2 - b^2}$, and m^2 and λ^i_{mn} are separation constants. The superscript i indicates a function appropriate to the potential region inside the well ($\xi < \xi_0$), while a superscript o will indicate these properties outside ($\xi > \xi_0$). $\Phi_m(\varphi)$ is equal to $A \sin m\varphi + B \cos m\varphi$, and since Φ_m must be single valued, m is an integer. The index n orders the eigenvalues λ_{mn} in order of increasing value and is chosen to have the possible values $n = m, m+1, m+2, \ldots$. This choice is convenient since in the spherical limit, where a tends to b, the eigenfunction given below reduces to a single term Ψ_{mn} with $n = l$, l being the angular momentum quantum number of the particle for the spherical case.[5]

Since the method is primarily designed to assess orientation effects in electron transfers between delocalized π systems, only states with no ξ-type nodes, and one η-type node are considered.[4] These states are odd with respect to reflection in the xy plane and are labeled (m,π); they are π-like states with azimuthal quantum number m. (A more complete description of the states is given elsewhere.[3,4])

To satisfy the quantization conditions, namely the continuity of the wave function and of its normal derivative at the well boundary, the exact solution $\Psi_{m,\pi}$ is written as a linear combination of the separated solutions,[3] that is, as $\Sigma_{r=0}^{\infty} C_n^i \Psi_{mn}^i$ for $\xi < \xi_0$, and as $\Sigma_{r=0}^{\infty} C_n^o \Psi_{mn}^o$ for $\xi > \xi_0$. Here, $n = 2r + m + 1$. Quantization is accomplished by iterating the energy E until $\Psi_{m,\pi}$ and its derivative are continuous at the well boundary $\xi = \xi_0$.

IV. APPROXIMATE SINGLE-WELL EIGENFUNCTIONS AND H_{BA} CALCULATION

The two new approximations made in the present paper to obtain single-well functions for use in calculating H_{BA} are the following: (1) The sums for the inner and outer quantized wave functions are each truncated to a single term, one inside and one outside the well, and (2) each R_{mn} and S_{mn}, inside and outside the well, is evaluated semiclassically rather than as a sum of known special functions.

The first approximation was prompted by two observations: (a) In the spherical limit the inner and outer wave functions are each represented by a single mn term. (For the case of π-like states this single term has $n = m + 1$.[3]) Since an oblate spheroid can be viewed as a "flattened sphere" it is reasonable that the use of only one term in the sum will be adequate when the eccentricity is not too high. (b) Empirically, we noted in our numerical calculations[3,4] that both inside and outside the potential well it was common for a single C_n^i and a single C_n^o to dominate the other coefficients for the states considered.

In view of approximation (1) above, the total wave function, for the (m,π) states of interest here may now be written as

$$\Psi_{m,\pi} \cong \begin{cases} C^i_{m+1}\Psi^i_{m,m+1}(\xi,\eta,\varphi); & \xi < \xi_0 \\ C^o_{m+1}\Psi^o_{m,m+1}(\xi,\eta,\varphi); & \xi > \xi_0. \end{cases} \tag{5}$$

Within this approximation the quantization conditions can now be satisfied only approximately at the well boundary:

$$C^i_{m+1}\Psi^i_{m,m+1} \cong C^o_{m+1}\Psi^o_{m,m+1} \quad (\xi = \xi_0), \tag{6a}$$

$$C^i_{m+1}\left.\frac{\partial\Psi^i_{m,m+1}}{\partial\xi}\right|_{\xi=\xi_0} \cong C^o_{m+1}\left.\frac{\partial\Psi^o_{m,m+1}}{\partial\xi}\right|_{\xi=\xi_0}. \tag{6b}$$

To satisfy Eq. (6a) both sides were squared and then integrated over η and φ at $\xi = \xi_0$, thereby averaging over the

boundary. Taking the square root, and following the same procedure for Eq. (6b) one obtains an equality of $C^{\prime}_{m+1}R^{\prime}_{m,m+1}(\xi_0)$ and of $C^{o}_{m+1}R^{o}_{m,m+1}(\xi_0)$ and also of their derivatives, when $S^{\prime}_{m,m+1}$, $S^{o}_{m,m+1}$ and Φ_m are each normalized to unity. Thereby, the ratio yields

$$\frac{1}{R^{\prime}_{m,m+1}(\xi)}\frac{d}{d\xi}R^{\prime}_{m,m+1}(\xi)|_{\xi=\xi_0} = \frac{1}{R^{o}_{m,m+1}(\xi)}\frac{d}{d\xi}R^{o}_{m,m+1}(\xi)|_{\xi=\xi_0}. \quad (7)$$

This equation serves to determine the approximate single-site wave function to within a normalization constant (Appendix A).

A semiclassical approximation is now introduced to simplify evaluation of R_{mn} and S_{mn} both inside and outside the well. In previous applications[3,4] the individual inner and outer R_{mn}'s and inner and outer S_{mn}'s were evaluated instead through series expansions in spherical Bessel functions and associated Legendre functions,[5,11] a process which can be time consuming. In the present study, semiclassical approximations were used for $S^{\prime}_{mn}$, S^{o}_{mn}, $R^{\prime}_{mn}$, and R^{o}_{mn} (uniform semiclassical approximations for the first two and primitive for the latter two, for reasons given in Appendix A). The resulting functions are seen (in Tables II, III, V, and VI given later) to be accurate. Previous uniform semiclassical approximations to *prolate* spheroidal wave functions, described by Sink and Eu,[12] have a number of differences from ours.[13] Our expressions for the wave functions and the procedure for calculating H_{BA} are given in Appendix A. The semiclassical treatment of $S^{\prime}_{mn}(\eta)$ itself involves four turning points for the states of interest in the present article.

The general procedure used for calculations of H_{BA} (both approximate and exact) was to choose a value for E which yielded the desired decay of H_{BA} with distance, after adjusting V_0. Thus, an accurate quantization of the energy for a given value of the potential was not needed. What is required is, given this decay, that the orientation dependence of H_{BA} be accurate for the states of interest. Nevertheless, for completeness, results for quantization of E are given in Appendix B.

V. RESULTS AND DISCUSSION

In this section the exact and approximate results for H_{BA} are compared and discussed for a number of states of interest. The physical significance of these (m,π) states was discussed earlier.[3,4] In particular, $(4,\pi)$ states are used to model the HOMO's of porphyrin derivatives and $(5,\pi)$ states to model the LUMO's in such molecules. The value of E (and hence of V_0) is chosen so as to give a fall off with distance of the rate which is fairly consistent with presently available data. The exact[3,4] and approximate electronic matrix elements H_{BA} so calculated are compared below in Table I and in Figs. 3, 4, and 6.

To describe the orientation of the two wells for the calculation of H_{BA} the (R,Θ) coordinate system shown in Fig. 2 is used. Unless otherwise specified, the xy planes of both wells are chosen to be parallel and the centers of the wells are held at a given separation distance R. The angle $\Theta = 0°$ (Fig. 2) corresponds to a "face-to-face" configuration and $\Theta = 90°$ to an "edge-to-edge" one.

TABLE I. Exact and approximate H_{BA}'s for a pair of $(4,\pi)$ states as a function of distance at $\Theta = 0°$ and $\Theta = 90°$.

Θ (deg)	R(Å)	H^{ex}_{BA} [a]	H^{sp}_{BA} [b]	H^{sphere}_{BA} [c]
0°	10	3.8(− 4) [d]	3.0(− 4)	7.0(− 4)
	15	2.0(− 6)	1.8(− 6)	2.2(− 6)
	20	2.2(− 8)	2.1(− 8)	2.0(− 8)
	25	3.8(− 10)	3.7(− 10)	3.0(− 10)
90°	10	− 4.1(− 2)	− 5.8(− 2)	− 9.9(− 3)
	15	− 1.3(− 4)	− 1.5(− 4)	− 4.5(− 5)
	20	− 1.5(− 6)	− 1.7(− 6)	− 5.8(− 7)
	25	− 3.0(− 8)	− 3.4(− 8)	− 1.2(− 8)

[a] For each $(4,\pi)$ state $E = -1.1525$ eV, $V_0 = 17.352\,97$ eV, $a = 4.85$ Å, $b = 2.55$ Å.
[b] For each $(4,\pi)$ state $E = -1.1525$ eV, $V_0 = 17.541\,21$ eV, $a = 4.85$ Å, $b = 2.55$ Å.
[c] For each $(4,\pi)$ spherical state $E = -1.1525$ eV, $V_0 = 18.0313$ eV, $r = 3.915$ Å.
[d] The numbers in parentheses are the powers of ten by which each entry should be multiplied.

The exact and approximate H_{BA}'s are presented as functions of distance for transfer between two $(4,\pi)$ states, for the $\Theta = 0°$ and $\Theta = 90°$ orientations in Table I. The agreement is seen to be good. The deviation in Table I is largest at small R, and, especially in the $\Theta = 0°$ orientation, is due to the contribution of other states in the exact state sum over $R_{mn}S_{mn}$ [cf. Eq. (6) of Ref. 3] at these small R's. It is clear that this contribution from other n's is only serious at very small R. For comparison, results using spherical wells of similar volume and energy are also given in Table I. They are seen to be significantly less accurate than the present approximation to the spheroidal problem, particularly at $\Theta = 0°$.

In Fig. 3 exact and approximate results for transfer between two $(5,\pi)$ states are compared at constant edge-to-edge distance for various Θ's. As the edge-to-edge distance increases from 0 to 4 Å, the accuracy of the present approxi-

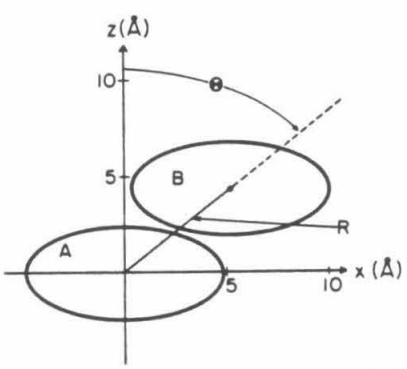

FIG. 2. Coordinate system used to specify the mutual orientation of wells A and B. The x axes of the wells are parallel and lie in the plane of the figure, as do the z axes.

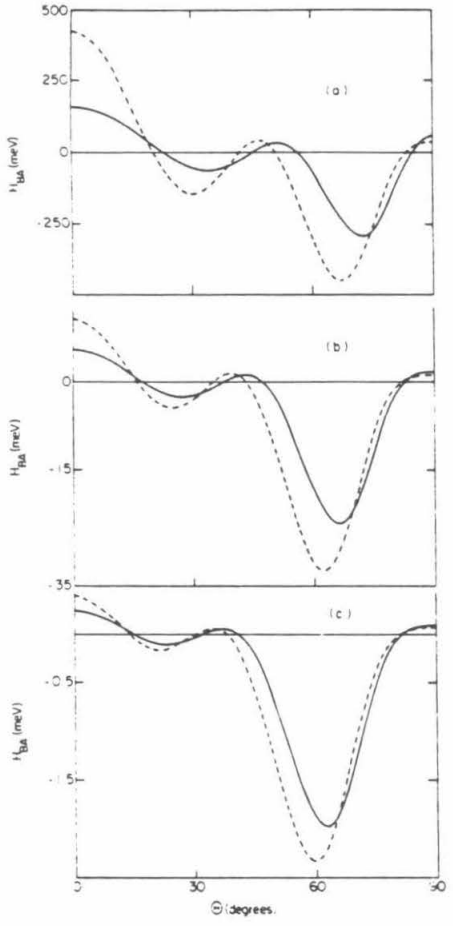

FIG. 3. The matrix element H_{BA} as a function of Θ at several fixed edge-to-edge separations for $(5,\pi)\rightarrow(5,\pi)$ transfer. For the donor and acceptor states $a = 5$ Å, $b = 2$ Å, $E = -2.8$ eV, - - - corresponds to the exact calculations where $V_0 = 26.3022$ eV. — corresponds to the semiclassical calculations where $V_0 = 25.532$ eV. (a) Edge-to-edge separation is 0 Å. (b) Edge-to-edge separation is 2 Å. (c) Edge-to-edge separation is 4 Å.

mate calculation also increases. The agreement is good for an edge-to-edge distance of 4 Å, and for larger separations the agreement remains good.

In Fig. 4 H_{BA}'s for the same set of orientations are given for transfer between $(5,\pi)$ and $(4,\pi)$ states. Calculations similar to those in Figs. 3 and 4 have been used previously[3,4] to model the orientation dependence of the electron transfer rate between two porphyrins. Again, at all distances the approximate results for the H_{BA}'s show similar behavior to the exact ones and for an edge-to-edge separation of 4 Å or larger the agreement is good.

Results for a different class of orientations (cf. Fig. 5) are given in Fig. 6. For these results, the wells are held at a given R, in the edge-to-edge ($\Theta = 90°$) orientation, but the xy planes are twisted about the line of centers through an angle γ relative to each other. The agreement is again good at all distances.

The present approximation has several advantages over the exact method developed in Ref. 3: (1) The present method is easier to implement. In the exact method the individual inner and outer R_{mn}'s and inner and outer S_{mn}'s were constructed as sums of known special functions. Each sum was then checked for convergence at all values of the argument for which the function was evaluated. Moreover, the total wave function was itself (in principle) an infinite sum which had to be checked for convergence at each evaluation. In the present method each inner and outer R_{mn} and each inner and

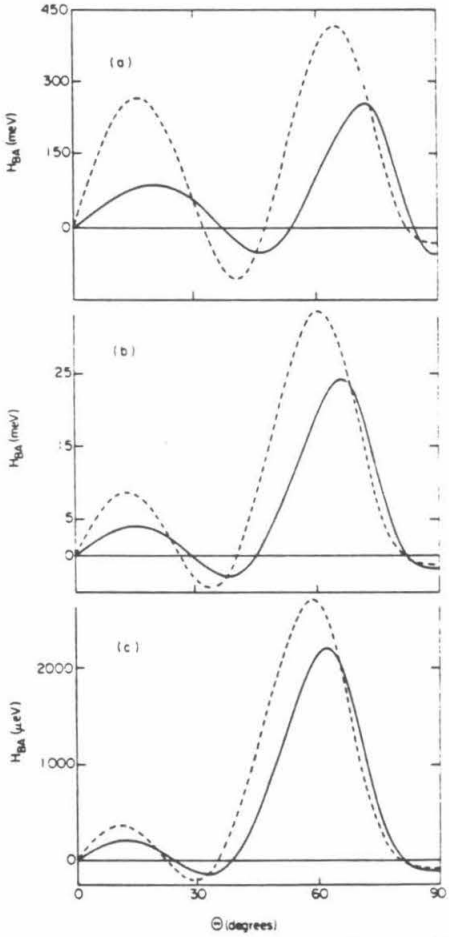

FIG. 4. The matrix element H_{BA} as a function of Θ at several fixed edge-to-edge separations for $(5,\pi)\rightarrow(4,\pi)$ transfer. For the donor and acceptor states $a = 5$ Å, $b = 2$ Å, $E = -2.8$ eV. For the exact calculations (- - -) the donor V_0 is 26.3022 eV and the acceptor V_0 is 22.199 eV. For the semiclassical calculations (—) the donor V_0 is 25.532 eV and the acceptor V_0 is 21.499 eV. (a) Edge-to-edge separation is 0 Å. (b) Edge-to-edge separation is 2 Å. (c) Edge-to-edge separation is 4 Å.

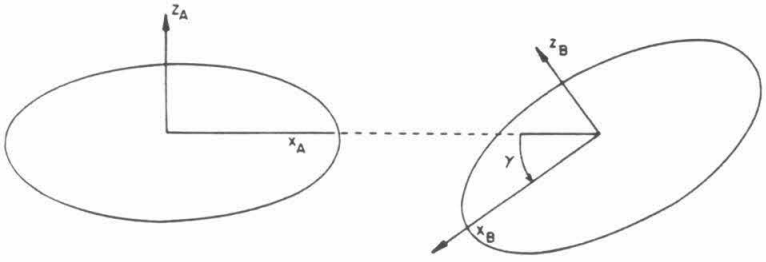

FIG. 5. Coordinate system used to specify the mutual orientation of the wells for the calculations presented in Fig. 6. The x axes of the wells lie in the plane of the figure. For $\gamma = 0°$ the x axes lie along the same line but are antiparallel.

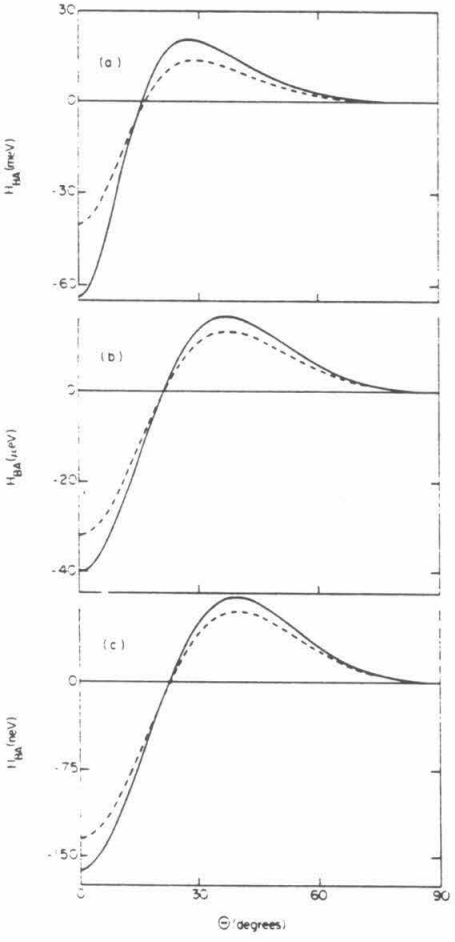

FIG. 6. The matrix element H_{BA} as a function of γ at several fixed edge-to-edge separations for $(5,\pi)\rightarrow(5,\pi)$ transfer. For the donor and acceptor states $a = 5$ Å, $b = 2$ Å, $E = -1.867$ eV. For the exact calculations (- - -) the donor and acceptor V_0 is 25.191 eV. For the semiclassical calculations (—) the donor and acceptor V_0 is 24.438 eV. (a) Edge-to-edge separation is 0 Å. (b) Edge-to-edge separation is 5 Å. (c) Edge-to-edge separation is 10 Å.

outer S_{mn} is evaluated as a single term, with convergence needed only for the respective integrals involved in the semiclassical expressions. The problem of convergence of a sum thus disappears. (2) The current method is considerably faster computationally. For each geometry in Figs. 3, 4, and 6, and Table I, the current method, treating H_{BA} as a three-dimensional volume integral, required about 10 min CPU time (VAX 11-780) while the exact method required about 50 times longer.[14] (A method of reducing computation time for the exact method by reducing the dimensionality of the H_{BA} integral is given in Ref. 4. It could be adapted using the present approximations to the wave functions, but we have not done so. It is expected to give essentially the same results as the present three-dimensional integration.) (3) The accuracy of the present method supports the simple conceptual previously introduced[3,4] to understand the orientation dependence of H_{BA}. Previously, this simple conceptual model was understood[3] by analogy with results from the use of spherical wells, where the inner and outer wave functions are each single terms. The spheroidal functions were envisioned as distorted spherical functions. Here, a related assumption is made explicitly by treating the inner and outer Ψ's as sin-

TABLE II. Relative values of $S^0_{mn}(\eta)$'s for various η's.

	$m = 5, n = 6$[a]		$m = 4, n = 5$[b]	
η	Semiclassical[c]	Exact	Semiclassical[c]	Exact
0.9	9.83(1)[d]	9.83(1)	1.93(1)	1.92(1)
0.8	4.71(2)	4.70(2)	6.81(1)	6.79(1)
0.7	1.06(3)	1.06(3)	1.30(2)	1.30(2)
0.6	1.71(3)	1.71(3)	1.89(2)	1.89(2)
0.5	2.24(3)	2.24(3)	2.31(2)	2.31(2)
0.4	2.48(3)	2.48(3)	2.44(2)	2.44(2)
0.3	2.36(3)	2.36(3)	2.23(2)	2.23(2)
0.2	1.84(3)	1.84(3)	1.70(2)	1.70(2)
0.1	1.01(3)	1.01(3)	9.21(1)	9.21(1)

[a] For both exact and semiclassical cases, $E = -2.8$ eV, $V_0 = 26.3022$ eV, $a = 5$ Å, $b = 2$ Å, $\lambda_{56}^{0,ex} = 44.95$, $\lambda_{56}^{0,sc} = 45.17$.

[b] For both exact and semiclassical cases, $E = -2.8$ eV, $V_0 = 22.1985$ eV, $a = 5$ Å, $b = 2$ Å, $\lambda_{45}^{0,ex} = 33.36$, $\lambda_{45}^{0,sc} = 33.67$.

[c] The semiclassical function was set equal to the exact function at $\eta = 0.4$. This was done for comparison purposes only and is not required for the H_{BA} calculations presented here.

[d] The numbers in parentheses are the powers of ten by which each entry should be multiplied.

TABLE III. Relative values of $S'_{mn}(\eta)$'s for various η's.

	$m=5,n=6$[a]		$m=4,n=5$[b]	
η	Semiclassical[c]	Exact	Semiclassical[c]	Exact
0.9	8.03(3)[d]	8.03(3)	1.28(3)	1.28(3)
0.8	1.78(4)	1.78(4)	2.15(3)	2.16(3)
0.7	1.94(4)	1.94(4)	2.07(3)	2.07(3)
0.6	1.60(4)	1.60(4)	1.58(3)	1.59(3)
0.5	1.13(4)	1.14(4)	1.08(3)	1.08(3)
0.4	7.35(3)	7.36(3)	6.81(2)	6.84(2)
0.3	4.44(3)	4.45(3)	4.06(2)	4.08(2)
0.2	2.45(3)	2.46(3)	2.23(2)	2.25(2)
0.1	1.08(3)	1.09(3)	9.79(1)	9.88(1)

[a] E, V_0, a, and b are the same as for the $m=5$, $n=6$ state of Table II. $\lambda_{56}^{\text{sem}} = -0.1111$, $\lambda_{56}^{\text{exc}} = 0.4718$.
[b] E, V_0, a, and b are the same as for the $m=4$, $n=5$ state of Table II. $\lambda_{45}^{\text{sem}} = -9.371$, $\lambda_{45}^{\text{exc}} = -8.790$.
[c] See Ref. c of Table II with $\eta = 0.4$ replaced by $\eta = 0.6$.
[d] See Ref. d of Table II.

TABLE V. Relative values of $R^{o}_{mn}(\xi)$'s for various ξ's.

	$m=5,n=6$[a]		$m=4,n=5$[b]	
ξ	Semiclassical[c]	Exact	Semiclassical[c]	Exact
1.0	3.47(−2)[d]	3.47(−2)	1.44(−2)	1.44(−2)
2.0	2.03(−4)	2.05(−4)	1.12(−4)	1.13(−4)
3.0	1.86(−6)	1.88(−6)	1.20(−6)	1.21(−6)
4.0	2.19(−8)	2.21(−8)	1.55(−8)	1.57(−8)
5.0	2.97(−10)	3.00(−10)	2.23(−10)	2.27(−10)
6.0	4.38(−12)	4.43(−12)	3.44(−12)	3.50(−12)
7.0	6.83(−14)	6.90(−14)	5.53(−14)	5.63(−14)
8.0	1.11(−15)	1.12(−15)	9.18(−16)	9.35(−16)

[a] E, V_0, a, and b are the same as for the $m=5$, $n=6$ state of Table II. $\lambda_{56}^{0,\text{sem}} = 44.95$, $\lambda_{56}^{0,\text{exc}} = 45.17$.
[b] E, V_0, a, and b are the same as for the $m=4$, $n=5$ state of Table II. $\lambda_{45}^{0,\text{sem}} = 33.36$, $\lambda_{45}^{0,\text{exc}} = 33.67$.
[c] See Ref. c of Table II with $\eta = 0.4$ replaced by $\xi = 1.0$.
[d] See Ref. d of Table II.

gle-term functions. The accuracy of these results therefore supports this model.

Although the goal of this paper is the calculation of H_{BA}'s, it is interesting to also compare the shape of the wave functions used with the exact ones. We do this next. More precisely we select the principal $R_{mn}S_{mn}$ term in the exact sum (largest coefficient) and compare (in Tables II to VI given later) its R_{mn} and S_{mn}, inside and outside the well, with those of the corresponding approximate functions used in the present single-term calculation of H_{BA}. They are compared on a relative basis to emphasize their similar shape. (Normalized wave functions were, as already noted, used to calculate H_{BA}.) Also included in these comparisons are the exact and semiclassical λ_{mn}'s inside and outside the well.

The exact and approximate results for the S^{o}_{mn}'s and λ^{o}_{mn}'s for two of the states used in the present H_{BA} calculations are compared in Table II. The agreement for the S^{o}_{mn}'s and for the λ^{o}_{mn}'s is generally better than 1%. In Table III, exact and approximate S'_{mn}'s and λ'_{mn}'s are compared for the same two states. The agreement for the S'_{mn}'s is again excellent, the largest error being less than 1%. (The agreement for both the R^{o}_{mn}'s and R'_{mn}'s, discussed later, is also good.) The λ'_{mn}'s themselves are somewhat inaccurate, though the splittings are in good agreement with those of the exact λ'_{mn}'s (Table IV). (A similar problem was encountered by Sink and Eu in the prolate spheroidal problem.[12]) The inaccuracy is seen, however, not to seriously affect the semiclassical S'_{mn}'s and R'_{mn}'s.

The exact and semiclassical R^{o}_{mn}'s are compared in Table V for the same two states as in Tables II and III. For comparison purposes, the functions are equated at the smallest ξ. The agreement is good over the entire region of interest. Similar accuracy is obtained for other states. The λ^{o}_{mn} values used in the calculations of R^{o}_{mn}'s for Table V were from exact and semiclassical methods, respectively. The exact and semiclassical R'_{mn}'s are compared in Table VI. The agreement is again good and similar accuracy can be expected for other states.

The accuracy of the semiclassical functions and the agreement of the semiclassical and exact H_{BA}'s indicate that the relevant shapes of the semiclassical and exact wave functions are quite similar. The shapes of the exact $(4,\pi)$ and $(5,\pi)$ states are compared elsewhere[4] to the shapes of porphyrin HOMO's and LUMO's obtained in molecular orbital calculations and are found to be in qualitative agreement. It would be useful to compare also the present H_{BA} results with calculations which might be based on the corresponding molecular orbital wave functions. For face-to-face orientations T_{BA} has been evaluated using molecular orbital techniques.[15,16] Molecular orbital calculations of H_{BA} have not

TABLE IV. Corrected λ'_{mn}'s.

	$m=5$[a]			$m=4$[b]	
λ'_{ij}	Exact	Semiclassical	λ'_{ij}	Exact	Semiclassical
λ'_{55}	−0.293	0.381	λ'_{44}	−9.49	−8.85
λ'_{56}	−0.111	0.562	λ'_{45}	−9.37	−8.73
$\lambda'_{56}-\lambda'_{55}$	0.182	0.181	$\lambda'_{45}-\lambda'_{44}$	0.12	0.12

[a] E, V_0, a, and b are the same as for the $m=5$, $n=6$ state of Table II.
[b] E, V_0, a, and b are the same as for the $m=4$, $n=5$ state of Table II.

TABLE VI. Relative values of $R^{i}_{mn}(\xi)$'s for various ξ's.

	$m=5,n=6^a$		$m=4,n=5^b$	
ξ	Semiclassical[c]	Exact	Semiclassical[c]	Exact
0.05	3.24(−2)[d]	3.18(−2)	3.38(−2)	3.35(−2)
0.10	6.25(−2)	6.14(−2)	6.51(−2)	6.48(−2)
0.15	8.80(−2)	8.68(−2)	9.19(−2)	9.16(−2)
0.20	1.07(−1)	1.06(−1)	1.12(−1)	1.12(−1)
0.25	1.18(−1)	1.18(−1)	1.24(−1)	1.24(−1)
0.30	1.20(−1)	1.20(−1)	1.27(−1)	1.27(−1)
0.35	1.13(−1)	1.13(−1)	1.20(−1)	1.20(−1)
0.40	9.59(−2)	9.73(−2)	1.04(−1)	1.04(−1)
0.45	7.13(−2)	7.31(−2)	8.02(−2)	7.99(−2)
0.50	4.08(−2)	4.29(−2)	5.00(−2)	4.93(−2)

[a] E, V_o, a, and b are the same as for the $m=5$, $n=6$ state of Table II. $\lambda^{sym}_{56} = -0.111$, $\lambda^{asym}_{56} = 0.562$.

[b] E, V_o, a, and b are the same as for the $m=4$, $n=5$ state of Table II. $\lambda^{sym}_{45} = -9.37$, $\lambda^{asym}_{45} = -8.73$.

[c] See Ref. c of Table II with $\eta = 0.4$ replaced by $\xi = 0.30$.

[d] See Ref. d of Table II.

been made for the variety of orientations examined here. Such a study should include the role of the solvent molecules, e.g., via a superexchange mechanism, and such molecular orbital-based calculations do not appear to be available as yet.

VI. CONCLUSION

A semiclassical plus single-term approximation for calculating the electron transfer matrix element H_{BA} has been formulated. It was shown to yield good agreement with results[4] in which the exact solution of the Schrödinger equation for the same model potential was used. This method also has much greater computational efficiency. In future applications of the model of Ref. 3 to the calculation of mutual orientation and separation distance effects, use of this method should be appropriate.

ACKNOWLEDGMENTS

It is a pleasure to acknowledge support of this research by the Office of Naval Research. RJC gratefully acknowledges the support of a National Science Foundation Predoctoral fellowship, 1979–1982. SJK gratefully acknowledges the support of a Natural Sciences and Engineering Research Council of Canada postgraduate scholarship, 1984–1985. The calculations reported in this paper made use of the Dreyfus-NSF theoretical chemistry computer which was funded through grants from the Camille and Henry Dreyfus Foundation, the National Science Foundation, and the Sloan Fund of the California Institute of Technology.

APPENDIX A: PRESCRIPTION FOR CALCULATING THE R_{mn}'s, S_{mn}'s, λ_{mn}'s AND H_{BA}

To facilitate use of the present method, details are given here on the calculation of H_{BA}. To this end, the R_{mn}'s, S_{mn}'s and λ_{mn}'s are calculated first, for any given E and V.

In obtaining a uniform semiclassical solution for S^{o}_{mn}, S^{o}_{mn} is converted[12,17] to a function $(1-\eta^2)^{1/2}S^{o}_{mn}$, whose differential equation contains no first derivatives. The comparison function chosen for making the uniform approximation is $(1-\nu^2)^{1/2}P^{m}_{l}(\nu)$,[12] where $P^{m}_{l}(\nu)$ is the associated Legendre function. Thereby, we have

$$S^{o}_{mn}(\eta) \cong A\frac{(1-\nu^2)^{1/2}}{(1-\eta^2)^{1/2}}P^{m}_{l}(\nu), \tag{A1}$$

where A is a constant which normalizes $S^{o}_{mn}(\eta)$, and where the function $\nu(\eta)$ is defined below.

The mapping $\eta \rightarrow \nu(\eta)$ leads in a standard way[12,18] to the equation

$$\int_{-\eta_{TP}}^{+\eta_{TP}} p_\eta \, d\eta = \int_{-\nu_{TP}}^{\nu_{TP}} p_\nu \, d\nu, \tag{A2}$$

where p_η is the classical η momentum

$$p^2_\eta = \frac{\lambda^{o}_{mn} + \eta^2 d^2 k_o^2/4}{(1-\eta^2)} - \frac{(m^2-1)}{(1-\eta^2)^2}, \tag{A3}$$

and p_ν is the classical ν momentum

$$p^2_\nu = \frac{l(l+1)}{1-\nu^2} - \frac{(m^2-1)}{(1-\nu^2)^2}, \tag{A4}$$

with $l=n$. At $\eta = \pm\eta_{TP}$, $p_\eta = 0$ while $p_\nu = 0$ at $\nu = \pm\nu_{TP}$. The left-hand side of Eq. (A2) was evaluated numerically, using a standard routine. The right-hand side equals $\{[l(l+1)]^{1/2} - (m^2-1)^{1/2}\}\pi$. The quantized value of λ^{o}_{mn} which appears in Eq. (A3) is that which permits Eq. (A2) to be satisfied.

The ν in Eq. (A1) is given by Eq. (A2) with the upper (or lower) limits of integration on each side of the equation replaced by η and $\nu(\eta)$.[19] (The choice of which set of turning points to use is a matter of convenience in performing the integration. In principle either choice will suffice.) With this $\nu(\eta)$ the $S^{o}_{mn}(\eta)$ given in Eq. (A1) was calculated for subsequent use in the calculation of H_{BA}.

The function $R^{o}_{mn}(\xi)$, the "radial" function outside the potential well, satisfies Eq. (4c), with the i superscripts and subscripts there replaced by o's. In the present study the following primitive semiclassical approximation[12,17] for $R^{o}_{mn}(\xi)$ sufficed because of the absence of turning points for the ξ motion:

$$R^{o}_{mn}(\xi) \cong \left[\exp\left(-\int_{\xi_o}^{\xi} |p_\xi| d\xi\right)\right] \Big/ (\xi^2+1)^{1/2}|p_\xi|^{1/2}, \tag{A5}$$

where the classical ξ momentum p_ξ is defined by

$$p^2_\xi = c^2_o - \{[(c^2_o + \lambda^{o}_{mn})(\xi^2+1) - (m^2-1)]/(\xi^2+1)^2\},$$

with $c^2_o = d^2k^2_o/4$ and where λ^{o}_{mn} was calculated above.

The calculation of λ^{i}_{mn} and S^{i}_{mn} is lengthier and is discussed at the end of this Appendix.

The inner radial function $R^{i}_{mn}(\xi)$ satisfies Eq. (4c). The tendency towards an absence of turning points, i.e., for the effective energy for the ξ motion to exceed the effective potential energy for all ξ, increases with increasing d, increasing k^2_i and decreasing n. For the (m,π) states and choice of parameters appropriate to the modeling of large aromatic systems discussed here there are no turning points for the ξ motion in the region $\xi < \xi_{0}$, and so a primitive semi-

classical approximation suffices for $R^{i}_{mn}(\xi)$. The boundary condition for π-like states is that the wave function be zero in the xy plane. Thereby, it is also zero on the disk of diameter d, centered at the origin, in the xy plane, and hence at $\xi = 0$. (It is also zero at $\eta = 0$.) The primitive semiclassical $R^{i}_{mn}(\xi)$ satisfying this condition is

$$R^{i}_{mn}(\xi) \cong \left[\sin\left(\int_0^{\xi} |p_\xi| d\xi\right)\right] \Big/ (\xi^2+1)^{1/2} |p_\xi|^{1/2}, \tag{A6}$$

where p_ξ^2 is the same as that given following Eq. (A5), but with o subscripts and superscripts replaced by i's.

All the components of $\Psi^{o}_{m,m+1}$ and $\Psi^{i}_{m,m+1}$ have now been considered [$\Phi^{i,o}_{m}(\varphi) = B\cos m\varphi + C\sin m\varphi$, with appropriate normalization] and thus the next step is to satisfy the quantization conditions. This is done by choosing the desired value of E and then using a root search technique (we used the Newton–Raphson method) to find the value of the well depth V_0 which allows Eq. (7) of the text to be satisfied. C^{o}_{m+1}, and C^{i}_{m+1} are determined using Eq. (6a) and normalizing the $\Psi_{m,\pi}$ defined in Eq. (5) of the text. The entire procedure is followed for both wells A and B. H_{BA} can then be calculated straightforwardly from Eq. (3b) of the text using nested numerical integration to perform the three-dimensional integral. We note that the integration only needs to be performed over well B, since this is the only region where V^{B} is nonzero.

In the above discussion we deferred consideration of S^{i}_{mn} and λ^{i}_{mn}. We now treat them by first describing a new procedure for defining localized wave functions.

First introducing[12] the function $U^{i}_{mn}(\eta) = (1-\eta^2)^{1/2} S^{i}_{mn}(\eta)$, as noted earlier, then using[20] the Bethe modification, namely, substituting m^2 for $m^2 - 1$, we obtain an equation for $U^{i}_{mn}(\eta)$:

$$\frac{d^2}{d\eta^2} U^{i}_{mn}(\eta) - V^{\text{eff}}(\eta) U^{i}_{mn}(\eta) = 0, \tag{A7}$$

where

$$V^{\text{eff}}(\eta) = [m^2 - (\lambda^{i}_{mn} + c_i^2\eta^2)(1-\eta^2)]/(1-\eta^2)^2,$$

with

$$c_i^2 \equiv d^2 k_i^2/4 = d^2\mu(E+V_0)/2\hbar^2.$$

This $V^{\text{eff}}(\eta)$ serves as an effective "$V - E$" term for the η motion.

When c_i^2 is zero the numerator in $V^{\text{eff}}(\eta)$ is quadratic in η. For $c_i^2 \neq 0$, this numerator is a quartic function which, for large enough c_i^2, has four real zeros. Examples of plots of $V^{\text{eff}}(\eta)$ for various positive values of V_0 and thus for various c_i^2's are given in Fig. 7. It is seen that as V_0 and thus as c_i^2 increases, $V^{\text{eff}}(\eta)$ changes from having two zeros to having four. For the states of interest in the present paper $V^{\text{eff}}(\eta)$ in Eq. (A7) typically has four zeros (i.e., the problem has four turning points), and we devised the following method for obtaining S^{i}_{mn}. [Had there been only two turning points an equation analogous to Eq. (A1) for $S^{o}_{mn}(\eta)$ would have been appropriate.]

In principle, a four turning-point problem can be treated with a comparison function that arises from a potential which itself yields four turning points, but such functions are typically as complicated as $S^{i}_{mn}(\eta)$ itself. Accordingly, results for two single-well problems were used, noting that the eigenvalues of a symmetric double well potential for a high barrier occur in pairs and the eigenfunctions can be represented to a high degree of accuracy by symmetric and antisymmetric combinations of the single-well wave functions.[21] Single-well potentials were devised for the portions of the wave function localized to the left- and the right-hand side of $\eta = 0$. Linear combinations of two semiclassical single-well eigenfunctions then yielded an approximate $S^{i}_{mn}(\eta)$.

For this purpose we introduce an effective single-well $V^{s}_{i}(\eta)$ to replace $V^{\text{eff}}(\eta)$, so as to yield a wave function largely localized in the $(-1<\eta<0)$ region, (cf. Fig. 8)[22]:

$$V^{s}_{i}(\eta) = \begin{cases} \dfrac{m^2 - (\lambda^{i}_{mn} + c_i^2\eta^2)(1-\eta^2)}{(1-\eta^2)^2} & (-1<\eta<0),(\eta_i<\eta<1) \\ V^{s} & (0<\eta<\eta_i) \end{cases}, \tag{A8}$$

where V^{s} equals $m^2 - \lambda^{i}_{mn}$ and η_i is the η in the interval (0,1) where $V^{s}_{i}(\eta_i) = V^{s}$. The single-well potential for a wave function localized between $0<\eta<1$ is simply the reflection of the potential depicted in Fig. 8 about $\eta = 0$. Each of these effective single-well potentials yields a two-turning point problem which can be solved using a uniform approximation based on a comparison equation for the two-turning point problem. The harmonic oscillator equation was chosen for the latter.[23] A zeroth order separation constant λ^{i}_{mn} is then obtained semiclassically from the single-well problem in a way analagous to the determination of λ^{o}_{mn}. The analog of Eq. (A2) for the determination of λ^{i}_{mn} is

$$\int_{-\eta^1_{TP}}^{\eta^2_{TP}} [V^{s}_{i}(\eta)]^{1/2} d\eta = \int_{-x_{TP}}^{+x_{TP}} \left[(2N+1) - \frac{x^2}{2}\right]^{1/2} dx = (2N+1)\frac{\pi}{2}, \tag{A9}$$

where $V^{s}_{i}(\eta)$ is defined in Eq. (A8), x_{TP} is the x for which the x integrand vanishes, and the $\eta^{1,2}_{TP}$'s are the values of η for which the η integrand vanishes. The first integral in Eq. (A9) was evaluated numerically, choosing λ^{i}_{mn} so as to satisfy Eq. (A9).

The choice of the quantum number N for the harmonic oscillator comparison wave function $\varphi_N(x)$ is determined by the state to be modeled. The number of nodes for the function $S^{i}_{mn}(\eta)$ (excluding those at $\eta = \pm 1$) is $n - m$. Thereby, $S^{i}_{m,m}(\eta)$ has no nodes, while $S^{i}_{m,m+1}(\eta)$ has one. The number of nodes of $\varphi_N(x)$ is N. Since pairs of φ_N's are combined, one member from each well, $S^{i}_{m,m}$ states are obtained by taking the symmetric combination of two ground-state harmonic oscillator-like wave functions, $\varphi_0(x)$, regardless of the value of m. For a π state, we need consider only states where $n = m + 1$. $S^{i}_{m,m+1}$ is obtained by taking

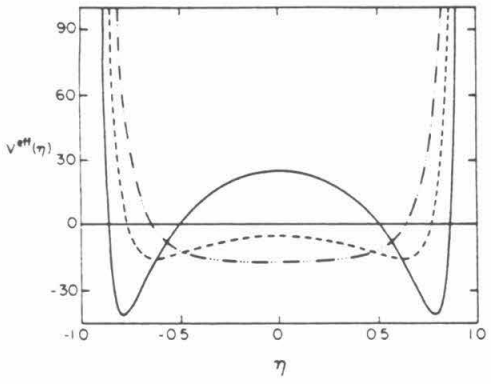

FIG. 7. Effective potential for S'_{mn} as a function of η for three different values of V_0. The other parameters used in all 3 plots are $a = 5$ Å, $b = 2$ Å, $m = 5$, $n = 6$, and $E = -2.8$ eV. — corresponds to $V_0 = 26.3022$ eV and $\lambda'_{56} = 0.3807$. - - - corresponds to $V_0 = 12.00$ eV and $\lambda'_{56} = 30.60$. - ··· - corresponds to $V_0 = 3.00$ eV and $\lambda'_{56} = 42.02$.

the antisymmetric combination of the two $\varphi_0(x)$ wave functions. (Similar reasoning shows that for S'_{mn} states for which $n > m + 1$, and when there are four turning points, linear combinations of two φ_N's with $N = 1,2,...$, would be used.)

Thus $S'_{m,m+1}$ is then given by

$$S'_{m,m+1}(\eta) = \frac{A}{(1-\eta^2)^{1/2}}\,[U_l(\eta) - U_r(\eta)], \quad \text{(A10)}$$

where $U_l(\eta)$ is $\exp(-x_l^2(\eta))$, i.e., a ground state harmonic oscillator wave function in the new variable $x_l(\eta)$ for the left-hand side single well; $x_l(\eta)$ is defined by Eq. (A9) with the upper or lower integration limits replaced by η and $x_l(\eta)$.[24] Similar definitions apply to $U_r(\eta)$ and x_r but with l's replaced by r's and with $V_r^s(\eta)$ as the single-well potential for a wave function "localized" in $0 \leqslant \eta \leqslant 1$. A is a constant which normalizes $S'_{m,m+1}(\eta)$.

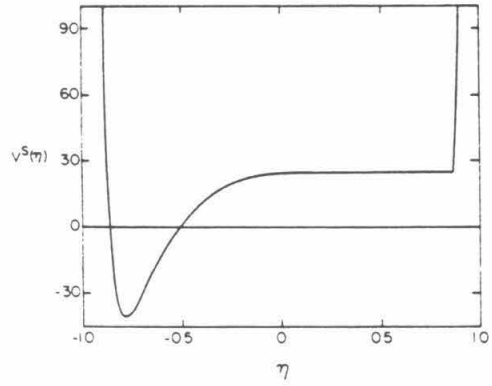

FIG. 8. Effective single-well potential for a localized S'_{mn} state, localized between $-1 \leqslant \eta \leqslant 0$ as a function of η. The parameters a, b, m, n, and E are the same as in Fig. 7, and $V_0 = 26.3022$ eV.

The above $\lambda'_{m,m+1}$'s can be termed zeroth order $\lambda'_{m,m+1}$'s. We also calculated "corrected" $\lambda'_{m,m+1}$'s which allow for the splitting of the eigenvalues by tunneling in the double-well problem. To do this we use the above U_l and U_r as basis functions, and obtain solutions of Eq. (A7) by solving

$$\begin{bmatrix} F_{ll} & F_{lr} \\ F_{rl} & F_{rr} \end{bmatrix} \begin{bmatrix} c_1 \\ c_2 \end{bmatrix} = \lambda \begin{bmatrix} 1 & G_{lr} \\ G_{rl} & 1 \end{bmatrix} \begin{bmatrix} c_1 \\ c_2 \end{bmatrix}, \quad \text{(A11)}$$

where F_{ij} denotes the matrix element $\langle U_i|F|U_j\rangle$ of

$$F = (1-\eta^2)(d^2/d\eta^2) + [m^2/(1-\eta^2)] - c_i^2\eta^2$$

and G_{ij} denotes $\langle U_i|U_j\rangle$. Equation (A11) yields two eigenvalues $\lambda_{m,m}$ and $\lambda_{m,m+1}$. This corrected $\lambda'_{m,m+1}$ was used in the calculation of $R'_{m,m+1}$ utilizing Eq. (A6)[25] and so to obtain the results given in the various tables and figures. However, we have found that for the parameters and states employed here, use of the zeroth order $\lambda'_{m,m+1}$, i.e., values without the splitting, gave results for the R'_{mn}'s which differed negligibly in the domain of interest and hence could have been used instead.

APPENDIX B: SEMICLASSICAL ENERGY EIGENVALUES

Using the semiclassical approximations to the individual R_{mn}'s and S_{mn}'s, and inside and outside the well, together with the single-term approximation, the energy values can be calculated using Eqs. (6) and (7) for given values of the potential and for various states. When V_0, a, and b for $m = 5$, $n = 6$ were chosen to be the values in Table II (Ref. a), the exact value of E was -2.8 eV, but the approximate value was -3.46 eV. To obtain the desired E of -2.8 eV in the approximate quantization, a V_0 of 25.5316 eV was needed and was used. When V_0, a, and b for $m = 4$, $n = 5$ were chosen to be the values in Table II (Ref. b) the exact value of E was -2.8 eV, while the approximate value was -3.39 eV. To obtain the desired E of -2.8 eV in the approximate quantization, a V_0 of 21.4993 eV was needed and used.

There is seen to be a fairly large error in this calculated eigenvalue, a result not unexpected, because of the observed contribution of several terms to the total wave functions near the well boundary. As was seen previously, however, these single-term functions are still accurate enough to yield reasonable results for H_{BA}.

[1]R. A. Marcus and N. Sutin, Biochim. Biophys. Acta. **811**, 265 (1985).
[2](a) S. A. Rice and M. J. Pilling, Prog. React. Kinet. **9**, 93 (1978); (b) B. Brocklehurst, J. Phys. Chem. **83**, 536 (1979); (c) A. B. Doktorov, R. F. Khairutdinov, and K. I. Zamaraev, Chem. Phys. **61**, 351 (1981).
[3]P. Siders, R. J. Cave, and R. A. Marcus, J. Chem. Phys. **81**, 5613 (1984).
[4]R. J. Cave, P. Siders, and R. A. Marcus, J. Phys. Chem. (submitted).
[5]C. Flammer, *Spheroidal Wave Functions* (Stanford University, Stanford, CA, 1957).
[6]V. G. Levich and R. R. Dogonadze, Collect. Czech. Chem. Commun. **26**, 193 (1961); English Translation, O. Boshko, University of Ottawa, Ontario, Canada.
[7]R. R. Dogonadze, A. M. Kuznetsov, and M. A. Vorotyntsev, Phys. Status Solidi B **54**, 125 (1972), **54**, 425 (1972).
[8]N. R. Kestner, J. Logan, and J. Jortner, J. Phys. Chem. **78**, 2148 (1974).
[9]B. S. Brunschwig, J. Logan, M. D. Newton, and N. Sutin, J. Am. Chem. Soc. **102**, 5798 (1980).
[10]P. Siders and R. A. Marcus, J. Am. Chem. Soc. **103**, 741 (1981).
[11]D. B. Hodge, J. Math. Phys. **11**, 2308 (1970).

[12]M. L. Sink and B. C. Eu, J. Chem. Phys. **78**, 4887 (1983).

[13]Sink and Eu (Ref. 12) treated the analogous prolate spheroidal problem, related to the present S^{e}_{mn} and R^{e}_{mn}. There are a number of differences between our treatment and theirs: (a) They do not have a boundary ξ_0 and hence do not need the "inner" wave functions. (b) They make the Langer modification [R. E. Langer, Phys. Rev. **51**, 669 (1937), M. S. Child, *Molecular Collision Theory* (Academic, New York, 1974), p. 44], i.e., they set $l(l+1)\rightarrow(l+\frac{1}{2})^2$ whereas we do not. (c) They also make an adjusted Bethe modification (Ref. 12) [H. A. Bethe, Hand. Physik **24** Part 1, 273 (1933) (cf. Ref. 2, p. 411)] $(m^2-1)\rightarrow(m+d)^2$, where d is a small positive constant chosen to give the best approximate λ^{e}_{mn}'s. We comment on these differences as follows: (a) The presence of the boundary leads to our having to treat the four turning-point problem. (b) When the Langer modification is avoided the S^{e}_{mn} reduce asymptotically to the corresponding P^{m}_{l}, as $n\rightarrow\infty$. [The difference between using and not using the Langer modification is quite small ($<0.1\%$ in S^{e}_{mn}) for the states examined here.] (c) The interest of Sink and Eu was in constructing a single uniform approximation for all mn states. Had they not adjusted the Bethe modification their method would not have yielded a single-valued mapping function for the case of $n=m=0$. In the present case, where only high n and m states are considered, the question of single valuedness for the mapping variable did not arise and a Bethe modification for S^{e}_{mn} was not needed. The Bethe modification for the η spheroidal equation is used when a harmonic oscillator comparison function is used, for the latter involves a mapping of the interval $(-1,1)$ onto the infinite interval $(-\infty,\infty)$. Accordingly, we used the Bethe modification for S^{o}_{mn} but not for S^{e}_{mn}, since we used an associated Legendre comparison function for S^{e}_{mn} rather than a harmonic oscillator comparison function.

[14]Of this factor of 50, a factor of 20 simply arises from the use of the single-term wave function and a factor of about 2.5 from the use of the semiclassical approximations in the wave functions.

[15]M.-H. Whangbo and K. R. Stewart, Isr. J. Chem. **23**, 133 (1983).

[16]W. J. Pietro, D. E. Ellis, T. J. Marks, and M. A. Ratner, Mol. Cryst. Liq. Cryst. **105**, 273 (1984).

[17]S. S. Gershtein, L. I. Ponomarev, and T. P. Puzyninca, Sov. Phys. JETP **21**, 418 (1965). These authors treated the analogous prolate spheroidal problem, and for it they justified the replacement of m^2-1 in Eqs. (A3) and (A4) by m^2 (Bethe modification).

[18]Uniform semiclassical treatments for second order differential equations having no first derivatives are discussed by S. C. Miller, Jr. and R. H. Good, Jr., Phys. Rev. **91**, 174 (1953); A. Erdélyi, J. Math. Phys. **1**, 16 (1960).

[19]The values of the ν integrals are then as follows. For $|\nu|>|\nu_{TP}|$:

$$\int_{\pm|\nu_{TP}|}^{\pm\nu} p_\nu\,d\nu=\frac{i(m^2-1)^{1/2}}{2}\times\ln\left[\frac{(m^2-1)^{1/2}\nu+[(m^2-1)-l(l+1)(1-\nu^2)]^{1/2}}{(m^2-1)^{1/2}\nu-[(m^2-1)-l(l+1)(1-\nu^2)]^{1/2}}\right]$$
$$-i[l(l+1)]^{1/2}\times\ln\left|\frac{[(m^2-1)-l(l+1)(1-\nu^2)]^{1/2}+[l(l+1)]^{1/2}\nu}{[l(l+1)-(m^2-1)]^{1/2}}\right|.$$

For $-\nu_{TP}<\nu<\nu_{TP}$:

$$\int_{-\nu_{TP}}^{\nu} p_\nu\,d\nu=\{[l(l+1)]^{1/2}-(m^2-1)^{1/2}\}\frac{\pi}{2}-(m^2-1)^{1/2}\times\arctan\left\{\frac{\nu(m^2-1)^{1/2}}{[l(l+1)(1-\nu^2)-(m^2-1)]^{1/2}}\right\}+[l(l+1)]^{1/2}\times\arcsin\left\{\frac{\nu[l(l+1)]^{1/2}}{[l(l+1)-(m^2-1)]^{1/2}}\right\}.$$

[20]H. A. Bethe, Ref. 13.

[21]M. A. Morrison, T. L. Estle, and N. F. Lane, *Quantum States of Atoms, Molecules, and Solids* (Prentice–Hall, New Jersey, 1976), p. 276.

[22]This procedure has elements in common with that used by V. Lopez, V. K. Babamov, and R. A. Marcus [J. Chem. Phys. **81**, 3962 (1984)] for a different double-well problem.

[23]Unlike the case of S^{e}_{mn}, the associated Legendre equation was not used. The single-well solutions are quite different from associated Legendre functions.

[24]The x integrals are then as follows: For $|x|>|x_{TP}|$:

$$\int_{\pm|x_{TP}|}^{\pm|x|} p_x\,dx=\frac{ix}{2}[x^2-(2N+1)]^{1/2}-i(N+1/2)\ln\left|\frac{x+[x^2-(2N+1)]^{1/2}}{[(2N+1)]^{1/2}}\right|.$$

For $-x_{TP}<x<x_{TP}$:

$$\int_{-x_{TP}}^{x} p_x\,dx=\frac{x}{2}[(2N+1)-x^2]^{1/2}+(N+1/2)\times\arcsin\left[\frac{x}{(2N+1)^{1/2}}\right]+(N+1/2)\frac{\pi}{2}.$$

[25]The zeroth order λ'_{mn}'s are used for the S'_{mn}'s, in order that the zeros of the comparison function and the original function U'_{mn}, are mapped onto one another by Eq. (A9).

Chapter 2: A Test of Two Approximate Two-State Treatments for the Dynamics of H-atom Transfer Between Two Heavy Particles

[The text of this chapter appeared in: S. J. Klippenstein, V. K. Babamov, and R. A. Marcus, J. Chem. Phys. **85**, 1924 (1986).]

ABSTRACT

Reactive transition probabilities and Boltzmann-averaged reactive transition probabilities for a slightly off-resonant model H-atom transfer system with an appreciable energy barrier are calculated using the approximate methods of Babamov *et al.* and of Crothers-Stückelberg. Both are compared with the corresponding quantities obtained from a numerical two-state treatment of the same model system. The method of Babamov *et al.* is seen to give more accurate results for the transition probabilities at energies below and around the reaction threshold, and much more accurate results for the Boltzmann-averaged probabilities in a wide range of temperatures than the second method. The relative merits of the two formulae are discussed.

I. INTRODUCTION

There have been a number of recent theoretical studies on the dynamics of chemical reactions in which an H atom is exchanged between two different heavier atoms or molecular fragments.[1–14] A method for reducing the dynamics of the reactive collision to two coupled ordinary differential equations, in the case when the initial reactant state and the final product state are nearly degenerate, was proposed recently by Babamov *et al.*[5,7] and applied to a collinear collision using a model LEPS potential energy surface for such reaction. This two-state method, which is only applicable to reactions with a substantial potential energy barrier to the reaction, has been shown[9] to give results for the transition probabilities in good agreement with the corresponding accurate (many states) coupled-channel calculations.[9]

A simple analytical formula for the reactive transition probabilities within the two-state approximation has also been proposed by Babamov *et al.*[6] and shown to give results in good agreement in the threshold region with those obtained from a numerical solution of the two-state model, and thus with the results of the accurate coupled channel calculations. The principal purpose of these treatments[5–8] has been to provide a practical simplified treatment of the dynamics of chemical reactions which correctly simulates the quantum mechanical tunneling of the light H-atom and is also accurate in the range of energies which contribute significantly to the kinetics of the reaction under typical conditions.

More recently the use of the Crothers-Stückelberg (CS) perturbed symmetric resonance formula[15,16] has been suggested[11,12] as an alternative simplified analytical treatment of the two-state model. The two methods have been applied[12] to an approximate analytical fit of the two-state representation of Babamov *et al.* for comparison purposes. However, the use of an incorrect analytical fit to the two-state model[17] and the overlooking of the importance of the near-threshold region led to an incorrect conclusion[12] about the relative usefulness of the two methods.

In this paper reactive transition probabilities from the two approximate methods are compared with those obtained from the exact two-state (numerical) treatment, for the model system of Ref. 9, as a function of the total energy. The results are also given in terms of Boltzmann-averaged reaction rate probabilities $P_{02}(T)$. Limitations of the CS method, already specifically mentioned by Bárány and Crothers,[16] will be seen to appear here in the threshold region.

II. TWO-STATE APPROXIMATION AND REACTIVE TRANSITION PROBABILITY CALCULATIONS

Starting with the Schrödinger equation for the collision in mass-weighted polar (hyperspherical[18]) coordinates and expanding the solution in terms of the eigenfunctions for the "vibrational" motion[5,19] $\eta_i(\theta;\rho)$

$$\psi(\theta,\rho) = \varphi_1(\rho)\eta_1(\theta;\rho) + \varphi_2(\rho)\eta_2(\theta;\rho) \tag{1}$$

one obtains, after some manipulation, a pair of coupled ordinary differential equations in the adiabatic representation:[5,19,20]

$$\left[-\frac{\hbar^2}{2m_H}\frac{d^2}{d\rho^2} + \epsilon_1(\rho) - E + \frac{Q_{11}}{2}\right]\varphi_1(\rho) = iP_{12}\frac{d\varphi_2(\rho)}{d\rho} - \frac{Q_{12}}{2}\varphi_2(\rho),$$

$$\left[-\frac{\hbar^2}{2m_H}\frac{d^2}{d\rho^2} + \epsilon_2(\rho) - E + \frac{Q_{22}}{2}\right]\varphi_2(\rho) = iP_{21}\frac{d\varphi_1(\rho)}{d\rho} - \frac{Q_{21}}{2}\varphi_1(\rho), \tag{2}$$

where m_H is the mass of the H-atom, E is the energy, the $\epsilon_i(\rho)$'s are the eigenvalues associated with the η_i, and the P_{ij}'s and Q_{ij}'s are matrix elements defined in Ref. 19. A closely related, but not entirely equivalent, pair of coupled equations in the diabatic representation can also be defined:[7,21]

$$\left\{-\frac{d^2}{d\rho^2} + \frac{2m_H}{\hbar^2}[V_{11}(\rho) - E]\right\}\Psi_1(\rho) = \frac{-2m_H}{\hbar^2}V_{12}(\rho)\Psi_2(\rho),$$

$$\left\{-\frac{d^2}{d\rho^2} + \frac{2m_H}{\hbar^2}[V_{22}(\rho) - E]\right\}\Psi_2(\rho) = \frac{-2m_H}{\hbar^2}V_{12}(\rho)\Psi_1(\rho). \tag{3}$$

The Ψ_i in Eq. (3) are the coefficients in an expansion

$$\psi(\theta,\rho) = \Psi_1(\rho)\zeta_1(\theta;\rho) + \Psi_2(\rho)\zeta_2(\theta;\rho), \tag{4}$$

in which the ζ_i are localized vibrational wavefunctions obtained as linear combinations of the η_i. The matrix **V** in Eq. (3), with elements V_{ij}, can be obtained by applying to the diagonal matrix of the ϵ_i's the orthogonal transformation[21,22] that converts the adiabatic vibrational basis $\eta_i(\theta;\rho)$ into a diabatic one $\zeta_i(\theta;\rho)$. The ϵ_i's in Eq. (2) are then related to the V_{ij}'s by

$$\epsilon_{1,2} = \frac{1}{2}(V_{11} + V_{22}) \mp \sqrt{\frac{1}{4}(V_{22} - V_{11})^2 + V_{12}^2}, \tag{5}$$

where the minus sign is for ϵ_1.

It has been shown[9] that the reactive transition probabilities $P_{02}(E)$ obtained from a numerical solution of Eq. (3) for the slightly off-resonant model system considered here are in good agreement with those of a 12-state accurate numerical quantum mechanical calculation[9] for the same system. Thus, the two-state treatment based on Eq. (3) provides an accurate simulation of the dynamics for the model system studied.

Babamov *et al.* gave[6] a simple analytical partially "exponentiated" distorted wave expression for the reactive transition probability from state n of the reactants to state m of the products, assuming approximately equal slopes[23] in plots of V_{11} and V_{22} versus ρ at the classical turning points:

$$P_{nm}^{B}(E) = \exp\left(\frac{-\Delta^2}{\alpha F}\right) \sin^2\left\{\left[\left(\frac{2\pi}{\alpha F}\right)\left[\frac{m_H}{\hbar^2}V_{12}(\rho_0)\right]^2 \exp\left(\frac{\alpha^3}{12F}\right)\right]^{1/2}\right\}, \tag{6}$$

where

$$\Delta = \frac{m_H}{\hbar^2}\left[V_{22}(\rho_0) - V_{11}(\rho_0)\right], \quad \alpha = \left[-\frac{d}{d\rho}\ln V_{12}(\rho)\right]_{\rho=\rho_0},$$

$$F = \left[-\frac{m_H}{\hbar^2}\frac{d}{d\rho}V^0(\rho)\right]_{\rho=\rho_0}. \tag{7}$$

Here, ρ_0 is the classical turning point for the ρ-motion on a mean potential $V^0(\rho) = [V_{11}(\rho) + V_{22}(\rho)]/2$. The approximations contained in Eq. (6) are given in the Discussion. Another formula proposed by Babamov *et al.*[6] is treated in

the Appendix. It should be stressed that the formula in the Appendix gives better results at higher energies than Eq. (6), and reduces to the exact two-state answer when Δ vanishes, but gives similar results in the threshold region. Eq. (6) is easier to use than the equation in the Appendix.

The Crothers-Stückelberg expression P_{nm}^{CS} for the reactive transition probability, for a transition from state n to state m, in a perturbed symmetric resonance problem, is given by:[15,16]

$$P_{nm}^{\mathrm{CS}}(E) = \mathrm{sech}^2\ \delta\ \sin^2(\sigma + \phi), \tag{8}$$

where

$$\sigma + i\delta = \int_{\rho_1}^{\rho_*} k_1(\rho)d\rho - \int_{\rho_2}^{\rho_*} k_2(\rho)d\rho, \tag{9}$$

$k_i(\rho) = \left\{2m_H\left[E - \epsilon_i(\rho)\right]/\hbar^2\right\}^{1/2}$, ρ_i is the classical turning point for the ρ-motion on the adiabatic potential $\epsilon_i(\rho)$, and ρ_* is the complex-valued ρ at which $\epsilon_1(\rho) = \epsilon_2(\rho)$. ϕ is a phase correction which to a good approximation[16] is zero for the perturbed symmetric resonance problem.

Nakamura *et al.*[12] recently suggested the application of Eq. (8) to the collinear H-transfer system studied in Ref. 9. As seen from Eqs. (8) and (9), the use of the formula does not explicitly require knowledge of the full coupled equations (2). It does, however, require knowledge of the two adiabatic potentials $\epsilon_i(\rho)$ in the complex plane, in order to determine the complex-valued crossing-point ρ_* and to perform the integration in the complex plane. One procedure[11,12,14] for implementing the formula is to attempt to construct an analytic representation of the diabatic matrix elements V_{ij} in Eq. (3) by making simple approximate analytic fits to a known numerical description of the latter. The adiabatic potentials are then determined from Eq. (5), with analytic continuation serving to extend them into the complex plane. This continuation yields a value for ρ_*, namely the value of ρ where the square root in Eq. (5) vanishes. This procedure appears to be the one used by Nakamura and Ohsaki[12].

The functional form assumed by the latter authors for the V_{ij}'s is[12]

$$V_{11}(\rho) = A \exp\left[-\frac{G}{A}(\rho - \rho_c)\right], \quad V_{22}(\rho) = V_{11}(\rho) - \Delta_0,$$

$$V_{12}(\rho) = \{B + C \exp[\beta(\rho - \rho_c)]\}^{-1}, \tag{10}$$

where A, B, C, G, Δ_0, and β, are all constants obtained from a fitting procedure, and ρ_c is an arbitrarily chosen constant.

In our applications we adopt the functional form of Nakamura and Ohsaki given by Eq. (10) and determine the parameters by fitting the values of V_{11}, V_{22}, V_{12}, the first derivative of V^0, and the first and second derivatives of V_{12} to the corresponding quantities in the numerical two-state representation, all at a given ρ_c. The parameter ρ_c in Eq. (10) was chosen in Sec. III to be 31.75 bohr, which is approximately the value of ρ at the classical turning-point at energies near the threshold energy. Other possible ways of applying the formula and of choosing ρ_c are explored in the Appendix.

III. RESULTS AND DISCUSSION

Since both the method of Babamov *et al.* and the CS method are based on the two-state approximation, the results for these methods are compared with those from a numerical solution of the two-state model. The two-state representation was used for a model LEPS surface for H-atom transfer between two heavy atoms.[24] The transition probability $P_{02}(E)$ obtained from the exact numerical solution of the two coupled equations as well as those from the two approximate formulae, $P_{02}^{B}(E)$ and $P_{02}^{CS}(E)$, were calculated for various energies. A plot of these quantities versus total energy is given in Fig. 2.1. One can see that at the lower energies the results of the formula of Babamov *et al.*, $P_{02}^{B}(E)$ are in excellent agreement with those of the numerical solution of the two-state model $P_{02}(E)$. The agreement gradually becomes worse as the energy increases well above the threshold. The results of the Crothers-Stückelberg formula $P_{02}^{CS}(E)$ on the other hand are quite inaccurate at energies near and below the reaction

threshold and become more accurate at higher energies. At a total collision energy of 10.0 kcal/mol, $P_{02}^{CS}(E)$ is seen to be too large by a factor of about 6. At higher energies, $P_{02}^{CS}(E)$ is still not in good agreement with $P_{02}(E)$ although it does have the correct shape and is in better agreement than $P_{02}^{B}(E)$. Another formula of Babamov *et al.* which is more accurate than Eq. (6) at higher energies, albeit somewhat more laborious to evaluate, is discussed in the Appendix.

In chemical reactions the quantity of primary interest is the reaction rate constant. For a collinear reaction a one-dimensional rate constant for the reaction from quantum state n of the reactants to form state m of the products can be defined as

$$k_{nm}(T) = \left(\frac{kT}{2\pi\mu}\right)^{1/2} P_{nm}(T), \tag{11}$$

where

$$P_{nm}(T) = \int_0^\infty P_{nm}(E) \exp\left(\frac{-E}{kT}\right) \frac{dE}{kT}, \tag{12}$$

μ is the Cl-HBr reduced mass and E is the translational energy of the reactants.

In Fig. 2.2 plots of $\log_{10} P_{02}(T)$, $\log_{10} P_{02}^{B}(T)$ and $\log_{10} P_{02}^{CS}(T)$ versus $1/T$ are given. At $T = 300°K$, the values of $P_{02}(T)$, $P_{02}^{B}(T)$, and $P_{02}^{CS}(T)$ are 6.2×10^{-6}, 6.3×10^{-6}, and 2.8×10^{-5}, respectively. At $T = 600°K$, they are 1.6×10^{-3}, 1.5×10^{-3}, and 2.7×10^{-3}, respectively. The corresponding one-dimensional rates ($k_{02}(T)$, $k_{02}^{B}(T)$ and $k_{02}^{CS}(T)$) given by Eq. (11) are 7.9×10^{-2}, 8.0×10^{-2} and 3.6×10^{-1} cm molecule^{-1} s^{-1} at $T = 300°K$. At $T = 600°K$ they are 29, 27 and 49 cm molecule^{-1} s^{-1}.

The rate constants $k_{02}(T)$ calculated using the $P_{02}(E)$ obtained from the exact numerical solution of the two-state problem are in good agreement with the rate constants calculated by Garrett *et al.*[13] using the $P_{02}(E)$ obtained from the accurate twelve channel[9] numerical solution. For example at $T = 300°K$ the twelve channel rate constant[13] is 6.37×10^{-2} cm molecule^{-1} s^{-1} as compared with the above two channel rate constant of 7.9×10^{-2} cm molecule^{-1} s^{-1}. At $T = 600°K$ the twelve channel result is 24.9 cm molecule^{-1} s^{-1} as compared

with the above two channel result of 29 cm molecule^{-1} s^{-1}.

Approximate semiclassical calculations of one-dimensional rate constants summed over the final states have been reported by Garrett *et al.*[13] for the same model system using various versions of variational transition state theory[25]. Those rates, which are also in good agreement with the corresponding results obtained from the accurate twelve channel quantum mechanical calculations[13], are not directly comparable to the state to state rates presented here.

The effective reaction threshold occurs at a translational energy of $\approx$ 7 kcal/mol[26] which, when equated to kT, corresponds to a temperature T of $3500°K$. Hence, for temperatures of practical interest the major contribution to $P_{nm}(T)$ arises from the reaction probabilities $P_{nm}(E)$ in the near-threshold region. Thus, although the application of the CS expression is better at high energies than the method of Babamov *et al.*, one sees that as far as the important temperature region is concerned, the Boltzmann-averaged Babamov probabilities $P_{02}^{B}(T)$ are in better agreement with the exact two-state result $P_{02}(T)$ than are the Boltzmann-averaged CS probabilities $P_{02}^{\mathrm{CS}}(T)$, for the model system studied (high energy barrier).

Some remarks about the "threshold region" are perhaps relevant here: At $125°K$, 80% of the integral $P_{02}(T)$ in Eq. (12) is contributed by energies equal to or less than 11.0 kcal/mol. At $250°K$ and $500°K$ the corresponding energies are $\leq$ 11.3 and $\leq$ 11.8 kcal/mol respectively. In these energy regions the $P_{02}^{B}(E)$ curve in Fig. 2.1 is seen to be accurate.

In order to study the possibility that the differences between the P_{02}^{CS}'s and the P_{02}'s are due to problems with the analytical fits, calculations were performed assuming that the dynamics occur on given analytical diabatic potentials of the form of Eq. (10). In Fig. 2.3 the quantities $P_{02}(E)$, $P_{02}^{B}(E)$ and $P_{02}^{\mathrm{CS}}(E)$ are calculated using these analytic diabatic potentials, $P_{02}^{\mathrm{CS}}(E)$ thus being the same as before. They are compared there as a function of total energy. Once again one sees that $P_{02}^{B}(E)$ is much better than $P_{02}^{\mathrm{CS}}(E)$ at energies near and below

the reaction threshold. Also, the superiority of the $P_{02}^{CS}(E)$ over the $P_{02}^{B}(E)$ at higher energies is again evident. Comparison of Figs. 2.1 and 2.3 also shows that at high energies there is a large discrepancy between $P_{02}(E)$ for the exact potentials and $P_{02}(E)$ calculated for the dynamics on the analytical fit in Eq. (10).

In Fig. 2.4 plots of $\log_{10} P_{02}(T)$, $\log_{10} P_{02}^{B}(T)$ and $\log_{10} P_{02}^{CS}(T)$ versus $1/T$ are given. The results observed in Fig. 2.4 reemphasize the fact that the transition probability versus energy dependence at high energies is not important for this model system, in determining the low to moderate temperature Boltzmann-averaged reactive transition probabilities. Thus, one can conclude that the discrepancies between $P_{02}^{CS}(T)$ and $P_{02}(T)$ found in Fig. 2.2 are not due to the analytical fit, but to the breakdown of the CS approximation in the threshold region.

We turn next to a discussion of the error of the CS approximation in the threshold region. Bárány and Crothers pointed out[16] that as one condition of validity of Eq. (8) the real phase σ in Eq. (9) should not be small, more specifically not $\lesssim 1$. Values of σ are given in Table 2.1. Comparison with Fig. 2.4 shows that Eq. (8) for $P_{02}^{CS}(E)$ indeed becomes invalid when $\sigma \lesssim 1$, confirming their prediction. At least in part, it is the smallness of the ρ-momentum which makes σ small in the threshold region.

We mention here some pertinent approximations used in obtaining Eq. (6) for $P_{nm}^{B}(E)$, though they are evident in the derivation given in Refs. 5 and 6: (1) There are no potential wells in the V_{ii}'s as a function of ρ contributing importantly at the energy of interest. (This point, explicitly noted elsewhere,[5,27] follows from the derivation[5–7,28] which excludes[27] this possibility.) (2) The transition is largely localized in the vicinity of the classical turning-point ρ_0.[29,30] (3) The resonance defect Δ at ρ_0 is small relative to the vibrational spacing, at least if Eq. (6) is used in the higher energy region.

In virtue of (3) the accuracy of the formula at energies above the threshold

region can be expected to gradually deteriorate with increasing resonance defect. However, it should be kept in mind that a good two-state approximation for the type of problem discussed above, valid in a wide energy region (as distinct from the threshold region), can only be made if the resonance defect Δ is small compared to the vibrational level spacing.

IV. CONCLUDING REMARKS

The formula of Babamov *et al.*, as shown in Figs. 2.1-2.4 above and Fig. 2.5 given in the Appendix, is an accurate approximation for energies near and below the reaction threshold, for this case of a high barrier slightly off-resonant reaction. At high energies the method is less accurate, but as seen in the previous section, these higher energies are not as important in determining the quantity of chemical interest $k_{nm}(T)$ for such reactions. In addition, the formula of Babamov *et al.*, given by Eq. (6), is a simple analytical formula and is expressed in terms of parameters that can be readily extracted from the numerical diabatic potentials.

The results obtained using the CS expression, on the other hand, are inaccurate at energies near and below the threshold for the present system, and begin to be accurate only at energies well above the threshold energy for this system. Thus, the important quantity $k_{nm}(T)$ is not accurately given for this system at low and moderate temperatures by the CS expression. A second difficulty with the CS formula (Eqs. (8) and (9)), which may hinder its wide applicability at present, is that the adiabatic potentials must be known in the complex plane and the complex integrals must somehow be evaluated. Thus far, for that reason, the only applications of the CS formula to H-atom transfers have involved constructing a set of approximate diabatic potentials rather than using the adiabatic potentials directly.

It may be emphasized that the results presented here do not bear any relation to the applicability of the Crothers-Stückelberg formula to problems in which the energies of interest are well above the threshold. The CS formula, as well as other simpler semiclassical formulae, should be applicable to problems for which the

transition probabilities at higher energies are the important ones. One example is the calculation of electron transfer cross sections in medium energy (Kev) atomic collisions for which such formulae are frequently used. The applicability of the CS formula to a low barrier reaction has been discussed elsewhere.[11,12,27]

ACKNOWLEDGMENTS

It is a pleasure to acknowledge support of this research by the Office of Naval Research. SJK gratefully acknowledges the support of a Natural Sciences and Engineering Research Council of Canada postgraduate scholarship, 1984-1986.

APPENDIX. ALTERNATIVE PROBABILITY CALCULATIONS

An alternative expression for the transition probability obtained by Babamov *et al.*[6,7] is

$$P_{nm}^{B'}(E) = \exp\left(\frac{-\Delta^2}{\alpha F}\right) \sin^2\left(\xi_0^s - \xi_0^a\right), \qquad (A1)$$

where ξ_0^s and ξ_0^a are the elastic phase shifts for the ρ-motion on the "symmetrized" potentials,

$$\epsilon^s(\rho) = \frac{1}{2}\left[V_{11}(\rho) + V_{22}(\rho)\right] - V_{12}(\rho)$$

$$\epsilon^a(\rho) = \frac{1}{2}\left[V_{11}(\rho) + V_{22}(\rho)\right] + V_{12}(\rho). \qquad (A2)$$

In Fig. 2.5 plots of $P_{02}(E)$, $P_{02}^{B}(E)$ and $P_{02}^{B'}(E)$ versus energy are given. At energies near the reaction threshold and below they are all equivalent. However, at higher energies $P_{02}^{B'}(E)$ is seen to have the correct phase, whereas $P_{02}^{B}(E)$ does not. This difference in phase does not significantly affect the calculation of the Boltzmann-averaged transition probabilities for moderate and low temperatures. Two other expressions[31] given by Babamov *et al.* are not examined here. Our current calculations showed that they lead to reaction probabilities very similar to those of $P_{02}^{B}(E)$ and $P_{02}^{B'}(E)$. When Δ vanishes Eq. (A1) reduces to the exact two-state formula.[19]

We turn next to the choice of the value of ρ_c used in the functional forms for the V_{ij}'s (Eq. (10)) in the CS calculations. The choice of this ρ_c depends on the choice of the ρ-region which needs to be the best represented. One can either use a single ρ_c, regardless of the collision energy, or let the choice of ρ_c depend on that energy. In obtaining the real parts of the integrals in Eq. (9) one may use either the adiabatic potentials calculated from the analytic diabatic potentials of Eq. (10), or the adiabatic potentials calculated from the real (numerical) diabatic potentials (i.e., not the fits to the diabatics). The adiabatic potentials calculated from the analytic diabatic potentials of Eq. (10) must be used in the determination of the imaginary parts of the integrals in Eq. (9).

For Fig. 2.6 we introduce the following notation: $P_{nm}^{CS}(E)$ corresponds (as before) to calculations using the analytic fits of Eq. (10) at $\rho_c = 31.75$ bohr, independent of the energy, for both the real and imaginary parts of the integrals in Eq. (9). $P_{nm}^{CS'}(E)$ corresponds to calculations using the fits of Eq. (10), with $\rho_c = \rho_0$ (the classical turning point for the mean potential $V^0(\rho)$ previously defined) at every collision energy, for both the real and imaginary parts of the integrals. Finally, $P_{nm}^{CS''}(E)$ corresponds to using the actual diabatic potentials to calculate the adiabatic ones for the real parts of the integrals and using fits, with $\rho_c = \rho_0$ at every collision energy, for the imaginary parts of the integrals.

The $P_{02}^{CS}(E)$'s are plotted along with $P_{02}(E)$ as a function of total energy in Fig. 2.6. $P_{02}^{CS''}(E)$ shows the best agreement at higher energies and also involves the most complicated calculations. At energies well below the reaction threshold, not shown in Fig. 2.6, $P_{02}^{CS'}(E)$ and $P_{02}^{CS''}$ are both less accurate than $P_{02}^{CS}(E)$ and thus result in less accurate Boltzmann-averaged reactive transition probabilities.

REFERENCES

[1] E. J. Shipsey, J. Chem. Phys. **58**, 232 (1973).

[2] M. Baer, J. Chem. Phys. **62**, 305 (1975).

[3] M. Ya. Ovchinnikova, Chem. Phys. **36**, 85 (1979).

[4] J. A. Kaye and A. Kuppermann, Chem. Phys. Lett. **92**, 574 (1982).

[5] V. K. Babamov, V. Lopez and R. A. Marcus, J. Chem. Phys. **78**, 5621 (1983); *ibid* **81**, 4182 (1984).

[6] V. K. Babamov, V. Lopez and R. A. Marcus, Chem. Phys. Lett. **101**, 507 (1983).

[7] V. K. Babamov, V. Lopez and R. A. Marcus, J. Chem. Phys. **80**, 1812 (1984); *ibid* **81**, 4181 (1984).

[8] V. Lopez, V. K. Babamov and R. A. Marcus, J. Chem. Phys. **81**, 3962 (1984).

[9] N. AbuSalbi, D. J. Kouri, V. Lopez, V. K. Babamov and R. A. Marcus, Chem. Phys. Lett. **103**, 458 (1984).

[10] J. Manz and H. H. R. Schor, Chem. Phys. Lett. **107**, 549 (1984).

[11] H. Nakamura, J. Phys. Chem. **88**, 4812 (1984); *ibid* **89**, 5862 (1985).

[12] H. Nakamura and A. Ohsaki, J. Chem. Phys. **83**, 1599 (1985).

[13] B. C. Garrett, N. AbuSalbi, D. J. Kouri and D. G. Truhlar, J. Chem. Phys. **83**, 2252 (1985).

[14] P. V. Coveney, M. S. Child and J. Römelt, Chem. Phys. Lett. **120**, 349 (1985).

[15] D. S. F. Crothers, Adv. Phys. **20**, 405 (1971).

[16] A. Bárány and D. S. F. Crothers, Phys. Scr. **23**, 1096 (1981).

[17] The incorrectness of the fit as a whole is evident from the lack of resemblance between the circle-results shown in Fig. 6 of Ref. 12 and the solid-line results shown in Fig. 3 of Ref. 7 (also shown in Fig. 2.1 here). An effective mass of 9000 a.u. was used in Ref. 12, whereas the correct mass to use should have been 1837.1 a.u. The value of the mass was not explicitly given[20a] in Refs.

5-9. The use of an incorrect mass converted the original nearly degenerate problem into one where the off-resonance became equal to about one quarter the spacing of the vibrational energy levels.

[18] A. Kuppermann, J. A. Kaye and J. P. Dwyer, Chem. Phys. Lett. **74**, 257 (1980).

[19] V. K. Babamov and R. A. Marcus, J. Chem. Phys. **74**, 1790 (1981).

[20] (a) The term $\hbar^2/m_H$ in Eq. (2) (or the term $m_H/\hbar^2$ in Eq. (3)) was intentionally omitted from the Schrödinger equation in Ref. 19 and Refs. 5-9. The term $m_H/\hbar^2$, which in atomic units has a value of 1837.1, should be inserted into the Schrödinger equation and all the formulae derived from it if one wants to reproduce any of the final results using the values for the potential matrix elements given in the Figures in Refs. 5,7, and 19. The manner in which that term should be inserted into the formulae is as $m_H/\hbar^2$ multiplying each variable which has a dimension of energy.

(b) The units in Fig. 8 of Ref. 5 and Fig. 2 of Ref. 7 were not specified. These energies are in kcal/mol when they are multiplied by an appropriate conversion factor: $[627.503/(2 \times 1837.1)]$ (This is $1/2m_H$ in hartrees converted to kcal/mol.)

[21] V. K. Babamov, Two-State Representation of H-Atom Transfer Reactions, J. Phys. Chem. (to be submitted).

[22] The transformation in Ref. 21 that transforms the η_i into the ζ_i is defined as the one that maximizes the difference of the expectation values of θ in the two ζ_i. This approach allows one to calculate the potential matrix elements V_{ij} up to higher energies than the approach in Ref. 7. However, the final results for $P^B_{nm}(E)$ near and below the threshold region are negligibly different from those calculated by the procedure in Ref. 7.

[23] In M. V. Basilevsky, G. E. Chudinov and V. M. Ryaboy, Chem. Phys. *in press*, the light atom transfer problem is treated without assuming approximately equal slopes.

[24] The LEPS surface used has the asymptotic parameters of the ClHBr system. It is, however, not intended to accurately mimic the real ClHBr potential energy surface. (The barrier height of 11 kcal/mol[13] for this LEPS surface is too high. In particular the collinear activation energy obtained from Fig. 2.2 is about 7 kcal/mol whereas the experimental 3-dimensional activation energy is about 1 kcal/mol. E.g., see C.-C. Mei and C. B. Moore, J. Chem. Phys. **67**, 3936 (1977), and R. Rubin and A. Persky, J. Chem. Phys. **79**, 4310 (1983).) The principal interest of this paper is in making comparisons for a given model surface with a substantial activation energy, and not in obtaining accurate reaction probabilities for the actual ClHBr system.

[25] D. G. Truhlar and B. C. Garrett, Annu. Rev. Phys. Chem. **35**, 159 (1984), and references cited therein.

[26] The zero-point vibrational energy of the HBr well is 3.83 kcal/mol and the classical barrier height is 11.0 kcal/mol.[13] Thus the energy above the zero-point energy at the effective reaction threshold is $\approx$ 7 kcal/mol, which is close to the activation energy of 7 kcal/mol for $P_{02}(T)$ in Fig. 2.2.

[27] V. K. Babamov and V. Lopez, J. Phys. Chem. **90**, 215 (1986). These authors point out that a recent treatment of a low barrier system[11] inadvertently overlooked the stated limitation of no potential energy wells for the energies of interest.

[28] It was stated incorrectly in Ref. 7 that Eq. (3.6) there should apply even for reactions having a barrier of only a few kcal/mol for which "the latter plot [meaning $V_{ii}(\rho)$] may have a well as a function of ρ, which leads to quasibound states or resonances in the strong interaction region." In the above quote the "latter plot" should have read "the lower $\epsilon_i(\rho)$". As shown in Ref. 9 it is the well in the lower adiabatic potential $\epsilon_i(\rho)$ that is responsible for the resonances. Eq. (A1) applies when there are such wells but not Eq. (6).

[29] Thereby, in order that the V_{ii}'s be approximated legitimately by straight

lines as in Ref. 5, the α in Eq. (7) should not be too small. In applications with realistic surfaces we expect that the slope $-dV_{12}/d\rho$ will be large enough for approximation (2) to be valid.

[30] The discrepancy in Fig. 2.3 between $P_{02}^{B}(E)$ and $P_{02}(E)$ for $E > 12$ kcal/mol can be understood in terms of the breakdown of approximation (2) at those high energies when the "analytical fit" given by Eq. (10) is used there: The resulting α tends to zero in that case, causing the exponential in Eq. (6) to be abnormally small and the frequency of the oscillations in the sinusoidal term to be too large. In contrast, the original V_{12} [Fig. 8 of Ref. 5] is not a constant at ρ_0 (and hence $\alpha \neq 0$) when $E \sim 12$ kcal/mol.

[31] The two alternative expressions are obtained by an average over the exponential quantity in Eqs. (6) and (A1) respectively. This averaging procedure is defined in Eqs. (3.5) to (3.8) of Ref. 7.

Table 2.1: Crothers-Stückelberg σ as a Function of Energy.

E^a (kcal/mol)	σ
7.0	0.22
7.5	0.24
8.0	0.26
8.5	0.29
9.0	0.33
9.5	0.39
10.0	0.50
10.5	0.72
11.0	1.25
11.5	2.10
12.0	2.95
12.5	3.70
13.0	4.39
13.5	4.99

[a] Total energy measured relative to the minimum of the HBR potential.

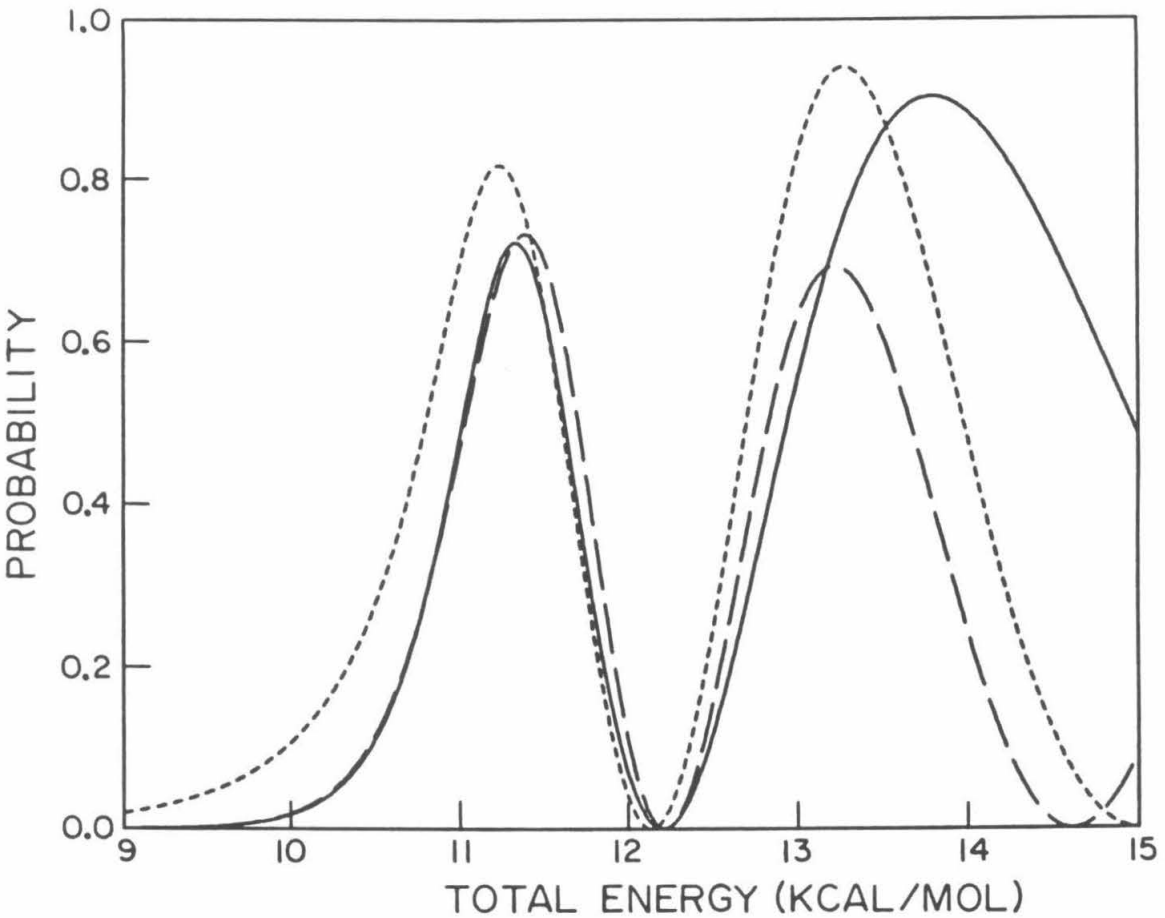

FIG. 2.1. The probabilities P_{02} as a function of the total energy E measured relative to the minimum of the HBr potential. The translational energy is 3.83 kcal/mol (i.e., the zero-point energy of the HBr well) less than E. $P_{02}(E)$ is the two-state numerical reactive transition probability and is denoted by —— . $P_{02}^{B}(E)$ is the reactive transition probability of Babamov *et al.*, calculated from Eq. (6), and is denoted by — — . $P_{02}^{CS}(E)$ is the reaction transition probability calculated from the CS expression, Eqs. (8) and (9), and is denoted by - - - .

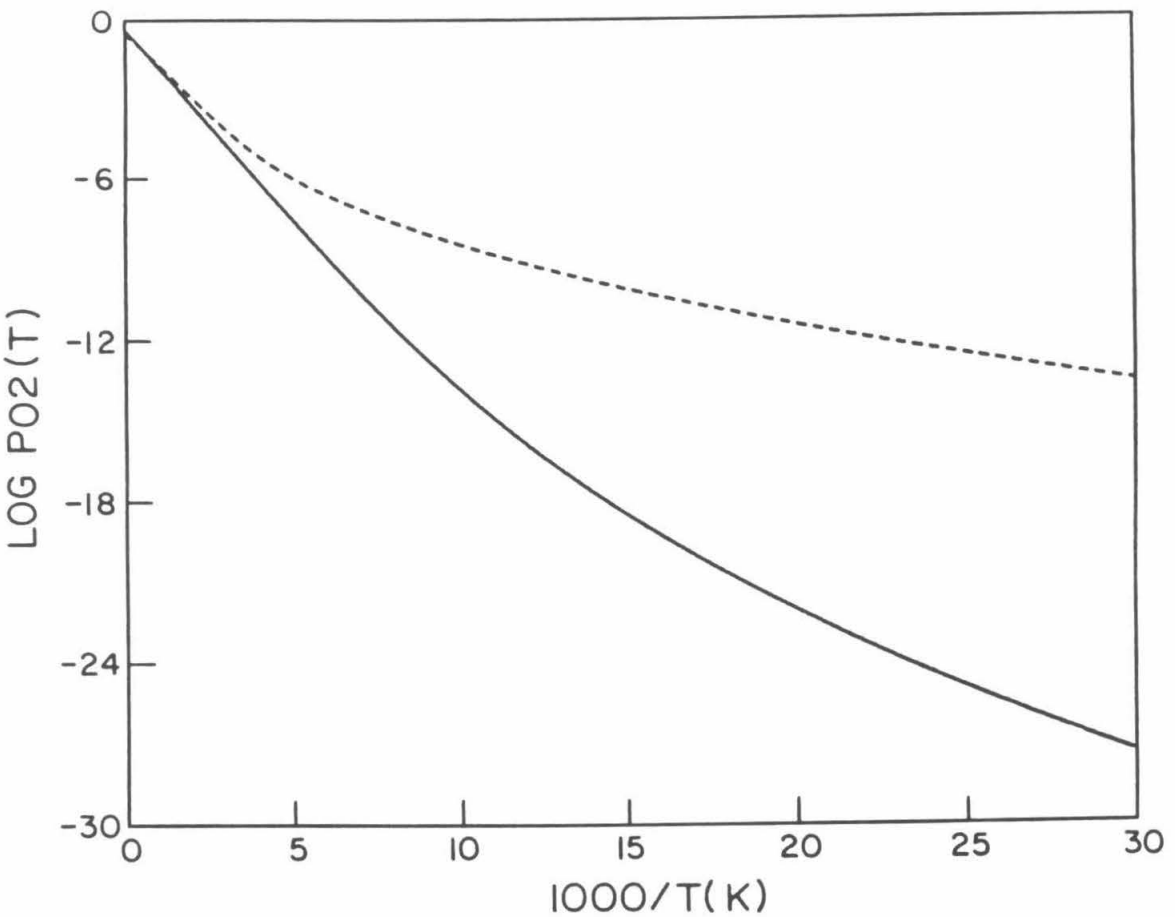

FIG. 2.2. Log_{10} of the probabilities P_{02} as a function of $1/T$ ($^\circ K$). $P_{02}(T)$ is the Boltzmann-averaged numerical transition probability and is denoted by — – . $P_{02}^{B}(T)$, the Boltzmann-averaged transition probability from the method of Babamov *et al.*, is denoted by — — (This plot is not visible since it coincides with that of $P_{02}(T)$). $P_{02}^{\text{CS}}(T)$, the Boltzmann-averaged transition probability from the CS method, is denoted by - - - .

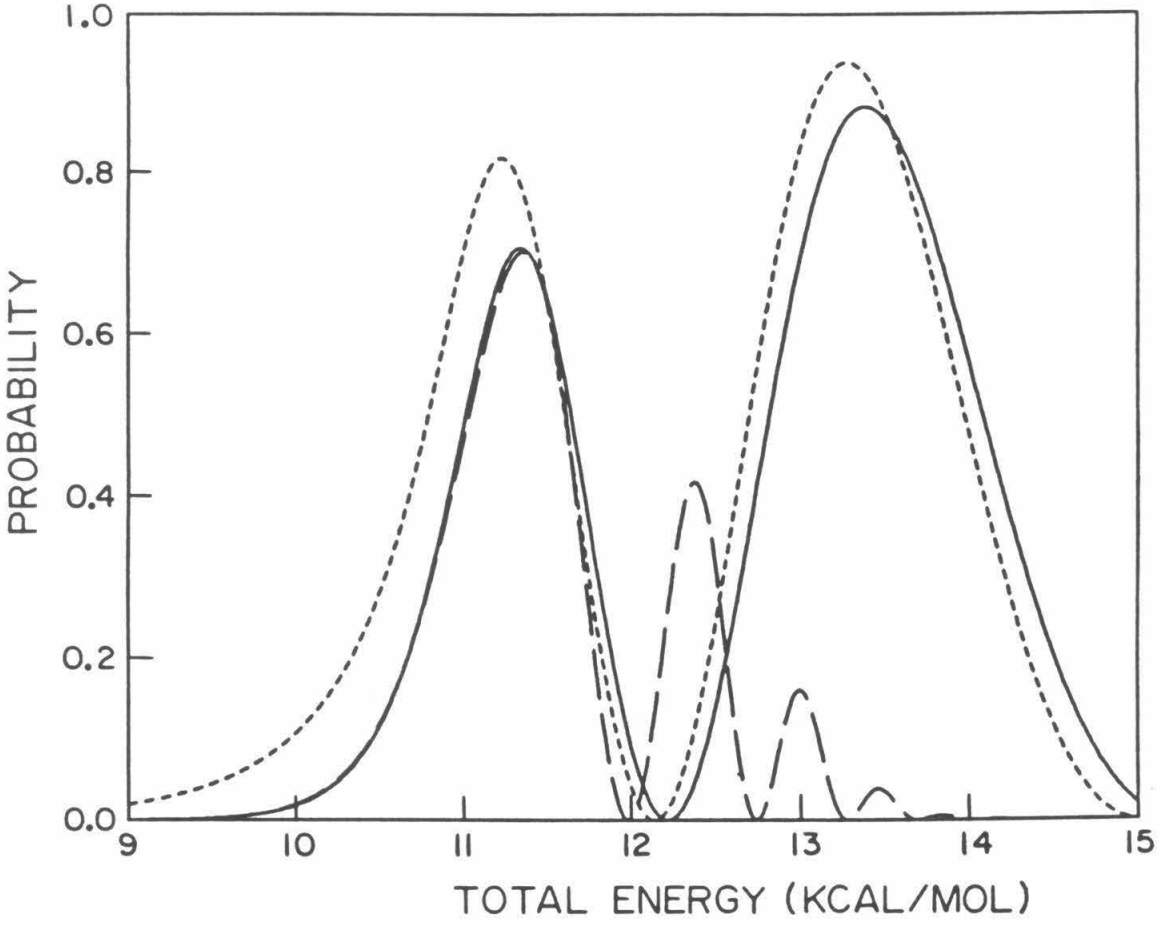

FIG. 2.3. The probabilities P_{02}, as a function of the total energy measured relative to the minimum of the HBr potential, obtained using model analytical diabatic potentials for all the calculations. The potential parameters used, as defined in Eq. (10), were $A = 6.880$ kcal/mol, $G = 1.062$ kcal/(mol bohr), $\rho_c = 31.75$ bohr, $\Delta_0 = 0.4162$ kcal/mol, $B = 0.9269$ mol/kcal, $C = 4.228$ mol/kcal, and $\beta = 2.052$ bohr^{-1}. $P_{02}(E)$ is denoted by —— , $P_{02}^{B}(E)$ by — — and $P_{02}^{CS}(E)$ by - - - . The discrepancy between the solid and long-dashed lines for $E > 12$ kcal/mol is discussed in the text.

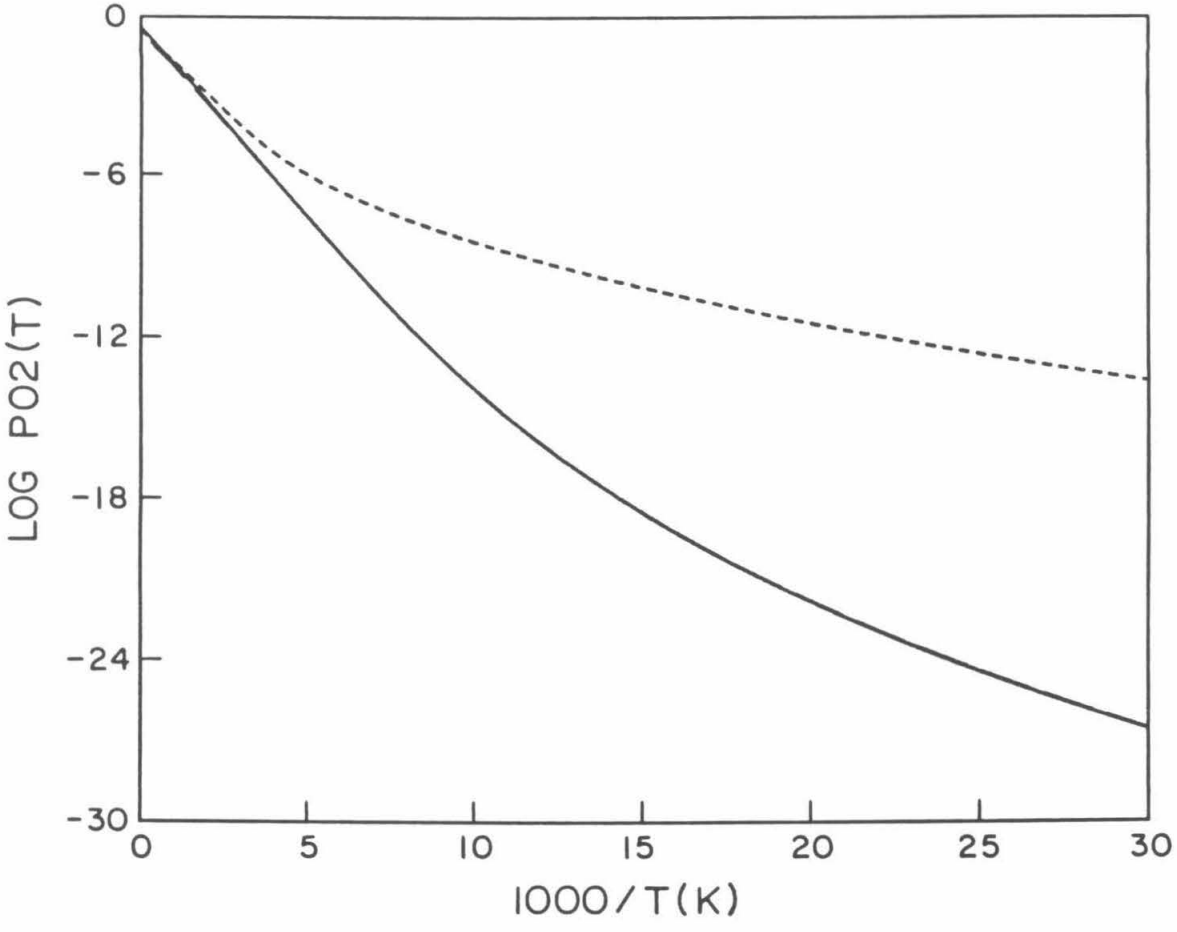

FIG. 2.4. Log_{10} of the probabilities P_{02} as a function of $1/T$ ($^{\circ}K$) for which model analytical diabatic potentials are used for all the calculations. The potential parameters used were as in Fig. 2.3. $P_{02}(T)$ is denoted by —— . $P_{02}^{B}(T)$ is denoted by — — (This plot is not visible since it coincides with that of $P_{02}(T)$). $P_{02}^{CS}(T)$ is denoted by - - - .

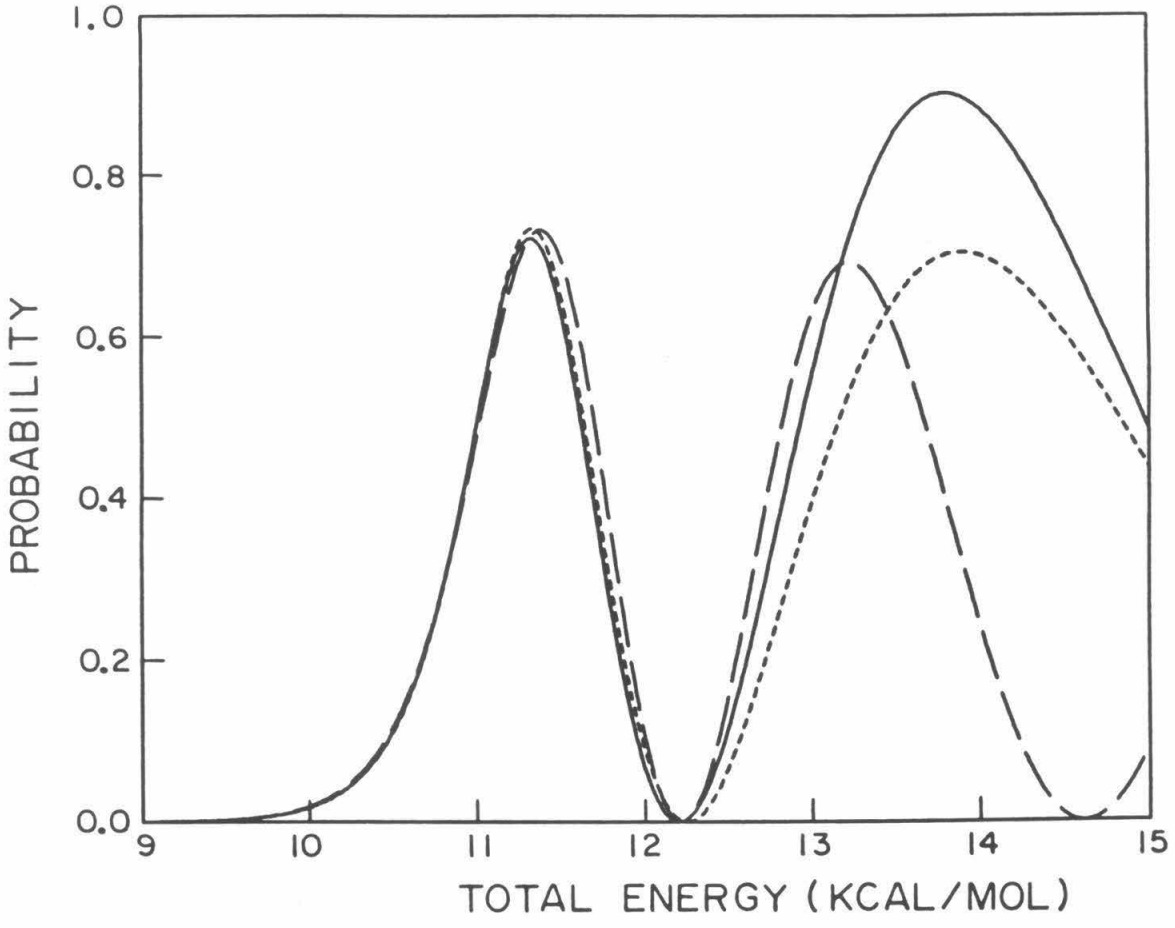

FIG. 2.5. The probabilities P_{02} as a function of the total energy measured relative to the minimum of the HBr potential. $P_{02}(E)$ is denoted by —— , $P_{02}^{B}(E)$ by — — and $P_{02}^{B'}(E)$ by - - - .

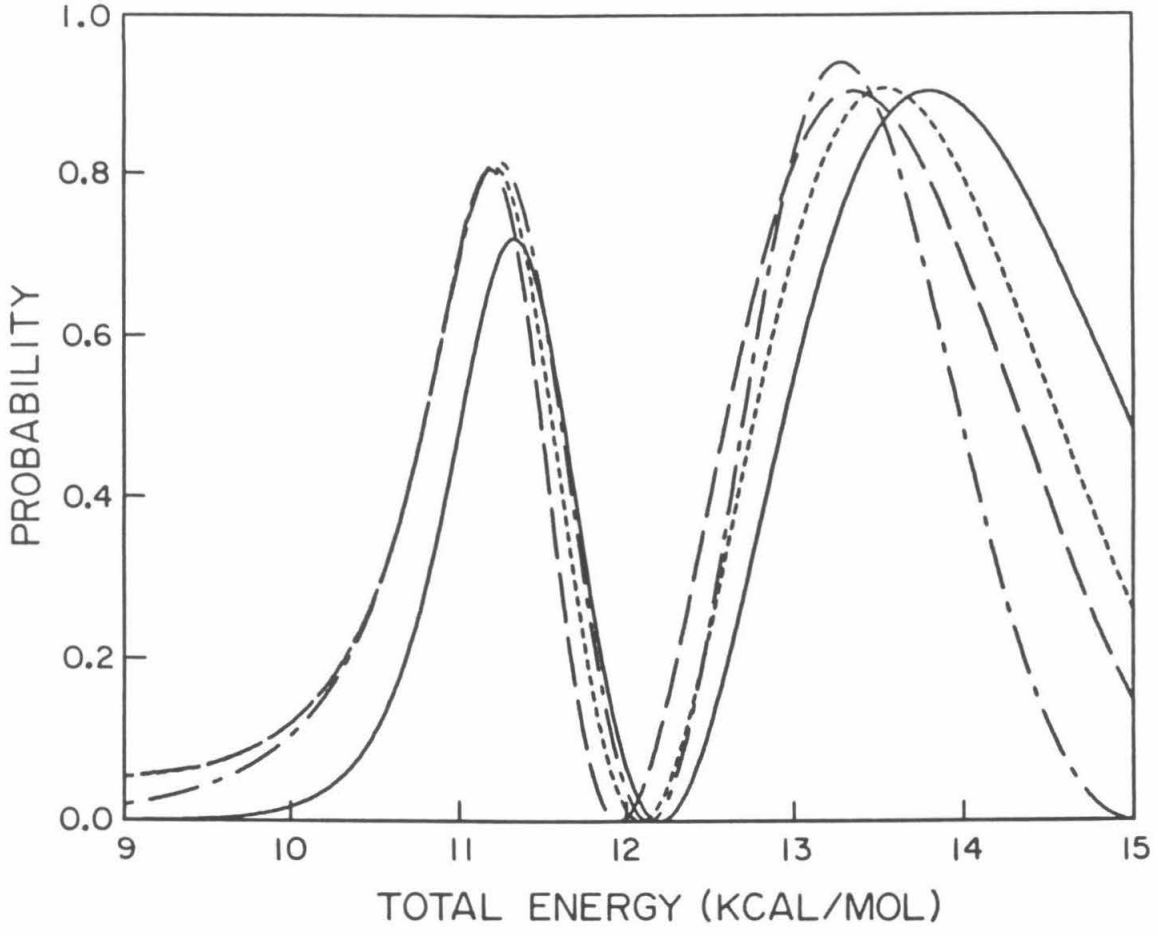

FIG. 2.6. The probabilities P_{02} as a function of the total energy measured relative to the minimum of the HBr potential. $P_{02}(E)$ is denoted by ——, $P_{02}^{CS}(E)$ by — - —, $P_{02}^{CS'}(E)$ by — — and $P_{02}^{CS''}(E)$ by - - - .

Chapter 3: Iteratively Determined Effective Hamiltonians for the Adiabatically Reduced Coupled Equations Approach to Intramolecular Dynamics Calculations

[The text of this chapter appeared in: S. J. Klippenstein, G. A. Voth, and R. A. Marcus, J. Chem. Phys. **85**, 5019 (1986).]

ABSTRACT

An iterative procedure is proposed for determining increasingly accurate effective Hamiltonians for use in the adiabatically reduced coupled equations approach to intramolecular dynamics calculations [J. Chem. Phys. **84**, 2254 (1986)]. The relationships between this iterative determination of the effective Hamiltonian, which is based on an adiabatic approximation, and some other partitioning methods for determining an effective Hamiltonian are discussed. The present iterative procedure provides accurate agreement with the exact dynamics for the two specific model systems studied.

I. INTRODUCTION

In recent years, there has been considerable theoretical and experimental interest in the quantum dynamics of initially prepared nonstationary states in isolated polyatomic molecules. More specifically, the time-evolution of initially prepared states resulting from vibronic,[1] vibrational,[2] and rovibrational[3] coupling mechanisms is of particular interest. The "exact" treatment of the dynamics of these states requires, in typical situations, the numerical diagonalization of a Hamiltonian matrix having a very large number of basis states. Since there are, at present, computational limitations on the size of matrices which can be diagonalized, methods which reduce the size of the Hamiltonian matrix to be diagonalized, or, alternatively, new methods for determining the quantum dynamics,[4] must be developed.

By virtue of clever numerical methods, several authors have been able to increase the number of basis states which may be included in a typical calculation. For example, Nauts and Wyatt[5] have developed the recursive residue generation method (RRGM) to determine the relevant time-dependent transition amplitudes directly without requiring the diagonalization of the Hamiltonian matrix. Moreover, Tietz and Chu,[6] as well as Chang and Wyatt,[7] have implemented artificial intelligence algorithms in their studies of multiphoton excitation of molecules which allowed them to consider a large number of basis states and then to include in their dynamical calculations only those states which had the largest effect on the dynamics. These methods represent potentially quite powerful numerical approaches for obtaining the dynamics of nonstationary states.

Recently, Voth and Marcus[8] have developed an approximate dynamical approach which is based on a partitioning[8,9] of the basis set into a subset of states which are resonant and/or strongly interacting with the initial state, and a subset of states containing the remaining off-resonant/weakly coupled states.[8] Their approach then treats the off-resonant/weakly coupled states in an effective manner by virtue of an adiabatic approximation. This latter method also allows one

to determine the dynamics directly by integrating the effective coupled equations and hence does not rely on a calculation (and computer storage) of the eigenvalues and eigenvectors of the system.

In this article, an iterative scheme is applied to the adiabatically reduced coupled equations approach of Voth and Marcus[8]. With each iterative step, new effective coupled equations for the resonant/strongly coupled subspace are obtained, and hence a new effective Hamiltonian is derived. If the initial adiabatic approximation is a good one (cf. discussion in Ref. 8), the resulting dynamics calculated from the effective coupled equations exhibit accurate agreement with the exact dynamics.

The derivation of the reduced coupled equations is reviewed in Sec. II, and the iterative scheme is presented there. In Sec. III the present time-dependent method for determining the effective coupled equations is shown to be related to the iterative solution of an equation for the effective interaction in nuclei derived from a time-independent viewpoint by Schucan and Weidenmüller[10]. The relationship of the present effective Hamiltonian to that given by Lee and Suzuki[11] and to the partitioning formalism of Löwdin[12] is also discussed in Sec. III. An application of the effective coupled equations to two model problems is given in Sec. IV, and the results are discussed in Sec. V. Concluding remarks appear in Sec. VI.

II. THEORY

A. Coupled Equations

The time-dependent wavefunction (in atomic units) is expanded as[8,13]

$$|\Psi(t)\rangle = \exp\left(-i\,\langle H\rangle\, t\right) \sum_{i=1}^{N} b_i(t)\,|\varphi_i\rangle \ , \tag{1}$$

where the basis states $|\varphi_i\rangle$ are eigenfunctions of a suitably chosen zeroth-order Hamiltonian H_0 , and $\langle H\rangle$ is the expectation value of the total Hamiltonian $H(= H_0 + V)$, defined as $\langle H\rangle = \langle\Psi(t)|H|\Psi(t)\rangle$. By substituting this expansion

for $|\Psi(t)\rangle$ into the time-dependent Schrödinger equation and using the orthonormal properties of the $\{|\varphi_i\rangle\}$ basis, the following coupled first-order differential equations for the amplitudes $b_i(t)$ are obtained:

$$\frac{db_j(t)}{dt} = i\,\langle H\rangle\, b_j(t) - i\sum_{i=1}^{N} H_{ji} b_i(t)\ , \tag{2}$$

where $H_{ji} = \langle\varphi_j\,|H|\,\varphi_i\rangle$.

The zeroth-order basis is now partitioned into a subset of states which are nearly resonant with and/or strongly coupled to the initial state and another subset containing all remaining off-resonant/weakly coupled states. The coupled equations may then be written in vector-matrix notation as[8]

$$\frac{d}{dt}\mathbf{b}^R(t) = i\left(\langle H\rangle\,\mathbf{1}^R - \mathbf{H}^R\right)\mathbf{b}^R(t) - i\mathbf{V}^{RO}\mathbf{b}^O(t) \tag{3}$$

$$\frac{d}{dt}\mathbf{b}^O(t) = i\left(\langle H\rangle\,\mathbf{1}^O - \mathbf{H}^O\right)\mathbf{b}^O(t) - i\mathbf{V}^{OR}\mathbf{b}^R(t)\ . \tag{4}$$

By denoting the dimension of the resonant/strongly coupled subspace by N_R and the off-resonant/weakly coupled subspace by N_O, the quantities in Eqs. (3) and (4) are defined as follows: $\mathbf{b}^R(t)$ $[\mathbf{b}^O(t)]$ is an N_R (N_O)-dimensional column vector containing the amplitudes for the resonant (off-resonant) states, $\mathbf{1}^R$ $(\mathbf{1}^O)$ is the $N_R \times N_R (N_O \times N_O)$ identity matrix, $\mathbf{H}^R$ $(\mathbf{H}^O)$ is the $N_R \times N_R$ $(N_O \times N_O)$ Hamiltonian sub-matrix for the resonant (off-resonant) states, and $\mathbf{V}^{RO}$ $(\mathbf{V}^{OR})$ is the $N_R \times N_O$ $(N_O \times N_R)$ coupling matrix between the two subspaces.

B. Iterative Scheme for the Effective Coupled Equations

The adiabatic approximation given in Ref. 8 was based on the physical property that the off-resonant amplitudes $\mathbf{b}^O(t)$ will remain negligibly small during the time evolution, and hence the derivatives $d\mathbf{b}^O(t)/dt$ in Eq. (4) are effectively equal to zero. The validity of this approximation depends on the partitioning scheme, and the reader is referred to Ref. 8 for further details in that regard. With the approximation of $d\mathbf{b}^O(t)/dt \simeq 0$, which hereafter will be termed the

"zeroth-order" approximation, effective coupled equations for calculating the dynamics of the resonant amplitudes may be derived.[8] It will be shown here how increasingly accurate higher-order effective coupled equations can be derived iteratively by obtaining improved approximations for the off-resonant derivatives in Eq. (4).

Equation (3) can be rewritten in the form

$$\mathbf{V}^{RO}\mathbf{b}^{O}(t) = i\frac{d}{dt}\mathbf{b}^{R}(t) + \left(\langle H\rangle\,\mathbf{1}^{R} - \mathbf{H}^{R}\right)\mathbf{b}^{R}(t), \tag{5}$$

and Eq. (4) can also be rearranged to give

$$\mathbf{b}^{O}(t) = -i\left(\langle H\rangle\,\mathbf{1}^{O} - \mathbf{H}^{O}\right)^{-1}\frac{d}{dt}\mathbf{b}^{O}(t) + \left(\langle H\rangle\,\mathbf{1}^{O} - \mathbf{H}^{O}\right)^{-1}\mathbf{V}^{OR}\mathbf{b}^{R}(t). \tag{6}$$

As mentioned before, the zeroth-order adiabatic approximation used in Ref. 8 was

$$\frac{d}{dt}\mathbf{b}^{O}(t) \simeq 0, \tag{7}$$

which, when substituted into Eq. (6), yields

$$\mathbf{b}^{O}(t) \simeq \left(\langle H\rangle\,\mathbf{1}^{O} - \mathbf{H}^{O}\right)^{-1}\mathbf{V}^{OR}\mathbf{b}^{R}(t). \tag{8}$$

Substitution of this expression for $\mathbf{b}^{O}(t)$ into Eq. (3) gives

$$\frac{d}{dt}\mathbf{b}^{R}(t) \simeq -i\mathbf{H}^{R}_{eff,0}\mathbf{b}^{R}(t), \tag{9}$$

where the zeroth-order effective Hamiltonian is given by

$$\mathbf{H}^{R}_{eff,0} = \mathbf{H}^{R} - \langle H\rangle\,\mathbf{1}^{R} + \mathbf{V}^{RO}\left(\langle H\rangle\,\mathbf{1}^{O} - \mathbf{H}^{O}\right)^{-1}\mathbf{V}^{OR}\ . \tag{10}$$

An iterative formula for the general n'th-order effective Hamiltonian, $\mathbf{H}^{R}_{eff,n}$, may be derived as shown below, for which the corresponding coupled equations are given by

$$\frac{d}{dt}\mathbf{b}^{R}(t) \simeq -i\mathbf{H}^{R}_{eff,n}\mathbf{b}^{R}(t), \tag{11}$$

where

$$\mathbf{H}^R_{eff,n} = \left[\mathbf{1}^R + \mathbf{F}^{-1}\left(\mathbf{H}^R_{eff,n-1} + \langle H\rangle\,\mathbf{1}^R - \mathbf{H}^R\right)\right]^{-1}\mathbf{H}^R_{eff,0} \quad , \tag{12}$$

and

$$\mathbf{F}^{-1} = \mathbf{V}^{RO}\left(\langle H\rangle\,\mathbf{1}^O - \mathbf{H}^O\right)^{-1}\left(\mathbf{V}^{RO}\right)^{-1}. \tag{13}$$

Equations (11) - (13) constitute the central result of the present paper.

To derive Eqs. (11) - (13), Eq. (5) is first rewritten as

$$\mathbf{b}^O(t) \;\simeq\; \left(\mathbf{V}^{RO}\right)^{-1}\left(\mathbf{H}^R_{eff,n-1} + \langle H\rangle\,\mathbf{1}^R - \mathbf{H}^R\right)\mathbf{b}^R(t), \tag{14}$$

where $\left(\mathbf{V}^{RO}\right)^{-1}$ is a "left" inverse, and $id\mathbf{b}^R(t)/dt$ in Eq. (5) has been taken to be equal to $\mathbf{H}^R_{eff,n-1}\mathbf{b}^R(t)$ (i.e., it is taken from the previous iteration). For example, the first-order approximation to $\mathbf{b}^O(t)$ is obtained by replacing $id\mathbf{b}^R(t)/dt$ in Eq. (5) by $\mathbf{H}^R_{eff,0}\mathbf{b}^R(t)$. By taking the derivative of Eq. (14) and then substituting the resulting expression for $d\mathbf{b}^O(t)/dt$ into Eq. (6), an approximation for $\mathbf{b}^O(t)$ is obtained, namely

$$\begin{aligned}\mathbf{b}^O(t) \simeq -i\left(\langle H\rangle\,\mathbf{1}^O - \mathbf{H}^O\right)^{-1}\left(\mathbf{V}^{RO}\right)^{-1}\left(\mathbf{H}^R_{eff,n-1} + \langle H\rangle\,\mathbf{1}^R - \mathbf{H}^R\right)\frac{d}{dt}\mathbf{b}^R(t) \\ + \left(\langle H\rangle\,\mathbf{1}^O - \mathbf{H}^O\right)^{-1}\mathbf{V}^{OR}\mathbf{b}^R(t).\end{aligned} \tag{15}$$

Substitution of Eq. (15) for the off-resonant amplitudes into Eq. (3) and collecting the terms for $d\mathbf{b}^R(t)/dt$ yields the n'th-order effective coupled equations given by Eqs. (11) - (13).

The present iterative procedure can be repeated *ad infinitum* to give, in principle, better and better approximations to the off-resonant amplitudes and hence to give more and more accurate effective coupled equations. However, the accuracy of the coupled equations determined from this procedure depends crucially on how good the initial choice for the time derivatives of the off-resonant states is. (This choice was zero in the present case.[8]) When the initial approximation for those derivatives is not a sufficiently accurate one, the iterative

procedure may give qualitatively incorrect results for the dynamics. From the nature of the iterative formula, it is clear that the convergence properties depend very much on the "magnitude" of $\mathbf{V}^{RO}$ (or $\mathbf{V}^{OR}$) relative to the "magnitude" of $(\langle H \rangle \mathbf{1}^O - \mathbf{H}^O)$.[8]

The following notation is introduced here to simplify the expressions for the effective Hamiltonians:

$$\begin{aligned} \mathbf{V}_0 &= \mathbf{H}^R_{eff,0} \\ \mathbf{V}_i &= \mathbf{V}^{RO} \left(\langle H \rangle \mathbf{1}^O - \mathbf{H}^O \right)^{-(i+1)} \mathbf{V}^{OR}, \quad i \geq 1. \end{aligned} \tag{16}$$

For example, the first-order effective Hamiltonian is now given by

$$\begin{aligned} \mathbf{H}^R_{eff,1} &= \left[\mathbf{1}^R + \mathbf{V}^{RO} \left(\langle H \rangle \mathbf{1}^O - \mathbf{H}^O \right)^{-2} \mathbf{V}^{OR} \right]^{-1} \mathbf{H}^R_{eff,0} \\ &= \left(\mathbf{1}^R + \mathbf{V}_1 \right)^{-1} \mathbf{V}_0, \end{aligned} \tag{17}$$

and the second-order effective Hamiltonian by

$$\mathbf{H}^R_{eff,2} = \left[\mathbf{1}^R + \mathbf{V}_1 - \mathbf{V}_2 \left(\mathbf{1}^R + \mathbf{V}_1 \right)^{-1} \mathbf{V}_0 \right]^{-1} \mathbf{V}_0 \, . \tag{18}$$

C. Expansions of the Effective Hamiltonian

The effective Hamiltonian determined from the present iterative procedure may be expanded in various ways. For example, due to computational limitations, it may not always be desirable to invert the matrix $\left(\langle H \rangle \mathbf{1}^O - \mathbf{H}^O \right)$ present in $\mathbf{V}_i$ [Eq. (16)]. In that case, the following expansion could prove useful (e.g., Ref. 12, with $\langle H \rangle$ replaced by an energy eigenvalue E):

$$\left(\langle H \rangle \mathbf{1}^O - \mathbf{H}^O \right)^{-1} = \left(\langle H \rangle \mathbf{1}^O - \mathbf{E}^O \right)^{-1} \sum_{n=0}^{\infty} \left[\mathbf{V}^O \left(\langle H \rangle \mathbf{1}^O - \mathbf{E}^O \right)^{-1} \right]^n , \tag{19}$$

where the matrix $\mathbf{H}^O$ has been separated into $\mathbf{E}^O + \mathbf{V}^O$, with $\mathbf{E}^O$ containing the diagonal elements of $\mathbf{H}^O$ and $\mathbf{V}^O$ containing the off-diagonal elements of $\mathbf{H}^O$. Since the matrix $\left(\langle H \rangle \mathbf{1}^O - \mathbf{E}^O \right)$ is a diagonal matrix and thereby trivial to invert, each of the terms in the expansion may be straightforwardly evaluated.

Another expansion which may prove useful is a series expansion in powers of $\mathbf{V}_i$ [cf. Eq. (16), and see, e.g., Ref. 10]. For example, the series expansion of $\mathbf{H}^R_{eff,2}$ in powers of $\mathbf{V}_i$ is given by

$$\mathbf{H}^R_{eff,2} = \sum_{m=0}^{\infty} \left[\mathbf{V}_2 \sum_{n=0}^{\infty} (-\mathbf{V}_1)^n \mathbf{V}_0 - \mathbf{V}_1 \right]^m \mathbf{V}_0, \tag{20}$$

With the further definition of

$$\mathbf{V}'_i = \left[\mathbf{1}^R + \mathbf{V}_1 \right]^{-1} \mathbf{V}_i, \qquad i \geq 0, \tag{21}$$

the second order effective Hamiltonian may be rewritten as

$$\mathbf{H}^R_{eff,2} = \left(\mathbf{1}^R - \mathbf{V}'_2 \mathbf{V}'_0 \right)^{-1} \mathbf{V}'_0. \tag{22}$$

A final series expansion which may prove useful is one in powers of $\mathbf{V}'_i$ [see, e.g., Ref. 10], which for $\mathbf{H}^R_{eff,2}$ is given by

$$\mathbf{H}^R_{eff,2} = \sum_{n=0}^{\infty} (\mathbf{V}'_2 \mathbf{V}'_0)^n \mathbf{V}'_0. \tag{23}$$

III. RELATIONSHIP TO OTHER PARTITIONING TECHNIQUES

The relationship between the present time-dependent method for determining the effective coupled equations, and hence the effective Hamiltonian, and some time-independent methods[10–12,14–16] for determining eigenvalues using effective Hamiltonians is discussed next. For the purpose of comparison, the preceeding dynamical analysis of Sec. II B may be viewed as a complementary way of determining an effective Hamiltonian, although the focus of the present paper is towards a determination of the dynamics rather than the eigenvalues.

Several authors (e.g., Refs. 10, 11, 14-16) have used partitioning techniques to construct an effective interaction Hamiltonian for the determination of a subset of energy levels in nuclei. A summary of the work in this field is given in Ref.

16. One frequently used formula for determining the effective interactions is the Des Cloiseaux and Brandow expansion,[14,15] given in the present notation[17] by

$$\mathbf{H}^R_{eff} = \mathbf{H}^R - \lambda \mathbf{1}^R + \sum_{n=0}^{\infty} \frac{d^n}{(dE)^n} \mathbf{V}^{RO} \left(E\mathbf{1}^O - \mathbf{H}^O\right)^{-1} \mathbf{V}^{OR} \Big|_{E=\lambda} \frac{1}{n!} \left(\mathbf{H}^R_{eff}\right)^n . \quad (24)$$

In this equation, the quantity λ is taken to be a general parameter which should, in principle, be chosen to give the best agreement between the eigenvalues of the effective Hamiltonian and the corresponding eigenvalues of the exact Hamiltonian. For a non-degenerate resonant subspace, deciding upon the appropriate choice of λ is non-trivial.[17] Following our analysis in Ref. 8, we make the choice $\lambda = \langle H \rangle$, since it gave the most accurate effective coupled equations for calculating the resonant state *dynamics*. The relationship of the effective Hamiltonians determined by the present iterative scheme to those determined by previous authors[10–12,14–16] can also be shown, noting that we have replaced their λ by our $\langle H \rangle$.

Schucan and Weidenmüller[10] (SW) have considered the application of partitioning techniques to the determination of energy levels in nuclei. SW derived the following equation for the effective interaction:[17]

$$\mathbf{H}^R_{eff} = \left[\mathbf{1}^R + \mathbf{F}^{-1} \left(\mathbf{H}^R_{eff} + \lambda \mathbf{1}^R - \mathbf{H}^R\right)\right]^{-1} \mathbf{V}_0, \quad (25)$$

where this $\mathbf{F}^{-1}$ denotes $\mathbf{V}^{RO} \left(\lambda \mathbf{1}^O - \mathbf{H}^O\right)^{-1} \left(\mathbf{V}^{RO}\right)^{-1}$, and $\mathbf{V}_0$ is given in terms of λ by $\mathbf{H}^R - \lambda \mathbf{1}^R + \mathbf{V}^{RO} \left(\lambda \mathbf{1}^O - \mathbf{H}^O\right)^{-1} \mathbf{V}^{OR}$. This equation is equivalent[10] to the implicit equation for $\mathbf{H}^R_{eff}$ given by the Des Cloiseaux and Brandow expansion [Eq. (24)]. Comparison of Eq. (25) above for the SW effective interaction with Eq. (12) for the present n'th-order effective Hamiltonian shows that $\mathbf{H}^R_{eff,n}$ is just the n'th iterative solution to Eq. (25), with the *specific* choice of $\lambda = \langle H \rangle$. SW discuss solving Eq. (25) iteratively, and, by making expansions in powers of $\mathbf{V}_i$'s or $\mathbf{V}'_i$'s, they derive series expansions for the effective Hamiltonian which are similarly related to n'th order forms of Eqs. (20) and (23) by making the choice $\lambda = \langle H \rangle$. Discussions of the convergence properties of the eigenvalues of

the unexpanded and various expanded forms of the effective Hamiltonians are given in Refs. 10, 11, and 14-16, for example.

Recently, Lee and Suzuki[11] have derived an iterative formula for an effective Hamiltonian $\mathbf{H}_n$ for use in obtaining the eigenvalues in the case of a degenerate subspace. This formula, generalized to the case of a non-degenerate subspace,[16,17] is given in the present notation [Eq. (16)] by

$$\mathbf{H}_0 = \mathbf{V}_0$$

$$\mathbf{H}_n = \left[\mathbf{1}^R + \mathbf{V}_1 - \sum_{m=2}^{n} (-)^m \mathbf{V}_m \prod_{k=n-m+2}^{n} \mathbf{H}_{k-1} \right]^{-1} \mathbf{V}_0, \quad n \geq 1 \qquad (26)$$

with $\mathbf{V}_0$ given as in the expression following Eq. (25) and with the $\mathbf{V}_i$'s for $i > 0$ given by Eq. (16) and having the $\langle H \rangle$ replaced by λ. In Appendix A, it is shown that the present $\mathbf{H}^R_{eff,n}$ is equivalent to the n'th-order effective Hamiltonian $\mathbf{H}_n$ of Lee and Suzuki[11], given by Eq. (26), once the specific choice of $\lambda = \langle H \rangle$ is made.

The eigenvalues obtained from the present iterative scheme for the effective Hamiltonian are also related to the Newton-Raphson technique for determining the eigenvalues for the exact partitioned Hamiltonian of Löwdin.[12] The exact partitioned Hamiltonian is given in the present notation by[8]

$$\mathbf{H}^R_{exact} = \mathbf{H}^R + \mathbf{V}^{RO} \left(E\mathbf{1}^O - \mathbf{H}^O \right)^{-1} \mathbf{V}^{OR}, \qquad (27)$$

where the constant factor $-\langle H \rangle \mathbf{1}^R$ has been omitted. The eigenvalues are then determined by solving the secular equation

$$\det \left| \mathbf{H}^R_{exact} - E\mathbf{1}^R \right| = 0, \qquad (28)$$

which, due to the dependence of $\mathbf{H}^R_{exact}$ on E, may require the use of a root search technique such as the Newton-Raphson method.[12]

The relationship between the Newton-Raphson solution to the above secular equation and the present effective Hamiltonian method may be established in the

case of a one-dimensional resonant subspace. In this situation, the expression for the eigenvalue derived from the first-order effective Hamiltonian is identical with the expression derived from the first iteration of the the Newton-Raphson method with the initial guess for E of $\langle H \rangle$. However, the relationship between the higher-order effective Hamiltonians and further iterations of the Newton-Raphson method (as well as for resonant subspaces of dimension greater than one) requires further investigation.

The effective Hamiltonian method for determining eigenvalues is also related to various other formulations of degenerate or nearly degenerate perturbation theory. These relationships are not as relevant to the dynamical analysis of the present paper and will not be discussed here. Further discussions in that regard are given in Refs. 18 and 19.

IV. APPLICATIONS

In order to illustrate the possible applications of this technique and the accuracy of the effective coupled equations, two model systems are considered here. The zeroth-order energy levels and couplings for the first system studied are depicted schematically in Fig. 3.1. The four basis states for this system are separated into two resonant states $|\varphi_1\rangle$ and $|\varphi_2\rangle$ and two off-resonant states $|\varphi_3\rangle$ and $|\varphi_4\rangle$. The state $|\varphi_1\rangle$ is taken to be the initially prepared state. This effective two-level model has features in common with the energy transfer dynamics of the local mode states in a model of H_2O.[8,20] In the present model, the relevant matrix elements are given by $\mathbf{H}^R = E_1 \mathbf{1}^R$, $H^O_{ii} = E_1 + \Delta$, $H^O_{12} = H^O_{21} = V_2$, and $V^{RO}_{ij} = V^{OR}_{ij} = V_1 \delta_{ij}$.

By using the formulas for the zeroth- and first-order effective Hamiltonians given in Eqs. (10) and (17), the following analytic result for the time-dependent probability $P_1(t)$ of the initial zeroth-order state is obtained:

$$P_1(t) = \left| b_1^R(t) \right|^2 = \cos^2 (\Omega_i t/2), \qquad (i = 0,1) \tag{29}$$

where the zeroth- and first-order effective frequencies Ω_0 and Ω_1 are given, re-

spectively, by

$$\Omega_0 = \left| \frac{2V_1^2 V_2}{\Delta^2 - V_2^2} \right| , \tag{30}$$

$$\Omega_1 = \left| \frac{2\left(\Delta^2 - V_2^2\right)\left\{\left[\left(\Delta^2 - V_2^2\right)^2 + V_1^2\left(\Delta^2 + V_2^2\right)\right] V_1^2 V_2 - 2\Delta^2 V_1^4 V_2\right\}}{\left[\left(\Delta^2 - V_2^2\right)^2 + V_1^2\left(\Delta^2 + V_2^2\right)\right]^2 - 4\Delta^2 V_1^4 V_2^2} \right| . \tag{31}$$

An analogous analytical formula for the second-order effective frequency Ω_2 can be obtained from Eq. (18), although it is omitted here for brevity. The "exact" frequency,[21] which would appear instead of Ω_i in Eq. (29), is denoted below by Ω.

The time evolution of $P_1(t)$ is plotted in Fig. 3.2 for the exact, zeroth- and first-order coupled equations. The parameters used in making this plot were $V_1 = -43.9, V_2 = -50.6, \Delta = 337.7$ cm^{-1}. For these parameters, the values of Ω_0, Ω_1 and Ω_2 were calculated to be 1.7495, 1.6588 and 1.6614 cm^{-1}, respectively, while the result for Ω is 1.6613 cm^{-1}. In Fig. 3.3, the initial state probability $P_1(t)$ is plotted once again, but now for the exact, zeroth- and second-order coupled equations, and with the zeroth-order detuning Δ decreased to 150 cm^{-1}. In this case, the values of Ω_0, Ω_1 and Ω_2 were calculated to be 9.781, 7.056 and 7.481 cm^{-1}, respectively, while the result for Ω is 7.426 cm^{-1}. In Table 3.1, the resonant subspace eigenvalues for the above two sets of parameters, as calculated from the exact, zeroth-, first- and second-order effective Hamiltonians, are given.

The second model system considered consists of 55 basis states, with the resonant subspace having 10 states and the off-resonant subspace having 45 states. The initial state energy H_{11}^R was arbitrarily set equal to zero and all the other diagonal elements of $\mathbf{H}^R$ were chosen to have random values between ± 10 cm^{-1}. The diagonal elements of $\mathbf{H}^O$ were chosen randomly within the limits $-55 \leq H_{ii}^O \leq -10$ cm^{-1} and $10 \leq H_{ii}^O \leq 55$ cm^{-1}. The off-diagonal elements of $\mathbf{H}^R$, $\mathbf{H}^O$, and all the elements of $\mathbf{V}^{RO}$ and $\mathbf{V}^{OR}$ were chosen randomly to be between ± 2 cm^{-1}. These matrices were made to be Hermitean. The initial

state probability $P_1(t)$ as calculated by the exact, zeroth- and first-order coupled equations is plotted in Fig. 3.4 for this system. In Table 3.2, the eigenvalues for the resonant subspace, as calculated from the exact Hamiltonian, and the zeroth- and first-order effective Hamiltonians, are given.

The probabilities in Figs. 3.2-3.4 obtained by integration of the effective coupled equations are seen to remain somewhat above the peaks and valleys of the exact probability curves. It is perhaps desirable to have the effective probability curves follow the "average" of the exact curves. For this purpose, a correction factor f_R, derived in Appendix B, may be used. This factor takes into account the small fraction of probability remaining, on the average, in the off-resonant states (cf. Appendix B) and is given by

$$f_R = 1 - \frac{1}{N_R} \sum_{i=1}^{N_R} M_{ii} \quad , \tag{32}$$

where the matrix M is

$$\mathbf{M} \;=\; \mathbf{V}^{RO}(\langle H \rangle \, \mathbf{1}^{O} - \mathbf{H}^{O})^{-2} \mathbf{V}^{OR} \quad . \tag{33}$$

In Figs. 3.5 and 3.6, all the initial state probabilities from Figs. 3.3 and 3.4 are plotted, but the approximate ones are now multiplied by the overall correction factor f_R.

V. DISCUSSION

From the results shown in Figs. 3.2-3.6, it is clear that by using such higher-order effective Hamiltonians one can obtain more accurate approximations to the dynamics than by just using the zeroth-order one. In addition, the results shown in Fig. 3.3 indicate that, even in the case of an interaction with the off-resonant states, which is fairly large relative to the splitting between the resonant and off-resonant subspaces, the approximate resonant state dynamics obtained from a higher-order effective Hamiltonian may still be able to reproduce the most important trends in the dynamics. However, in each case it is also apparent that

the zeroth-order approximation gives a reasonably good description of the correct "average" behavior, apart from a shift in the oscillation frequency. As mentioned before, this situation is necessary for the higher-order effective coupled equations to be accurate. In addition, Figs. 3.5 and 3.6 indicate that the correction factor f_R [Eq. (32)] is indeed useful for obtaining better "average" dynamics.

An inspection of the results given in Table 3.1 shows that the eigenvalues in the effective two-level model become more accurate with succesive steps in the iteration procedure. From the results given in Table 3.2 for the second model system, one can again see that the eigenvalues which are obtained from the first-order effective Hamiltonian are more accurate than those obtained from the zeroth-order effective Hamiltonian, with the ones closest to the initial state energy $\langle H \rangle \left(= H_{11}^R = 0\right)$ being the most accurately determined. In addition, calculations for this and other model systems have shown that more accurate dynamics and eigenvalues may also be obtained by increasing the dimension of the resonant subspace relative to the dimension of the off-resonant subspace. This result illustrates the potential power of a combined partitioning and iterative formalism.

It is also noted here that although the zeroth-order effective Hamiltonian is Hermitean, since $\mathbf{H}$ is Hermitean, the n'th-order effective Hamiltonian is not in general Hermitean. If desired, this situation can be remedied in various ways. For example, a Hermitean effective Hamiltonian may by obtained by defining it to be $\left(\mathbf{H}_{eff,n}^R + \mathbf{H}_{eff,n}^{R\dagger}\right)/2$. This simple symmetrization of the effective Hamiltonian has been used in nuclear physics applications,[19] but was found in those applications and in the present dynamical calculations to have a negligible effect. Other alternatives in this regard include transformations which make the initial non-Hermitean effective Hamiltonian Hermitean.[14,15,19]

VI. CONCLUDING REMARKS

An iterative procedure for obtaining increasingly accurate effective coupled

equations has been presented in the present paper. This procedure extends the adiabatic approximation developed by Voth and Marcus[8] and is related to several effective Hamiltonian techniques[10–12,14–16,18,19] used predominantly in the nuclear physics literature. A general prescription for obtaining the effective coupled equations, and hence an effective Hamiltonian, has been formulated. This prescription may be used to calculate the dynamics of a subset of resonant/strongly coupled states (relative to the initially prepared state). The model calculations performed to test the accuracy of the iterative procedure indeed yielded very encouraging results.

The results presented in this paper suggest the following possibilities for use of the higher-order effective coupled equations in intramolecular dynamics calculations: (1) as a test for the usefulness/accuracy of the zeroth-order adiabatically reduced coupled equations approach,[8] (2) as a means for obtaining more accurate dynamics in any given application of the zeroth-order coupled equations, and (3) as a means to obtain the approximate intramolecular dynamics in a situation where, due to computational limitations, one cannot obtain convergence of the zeroth-order dynamics by simply increasing the dimension of the resonant subspace. It is planned to give specific applications of the present theory in later publications.

ACKNOWLEDGEMENTS

It is a pleasure to acknowledge support of this research by the National Science Foundation. SJK gratefully acknowledges the support of a Natural Sciences and Engineering Research Council of Canada Postgraduate Scholarship, 1984 - 1986.

APPENDIX A: EQUIVALENCE OF EQ. (12) TO EQ. (26).

It is given that $\mathbf{H}_0 = \mathbf{H}^R_{eff,0}$, and so using the method of induction, the equality of the two effective Hamiltonians $\mathbf{H}^R_{eff,n}$ and $\mathbf{H}_n$ [Eqs. (12) and (26), respectively] may be established by assuming that $\mathbf{H}^R_{eff,n} = \mathbf{H}_n$ and then showing that $\mathbf{H}^R_{eff,n+1} = \mathbf{H}_{n+1}$.

Equation (12), with n replaced by $n+1$ and setting $\mathbf{H}^R_{eff,n} = \mathbf{H}_n$, yields

$$\begin{aligned} \mathbf{H}^R_{eff,n+1} &= \left[\mathbf{1}^R + \mathbf{F}^{-1}\left(\mathbf{H}_n + \langle H\rangle \mathbf{1}^R - \mathbf{H}^R\right)\right]^{-1} \mathbf{F}^{-1}\mathbf{F}\mathbf{V}_0 \\ &= \left[\mathbf{F} + \mathbf{H}_n + \langle H\rangle \mathbf{1}^R - \mathbf{H}^R\right]^{-1} \mathbf{F}\mathbf{V}_0, \end{aligned} \tag{A1}$$

recalling Eq. (16) for $\mathbf{V}_0$. There is also the identity,

$$\begin{aligned} \mathbf{H}_n &= \mathbf{V}_0 - \left(\mathbf{V}_0\mathbf{H}_n^{-1} - \mathbf{1}^R\right)\mathbf{H}_n \\ &= \mathbf{V}_0 - \left[\left(\mathbf{H}_n\mathbf{V}_0^{-1}\right)^{-1} - \mathbf{1}^R\right]\mathbf{H}_n. \end{aligned} \tag{A2}$$

Introducing the expression for $\mathbf{H}_n$, given by Eq. (26), into the first $\mathbf{H}_n$ term on the right hand side of Eq. (A2) yields

$$\begin{aligned} \mathbf{H}_n &= \mathbf{V}_0 - \left[\mathbf{V}_1 - \sum_{m=2}^{n} (-)^m \mathbf{V}_m \prod_{k=n-m+2}^{n} \mathbf{H}_{k-1}\right]\mathbf{H}_n \\ &= \mathbf{V}_0 - \sum_{m=2}^{n+1} (-)^m \mathbf{V}_{m-1} \prod_{k=n-m+3}^{n+1} \mathbf{H}_{k-1}, \end{aligned} \tag{A3}$$

upon using Eq. (16). Substituting this expression for $\mathbf{H}_n$ into Eq. (A1) yields

$$\mathbf{H}^R_{eff,n+1} = \left[\mathbf{F} + \mathbf{V}_0 + \langle H\rangle \mathbf{1}^R - \mathbf{H}^R - \sum_{m=2}^{n+1} (-)^m \mathbf{V}_{m-1} \prod_{k=n-m+3}^{n+1} \mathbf{H}_{k-1}\right]^{-1} \mathbf{F}\mathbf{V}_0 \tag{A4}$$

Observing that

$$\mathbf{F}\mathbf{V}_1 = \mathbf{V}_0 + \langle H\rangle \mathbf{1}^R - \mathbf{H}^R \tag{A5}$$

and

$$\mathbf{F}\mathbf{V}_m = \mathbf{V}_{m-1}, \qquad (m \geq 2) \tag{A6}$$

one sees that Eq. (A4) may be rewritten as

$$\begin{aligned} \mathbf{H}^{R}_{eff,n+1} &= \left\{ \mathbf{F} \left[\mathbf{1}^{R} + \mathbf{V}_1 - \sum_{m=2}^{n+1} (-)^m \mathbf{V}_m \prod_{k=n-m+3}^{n+1} \mathbf{H}_{k-1} \right] \right\}^{-1} \mathbf{F}\mathbf{V}_0 \\ &= \mathbf{H}_{n+1} \mathbf{V}_0^{-1} \mathbf{F}^{-1} \mathbf{F} \mathbf{V}_0 \\ &= \mathbf{H}_{n+1}, \end{aligned} \tag{A7}$$

upon using a result for the product of inverses, and introducing Eq. (26) (for $n+1$ instead of n).

APPENDIX B: DERIVATION OF THE CORRECTION FACTOR f_R.

The total probability $\langle\Psi(t)|\Psi(t)\rangle$ of the quantum dynamical system satisfies the condition

$$P_R(t) + P_O(t) = 1 \quad , \tag{B1}$$

where $P_R(t)$ and $P_O(t)$ are the resonant and off-resonant basis state probabilities, respectively (cf. Sec. II A). The latter two quantities may be written in terms of the vectors containing the resonant and off-resonant state amplitudes as

$$P_R(t) = \mathbf{b}^{R\dagger}(t)\mathbf{b}^R(t) \quad \text{and} \quad P_O(t) = \mathbf{b}^{O\dagger}(t)\mathbf{b}^O(t) \quad , \tag{B2}$$

respectively. If the probabilities are now long-time-averaged, the average resonant state probability $\bar{P}_R$ is given from Eq. (B1) as

$$\bar{P}_R = 1 - \bar{P}_O \quad , \tag{B3}$$

where $\bar{P}_R$ and $\bar{P}_O$ are given by

$$\bar{P}_i = \lim_{\tau\to\infty} \frac{1}{\tau}\int_0^\tau P_i(t)dt \; , \quad (i = R, O) \; . \tag{B4}$$

By virtue of Eq. (B2) and the "zeroth-order" adiabatic approximation for the amplitudes $\mathbf{b}^O(t)$ [Eq. (8)], the long-time-averaged off-resonant state probability may be approximated as

$$\bar{P}_O \simeq \lim_{\tau\to\infty} \left[\frac{1}{\tau}\sum_{i=1}^{N_R} M_{ii}\int_0^\tau |b_i^R(t)|^2 dt + \frac{1}{\tau}\sum_{i=1}^{N_R}\sum_{j\neq i}^{N_R} M_{ij}\int_0^\tau b_i^{R*}(t)b_j^R(t)dt\right] \; , \tag{B5}$$

where the matrix $\mathbf{M}$ is given by Eq. (33) of the text, and N_R is the dimension of the resonant subspace (cf. Sec. II A). This expression could, in principle, be evaluated from an actual dynamical calculation of the vector $\mathbf{b}^R(t)$ using the effective coupled equations [Eqs. (11)-(13)].

It is desirable, however, to obtain simple approximations for the long-time-averages of $|b_i^R(t)|^2$ and $b_i^{R*}(t)b_j^R(t)$ and to thereby simplify Eq. (B5). To achieve this goal, the resonant state basis functions $|\varphi_i^R\rangle$ are assumed to be adequately described as a linear combination of the resonant state eigenfunctions $|\psi_n^R\rangle$, i.e., as

$$|\varphi_i^R\rangle \simeq \sum_{n=1}^{N_R} C_{in} |\psi_n^R\rangle \quad . \tag{B6}$$

It is assumed here that the contributions from the off-resonant basis functions $|\varphi_i^O\rangle$ to the resonant eigenfunctions $|\psi_n^R\rangle$ are small. With the further assumption of strong mixing among the resonant basis functions due to the perturbation and their near degeneracy, the magnitude of the expansion coefficients $|C_{in}|$ may be approximated by $1/\sqrt{N_R}$. By virtue of these latter two approximations and the fact that $b_i^R(t) = \langle\varphi_i^R|\Psi(t)\rangle$, the first term in Eq. (B5) becomes

$$\lim_{\tau\to\infty} \frac{1}{\tau} \sum_{i=1}^{N_R} M_{ii} \int_0^\tau |b_i^R(t)|^2 dt \simeq \frac{1}{N_R} \sum_{i=1}^{N_R} M_{ii} \quad . \tag{B7}$$

The second term in Eq. (B5) is assumed to be approximately equal to zero since each $b_i^{R*}(t)b_j^R(t)$ term, with $i \neq j$, is highly oscillatory. With the above approximations for the long-time-averages in Eq. (B5), the simple approximate formula for $\bar{P}_O$ is obtained:

$$\bar{P}_O \simeq \frac{1}{N_R} \sum_{i=1}^{N_R} M_{ii} \quad . \tag{B8}$$

If dynamics calculations are performed using the effective coupled equations [Eqs. (11)-(13)] and an initial state probability normalized to unity, the results of Eqs. (B3) and (B8) suggest that the calculated resonant state probabilities should be multiplied by the correction factor

$$f_R \equiv 1 - \bar{P}_O \quad , \tag{B9}$$

where $\bar{P}_O$ is given by Eq. (B8). The factor f_R corrects phenomenologically for the small fraction of probability which is present, on the average, in the off-resonant "virtual" states.[8]

REFERENCES

[1] For reviews, see K. F. Freed, Top. Appl. Phys. **15**, 23 (1976); P. Avouris, W. M. Gelbart, and M. A. El-Sayed, Chem. Rev. **77**, 793 (1977); S. Mukamel and J. Jortner, in *Excited States*, edited by E. C. Lim (Academic, New York, 1977), Vol. 3, p. 57; W. Rhodes, J. Phys. Chem. **87**, 30 (1983); and references cited therein.

[2] For reviews, see V. E. Bondybey, Ann. Rev. Phys. Chem. **35**, 591 (1984); F. F. Crim, *ibid.* **35**, 657 (1984); E. B. Stechel and E. J. Heller, *ibid.* **35**,563 (1984); R. E. Smalley, J. Phys. Chem. **86**, 3504 (1982); M. L. Sage and J. Jortner, Adv. Chem. Phys. **47**, 293 (1981); S. A. Rice, *ibid.* **47**, 117 (1981).

[3] See, for example, K. T Chen, B. E. Forch, and E. C. Lim, Chem. Phys. Lett. **99**, 98 (1983); N. L. Garland and E. K. C. Lee, Faraday Discuss. Chem. Soc. **75**, 377 (1983); A. Lorincz, D. D. Smith, F. Novak, R. Kosloff, D. J. Tannor, and S. A. Rice, J. Chem. Phys. **82**, 1067 (1985); P. M. Felker and A. H. Zewail, *ibid.* **82**, 2994 (1985).

[4] We are concerned here with quantum mechanical approaches and hence will not consider the many useful semiclassical and classical approaches.

[5] A. Nauts and R. E. Wyatt, Phys. Rev. Lett. **51**, 2238 (1983); Phys Rev. A **30**, 872 (1984); I. Schek and R. E. Wyatt, J. Chem. Phys. **83**, 3028 (1985); **83**, 4650 (1985); **84**, 4497 (1986); K. F. Milfeld, J. Castillo, and R. E. Wyatt, *ibid.* **83**, 1617 (1985).

[6] J. V. Tietz and S. -I. Chu, Chem. Phys. Lett. **101**, 446 (1983).

[7] J. Chang and R. E. Wyatt, Chem. Phys. Lett. **121**, 307 (1985).

[8] G. A. Voth and R. A. Marcus, J. Chem. Phys. **84**, 2254 (1986).

[9] For a related, but somewhat different, partitioning approach to that given in Ref. 8, see R. A. White, A. Altenberger-Siczek, and J. C. Light, J. Chem. Phys. **59**, 200 (1973).

[10] (a) T. H. Schucan and H. A. Weidenmüller, Ann. Phys. **73**, 108 (1972); (b) *ibid.* **76**, 483 (1973).

[11] (a) S. Y. Lee and K. Suzuki, Phys. Lett. **91B**, 173 (1980); (b) K. Suzuki and S. Y. Lee, Prog. Theor. Phys. **64**, 2091 (1980). These authors use the notation $\mathbf{R}_n$ in place of $\mathbf{H}_n$.

[12] P. O. Löwdin, in *Perturbation Theory and Its Applications in Quantum Mechanics*, edited by C. H. Wilcox (Wiley, New York, 1966), p. 255 and references cited therein.

[13] The expansion of the wavefunction $|\Psi(t)\rangle$ in Eq. (1) is assumed to be composed of a finite number (=N) of basis states. In theory, an infinite number of basis states are required to completely represent most Hamiltonians, but, in practice, the basis set is usually truncated.

[14] J. Des Cloiseaux, Nucl. Phys. **20**, 321 (1960).

[15] B. H. Brandow, Rev. Mod. Phys. **39**, 771 (1967); in *Lectures in Theoretical Physics*, edited by K. T. Mahanthappa (Gordon and Breach, New York, 1969), Vol. 11 ; Ann. Phys. **57**, 214 (1970).

[16] T. T. S. Kuo, in *Lecture Notes in Physics*, edited by T. T. S. Kuo (Springer-Verlag, 1981), Vol. 144, p. 248.

[17] Note that in this article the resonant subspace is not necessarily degenerate and for this reason the Des Cloiseaux expansion is slightly modified here as discussed in Ref. 10(a). For the case of a degenerate subspace of energy E_o, the choice $\lambda = E_o$ is used. Similar remarks apply to most of the expansions of Schucan and Weidenmüller and Lee and Suzuki, as given here. We have adopted the notation and partitioning scheme from Ref. 8.

[18] D. J. Klein, J. Chem. Phys. **61**, 786 (1974).

[19] B. H. Brandow, Int. J. Quantum Chem. **15**, 207 (1979).

[20] J. S. Hutchinson, E. L. Sibert III, and J. T. Hynes, J. Chem. Phys. **81**, 1314 (1984).

[21] The "exact" frequency was determined from the splittings of the resonant state *eigenstates* (cf. Table 3.1).

Table 3.1: Eigenvalues for the Resonant Subspace in the Four-State Model System.

Δ^a	Exact	Second	First	Zeroth
337.7	-6.56266	-6.56274	-6.55932	-6.71268
	-4.90133	-4.90134	-4.90056	-4.96320
150.0	-16.61214	-16.66792	-16.223.89	-19.33843
	-9.18653	-9.18733	-9.16814	-9.60723

[a] The other parameters in the four-state model were $V_1 = -43.9$ and $V_2 = -50.6$ cm^{-1}. All units are in cm^{-1}.

Table 3.2: Eigenvalues for the Resonant Subspace in the 55-State Model System.[a]

Exact	First	Zeroth
-7.8342	-8.1506	-9.1006
-3.4768	-3.5308	-4.1809
-2.6149	-2.6338	-2.9832
-1.3356	-1.3344	-1.5533
0.6269	0.6268	0.7097
1.1780	1.1811	1.3642
4.5006	4.3520	5.3627
5.9862	6.1315	6.8652
6.1681	6.2137	7.3159
7.6073	7.7074	8.5667

[a] All units are cm^{-1}.

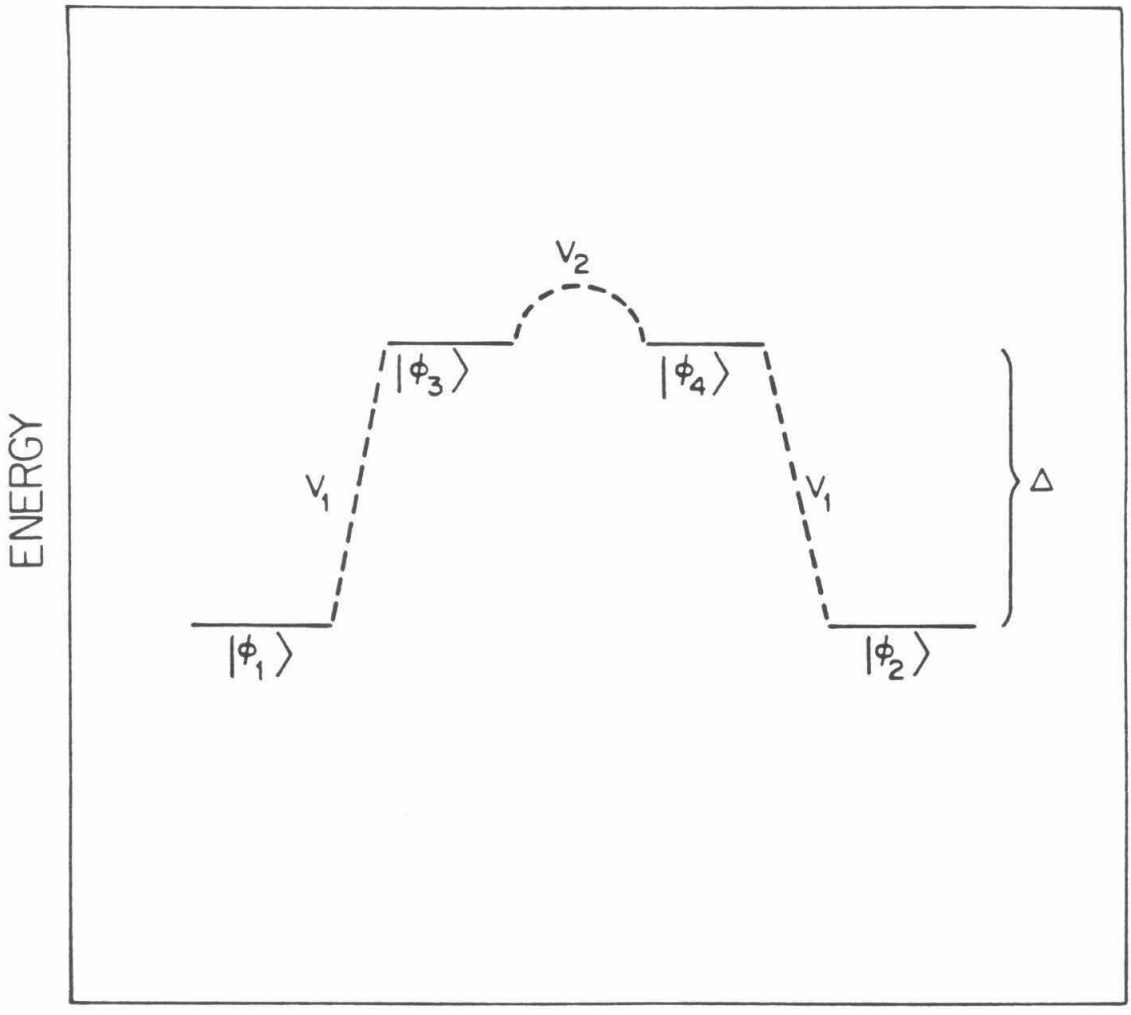

FIG. 3.1. A schematic diagram of the four-state model system used in Sec. IV. Dotted lines denote the couplings between the zeroth-order states, and $|\varphi_1\rangle$ is the initial state.

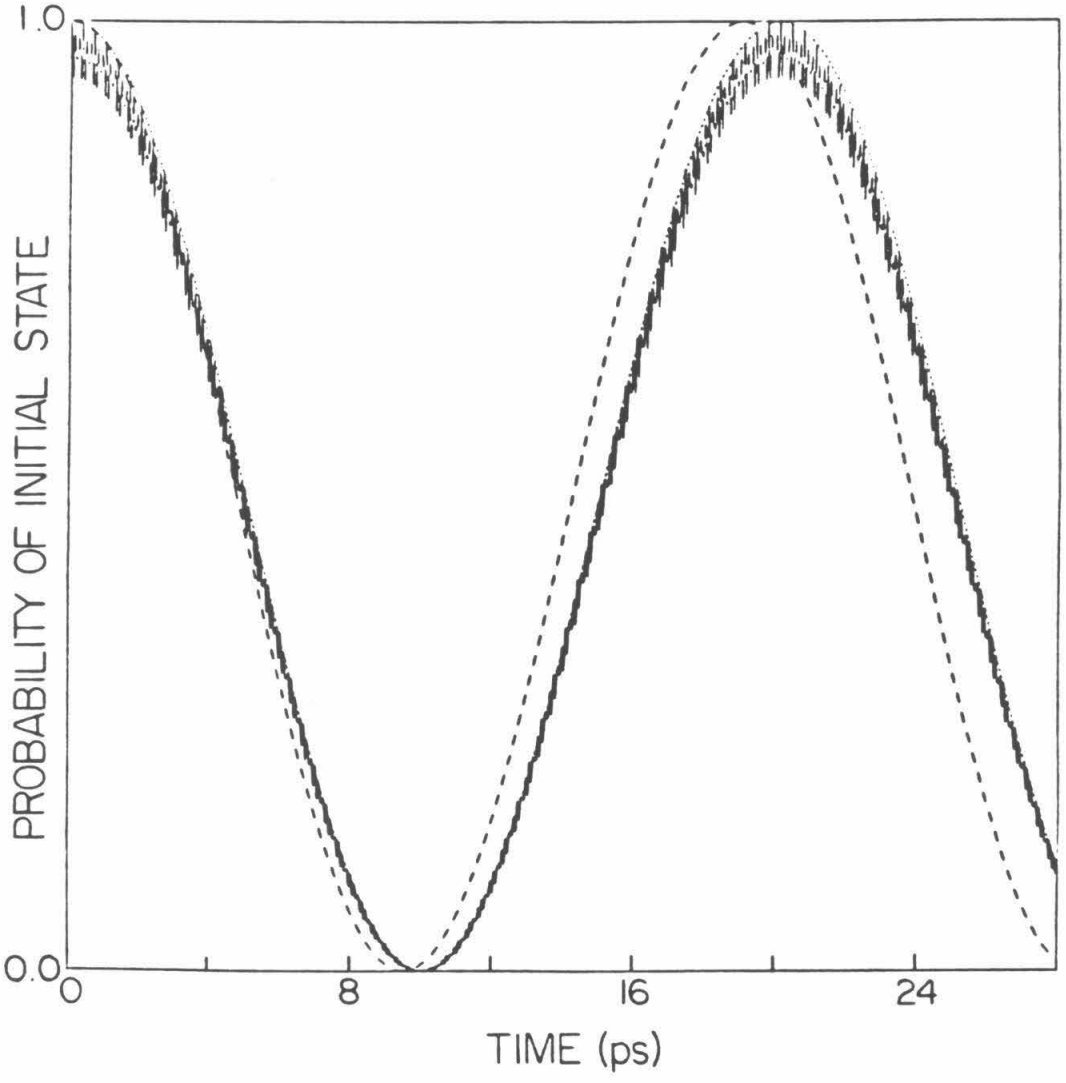

FIG. 3.2. Initial state probability $P_1(t)$ for the model system shown in Fig. 3.1, with $\Delta = 337.7$, $V_1 = -43.9$ and $V_2 = -50.6$ cm^{-1}. The exact results are given by the solid line, the zeroth-order results by the long dashed line and the first-order results by the short dashed line.

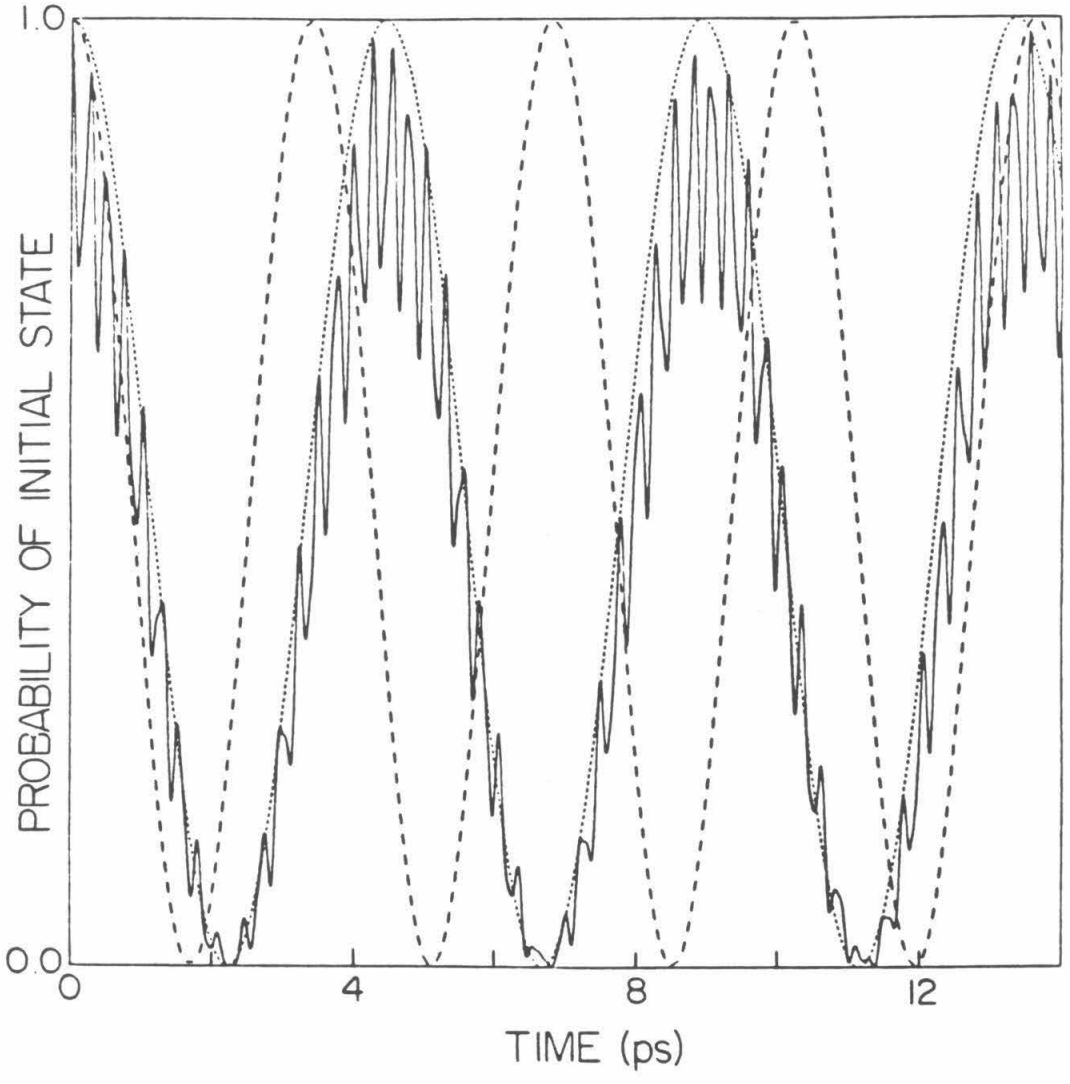

FIG. 3.3. Initial state probability $P_1(t)$ for the model system shown in Fig. 3.1, with $\Delta = 150.0$, $V_1 = -43.9$ and $V_2 = -50.6$ cm^{-1}. The exact results are given by the solid line, the zeroth-order results by the long dashed line and the second-order results by the short dashed line.

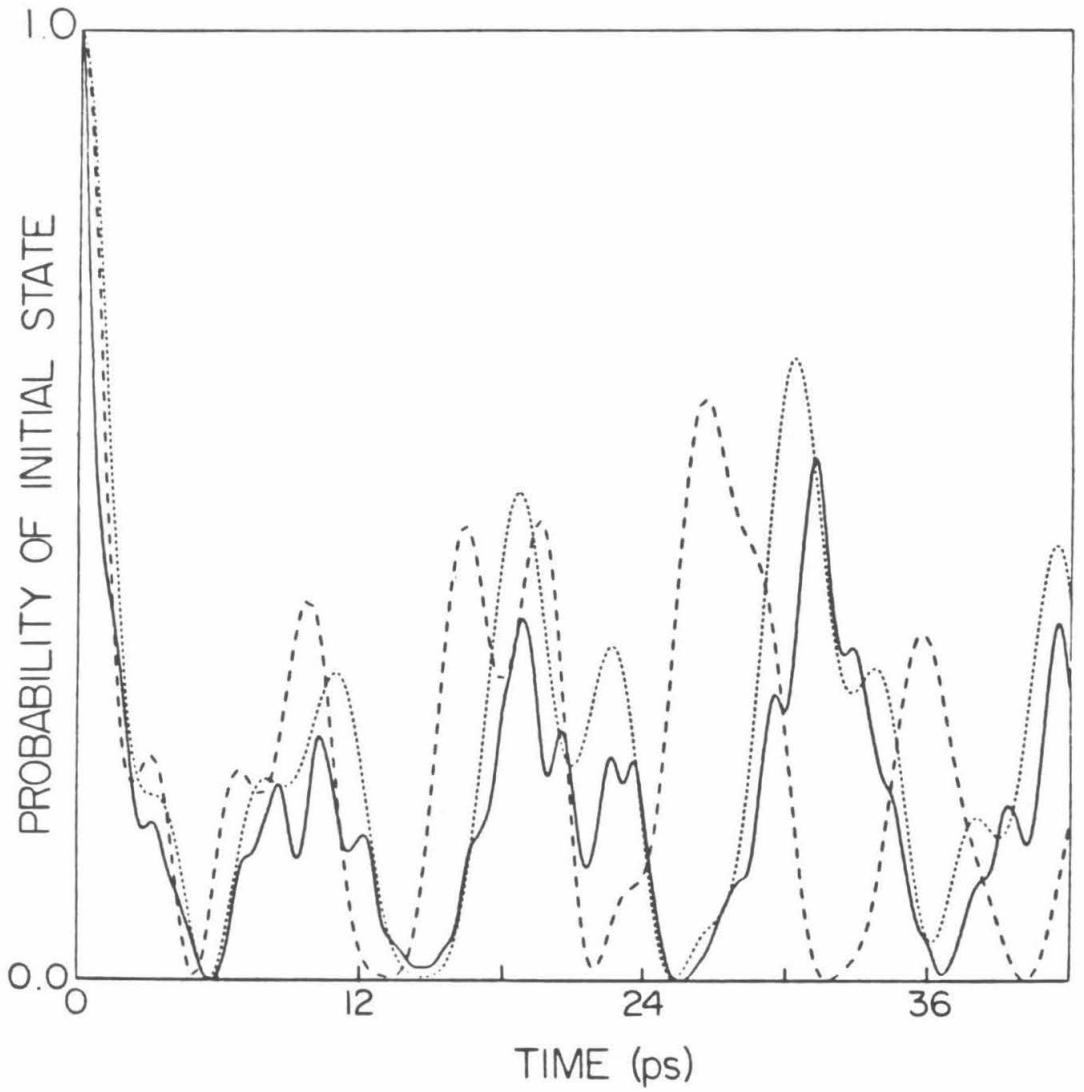

FIG. 3.4. Initial state probability $P_1(t)$ for the second model system discussed in Sec. IV of the text. The exact results are given by the solid line, the zeroth-order results by the long dashed line and the first-order results by the short dashed line.

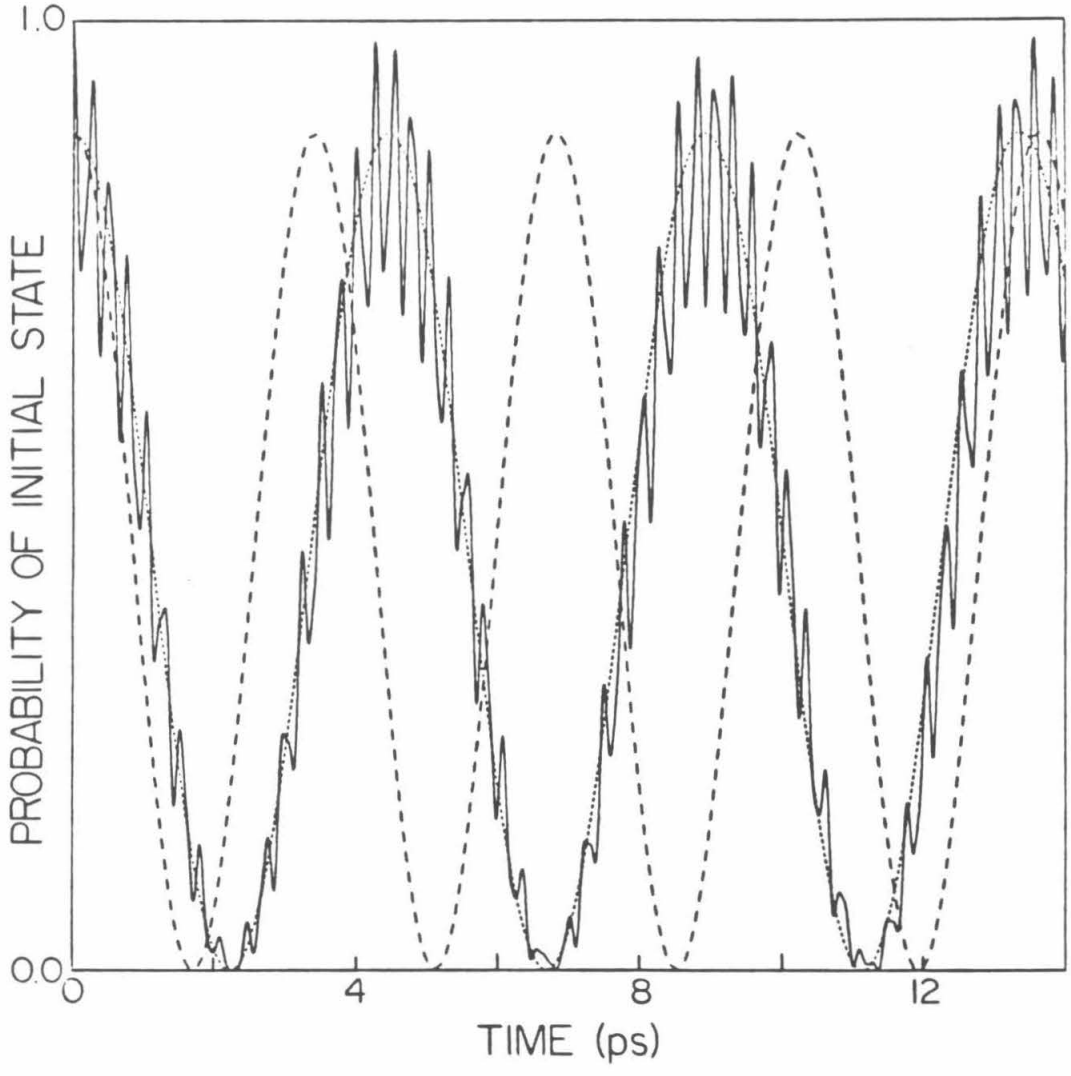

FIG. 3.5. "Corrected" initial state probability $P_1(t) \times f_R$ for the model system shown in Fig. 3.1, with $\Delta = 150.0$, $V_1 = -43.9$ and $V_2 = -50.6$ cm^{-1}. The exact results (with no correction factor) are given by the solid line, the zeroth-order results by the long dashed line and the second-order results by the short dashed line.

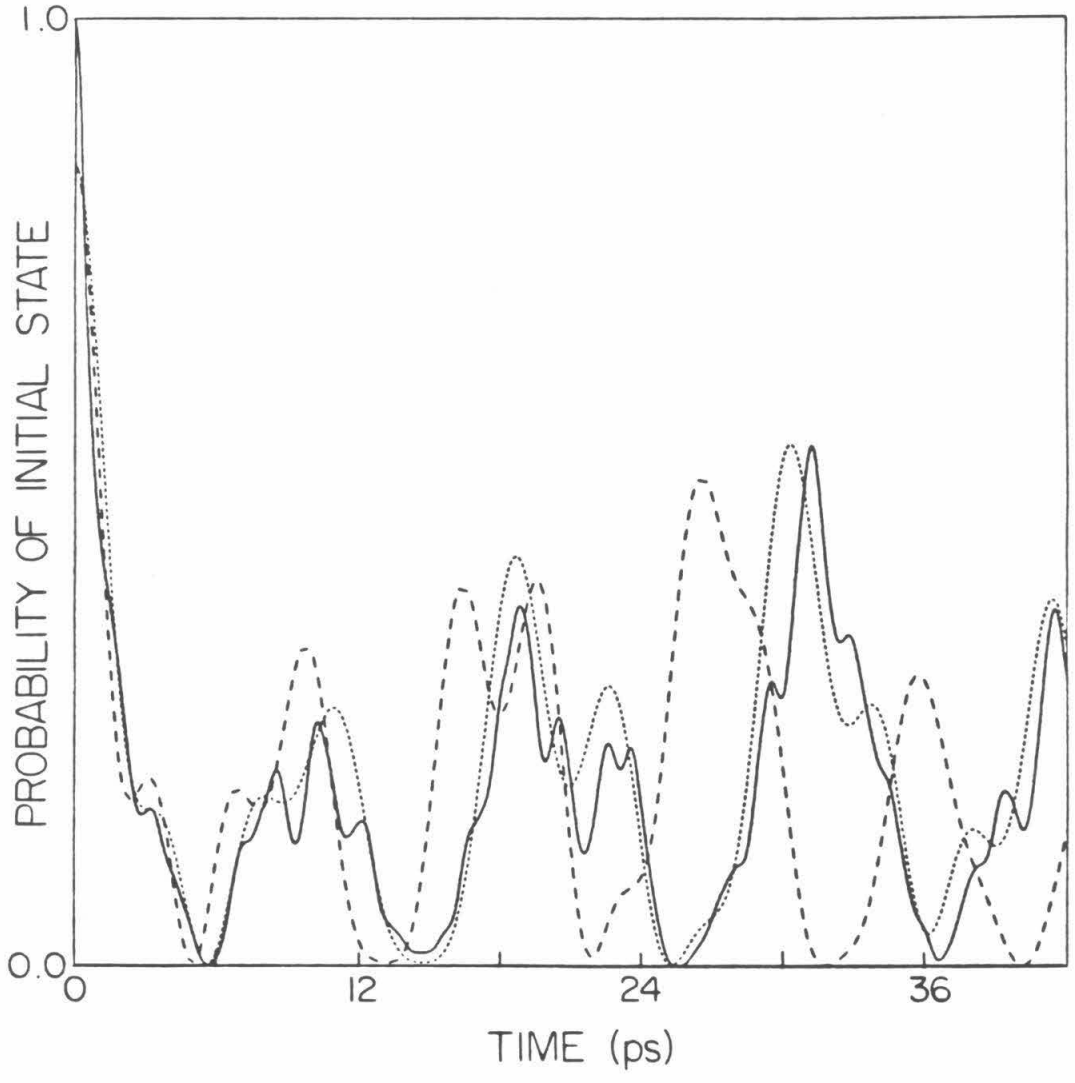

FIG. 3.6. "Corrected" initial state probability $P_1(t) \times f_R$ for the second model system discussed in Sec. IV of the text. The exact results (with no correction factor) are given by the solid line, the zeroth-order results by the long dashed line and the first-order results by the short dashed line.

Chapter 4: Application of Artificial Intelligence Methods to Intramolecular Dynamics Calculations

[The text of this chapter is in press and will appear in: S. M. Lederman, S. J. Klippenstein, and R. A. Marcus, Chem. Phys. Letts. (1988).]

ABSTRACT

The application of artificial intelligence (AI) methods to the determination of intramolecular quantum dynamics for multidimensional systems is described. An AI method based on a physically motivated search algorithm and evaluation function is considered. In both the cases of quantum beats and energy "dissipation" the results for the intramolecular vibrational energy redistribution within an eleven-coordinate model system are shown to be accurate with a considerably reduced number of basis states.

I. INTRODUCTION

The quantum dynamics of the intramolecular vibrational redistribution (IVR) of energy poses, in general, a quite difficult problem, because of the large number of basis states required for the correct modelling of the physical process. For this reason, many different approaches have been developed for increasing the number of basis states which may be effectively handled in the computations. Sometimes physical arguments have been used to limit consideration to only a few of the degrees of freedom.[1] In other approaches methods such as recursive residue generation,[2] partitioning,[3] and a generalized moment expansion[4] have been used.

A reduction in the number of basis states to the subset of dynamically important states is an alternative method for solving high dimensional problems. Recent experimental work has, in fact, provided examples of selective mode coupling among a subset of states.[5] In the present letter we use an AI method to select the states important to the dynamics and to examine convergence properties. AI methods are particularly well suited to performing the reduction in basis set size and thus more degrees of freedom may be considered, thereby contributing to the study of actual molecular systems.

We describe a method for applying AI to the treatment of the time-behavior of an initially prepared vibrational state and apply it to an eleven-coordinate model system. The results from this AI method tend to converge toward the "exact" results as the number of basis states generated by the AI method increases. Examples are given for the cases of quantum beats and of quasidissipative dynamics. AI methods have previously been applied to the study of the dynamics of multiphoton excitation[6] and to the determination of individual eigenvalues.[7] The basis for these applications was the use of AI search methods, as it is here. However, since the present application is to IVR, the search

algorithms and evaluation functions presented here are quite different from those given previously.

II. SEARCH ALGORITHM AND EVALUATION FUNCTION

In the IVR problem the probability distribution function among zeroth-order states is often initially localized and can be represented by a single basis state or a set of basis states. This probability becomes redistributed over some set of final basis states. However, this set of final basis states over which the probability is distributed is not in general known *a priori*. A search algorithm is discussed next for determining the dynamically important basis states and followed by a description of the evaluation function which is used to estimate the importance of each path in the search process.

The search algorithm,[8] which we have called a ***best incomplete paths search***, is a combination of a "beam search" and a "best-first search." A beam search considers all states directly coupled to every incomplete path whose evaluation function is above a certain minimum.* A best-first search considers only the most promising incomplete path as determined by the evaluation function EF for each path (the EF is described later). An example of the search is given in Fig. 4.1 in which the horizontal lines represent basis states with the first number above the line numbering the states in the order searched and the second number giving the evaluation function for the path to that basis state. The first part of the best incomplete paths search involves a beam search for the first two levels as seen in Fig. 4.1. In the example, every state directly coupled to the initial state (I.S.$\equiv$ 1) is found and this yields states 2, 3 and 4. The "X" after state 4 represents the fact that the evaluation function for its path of 0.1 is below the minimum (0.15 say) used for this example, and this path is thus removed from future consideration.

---

* The minimum is chosen through experience to reduce the number of states searched without removing states of importance. A more detailed discussion appears in Ref. 9.

The present beam search continues for one more step and all states coupled to states 2 and 3 are found (states 5, 6 and 7). Though the beam search considers many possible choices of paths simultaneously, it necessitates keeping track of a rapidly increasing list of paths. To avoid maintaining an unmanagable list of potential paths, a best-first search is then implemented for all future choices. The beam search is utilized for the first two steps because poor estimates by the evaluation function at early steps can cause important paths to be discounted unless many possible alternatives are considered.

The best-first search begins at the end of the second level of the two level beam search. In the example in Fig. 4.1, the path to basis state 5 has the highest evaluation function (0.7) of the three incomplete paths leading to states 5, 6 and 7. All states coupled to state 5 are then found and this yields a path to state 8. There are now three incomplete paths to states 6, 7 and 8, of which the path to state 8 has the highest evaluation function (0.6). When all states coupled to this state 8 are found this only gives state 9, which is a duplicate of state 5. This duplicate state (9) is removed from consideration (marked by "X") since it has a lower evaluation function for its path than the earlier path to state 5.† Removal of the new path to state 9 leaves two incomplete paths to states 6 and 7 for consideration. Since the evaluation function for the path to state 7 is greatest, all states coupled to state 7 are found to yield the paths to states 10 and 11. The best-first search process of considering the best incomplete path can continue but is stopped here for brevity of presentation.

The states included in the dynamical calculation are the states for those paths with the best evaluation function at each step in the best-first phase of the search. The states along the path are thereby included. In the example in Fig. 4.1, the path up to and including state 5 (states 1, 2 and 5) are chosen first. This is followed by the path to state 8 for which only state 8 has not been previously

† A further discussion of duplicate states and multiple paths to the same state is given in Ref. 9.

chosen. Finally, the path to state 7 is included for which states 3 and 7 are new. A new path of states is included for each step in the best-first search. The search process is stopped when a preassigned number of states for the dynamics has been chosen.

The choice of an evaluation function in the present work was based primarily on several considerations: (a) a high weighting for the most dynamically important states must be used in order to encourage these states to be accepted first; (b) the calculation of the evaluation function must be rapid since it has to be determined many times during the searching process; (c) paths should be encouraged to return to an energy near that of the initial state, reflecting the role of the uncertainty principle at long times. The evaluation function given below, motivated by perturbative expressions Ref. 10, is a heuristic combination of terms which encourage a return to the initial energy region and which still encourage some searching at energies near that of the previous energy level.

The evaluation function used here in the best incomplete paths search is given by

$$EF = \left| V_{12} \prod_{i=2}^{n} \frac{V_{i,i+1}}{\frac{1}{2}(\Delta E_{i,i+1} + \Delta E_{1,i+1})} \right| . \qquad (1)$$

Each factor after the product sign was set equal to unity whenever its magnitude exceeds unity (again motivated by perturbation arguments). $V_{i,i+1}$ and $\Delta E_{i,i+1}$ represent the Hamiltonian matrix element and energy difference, respectively, between the i and $i+1$ basis states and $\Delta E_{1,i+1}$ is the energy difference between the initial state and state $i+1$. The evaluation function EF gives an equal weighting to $\Delta E_{i,i+1}$ and $\Delta E_{1,i+1}$ for each state in the path. The evaluation function estimates the importance of the path and is a function of the specific path. The search algorithm compares the magnitude of the evaluation functions for the various states (for the particular paths), and selects states, and their paths, with the largest EF's. It does not maximize (in the sense of setting some derivative equal to zero) the evaluation function for a given state. Other

evaluations functions and search methods were studied and are discussed in detail elsewhere.[9] (This more detailed discussion introduces other terms and concepts such as a *goal state* and *expansion* of states.)

After the determination of the important subset of states by the AI procedure, the quantum dynamics of the system was then determined by full matrix diagonalization of this subset. From the resulting eigenvalues and eigenvectors the quantities of physical interest were determined.

III. MODEL SYSTEM

In the testing of the AI method an eleven-coordinate IVR problem involving a heavy central mass was examined.[11]. The model represents the system $C_a - C_b - M - CD_2 - C_c$ where M is a relatively heavy central mass that can act as a barrier to energy redistribution in the molecule, and C and D denote carbon and deuterium atoms.[12] C_a, C_b and C_c have as effective masses those of CH_3, CH_2 and CD_3, respectively. The Hamiltonian for the system is given by the sum of the Hamiltonians for the left and right ligands and the coupling term:

$$H = H_L + H_R + V_{LR} \ , \tag{2}$$

where

$$H_L = \frac{1}{2}\sum_{i=1}^{2}\sum_{j=1}^{2} P_i G_{ij} P_j + \sum_{i=1}^{2} D_i(1 - \exp[\alpha_i(r_i - r_i^e)])^2 \tag{3}$$

$$H_R = \frac{1}{2}\sum_{i=3}^{12}\sum_{j=3}^{12}\left[P_i\left(G_{ij} + \sum_{k=3}^{12}\frac{\partial G_{ij}}{\partial r_k} r_k\right) P_j\right] + \frac{1}{2}\sum_{i=3}^{12} k_i(r_i - r_i^e)^2 \tag{4}$$

$$V_{LR} = \lambda \frac{\cos\theta}{m} P_2 P_3 \ . \tag{5}$$

Here, r_i and P_i are the bond-coordinate and momentum, respectively. The left Hamiltonian, Eq. (3), contains two streching coordinates and the right Hamiltonian, Eq. (4), contains four stretching and five bending coordinates as in a

methane-like ligand (but our model system has a reduced C_2 symmetry).† G_{ij} is the Wilson **G** matrix[13] where it and its derivatives in Eqs. (3) and (4) are evaluated at the equilibrium value of the bond-coordinates. In Eq. (5) θ represents the fixed enclosed angle between the left and right ligand (i.e., the $C_b - M - C$ angle). The detailed parameters used in the model and a detailed discussion of its relevance to IVR calculations are given elsewhere.[12]

The approximate separability of the Hamiltonian into the left and right contributions suggested the use of a basis set with its elements given by the product of a wavefunction of a pre-diagonalized H_L and one of the normal modes of H_R, the latter found when the derivatives of the **G** matrix in H_R are omitted. H_L was pre-diagonalized because of the high energies of excitation used for the left ligand. The AI technique was applied to vibrational energy transfer between the left and right ligands. The system was initially "prepared" in a basis state that only had excess energy in the left ligand, and the amount of energy in the left ligand of the molecule as a function of time was studied.

The λ parameter in V_{LR} permits the variation of the kinetic coupling between left and right ligands in a way which mimics changing the central mass M. The advantage of using λ instead of actually changing the central mass is that the frequencies of the left and right ligands remain unchanged. Thus, a "pure" mass effect is achieved in this model calculation without the possibility of resonances accidentally being modified.

---

† The right Hamiltonian, H_R, in Eq. (4) contains 10 bond coordinates for which one of the bending coordinates is redundant and linearly dependent on the other four bending coordinates. The calculations were performed in symmetry coordinates which remove this redundant coordinate. Details are given in Ref. 13.

IV. RESULTS

The AI method described in Sec. II is compared with the "exact" result, for two different initial states and masses in Figs. 4.2 and 4.3. These "exact" results involved large calculations that were still practical with currently available computers by imposing a simple energy constraint on the basis states used in the calculation. In order to compare the results of the AI method with these exact results, the AI search was constrained to those basis states used in the exact calculations. These calculations were performed so as to determine the quality of the AI method, with the ultimate goal of using the developed technique without such a constraint on the basis states chosen, both for this and for other systems. In the present comparison, m in Eq. (5) is the mass of carbon. In Fig. 4.2, the basis set for this large, exact calculation consisted of all basis states within an energy of $\pm$ 1300 cm^{-1} of the initial state, thereby giving 1023 basis functions. Also, λ was set to 0.1655 to represent the mass of Ge. In Fig. 4.3 twice the mass of carbon was used giving a λ of 0.5, and all basis states within an energy of $\pm$ 650 cm^{-1} of the initial state were included, resulting in a basis set size of 1112 for the higher energy excitation.

In the exact calculations, the heavier mass system (Fig. 4.2) displayed vibrational quantum beats, whereas the lighter mass system (Fig. 4.3) showed, instead, a greater dissipation of energy from the left ligand into the right ligand. In both cases, results from the AI method are seen to be in good agreement with the exact results, especially at short times. Even though the quantum beats case resembles an effective three-state problem it involved many basis states for an accurate description. Thus, 125 basis states had to be generated by the AI method and used in the calculation of the dynamics in order to obtain good agreement with the exact results as given in Fig. 4.2. In a quantum beats case that resembled an effective two-state problem, 70 states were needed and will be discussed in Ref. 9. In the dissipative case only 20 states were generated by

the AI method for the plot in Fig. 4.3. These two situations, quantum beats and dissipation, represent different dynamical situations and serve to test the robustness of the present AI method.

V. DISCUSSION

The AI method presented here has several attractive features for studying IVR problems with many degrees of freedom. The AI technique can efficiently identify a subset of thousands of dynamically important states from a set of a million or more possible basis states. It should, however, be stressed that the AI search is performed within the set of basis states. Thus, it is still important that an intelligent choice be made for the zeroth-order description of the problem. Without the use of AI searching, the determination of the dynamics within a basis of a million of states is beyond the scope of currently available methods.[2–4] For the examples studied, the time spent in the AI searches is typically only a small fraction of the total computer time (e.g., < 1 % for the examples given here) needed to solve the problem. Furthermore the computer time for the AI search scales linearly with the number of basis states chosen (provided the number of basis states considered scales linearly with the number of basis states chosen, as is the case for the present model problem) but the dynamics scales as a cube of the number of basis states. Thus, the AI search will be a smaller percent of the total computer time for larger problems. Also, the computer time necessary for performing the AI methods on higher energy excitations of a molecule is comparable to that at lower molecular energy excitations, provided that the number of possible states searched by the AI method is the same, even though the total number of available states increases exponentially with energy.

In the present letter a search algorithm and evaluation function have been presented, and an AI technique has been applied to the determination of the dynamics for two common situations in IVR, quantum beats and dissipation. In the examples given, the AI search method was able to converge towards and

represent well the exact calculations. The AI method presented can be readily adapted for use in many problems, since only the description of the Hamiltonian needs to be changed. (A different problem might involve a different choice of search algorithm and/or evaluation function.) Thus, the present AI method is not only promising but can be readily applied to a range of problems.

ACKNOWLEDGMENTS

The authors would like to thank Walter Nadler for his help in several aspects of this research, as well as Vicente Lopez and Victor Fairen for their important contributions in developing the model Hamiltonian. It is a pleasure to acknowledge the support of the National Science Foundation, the U.S.-Spain Committee for Scientific and Technological Cooperation, and the Office of Naval Research.

REFERENCES

[1] E.g., K.T. Marshall and J.S. Hutchinson, J. Phys. Chem., 91 (1987) 3219; J.S. Hutchinson, J. Chem. Phys., 82 (1985) 22; J.S. Hutchinson, J.T. Hynes and W.P. Reinhardt, Chem. Phys. Lett., 108 (1984) 353.

[2] See, for example, A. Nauts and R. E. Wyatt, Phys. Rev. Lett. 51 (1983) 2238.

[3] See, for example, G.A. Voth and R.A. Marcus, J. Chem. Phys., 84 (1986) 2254; S.J. Klippenstein, G.A. Voth and R.A. Marcus, J. Chem. Phys., 85 (1986) 5019.

[4] See, for example, W. Nadler and R.A. Marcus, J. Chem. Phys., 86 (1987) 6982;

[5] W.R. Lambert, P.M. Felker and A.H. Zewail, J. Chem. Phys., 75 (1981) 5958; P.M. Felker and A.H. Zewail, Phys. Rev. Lett., 53 (1984) 501; P.M. Felker and A.H. Zewail, J. Chem. Phys., 82 (1985) 2961; 82 (1985) 2975; U. Schubert, E. Riedle and H.J. Neusser, J. Chem. Phys., 84 (1986) 5326; E. Riedle, H.J. Neusser and E.W. Schlag, J. Phys. Chem., 86 (1982) 4847.

[6] J.V. Tietz and S.-I. Chu, Chem. Phys. Letters 101 (1983) 446; J. Chang and R.E. Wyatt, Chem. Phys. Letters 121 (1985) 307; ibid., J. Chem. Phys. 85 (1986) 1826; ibid., 85 (1986) 1840.

[7] J. Chang, N. Moiseyev and R.E. Wyatt, J. Chem. Phys. 84 (1986) 4997

[8] A. Barr and E.A. Feigenbaum, The Handbook of Artificial Intelligence (Heuris-Tech Press, Stanford, 1981) Vol I, Ch. II.; N.J. Nilsson, Problem-Solving Methods in Artificial Intelligence (McGraw-Hill, New York, 1971) Ch. 1-5; P.H. Winston, Artificial Intelligence (Addison-Wesley, Reading, 1984) Ch. 4.

[9] S.M. Lederman and R.A. Marcus, J. Chem. Phys., in press.

[10] A. Messiah, Quantum Mechanics (North-Holland, Amsterdam, 1963) Vol II, Ch. XVI, §16.

[11] V. Lopez, V. Fairen, S.M. Lederman and R.A. Marcus, J. Chem. Phys. 84 (1986) 5494; S.M. Lederman, V. Lopez, G.A. Voth and R.A. Marcus, Chem. Phys. Letters 124 (1986) 93; V. Lopez and R.A. Marcus, Chem. Phys. Letters 93 (1982) 232.

[12] S.M. Lederman, V. Lopez, V. Fairen, G.A. Voth, and R.A. Marcus, J. Chem. Phys., to be submitted.

[13] E.B. Wilson, J.C. Decius and P.C. Cross, Molecular Vibrations (Dover, New York, 1955).

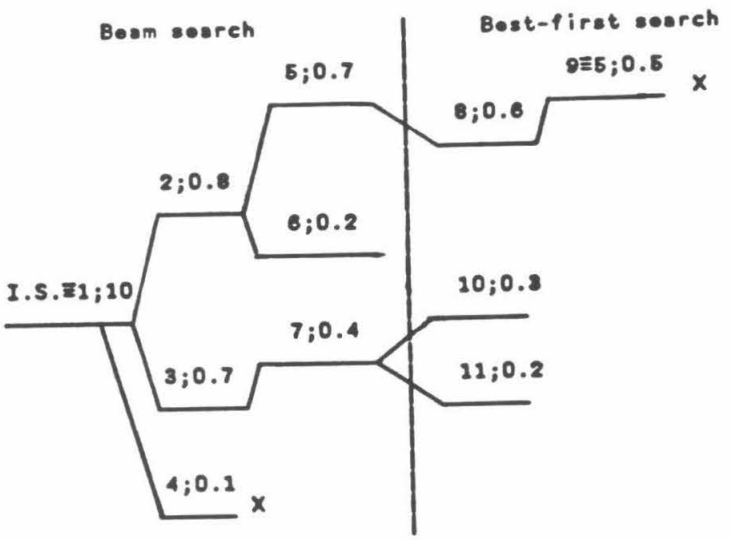

FIG. 4.1. Example of a best incomplete paths search in which two levels of beam search are performed. The horizontal lines represent states and the dashed diagonal connecting lines represent non-zero couplings. The first number above each line is the number given to the basis state (according to the order in which it is found in the search), and the second number is the evaluation function for the path leading to that basis state.

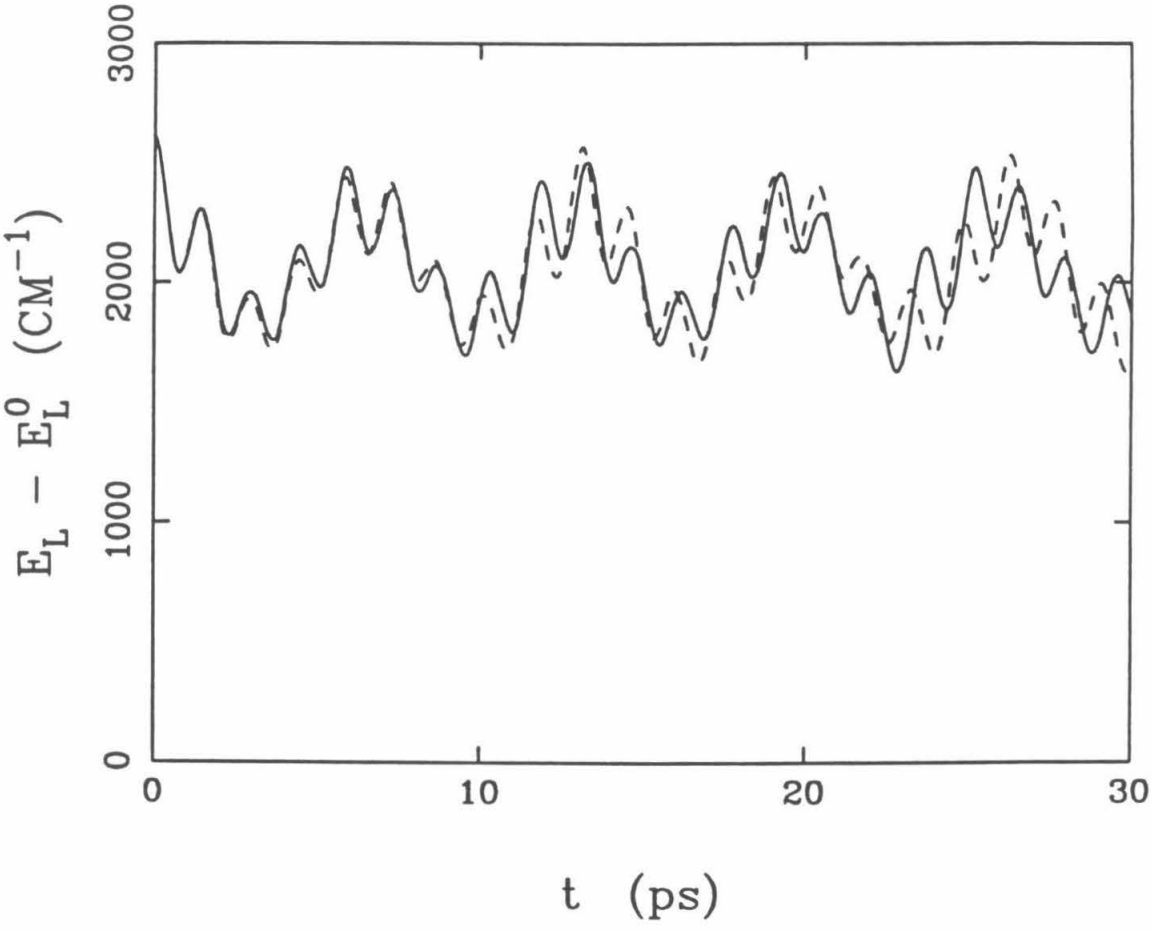

FIG. 4.2. Comparison of the results for the excess energy in the left ligand plotted *vs* the time, with $\lambda = 0.1655$ (mass of Ge). The solid line (—) is the exact result, the dashed line (- - - -) is the AI result. E_L denotes the energy, and E_L^0 the zero-point energy, in the left ligand.

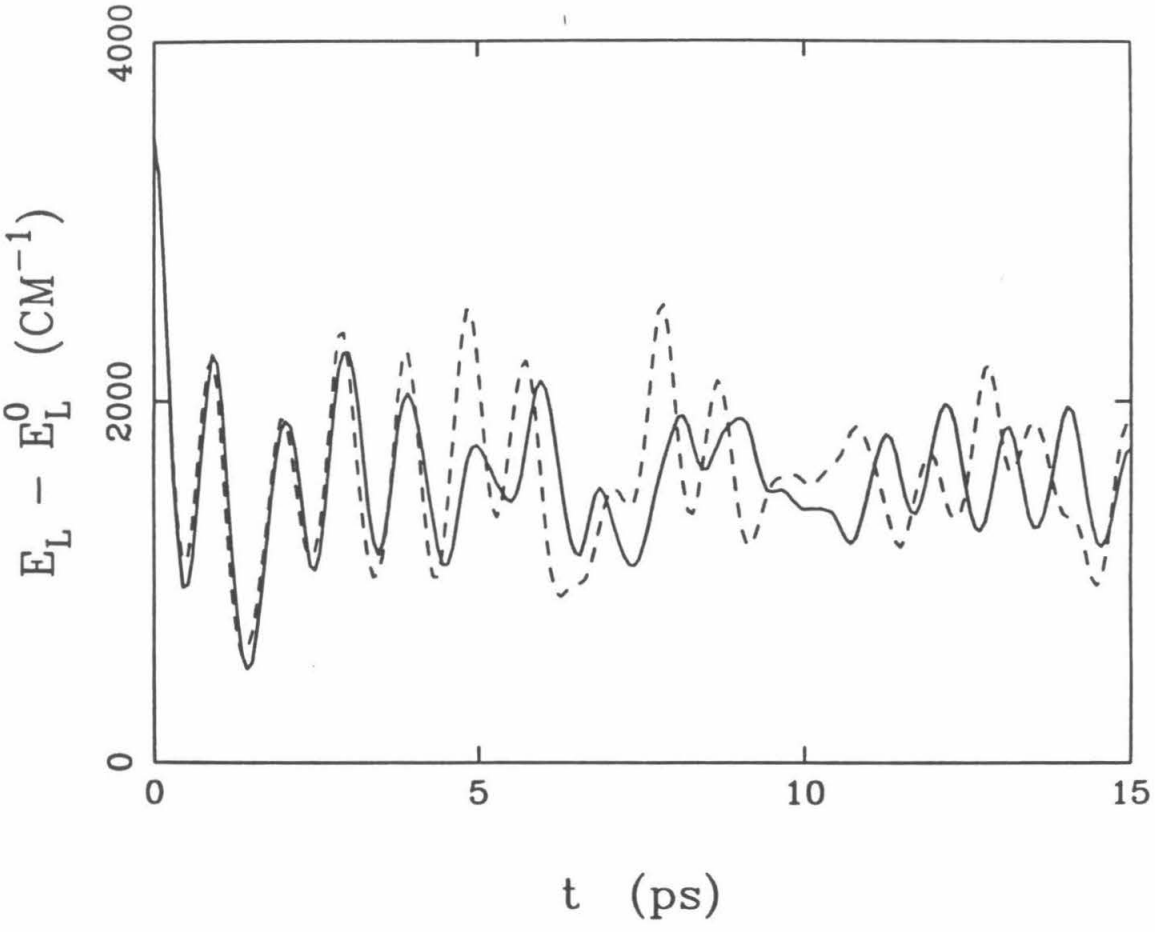

FIG. 4.3. As in Fig. 4.2 except $\lambda = 0.5$ (twice the mass of C).

Chapter 5: High Pressure Rate Constants for Unimolecular Dissociation / Free Radical Recombination: Determination of the Quantum Correction via Quantum Monte Carlo Path Integration

[The text of this chapter appeared in: S. J. Klippenstein and R. A. Marcus, J. Chem. Phys. **87**, 3410 (1987).]

ABSTRACT

The determination of a quantum correction factor for the transitional modes of a unimolecular dissociation / free radical recombination reaction having a transition state of varying looseness is described. The quantum correction factor for the high pressure canonical rate constant is calculated via Monte Carlo path integral evaluation of partition function ratios, and is applied to the recombination reaction $2CH_3 \rightarrow C_2H_6$.

I. INTRODUCTION

In RRKM theory the (microcanonical) unimolecular rate constant k_{EJ} is given by[1-3]

$$k_{EJ} = \frac{N^{\dagger}_{EJ}}{h\rho_{EJ}} , \tag{1}$$

where $N^{\dagger}_{EJ}$ is the number of states of the transition state with energy equal to or less than E, and with a given total angular momentum J; ρ_{EJ} is the density of states for the reactants at the given E and J. In the case of a unimolecular dissociation of the parent molecule into two particles, the coordinates which contribute to $N^{\dagger}_{EJ}$ are largely of two types: i) vibrational modes, usually of high frequency, whose characteristic motion doesn't change appreciably from the parent molecule to the transition state, and ii) the remaining modes whose characteristic motion does change. The latter consist, typically, of coupled degrees of freedom which are fragment bending plus overall rotational motions, and which subsequently become hindered relative rotations plus overall rotational motion in the transition state. In the fragment molecules these modes are typically the free rotations and relative translation of the two fragments. The fragment-fragment stretching in the parent molecule typically becomes the reaction coordinate itself.

Wardlaw and Marcus[4-7] separated the modes into these "conserved" and "transitional" modes, respectively. In this separation the conserved modes were treated quantum mechanically and the transitional modes were treated classically. Their result for the number of states of the transition state for a given energy and total angular momentum J was, thereby, given as the convolution

$$N^{\dagger}_{EJ} = \int_0^E N_V\left(E-\epsilon\right)\Omega_J\left(\epsilon\right)d\epsilon , \tag{2}$$

where $N_V(E-\epsilon)$ is the number of states in the conserved modes with energy less than or equal to $E-\epsilon$, and $\Omega_J(\epsilon)$ is the number of states in the transitional modes with total angular momentum equal to J, and with energy in the range ϵ to $\epsilon + d\epsilon$. $N_V(E-\epsilon)$ was calculated via a direct quantum count, while $\Omega_J(\epsilon)$

was obtained by transformation to action angle coordinates followed by "crude" Monte Carlo evaluation of the phase space integral. Purely *classical* Monte Carlo phase space volume calculations are described in, e.g., Refs. 8 – 17.

Many other approaches to the treatment of the transitional modes have been given previously. (See, e.g., Refs. 18 – 26.) However, the only treatment which has included all of the couplings within the transitional modes, while maintaining a quantum treatment for the conserved modes, appears to be that of Wardlaw and Marcus.[4–7] In a recent article, Pacey[27] has discussed and applied many of the approaches to the 2-dimensional hindered rotor motion on a model sinusoidal potential. Comparison of the results obtained for the partition function from the various approaches with that determined from the exact quantum partition function for the same model potential shows the differences between the various approaches can be significant. In another recent study on the bending / rotation problem, Hase *et al.*[28] have compared rate constants for the $H + CH_3 \rightarrow CH_4$ recombination reaction with the transitional modes treated as either classical hindered rotors or harmonic oscillators (quantum or classical). They find that the partition functions and rate constants can vary by about 10 % depending on how these modes are treated.

As noted in the studies of Wardlaw and Marcus, the question arises, what are the quantum corrections for the contribution of the transitional modes to the overall rate. When the transition state is nearly "loose" such a correction is expected to be minor. One direct approach to calculating the correction would be to determine the number of quantum states for the transitional modes as a function of energy and total angular momentum, and convolute that result with the quantum result for the "conserved" modes. This approach is currently under study. In the present manuscript, however, rather than looking at individual k_{EJ}'s, we have chosen to consider first the cumulative effect of the transitional modes by determining their quantum mechanical contribution to the high pressure canonical rate constant, $k_\infty(T)$, defined below. The position of the transition state is

determined variationally,[29,30,31] namely as that value (the "transition value") of the reaction coordinate for which the calculated $k_\infty(T)$ is a minimum.

In the present study we note that $k_\infty(T)$ is given by a ratio of partition functions and so the quantum mechanical corrections, aside from quantum corrections due to tunneling along the reaction coordinate, may be determined by considering the Monte Carlo path integral evaluation of partition function ratios. The correction factor can thus be obtained for any potential energy surface and is for the *canonical* rate constant. In Section II, for comparison, the canonical rate constant is determined using quantum partition functions for the conserved modes and classical partition functions for the transitional modes. The determination of the quantum correction for the transitional modes is presented in Sec. III. In Sec. IV results for the methyl radical recombination reaction: $2CH_3 \rightarrow C_2H_6$ are presented and discussed. The correction proves to be relatively small for the temperatures investigated.

II. DETERMINATION OF $k_\infty(T)$ USING CLASSICAL CANONICAL TST FOR THE TRANSITIONAL MODES

The canonical rate constant $k_\infty(T)$ is given in terms of $N^\dagger_{EJ}$ by[32]

$$k_\infty(T) = \frac{g_e}{hQ^r(T)} \int_0^\infty dE \sum_{J=0}^\infty (2J+1)\, N^\dagger_{EJ} \exp\left(-\beta E\right), \tag{3}$$

where $Q^r(T)$ is the partition function for the reactants (in the center of mass system and excluding electronic degrees of freedom), g_e is the ratio of the electronic partition function for the transition state to that for the reactants, and $\beta = 1/k_B T$. In a comparative study Wardlaw and Marcus have evaluated $k_\infty(T)$ at several levels.[6] In the first method they determined the location of the transition state variationally for each E and J and then evaluated the sum and integral in Eq. (3) numerically. In a second calculation, which represents an approximation to the first, they determined the transition state location for each E by minimizing a J-sampled integrand, and in a third calculation, which represents still a further approximation, they found the transition state location of

an ensemble which sampled over E and J at a given T. They noted that the three $k_\infty(T)$'s are related by $k_\infty^I(T) \leq k_\infty^{II}(T) \leq k_\infty^{III}(T)$, $k_\infty^I(T)$ being the correct one. This last calculation, $k_\infty^{III}(T)$, is equivalent[1,33] to determining $k_\infty(T)$ variationally from the expression

$$k_\infty(T) = g_e \frac{k_B T}{h} \frac{Q^\dagger}{Q^r} \,, \tag{4}$$

where $Q^\dagger$ is the partition function for the transition state. The $Q^\dagger$ and Q^r in Eq. (4) are calculated relative to the same energy zero. Separating the modes into the conserved modes (c) and the transitional modes (t) implies that

$$k_\infty(T) = g_e \frac{k_B T}{h} \frac{Q_c^\dagger}{Q_c^r} \frac{Q_t^\dagger}{Q_t^r} \,, \tag{5}$$

where $Q_c^\dagger$ and Q_c^r are the partition functions for the conserved modes at the transition state and at the reactant configuration, respectively. They can be evaluated using quantum oscillator partition functions. $Q_t^\dagger$ and Q_t^r are the partition functions for the transitional modes at the transition state and at the reactant configuration, respectively.

For a free radical recombination reaction, the classical partition function for the transitional modes of the reactants, Q_t^r, separates into the translational partition function for a particle of mass μ_{12}, where μ_{12} is the reduced mass of the two fragments, and the product of the classical free-rotor partition functions for the two reactant fragments, $\prod_{i=1}^{2} \sigma_i^{-1} \left[\pi \left(2k_B T/\hbar^2\right)^3 I_{A_i} I_{B_i} I_{C_i}\right]^{1/2}$, where I_{A_i}, I_{B_i}, and I_{C_i} are the moments of inertia of reactant fragment i, and σ_i is the symmetry number for reactant fragment i. The classical partition function for the transitional modes of the transition state is given by

$$Q_t^\dagger = \frac{1}{\sigma^\dagger} \int dp_{\theta_{12}} dp_{\phi_{12}} d\theta_{12} d\phi_{12} \left(\prod_{i=1}^{2} dp_{\theta_i} dp_{\phi_i} dp_{\psi_i} d\theta_i d\phi_i d\psi_i \right) \exp\left(-\beta H_t\right), \tag{6}$$

where $\sigma^\dagger$ is the symmetry factor for the transition state, θ_i, ϕ_i and ψ_i are the Euler angles[34] for the absolute orientation in space of fragment i, and θ_{12} and

ϕ_{12} describe the absolute orientation in space of the line of centers. H_t is the classical Hamiltonian for the transitional degrees of freedom and is given by

$$\begin{aligned} H_t = & \frac{1}{2I_d^\dagger}\left(p_{\theta_{12}}^2 + \frac{p_{\phi_{12}}^2}{\sin^2\theta_{12}}\right) \\ & + \sum_{i=1}^{2}\left\{\frac{1}{2I_{A_i}^\dagger \sin^2\theta_i}\left[(p_{\phi_i} - p_{\psi_i}\cos\theta_i)\cos\psi_i - p_{\theta_i}\sin\theta_i\sin\psi_i\right]^2\right. \\ & \left. + \frac{1}{2I_{B_i}^\dagger \sin^2\theta_i}\left[(p_{\phi_i} - p_{\psi_i}\cos\theta_i)\sin\psi_i + p_{\theta_i}\sin\theta_i\cos\psi_i\right]^2 + \frac{1}{2I_{C_i}^\dagger}p_{\psi_i}^2\right\} \\ & + V(R^\dagger, \theta_{12}, \phi_{12}, \Theta, \Phi, \Psi)\ , \end{aligned} \tag{7}$$

where $\Theta \equiv (\theta_1, \theta_2)$, $\Phi \equiv (\phi_1, \phi_2)$, $\Psi \equiv (\psi_1, \psi_2)$ and $V(R^\dagger, \theta_{12}, \phi_{12}, \Theta, \Phi, \Psi)$ is the potential energy for the given separation $R^\dagger$, and orientation of the rigid rotor fragments. $I_d^\dagger$ is the "diatomic" moment of inertia for the centers of mass of the two fragments and equals $\mu_{12}R^{\dagger^2}$. $I_{A_i}^\dagger, I_{B_i}^\dagger$, and $I_{C_i}^\dagger$ are the principal moments of inertia of the rigid body fragments with their transition state structure.

Evaluation of the integral over the momenta yields

$$\begin{aligned} Q_t^\dagger = & \frac{1}{\sigma^\dagger}\frac{2\pi I_d^\dagger k_B T}{h^2}\left\{\prod_{i=1}^{2}\left[8\pi^3 I_{A_i}^\dagger I_{B_i}^\dagger I_{C_i}^\dagger \left(k_B T/h^2\right)^3\right]^{1/2}\right\} \\ & \times \int d\theta_{12}\, d\phi_{12} \sin\theta_{12}\left(\prod_{i=1}^{2} d\theta_i\, d\phi_i\, d\psi_i \sin\theta_i\right)\exp\left[-\beta V(R^\dagger, \theta_{12}, \phi_{12}, \Theta, \Phi, \Psi)\right]. \end{aligned} \tag{8}$$

Upon integration over the θ_i, ϕ_i, and ψ_i for a fixed θ_{12} and ϕ_{12}, the result, by symmetry, is independent of the actual orientation in space, θ_{12} and ϕ_{12}, of the two fragments, and so the integral over θ_{12} and ϕ_{12} may be immediately evaluated to give

$$Q_t^\dagger = \frac{1}{\sigma^\dagger} Q_{t,d}^\dagger Q_{t,hr}^\dagger, \tag{9}$$

where $Q^{\dagger}_{t,d}$ is the usual classical diatomic partition function $2I^{\dagger}_{d}k_BT/\hbar^2$, and

$$Q^{\dagger}_{t,hr} = \left\{ \prod_{i=1}^{2} \left[8\pi^3 I^{\dagger}_{A_i} I^{\dagger}_{B_i} I^{\dagger}_{C_i} \left(k_BT/h^2 \right)^3 \right]^{1/2} \right\} \times \int \left(\prod_{i=1}^{2} d\theta_i d\phi_i d\psi_i \sin\theta_i \right) \exp\left[-\beta V(R^{\dagger}, 0, 0, \Theta, \Phi, \Psi) \right] , \tag{10}$$

with θ_{12} and ϕ_{12} having been set equal to zero.

For the case of a reasonably loose transition state, $Q^{\dagger}_{t,hr}$ can be evaluated via crude Monte Carlo integration.[35] For a tight transition state many of the configurations sampled will not contribute to the integral and one might revert to the calculation method of Wardlaw and Marcus[4–7] or else use some form of stratified sampling such as that discussed by Farantos *et al.*[11] for microcanonical RRKM determinations. In the present application to the methyl radical recombination reaction, crude Monte Carlo integration sufficed. The final Monte Carlo result for the rate constant for the case of free radical recombination is

$$k^{Cl}_{\infty}(T) = g_e \frac{\sigma_1\sigma_2}{\sigma^{\dagger}} R^{\dagger^2} \left(\frac{8\pi k_BT}{\mu_{12}} \right)^{1/2} \left\{ \prod_{i=1}^{N_v} \frac{\sinh\left(\frac{h\nu_i}{2k_BT} \right)}{\sinh\left(\frac{h\nu^{\dagger}_i}{k_BT} \right)} \right\} \times \left(\prod_{i=1}^{2} \frac{I^{\dagger}_{A_i} I^{\dagger}_{B_i} I^{\dagger}_{C_i}}{I_{A_i} I_{B_i} I_{C_i}} \right)^{1/2} \frac{1}{N_{MC}} \sum_{i=1}^{N_{MC}} \exp\left[-\beta V_i \right] , \tag{11}$$

where N_v is the number of conserved vibrational modes for the two fragments, and ν_i and $\nu^{\dagger}_i$ are the vibration frequencies for the i'th conserved mode of the reactants and of the transition state, respectively. V_i is the value of the potential for the i'th randomly selected configuration, and N_{MC} is the number of random points.

III. DETERMINATION OF THE QUANTUM PARTITION FUNCTION FOR THE TRANSITIONAL MODES

The primitive P-point discretization of the path integral expression for the

quantum transitional mode partition function is given by

$$Q_t^\dagger = \int d\mathbf{\Lambda}^1 \cdots d\mathbf{\Lambda}^P d\mathbf{\Omega}^1 \cdots d\mathbf{\Omega}^P \times \prod_{s=1}^{P} \rho_0\left(\mathbf{\Lambda}^{s+1}, \mathbf{\Lambda}^s; \beta/P\right) \rho_0\left(\mathbf{\Omega}^{s+1}, \mathbf{\Omega}^s; \beta/P\right) \exp\left[-\frac{\beta}{P} V\left(\mathbf{\Lambda}^s, \mathbf{\Omega}^s\right)\right] \tag{12}$$

where $\mathbf{\Lambda}^s$ refers to the line of centers orientations

$$\mathbf{\Lambda}^s = (\cos\theta_{12}^s, \phi_{12}^s) \ , \tag{13}$$

and $\mathbf{\Omega}^s$ refers to the Euler angles

$$\mathbf{\Omega}^s = \prod_{i=1}^{2} \mathbf{\Omega}_i{}^s = \prod_{i=1}^{2} (\cos\theta_i^s, \phi_i^s, \psi_i^s) \ . \tag{14}$$

In Eq. (12) $\mathbf{\Lambda}^{P+1} = \mathbf{\Lambda}^1$ and $\mathbf{\Omega}^{P+1} = \mathbf{\Omega}^1$, while $\rho_0\left(\mathbf{\Lambda}^{s+1}, \mathbf{\Lambda}^s; \beta/P\right)$ and $\rho_0\left(\mathbf{\Omega}^{s+1}, \mathbf{\Omega}^s; \beta/P\right)$, the "free density matrices," are the density matrices for the free-rotor system at a temperature PT. (The latter has $V(\mathbf{\Lambda}, \mathbf{\Omega}) \equiv 0$.)

In the present treatment the quantity of interest is the combined partition function for the hindered rotation of the two separate fragments and for the rotation of the line of centers. If the integrals over $\mathbf{\Omega}^s$ at fixed line of centers orientations $\mathbf{\Lambda}^s$ are performed first, the resulting expression is independent of $\mathbf{\Lambda}^s$ because there is no external field acting on the reacting pair. Thus the integrals over the $\mathbf{\Lambda}^s$ may be evaluated separately to give the partition function for the rotation of a diatomic molecule with point masses equal to those of the two fragments. Expressions for the remaining partition function for the hindered rotations are now easily obtained from the analogous expressions derived by Kuharski and Rossky,[36] who utilized some results of Schulman[37] and introduced a short-time ("fixed-axis") method[38] to determine the quantum partition function for the hindered translational and hindered rotational degrees of freedom of liquid H_2O and D_2O. A brief review of their derivations, with application to the present two-fragment case, is presented below for clarity.

The quantum partition function may be expressed as in Eq. (9) except that now $Q^{\dagger}_{t,d}$ and $Q^{\dagger}_{t,hr}$ are to be evaluated quantum mechanically. In particular

$$Q^{\dagger}_{t,hr} = \int d\mathbf{\Omega}^1 \cdots d\mathbf{\Omega}^P \prod_{s=1}^{P} \rho_0 \left(\mathbf{\Omega}^{s+1}, \mathbf{\Omega}^s; \beta/P\right) \exp\left[-\frac{\beta}{P} V\left(\mathbf{\Omega}^s\right)\right], \tag{15}$$

and $Q^{\dagger}_{t,d}$, the quantum diatomic partition function, is given (for $T > 2I^{\dagger}_d k_B/\hbar^2 \equiv \Theta_r^{-1}$) by the expansion[39]

$$Q^{\dagger}_{t,d} = \frac{T}{\Theta_r}\left[1 + \frac{1}{3}\left(\frac{\Theta_r}{T}\right) + \frac{1}{15}\left(\frac{\Theta_r}{T}\right)^2 + \frac{4}{315}\left(\frac{\Theta_r}{T}\right)^3 + \ldots\right]. \tag{16}$$

Using the least action approximation to the sum over all classical paths for the transition from the orientation $\mathbf{\Omega}^s$ to the orientation $\mathbf{\Omega}^{s+1}$ in the time period $\beta\hbar/P$ gives the free rotation matrix as[37]

$$\begin{aligned}\rho_0\left(\mathbf{\Omega}^{s+1}, \mathbf{\Omega}^s; \beta/P\right) = C \prod_{i=1}^{2} \left[D\left(\mathbf{\Omega}_i^{s+1}, \mathbf{\Omega}_i^s; \beta/P\right)\right]^{1/2} \\ \times \exp\left[-S_{Cl}\left(\mathbf{\Omega}_i^{s+1}, \mathbf{\Omega}_i^s; \beta/P\right)/\hbar\right]\end{aligned}, \tag{17}$$

where C is a constant, $D\left(\mathbf{\Omega}_i^{s+1}, \mathbf{\Omega}_i^s; \beta/P\right)$ is the Van Vleck determinant[40] associated with the transition from $\mathbf{\Omega}_i^s$ to $\mathbf{\Omega}_i^{s+1}$ in a time period of $\beta\hbar/P$, and $S_{Cl}\left(\mathbf{\Omega}_i^{s+1}, \mathbf{\Omega}_i^s; \beta/P\right)$ is the action along the least action classical path between the two orientations. In the exact free rotation matrix there are contributions from multiple rotations. However, for sufficiently large P ("sufficiently small times β/P") these contributions are negligible, and, in the limit of large enough P, Eq. (17) becomes exact.

A fixed-axis approximation is next introduced to determine the Van Vleck determinant and the classical action.[36] This fixed-axis approximation, which is valid for short times and is thus accurate at large P or high temperature, yields[36]

$$D_{FA}\left(\mathbf{\Omega}_i^{s+1}, \mathbf{\Omega}_i^s; \beta\hbar/P\right) = \frac{I^{\dagger}_{A_i} I^{\dagger}_{B_i} I^{\dagger}_{C_i}}{(\beta\hbar/P)^3}\left[\frac{\Gamma_i^{s+1,s}/2}{\sin\left(\Gamma_i^{s+1,s}/2\right)}\right]^2, \tag{18}$$

where $\Gamma_i^{s+1,s}$, the arc length of the rotation from orientation s to orientation $s+1$ of fragment i, is given by[36]

$$\Gamma_i^{s+1,s} = 2\cos^{-1}\left(\chi_i^{s+1,s}\right), \tag{19}$$

and $\chi_i^{s+1,s}$ is a quaternion parameter for the rotation from orientation $\mathbf{\Omega}_i^s$ to orientation $\mathbf{\Omega}_i^{s+1}$, the four of which, in general, are given in terms of Euler angles as[41,42]

$$\chi = \cos\frac{\theta}{2}\cos\frac{(\psi+\phi)}{2}, \quad \eta = \sin\frac{\theta}{2}\cos\frac{(\psi-\phi)}{2},$$
$$\xi = \sin\frac{\theta}{2}\sin\frac{(\psi-\phi)}{2}, \quad \zeta = \cos\frac{\theta}{2}\sin\frac{(\psi+\phi)}{2}\ . \tag{20}$$

The use of these quaternion parameters provides a convenient set of parameters to describe the orientation after a rotation has been performed on some initial orientation, and they also provide a convenient method for determining the relative orientation of two orientations. (See, e.g., Refs. 41 and 42.)

The least classical action for the rotation from orientation s to orientation $s+1$ of fragment i, in the fixed-axis approximation, is given by

$$S_{FA}\left(\mathbf{\Omega}_i^{s+1}, \mathbf{\Omega}_i^s; \beta/P\right) = \frac{\left(\Gamma_i^{s+1,s}\right)^2 P}{2\beta\hbar}\left(\hat{\mathbf{n}}_i^{s+1,s}\cdot\mathbf{I}\cdot\hat{\mathbf{n}}_i^{s+1,s}\right)\ , \tag{21}$$

where, using the quaternions, the rotation axis, $\hat{\mathbf{n}}_i^{s+1,s}$, is given in the principal axis frame by[36]

$$\hat{\mathbf{n}}_i^{s+1,s} = \frac{1}{\sin\left(\Gamma_i^{s+1,s}/2\right)}\left(\eta_i^{s+1,s}\hat{i} - \xi_i^{s+1,s}\hat{j} + \zeta_i^{s+1,s}\hat{k}\right), \tag{22}$$

and the last term in parentheses in Eq. (21) is a tensor product, $\mathbf{I}$ being the moment of inertia tensor in the principal axis frame. Equation (21) has the form which parallels the usual one for a free translational coordinate: a distance squared (here an arc length squared), multiplied by a mass (here a moment of inertia), and divided by twice a time, $\beta\hbar/P$.

The final expression for the quantum partition function for the hindered rotation of two rigid rotor molecules is thus

$$Q^{\dagger}_{t,hr_Q} = C \left[\prod_{i=1}^{2} \frac{I^{\dagger}_{A_i} I^{\dagger}_{B_i} I^{\dagger}_{C_i}}{(\beta\hbar/P)^3} \right]^{1/2} \int d\mathbf{\Omega}^1 \cdots d\mathbf{\Omega}^P \prod_{s=1}^{P} \left\{ \prod_{i=1}^{2} \frac{\Gamma_i^{s+1,s}/2}{\sin\left(\Gamma_i^{s+1,s}/2\right)} \right. \tag{23}$$
$$\left. \times \exp\left[-\frac{1}{\hbar} S_{FA}\left(\mathbf{\Omega}_i^{s+1}, \mathbf{\Omega}_i^{s}; \frac{\beta\hbar}{P} \right) \right] \right\} \exp\left[-\frac{\beta}{P} V\left(\mathbf{\Omega}^s\right) \right].$$

As discussed by Doll and Myers,[43] quantum partition functions may be obtained from Monte Carlo evaluation of an appropriate partition function ratio. In the present article two alternative partition function ratios were used to determine the quantum partition function. One alternative involves the determination of the ratio of the quantum partition function relative to that for two free-rotors:

$$\frac{Q^{\dagger}_{t,hr_Q}}{Q^{\dagger}_{t,fr_Q}} = \frac{\int d\Gamma A \exp\left[-\frac{\beta}{P} \sum_{s=1}^{P} V\left(\mathbf{\Omega}^s\right) \right]}{\int d\Gamma A}, \tag{24}$$

where

$$Q^{\dagger}_{t,fr_Q} = \int d\Gamma A, \tag{25a}$$

$$d\Gamma = d\mathbf{\Omega}^1 \cdots d\mathbf{\Omega}^P, \tag{25b}$$

and

$$A = \prod_{s=1}^{P} \rho_0\left(\mathbf{\Omega}^{s+1}, \mathbf{\Omega}^s; \beta/P\right). \tag{25c}$$

The quantum partition function for the free rotation of the two fragments in their transition state configuration, $Q^{\dagger}_{t,fr_Q}$, is given by the high temperature expansion[44]

$$Q^{\dagger}_{t,fr_Q} = Q^{\dagger}_{t,fr_{Cl}} \prod_{i=1}^{2} \left[1 + \frac{\hbar^2}{24 k_B T} \sum_{cyclic} \left(\frac{2}{I^{\dagger}_{A_i}} - \frac{I^{\dagger}_{A_i}}{I^{\dagger}_{B_i} I^{\dagger}_{C_i}} \right) \right], \tag{26}$$

where

$$Q^{\dagger}_{t,fr_{Cl}} = \prod_{i=1}^{2} 8\pi^2 \left[8\pi^3 I^{\dagger}_{A_i} I^{\dagger}_{B_i} I^{\dagger}_{C_i} \right]^{1/2} \left(k_B T/h^2 \right)^{3/2}. \tag{27}$$

Thus $Q^{\dagger}_{t,hr_Q}$ may be obtained from Eqs. (24) - (27) with Monte Carlo evaluation of the ratio given in Eq. (24). This alternative is once again restricted to reasonably loose transition states.

The other alternative is to calculate the ratio of the quantum to the classical partition function. The classical partition function for the hindered rotor degrees of freedom may be written as

$$Q^{\dagger}_{t,hr_{Cl}} = Q^{\dagger}_{t,fr_{Cl}} \frac{\int d\mathbf{\Omega}^1 \exp\left[-\beta V\left(\mathbf{\Omega}^1\right)\right]}{\int d\mathbf{\Omega}^1}. \tag{28}$$

Multiplying both sides of Eq. (28) by $Q^{\dagger}_{t,fr_Q}/Q^{\dagger}_{t,fr_{Cl}}$, and using Eq. (25a), yields

$$Q^{\dagger}_{t,hr_{Cl}} \frac{Q^{\dagger}_{t,fr_Q}}{Q^{\dagger}_{t,fr_{Cl}}} = \frac{\int d\Gamma A \int d\mathbf{\Omega}^1 \exp\left[-\beta V\left(\mathbf{\Omega}^1\right)\right]}{\int d\mathbf{\Omega}^1}, \tag{29}$$

where $d\Gamma$ and A are given by Eq. (25b) and Eq. (25c), respectively. Since $\int A d\mathbf{\Omega}^2 \cdots d\mathbf{\Omega}^P$ is independent of $\mathbf{\Omega}^1$, $\int d\Gamma A$ can be written as $(\int d\mathbf{\Omega}^1)(\int A d\mathbf{\Omega}^2 \cdots d\mathbf{\Omega}^P)$, and hence Eq. (29) may be written as

$$Q^{\dagger}_{t,hr_{Cl}} \frac{Q^{\dagger}_{t,fr_Q}}{Q^{\dagger}_{t,fr_{Cl}}} = \int d\Gamma A \exp\left[-\beta V\left(\mathbf{\Omega}^1\right)\right]. \tag{30}$$

Thus, using Eqs. (24), (25a), and (30), the ratio of the quantum to classical partition functions for the transitional modes may be written as

$$\frac{Q^{\dagger}_{t,hr_Q}}{Q^{\dagger}_{t,hr_{Cl}}} = \frac{Q^{\dagger}_{t,fr_Q}}{Q^{\dagger}_{t,fr_{Cl}}} \frac{\int d\Gamma A \exp\left[-\frac{\beta}{P}\sum_{s=1}^{P} V\left(\mathbf{\Omega}^s\right)\right]}{\int d\Gamma A \exp\left[-\beta V\left(\mathbf{\Omega}^1\right)\right]}. \tag{31}$$

The Monte Carlo calculation of this ratio is feasible regardless of how tight or loose the transition state is. On the other hand, the determination of $k^Q_\infty(T)$ (the quantum free radical recombination rate constant) from the $Q^{\dagger}_{t,hr_Q}$ in Eq. (24) requires only a *single* Monte Carlo integration, rather than, as in Eq (31), the Monte Carlo evaluation of both the ratio $Q^{\dagger}_{t,hr_Q}/Q^{\dagger}_{t,hr_{Cl}}$ and the quantity $Q^{\dagger}_{t,hr_{Cl}}$.

Importance sampling techniques[45,46] may now be used together with the fixed-axis approximation for A discussed above, in the Monte Carlo evaluation of the path integral ratios given in Eqs. (24) and (31). In particular, in the evaluation of Eq. (31) a weighting factor

$$W_j = A \exp\left[-\frac{\beta}{P} V\left(\mathbf{\Omega}^1\right)\right], \tag{32}$$

with A given by Eq. (25c), is used to determine whether to accept or reject each random step generated in accordance with the parameters described in the next section. The integrand in Eq. (31) which is summed up is then

$$Y_j = \exp\left\{-\frac{\beta}{P}\left[\sum_{s=1}^{P} V\left(\mathbf{\Omega}^s\right) - V\left(\mathbf{\Omega}^1\right) P\right]\right\}, \tag{33}$$

with the quantum to classical ratio being given by

$$\frac{Q^{\dagger}_{t,hr_Q}}{Q^{\dagger}_{t,hr_{Cl}}} = \frac{Q^{\dagger}_{t,fr_Q}}{Q^{\dagger}_{t,fr_{Cl}}} \sum_{j=1}^{N_{MC}} Y_j \,. \tag{34}$$

Multiplying the result of this Monte Carlo evaluation of Eq. (24) by the quantum correction factor for the diatomic term $Q^{\dagger}_{t,d}$ (given by the quantity in brackets in Eq. (16)) and then dividing by the quantum correction factor for Q^{r}_{t} (given by the term multiplying $Q^{\dagger}_{t,fr_{Cl}}$ in Eq. (26), with the transition state moments of inertia replaced by those for the reactant configuration) yields the ratio $k^{Q}_{\infty}(T)/k^{Cl}_{\infty}(T)$.

For the quantum to free-rotor ratio given in Eq. (24) the weighting factor is, instead,

$$W_j = A \,, \tag{35}$$

and the integrand in Eq. (24) is now given by

$$Y_j = \exp\left[-\frac{\beta}{P}\sum_{s=1}^{P} V\left(\mathbf{\Omega}^s\right)\right] \,. \tag{36}$$

The result of this Monte Carlo evaluation of Eq. (24) is next multiplied by the quantum expression for $Q^{\dagger}_{t,d}$, given by Eq. (16), to give the quantum result for

$Q_i^\dagger$. Substituting this result into Eq. (5) and inserting the quantum correction factor for Q_i^r yields the quantum free radical recombination rate constant, $k_\infty^Q(T)$.

IV. RESULTS AND DISCUSSION

The two formalisms described above were implemented for the methyl radical recombination reaction using the potential energy function employed by Wardlaw and Marcus.[5,6] The structure of the rigid body fragments for a given $R^\dagger$ were also taken to be as in Refs. 5, and 6. g_e, σ_{CH_3}, and $\sigma^\dagger$ were taken to be 1/4, 6, and 72, respectively.

For the evaluation of the quantum to free-rotor ratio the following procedure was followed: (1) One of the two fragments i was chosen randomly and an absolute orientation in space, which we will denote by $s = 0$, was chosen randomly.[47] The subsequent points (the path integral points in Eq. (12)) correspond to $s = 1, \cdots, P$. The molecule corresponding to fragment i, and path integral discretization point s will be denoted as (i, s), and the molecule corresponding to the $s = 0$ point is denoted by $(i, 0)$. For this method, this orientation has no effect on the weighting factor and so was always accepted. (2) Next, one of the discretization points s was chosen randomly, and then a rotation about a randomly chosen axis[48] of the old orientation of molecule (i, s) relative to molecule $(i, 0)$ was performed. The magnitude of the rotation was chosen as $R\ \delta_1^{fr}$, where R is a random number between 0 and 1, and δ_1^{fr}, the maximum magnitude of the rotation, was chosen to give a roughly 50% acceptance ratio[49] of the rotations. (3) The new orientation of molecule (i, s) relative to the zeroth order orientation $(i, 0)$ was then calculated using the formula for the composition of quaternions given in Eq. (33) of Ref. 41. (4) The new orientation of molecule (i, s) relative to that of $(i, s + 1)$, and that of $(i, s - 1)$ was next calculated from the known orientations of (i, s), $(i, s + 1)$, and $(i, s - 1)$ relative to that of $(i, 0)$, using the formula for relative quaternions given by Eq. (38) of Ref. 41. (5) The ratio of the weighting factor W_j, given in Eq. (35), for this new orientation relative

to W_j for the old orientation was calculated. If this number was greater than a random number between 0 and 1, then the rotation was accepted. Otherwise the rotation in step (2) was rejected and the old relative orientations of (i,s) to $(i,0)$, (i,s) to $(i,s+1)$, and (i,s) to $(i,s-1)$ were restored to their old values. (6) The absolute orientation in space of molecule (i,s) was then calculated, from Eq. (33) of Ref. 41 for the composition of quaternions, using the orientation of molecule (i,s) relative to that of molecule $(i,0)$ and the absolute orientation in space of molecule $(i,0)$. The new value of the integrand was then calculated from Eq. (36) using the new absolute orientation in space of molecule (i,s). This process was then repeated until the desired number of Monte Carlo points was reached.

The evaluation of the quantum to classical ratio was calculated in a similar manner except that now the weighting factor W_j given in Eq. (32) is used. In this case W_j does depend on the 'zeroth' order orientation so that step (1) now involves a rotation of random magnitude, within a maximum magnitude δ_0^{Cl}, of the 'zeroth' order orientation about a randomly chosen axis.[48] The maximum magnitude of the rotation here was much larger than that of step (2) (labelled δ_1^{Cl}) in order to allow for an efficient sampling over configuration space, as discussed by Kuharski and Rossky.[36] The other steps were identical to those in the quantum to free-rotor case, except in the present case the old $(i,0)$ absolute orientation also had to be restored in step (5) whenever a move was rejected. The overall acceptance ratio was once again kept at about 50%[49] by varying the parameters δ_0^{Cl} and δ_1^{Cl}.

All of the calculations discussed here were easily programmed and large computation times were not required.[50] The results for $k_\infty^{Cl}(T)$, $k_\infty^{Q}(T)$, and the ratio $k_\infty^{Q}(T)/k_\infty^{Cl}(T)$ obtained from these calculations are given in Table 5.1 for the four temperatures 300, 500, 1000, and 2000 K. All of the quantum results reported in Table 5.1 were calculated using $P = 6$ discretization points, since it was found that the results had converged by this value of P.[51] In the classical

calculations the estimated error, σ^{MC}, was evaluated from

$$\sigma^{MC} = \left[\left| f^2 - \sum_{i=1}^{N_{MC}} f_i^2 / N_{MC} \right| \Big/ N_{MC} \right]^{1/2} , \qquad (4.1)$$

where f is the Monte Carlo result for the quantity being evaluated (in the present case $k_\infty^{Cl}(T)$) and f_i is a particular value of the integrand. In the quantum calculations, due to the strong correlation between successive states, σ^{MC} was instead calculated from the variance of sequences of estimates to f (f being either $k_\infty^{Q}(T)$ or the ratio $k_\infty^{Q}(T)/k_\infty^{Cl}(T)$) over blocks of 100 to 1000 Monte Carlo steps. (See, e.g., Ref. 46.)

Comparison of the results for $k_\infty^{Cl}(T)$ given in Table 5.1, with those given in Table VII of Ref. 6, shows that within the Monte Carlo error bars the two calculations give the same result. One also sees from Table 5.1 that, within the Monte Carlo error bars, the quantum correction for recombination in the present case is negligible, and is at most about 1 to 2 %, and its temperature depednence is, within the statistical error, also negligible. At low temperatures one might expect that there would be a larger quantum correction for these modes. However, when the temperature is reduced the location of the transition state moves to larger separation distances and so the partition function for the transitional modes becomes more and more like the product of free-rotor partition functions for which the quantum correction is relatively minor (except at quite low temperatures in which case one expects the quantum corrections for the transitional modes of the transition state and for the transitional modes of the reactants to cancel). Conversely, at high temperatures one might expect a quantum correction due to the decrease in $R^\dagger$, causing an increase in the steepness of the potential energy function. That this is not the case here must be because the increase in temperature causing more classical behaviour balances out the increase in steepness causing quantum effects. In other systems which are "tighter" in the transition state region (have stronger fragment-fragment bending forces there) there may

be larger quantum effects and the present method may be used to determine the quantum correction.

It is interesting to compare these results with those which can be obtained from a generalized Wigner-Kirkwood expansion of the partition function.[52,53] For the present system of two symmetric tops plus a linear rigid rotor this expansion of the partition function is given by[52,53]

$$\frac{Q^{\dagger}_{t,hr_Q}}{Q^{\dagger}_{t,hr_{Cl}}} = \frac{Q^{\dagger}_{t,fr_Q}}{Q^{\dagger}_{t,fr_{Cl}}} \times \frac{\int d\theta_{12} d\phi_{12} \prod_{i=1}^{2} d\theta_i d\phi_i d\psi_i \exp(-\beta V) \left[1 - \beta^3 \hbar^2 \sum_k (\nabla_k V)^2 / 24 m_k\right]}{\int d\theta_{12} d\phi_{12} \prod_{i=1}^{2} d\theta_i d\phi_i d\psi_i \exp(-\beta V)} \quad , \tag{4.2}$$

where

$$\begin{aligned} \frac{1}{m_k}(\nabla_k V)^2 = \frac{1}{I_d^{\dagger}} \left[\left(\frac{\partial}{\partial \theta_{12}} V \right)^2 + \frac{1}{\sin^2 \theta_{12}} \left(\frac{\partial}{\partial \phi} V \right)^2 \right] \\ + \sum_{i=1}^{2} \left[\frac{1}{I_{A_i}^{\dagger}} \left(\frac{\partial}{\partial \theta_i} V \right)^2 + \frac{1}{I_{A_i}^{\dagger} \sin^2 \theta_i} \left(\frac{\partial}{\partial \phi_i} V - \frac{\partial}{\partial \psi_i} V \right)^2 \right. \\ \left. + \frac{1}{I_{C_i}^{\dagger}} \left(\frac{\partial}{\partial \psi_i} V \right)^2 \right] \end{aligned} \tag{4.3}$$

The derivation of the Wigner-Kirkwood expansion for symmetric tops and for diatomic rotors has been given previously, (see, e.g. Refs. 54, and 55).

Results based on Eqs. (4.2) and (4.3) are presented in Table 5.2. The Monte Carlo evaluations in the calculation of $k_{\infty}^{Q}(T)$ have been performed in exact analogy to the classical calculations of Table 5.1. The ratio calculations have been performed along the lines of the quantum calculations in Table 5.1. In both cases the derivatives given in Eq. (4.3) were calculated numerically, and, as a result of the extra potential calls thus required, the evaluation of Eq. (4.2) required more CPU time than the exact calculations. However, this would not

case if the potential was given in a form which was easily differentiated analytically. Comparison of the results given for $k_\infty^Q(T)$ in Tables 5.1 and 5.2 shows that the Wigner-Kirkwood result is approximately within the error bars of the nonperturbative result. The smallness of σ_{MC} in the last column of Table 5.2 is presumably because in that calculation of a ratio $k_\infty^Q(T)/k_\infty^{Cl}(T)$ only a small correction term had to be averaged.

Although the results given in Table 5.1 indicate a very small correction for the transitional modes of a relatively loose transition state at reasonable temperatures, there may still be a large correction to some of the k_{EJ}'s at lower energies. For some experimental situations quantities of particular interest are these k_{EJ}'s, and, for this reason, we are currently studying the possibility of obtaining accurate microcanonical correction factors. When only microcanonical rate constants, k_E, are needed, they can be obtained by inverse Laplace transformation of results at fixed R, provided one evaluates $k_{\infty,Q}(T)$ over a wide enough range of temperatures. However, the determination of the constant E *and* J rate constants requires a different approach.

ACKNOWLEDGMENTS

It is a pleasure to acknowledge support of this research by the National Science Foundation. SJK gratefully acknowledges the support of a Natural Sciences and Engineering Research Council of Canada Postgraduate Scholarship, 1984 - 1987.

REFERENCES

[1] P. J. Robinson and K. A. Holbrook, *Unimolecular Reactions* (Wiley, New York, 1972); W. Forst, *Theory of Unimolecular Reactions* (Academic, New York, 1973).

[2] R. E. Weston and H. A. Schwarz, *Chemical Kinetics* (Prentice-Hall, Englewood Cliffs, NJ, 1972).

[3] R. A. Marcus, J. Chem. Phys. **20**, 359 (1952); R. A. Marcus and O. K. Rice, J. Phys. Colloid. Chem. **55**, 894 (1951); R. A. Marcus, J. Chem. Phys. **43**, 2658 (1965); *ibid* **52**, 1018 (1970).

[4] D. M. Wardlaw and R. A. Marcus, Chem. Phys. Lett. **110**, 230 (1984).

[5] D. M. Wardlaw and R. A. Marcus, J. Chem. Phys. **83**, 3462 (1985).

[6] D. M. Wardlaw and R. A. Marcus, J. Phys. Chem. **90**, 5383 (1986).

[7] D. M. Wardlaw and R. A. Marcus, Adv. Chem. Phys., *in press.*

[8] R. Viswanathan, L. M. Raff, and D. L. Thompson, J. Chem. Phys., **81**, 3118 (1984);

[9] R. Viswanathan, L. M. Raff, and D. L. Thompson, J. Chem. Phys., **81**, 829 (1984).

[10] J. E. Adams, J. Chem. Phys., **78**, 1275 (1983).

[11] S. C. Farantos, J. N. Murrell, and J. C. Hajduk, Chem. Phys., **68**, 109 (1982).

[12] L. B. Bhuiyan and W. L. Hase, J. Chem. Phys., **78**, 5052 (1983).

[13] J. D. Doll, J. Chem. Phys., **74**, 1074 (1981).

[14] J. D. Doll, Chem. Phys. Letts. **72**, 139 (1980).

[15] A. J. Stace, J. Chem. Soc., Faraday Trans. 2, **78**, 959 (1982).

[16] R. M. Stratt and J. E. Adams, J. Chem. Phys., **78**, 2368 (1983).

[17] D. W. Noid, M. L. Koszykowski, M. Tabor and R. A. Marcus, J. Chem. Phys. **72**, 6169 (1980).

[18] S. W. Benson, *Thermochemical Kinetics*, 2nd ed. (Wiley, New York, 1976).

[19] D. M. Golden, J. Phys. Chem. **83**, 108 (1979).

[20] E. V. Waage and B. S. Rabinovitch, Int. J. Chem. Kinet. **3**, 105 (1971).

[21] D. B. Olson and W. C. Gardiner, Jr., J. Phys. Chem. **83**, 922 (1979).

[22] A. W. Miziolek and G. C. Pimentel, J. Chem. Phys. **65**, 4462 (1976).

[23] W. L. Hase, J. Chem. Phys. **57**, 730 (1972); *ibid* **64**, 2442 (1976).

[24] M. Quack and J. Troe, Ber. Bunsenges. Phys. Chem. **78**, 240 (1974).

[25] C. J. Cobos and J. Troe, Chem. Phys. Lett. **113**, 419 (1985); *ibid* J. Chem. Phys. **83**, 1010 (1985); *ibid* J. Phys. Chem. **90**, 3485 (1986).

[26] J. F. LeBlanc and P. D. Pacey, J. Chem. Phys. **83**, 4511 (1985).

[27] P. D. Pacey, J. Chem. Phys. **77**, 3540 (1982).

[28] W. L. Hase, S. L. Mondro, R. J. Duchovic and D. M. Hirst, J. Am. Chem. Soc., **109**, 2916 (1987).

[29] S. Glasstone, K. J. Laidler, and H. Eyring, *The Theory of Rate Processes*, (McGraw-Hill, New York, 1941).

[30] M. Quack and J. Troe, Ber. Bunsenges. Phys. Chem. **81**, 329 (1977).

[31] D. G. Truhlar and B. C. Garrett, Annu. Rev. Phys. Chem. **35**, 159 (1984).

[32] R. A. Marcus, J. Chem. Phys. **43**, 2658 (1965).

[33] Wardlaw and Marcus have separated phase space into three regions and calculated the contribution from only those regions which are dynamically allowed. This is not done in the present canonical treatment because there is not a well defined energy to determine which configurations are allowed.

[34] H. Goldstein, *Classical Mechanics*, 2nd ed. (Addison-Wesley, Reading, MA 1980).

[35] In the present case this involves choosing points in configuration space by choosing θ_i randomly between 0 and π and then choosing ϕ_i, and ψ_i randomly between 0 and 2π. The integral is then given by $\sum_{i=1}^{N_{MC}} \exp\left(-\beta V_i\right) \left(8\pi^2\right)^2 / N_{MC}$.

[36] R. A. Kuharski and P. J. Rossky, J. Chem. Phys. **82**, 5164 (1985).

[37] L. Schulman, Phys. Rev., **176**, 1558 (1968).

[38] In the fixed-axis approximation the least classical action is approximated by

the action for a rotation at constant angular velocity about the fixed-axis **n**. Kuharski and Rossky (Ref. 36) have shown that this action is the same as the least classical action to order $(\Delta t)^2$ and is thus valid for short times, which corresponds to large P or high temperatures.

[39] D. A. McQuarrie, *Statistical Mechanics*, (Harper and Row, New York, 1976).

[40] J. H. Van Vleck, Proc. Natl. Acad. Sci. **14**, 178 (1928).

[41] D. J. Evans, Mol. Phys., **34**, 317 (1977).

[42] D. J. Evans and S. Murad, Mol. Phys. **34**, 327 (1977).

[43] J. D. Doll and L. E. Myers, J. Chem. Phys., **71**, 2880 (1979); J. D. Doll, J. Chem. Phys. **81**, 3536 (1984).

[44] K. F. Stripp and J. G. Kirkwood, J. Chem. Phys. **19**,1131 (1951).

[45] J. P. Valleau and S. G. Whittington, in *Statistical Mechanics*, edited by B. J. Berne (Plenum, New York, 1977), p. 137.

[46] J. P. Valleau and G. M. Torrie, in *Statistical Mechanics*, edited by B. J. Berne (Plenum, New York, 1977), p. 169.

[47] E.g., $\theta_i = \pi\ R_1$, $\phi_i = 2\pi\ R_2$, and $\psi_i = 2\pi\ R_3$, where R_1, R_2, and R_3 are random numbers between 0 and 1.

[48] First, χ is set equal to $\cos(\Gamma/2)$, where Γ is the magnitude of the rotation. An axis of rotation is then chosen randomly by choosing a random point on a sphere of radius $\sqrt{1-\chi^2}$ and taking η, ξ, and ζ as the three cartesian coordinates of this point.

[49] The acceptance ratio is defined as the number of moves accepted divided by the number of moves attempted. It has been empirically determined that acceptance ratios of about 50% lead to the most rapid convergence. See, e.g., J. A. Barker, *Lattice Theories of the Liquid State* (MacMillan, New York, 1963).

[50] Typical computational times on a VAX 11/780 were, for the quantum calculations 30 minutes, and for the classical calculations 6 minutes.

[51] The initial configuration for each of the quantum calcualtions was taken to

be the configuration of minimum potential energy for the given $R^{\dagger}$. At the start of the quantum calculations 100 initialization steps were performed before starting the evaluation of the integral. After this the integrands were summed up for 40000 points. In the classical calculations no initialization procedure is needed and 50000 points were used in the calculation of the integral. The values of δ_0^{fr} used were 0.25, 0.20, 0.14, 0.09, for $T = 300$, 500, 1000, and 2000 K, respectively. The values of (δ_0^{Cl} , δ_1^{Cl}) were (1.0,0.22), (0.65,0.17), (0.45,0.09), and (0.4,0.06), for the same four temperatures.

[52] E. Wigner, Phys. Rev. **40**, 749 (1932).

[53] J. G. Kirkwood, Phys. Rev. **44**, 31 (1933).

[54] H. Friedmann, Adv. Chem. Phys. **4**, 262 (1976).

[55] J. G. Powles and G. Rickayzen, Mol. Phys. **38**, 1875 (1979); *ibid* **40**, 1533 (1980).

Table 5.1: Quantum Corrections from Path Integration

Temp (K)	$R^{\dagger}$[a] (Å)	$k_{\infty}^{Cl}(T)$[b] $\pm \sigma_{MC}$[c] (10^{13} cm^3 mol $^{-1}$)	$k_{\infty}^{Q}(T)$[d] $\pm \sigma_{MC}$[c] (10^{13} cm^3 mol $^{-1}$)	Ratio[e] $\pm \sigma_{MC}$[c]
300	4.2	5.06 ± 0.02	4.99 ± 0.02	1.002 ± 0.004
500	3.8	4.32 ± 0.03	4.31 ± 0.04	0.999 ± 0.006
1000	3.4	2.83 ± 0.03	2.75 ± 0.04	0.997 ± 0.007
2000	3.0	1.38 ± 0.02	1.34 ± 0.03	1.024 ± 0.008

[a] As determined in Ref. 6.

[b] As determined by the present classical Monte Carlo calculation.

[c] σ_{MC} refers to the Monte Carlo uncertainties determined as discussed in the text.

[d] As determined by the quantum to free-rotor ratio path integral ratio calculation. (See Eq. (24).)

[e] $k_{\infty}^{Q}/k_{\infty}^{Cl}$ as determined by the quantum to classical ratio path integral calculation. (See Eq. (31).)

Table 5.2: Quantum Corrections from Generalized Wigner-Kirkwood Expansion

Temp (K)	$R^{\dagger}$[a] (Å)	$k_{\infty}^{Q}(T)$[b] $\pm \sigma_{MC}$[c] (10^{13} cm^3 mol $^{-1}$)	Ratio[d] $\pm \sigma_{MC}$[c]
300	4.2	5.00 ± 0.03	0.990 ± 0.001
500	3.8	4.22 ± 0.05	0.980 ± 0.001
1000	3.4	2.70 ± 0.06	0.980 ± 0.001
2000	3.0	1.29 ± 0.05	0.982 ± 0.001

[a] As determined in Ref. 6.

[b] Determined by the direct evaluation of $k_{\infty}^{Q}(T)$ from the generalized Wigner-Kirkwood expansion.

[c] σ_{MC} refers to the Monte Carlo uncertainties determined as discussed in the text.

[d] Determined by the direct evaluation of $k_{\infty}^{Q}/k_{\infty}^{Cl}$ from the generalized Wigner-Kirkwood expansion calculation. The Monte Carlo error bars in this calulation are negligible.

Chapter 6: Unimolecular Reaction Rate Theory for Highly Flexible Transition States. I. Use of Conventional Coordinates

[The text of this chapter is in press and will appear in: S. J. Klippenstein and R. A. Marcus, J. Phys. Chem. (1988).]

ABSTRACT

An alternative method for implementing RRKM theory for unimolecular reactions with highly flexible transition states is described using conventional coordinates. The number of available states for motion in the transition state N_{EJ} is determined via an appropriate average over the absolute space orientations and body-fixed momenta of the two fragments. The results of calculations of N_{EJ} for the $C_2H_6 \rightarrow 2CH_3$ reaction (or alternatively for the corresponding recombination reaction) obtained from the present expression are shown to be equivalent numerically to those obtained previously by Wardlaw and Marcus.

I. INTRODUCTION

In recent years there has been an increase in the degree of molecular state selection available in experimental studies of unimolecular reactions.[1] Concurrent with this increase in state resolution has been an increased need for the theoretical determination of energy and angular momentum-resolved unimolecular dissociation or isomerization rate constants k_{EJ} for realistic potential energy surfaces. Previous calculations of k_{EJ} have included those involving fully classical methods (both trajectory calculations and variationally implemented RRKM theory),[2] the statistical adiabatic channel model,[3] and a partially quantum partially classical variationally implemented RRKM theory.[4] The present paper focuses on an alternative method for implementing the latter.

In RRKM theory the specific rate constant, k_{EJ}, for the dissociation or isomerization at a given energy E and total angular momentum quantum number J is given by [5]

$$k_{EJ} = \frac{N_{EJ}}{h\rho_{EJ}} , \tag{1}$$

where ρ_{EJ} is the density of states for the reactant at the given E and J. The quantity N_{EJ} is the number of available states for motion in the transition state, which is to be determined variationally, i.e., by finding a potential hypersurface for which N_{EJ} is minimized. In most practical applications the full hypersurface is not varied but rather some coordinate R, which describes the progress of the reaction. The value of R that gives a minimum in N_{EJ}, labeled $R^{\dagger}$, is a function of E and J.

In a recent series of articles,[4] Wardlaw and Marcus have shown how Monte Carlo integration techniques may be used to facilitate the calculation of N_{EJ}'s. The basis of this method is the introduction of an approximate separation of variables into the conserved modes, i.e., modes which do not change their nature in the transition from reactant to products, and the transitional modes, i.e., modes which do have a considerable such change. The conserved modes are typically vibrations and were treated quantum mechanically. In a unimolecular

dissociation the transitional modes are typically the fragment-fragment hindered rotations (or bending modes) and the overall rotations, and were treated classically. [A quantum correction for the latter for the high pressure (i.e., canonically averaged) k_{EJ}'s was recently given.[6]]

The number of states N_{EJ} is then given by the convolution[4]

$$N_{EJ} = \int_0^E N_V\,(E-\epsilon)\,\rho_J\,(\epsilon)\,d\epsilon, \tag{2}$$

where $N_V(E)$ is the number of quantum states for the conserved modes with an energy less than or equal to E, and $\rho_J(\epsilon)$ is the density of states for the transitional modes at the given energy ϵ and total angular momentum quantum number J for the given R. Upon introducing various canonical transformations using action-angle variables, Wardlaw and Marcus obtained $\rho_J\,(\epsilon)$ as a reduced phase space average of the product of triangle inequalities and a delta function in $\epsilon - H$, where H is the classical Hamiltonian for the relevant modes. In this reduced phase space average the total angular momentum was fixed, and the z-component of the total angular momentum and the two coordinates conjugate to these two momenta had been eliminated via an analytical integration. The problem was thereby reduced to a Monte Carlo integration of a given analytical expression over typically (for the case of two polyatomic fragments) six coordinates and six momenta.

In the present article a simple alternative method for evaluating N_{EJ} is presented, in which the transformation of variables to action-angle coordinates is avoided. For the conditions we have explored it is also shown how an alternative method for handling the integration limits can be used. The resulting overall method is very easily programmed and executed. In Sec. II a series of transformations is introduced which serves to reduce the dimensionality of the phase space integral, without making any transformations in the remaining variables. The resulting phase space integral is then evaluated as a free-rotation canonical average in Sec. III. Results for N_{EJ} from calculations using this method are

discussed and compared with previous results of Wardlaw and Marcus in Sec. IV.

II. DETERMINATION OF N_{EJ} USING ABSOLUTE SPACE ORIENTATIONS AND CONJUGATE MOMENTA

Since the rapid determination of accurate $N_V(E)$'s for Eq. (2) is usually possible through direct count algorithms,[7] the evaluation of N_{EJ} mainly involves finding a rapid method for determining $\rho_J(\epsilon)$. The first step in evaluating the latter involves the choice of an appropriate coordinate system. In the present article the coordinates chosen are the conventional Euler angles[8] $(\theta_i, \phi_i, \psi_i)$ for the *absolute* orientation in space of fragment i, denoted by $\mathbf{\Omega}_i$, and the two angles θ_{12} and ϕ_{12} which describe the spatial orientation of the line of centers of the two fragments. The conjugate momenta for these coordinates are then denoted by $\mathbf{p}_i = (p_{\theta_i}, p_{\phi_i}, p_{\psi_i})$, $p_{\theta_{12}}$, and $p_{\phi_{12}}$, respectively.

In terms of these coordinates $\rho_J(\epsilon)$ can be written as

$$\rho_J(\epsilon) = \frac{1}{\sigma h^8} \int \delta\left[\epsilon - H(\tau)\right] \hbar \delta\left[J\hbar - J_T(\tau)\right] d\tau \ , \tag{3}$$

where τ denotes the above described coordinates and their conjugate momenta. J_T is the magnitude of the total angular momentum as a function of the coordinates and momenta, and now a delta function in $J\hbar - J_T$ is present, unlike in the treatment of Wardlaw and Marcus, who used a fixed J_T as one of their action-angle coordinates. We have introduced the $\hbar$ in Eq. (3) with the following reasoning: Without it the right hand side of Eq. (3) would be the classical number of quantum states per unit energy per unit angular momentum J_T. By multiplying by $\hbar$ we have obtained the semiclassical equivalent of the number of states per unit energy for a given value of the angular momentum quantum number J.

The integral over ϵ in Eq. (2) can now be performed to yield

$$N_{EJ} = \frac{\hbar}{\sigma h^8} \int N_V\left[E - H(\tau)\right] \delta\left[J\hbar - J_T(\tau)\right] d\tau \ . \tag{4}$$

The above choice of conventional coordinates is convenient in that it allows for a *simple* evaluation of the Hamiltonian. However, the dimensionality of the phase-space integral should still be reduced by four, to obtain the dimensionality of integration used previously by Wardlaw and Marcus. To this end, several transformations of the coordinates and momenta describing the line of centers orientation and momenta are now introduced. These transformations, in conjunction with several observations about the dependence of the integral on certain variables, permit the desired reduction in dimensionality of the integral.

The first observation is that the integrand in Eq. (4) is independent of the direction of the total angular momentum vector $\mathbf{J}_T$ and, hence, of the value of J_{Tz}, the z-component of $\mathbf{J}_T$. Thus, the integral will be unchanged if $\mathbf{J}_T$ is restricted to lie along the z-axis by introducing a delta function in $J_T - J_{Tz}$, which singles out a particular J_{Tz}, multiplying again by $\hbar$ for reasons analogous to those described for Eq. (3), and then multiplying by the actual number of J_{Tz} quantum states (semiclassically speaking), for the given J_T, namely $2J+1$. Thereby,

$$N_{EJ} = \frac{(2J+1)\,\hbar^2}{\sigma h^8} \int N_V\left[E - H(\tau)\right] \delta\left[J\hbar - J_T(\tau)\right] \delta\left[J_T(\tau) - J_{Tz}(\tau)\right] d\tau. \tag{5}$$

The dimensionality of the integral in Eq. (5) can be reduced by two by performing an analytical integration over the arguments of the delta functions. To this end, a transformation of variables is needed to new variables which include J_T and J_{Tz} or their equivalents. For simplicity, the required transformation is divided into two steps with the first transformation being from θ_{12}, $p_{\theta_{12}}$, and $p_{\phi_{12}}$ to the Cartesian components of the orbital angular momentum l_x, l_y, and l_z:[9]

$$l_x = -p_{\theta_{12}} \sin\phi_{12} - p_{\phi_{12}} \cos\phi_{12} \cot\theta_{12},$$

$$l_y = p_{\theta_{12}} \cos\phi_{12} - p_{\phi_{12}} \sin\phi_{12} \cot\theta_{12}, \qquad l_z = p_{\phi_{12}}, \tag{6}$$

the Jacobian of the transformation being $|\partial(\theta_{12}p_{\theta_{12}}p_{\phi_{12}})/\partial(l_x l_y l_z)| = |\sin^2\theta_{12}/p_{\phi_{12}}|$. The latter equals $|l_z|/\left[(\cos\phi_{12}l_x+\sin\phi_{12}l_y)^2+l_z^2\right]$, thereby yielding

$$N_{EJ}=\frac{(2J+1)\hbar^2}{\sigma h^8}\int N_V\left[E-H(\tau')\right]\frac{\delta\left[J\hbar-J_T(\tau')\right]\delta\left[J_T(\tau')-J_{Tz}(\tau')\right]|l_z|}{(\cos\phi_{12}l_x+\sin\phi_{12}l_y)^2+l_z^2}d\tau', \tag{7}$$

where τ' denotes $\mathbf{\Omega}_i, \mathbf{p}_i, \phi_{12}, l_x, l_y, l_z$, and $d\tau'$ is the corresponding volume element.

The second transformation is from l_x, l_y, and l_z to J_T, θ, and ϕ, where the θ and ϕ are the polar coordinates of $\mathbf{J}_T$:

$$l_x+k_x=J_T\sin\theta\cos\phi,\quad l_y+k_y=J_T\sin\theta\sin\phi,\quad l_z+k_z=J_T\cos\theta. \tag{8}$$

Here, k_x, k_y and k_z are the Cartesian components of the sum of the space-fixed rotational angular momenta of the individual fragments $\mathbf{j}_i$, which in turn are given in terms of the $\mathbf{p}_i$ by[9]

$$\begin{aligned} j_{z_i}&=-\left[(\cos\theta_i p_{\phi_i}-p_{\psi_i})\cos\phi_i/\sin\theta_i+\sin\phi_i p_{\theta_i}\right],\\ j_{y_i}&=-\left[(\cos\theta_i p_{\phi_i}-p_{\psi_i})\sin\phi_i/\sin\theta_i-\cos\phi_i p_{\theta_i}\right],\qquad j_{z_i}=p_{\phi_i}. \end{aligned} \tag{9}$$

The Jacobian of the transformation is given in this case by $|\partial(l_x l_y l_z)/\partial(J_T\theta\phi)| = J_T^2\sin\theta$, yielding

$$\begin{aligned} N_{EJ}=\frac{(2J+1)\hbar^2}{\sigma h^8}\int N_V\left[E-H(\tau'')\right]\delta(J\hbar-J_T)\,\delta(J_T-J_T\cos\theta)\\ \times\frac{|J_T\cos\theta-k_z|\,J_T^2\sin\theta d\tau''}{\left[\cos\phi_{12}(J_T\sin\theta\cos\phi-k_x)+\sin\phi_{12}(J_T\sin\theta\sin\phi-k_y)\right]^2+(J_T\cos\theta-k_z)^2}, \end{aligned} \tag{10}$$

where τ'' denotes the variables $\mathbf{\Omega}_i, \mathbf{p}_i, \phi_{12}, J_T, \theta, \phi$.

The integrals over J_T and $\cos\theta$ may now be performed using the delta functions, whence

$$\begin{aligned} N_{EJ}=&\frac{(2J+1)\hbar^2}{\sigma h^8}\int N_V\left[E-H(\mathbf{\Omega}_i,\mathbf{p}_i,\phi_{12},J\hbar,\theta=0,\phi)\right]\\ &\times\frac{|J\hbar-k_z|\,J\hbar}{(\cos\phi_{12}k_x+\sin\phi_{12}k_y)^2+(J\hbar-k_z)^2}d\phi d\phi_{12}\prod_{i=1}^{2}d\mathbf{\Omega}_i d\mathbf{p}_i. \end{aligned} \tag{11}$$

Two final observations permit the analytic evaluation of the ϕ and ϕ_{12} integrations in Eq. (11) and thus complete the reduction in dimensionality of the integral. Firstly, in the Appendix it is shown that the integrand of Eq. (11) is independent of ϕ and therefore one may integrate over ϕ yielding a factor of 2π. Next, in the Appendix it is also shown that the dependence of the integrand on the three variables ϕ_1, ϕ_2, and ϕ_{12} occurs only via $\phi_1 - \phi_{12}$ and $\phi_2 - \phi_{12}$. Therefore, one may choose ϕ_{12} in the integrand to have any constant value, labeled ϕ^*_{12}, and then integrate over ϕ_{12}, yielding a value of 2π[10]. These steps yield

$$N_{EJ} = \frac{(2J+1)}{\sigma h^6} \int N_V \left[E - H\left(\mathbf{\Omega}_i, \mathbf{p}_i, \phi^*_{12}, J\hbar, \theta = 0\right)\right] \times \frac{|J\hbar - k_z|\, J\hbar}{\left(\cos\phi^*_{12} k_x + \sin\phi^*_{12} k_y\right)^2 + \left(J\hbar - k_z\right)^2} \prod_{i=1}^{2} d\mathbf{\Omega}_i d\mathbf{p}_i. \tag{12}$$

The above expression is seen to involve only conventional coordinates. A Monte Carlo evaluation of this integral requires some treatment of the sampling limits (e.g., assigning some maximum values for the $\mathbf{p}_i$'s). In the next section it is shown how the integral in Eq. (12) may conveniently be transformed into a form where importance sampling can be used in the Monte Carlo evaluation, thereby eliminating the need for this specific consideration of maximum values.

III. FREE-ROTATION CANONICAL AVERAGE

The first step in simplifying the Monte Carlo evaluation of N_{EJ} is to remove the dependence of T^0_i, the kinetic energy of rotation of fragment i about its center of mass, on its orientation θ_i, ϕ_i, ψ_i. This step serves to make the evaluation of weighting factors more efficient in the importance sampling Monte Carlo integration to follow. To remove this orientation dependence of T^0_i the space-fixed $\mathbf{p}_i$ are first transformed to the three fragment i-fixed components of the angular momenta, $p_{a_i}, p_{b_i}, p_{c_i}$, defined by[9]

$$p_{a_i} = -\cos\psi_i \csc\theta_i p_{\phi_i} + \cos\psi_i \cot\theta_i p_{\psi_i} + \sin\psi_i p_{\theta_i},$$

$$p_{b_i} = \sin\psi_i \csc\theta_i p_{\phi_i} - \sin\psi_i \cot\theta_i p_{\psi_i} + \cos\psi_i p_{\theta_i}, \quad p_{c_i} = p_{\psi_i}. \tag{13}$$

In terms of these new momenta T_i^0 is given by

$$T_i^0 = \frac{p_{a_i}^2}{2I_{A_i}^\dagger} + \frac{p_{b_i}^2}{2I_{B_i}^\dagger} + \frac{p_{c_i}^2}{2I_{C_i}^\dagger}, \tag{14}$$

where $I_{A_i}^\dagger$, $I_{B_i}^\dagger$, and $I_{C_i}^\dagger$, are the principal moments of inertia of the rigid body fragment i for the transition state structure. The Jacobian of the transformation in Eq. (13) introduces a factor of $\sin\theta_1 \sin\theta_2$ into the integrand of Eq. (12).

The next step is to select an appropriate weighting function. We recall that in importance sampling[11] a weighting function is introduced which has a large weight in the regions where the integrand is large and also for which the integral over the desired coordinates is known. The function $\exp\left[-\beta\left(T_1^0 + T_2^0\right)\right] \sin\theta_1 \sin\theta_2$ is suitable, since β may be chosen to restrict the momenta coordinates to the region where the mean value of the kinetic part of H is less than E, the region of importance to the integrand given in Eq. (12). In addition, the integral of this function over $\mathbf{\Omega}_i$, p_{a_i}, p_{b_i}, p_{c_i}, for $i = 1,2$ (i.e., the coordinates which specify the orientation in space of each fragment and the body-fixed momenta of each fragment) is just h^6 times the product of the free-rotation canonical partition functions for the two fragments, Q_0, defined by

$$\begin{aligned} Q_0 &\equiv \frac{1}{h^6} \int \exp\left[-\beta\left(T_1^0 + T_2^0\right)\right] \prod_{i=1}^{2} d\cos\theta_i d\phi_i d\psi_i dp_{a_i} dp_{b_i} dp_{c_i} \\ &= 8\pi \left(k_B T/\hbar^2\right)^3 \prod_{i=1}^{2} \left(I_{A_i}^\dagger I_{B_i}^\dagger I_{C_i}^\dagger\right)^{1/2}. \end{aligned} \tag{15}$$

Making the transformation described in Eq. (13) and introducing the above weight function into Eq. (12) by multiplying the integrand by $\exp\left(\beta \sum_{i=1}^{2} T_i^0\right) \exp\left(-\beta \sum_{i=1}^{2} T_i^0\right)$, Eq. (12) for N_{EJ} becomes

$$N_{EJ} = \frac{(2J+1)\, J\hbar}{\sigma} Q_0 \left\langle \frac{N_V\left(E - H\right) \left|J\hbar - k_z\right| \exp\left[\beta\left(T_1^0 + T_2^0\right)\right]}{\left(\cos\phi_{12}^* k_x + \sin\phi_{12}^* k_y\right)^2 + \left(J\hbar - k_z\right)^2} \right\rangle, \tag{16}$$

where $\langle f \rangle$ denotes an average with respect to the free-rotation weight function,

$$\langle f \rangle = \int f \exp\left[-\beta\left(T_1^0 + T_2^0\right)\right] \prod_{i=1}^{2} d\cos\theta_i d\phi_i d\psi_i dp_{a_i} dp_{b_i} dp_{c_i} / Q_0 h^6. \tag{17}$$

For each sampling point the integrand f is set equal to zero whenever $H > E$.

A Monte Carlo evaluation of Eq. (16) is now straightforward using crude sampling for the orientational coordinates and importance sampling[11] for the momentum coordinates, with $\exp[-\beta(T_1^0 + T_2^0)]$ as the weighting function. This sampling using the free-rotation canonical distribution is most effective in those cases in which the potential energy is not too large in the regions of importance to the original integral. This situation corresponds to large values of $R^\dagger$, since the interaction potentials are smaller at large $R^\dagger$. However, in the present calculations it was observed that the free-rotation sampling was reasonably efficient at all E's and J's of interest (e.g., see discussion and Table 6.1 in the next section.)

IV. RESULTS AND DISCUSSION

The formalism described above for evaluating N_{EJ} was applied to the methyl radical recombination reaction (or ethane dissociation) using the same potential energy function as that employed by Wardlaw and Marcus.[4b] The structure of the rigid body fragments for a given $R^\dagger$ was taken to be as in Ref. 4b, and σ was taken to be 72.

The results for N_{EJ} are given in Table 6.1, together with the previous results of Ref. 4c, the latter multiplied by $(2J+1)/\sigma$, since the results reported there are actually $N_{EJ}\sigma/(2J+1)$ (cf. Footnote in Ref. 4d). Also, no $J = 0$ results are presented here since the transformation given by Eq. (8) is not valid in this special case. In the calculations 80,000 Monte Carlo points were used and typical computation times were only 10 to 15 minutes on a Vax 11/780. The sampling temperature was chosen to keep the maximum kinetic energy sampled one to two times the maximum available energy (E minus the minimum $V(R)$ for the given R, minus the zero-point energy difference), since this choice seemed to give the most rapid convergence. At small $R^\dagger$ there is a slower convergence of this particular importance sampling because of the increased importance of the potential energy term, although, as we have noted previously, we did not encounter any difficulty in our current calculations. Had such a difficulty been

encountered we could have used a sampling method analogous to the earlier one.[4]

Inspection of the results given in Table 6.1 indicates that both methods give equivalent numerical results.[12] As mentioned previously, the action-angle transformations are now avoided and an alternative method for handling the integration limits has been used. To be sure, the action-angle transformations are straightforward albeit a little tedious. It may also be possible to implement in the method of Wardlaw and Marcus the same idea of avoiding these integration limits, although this possiblity has not yet been explored. The present calculation is very easily programmed and implemented.

ACKNOWLEDGMENTS

It is a pleasure to acknowledge support of this research by the National Science Foundation. SJK gratefully acknowledges the support of a Natural Sciences and Engineering Research Council of Canada Postgraduate Scholarship, 1984 - 1987.

APPENDIX. DEPENDENCE OF THE INTEGRAND IN EQ. (11) ON ϕ, ϕ_i, AND ϕ_{12}

The Hamiltonian may be written as $H = T^0 + V$, where T^0 is the kinetic energy and V is the potential energy. The kinetic energy may be written as

$$T^0 = T_1^0 + T_2^0 + T_{12}^0, \tag{A1}$$

where T_{12}^0 is the kinetic energy of rotation of the line of centers about the overall center of mass and T_i^0 is given by Eq. (14) of the text. T_{12}^0 is given by

$$T_{12}^0 = \frac{1}{2I_{di}^\dagger}\left(p_{\theta_{12}}^2 + \frac{p_{\phi_{12}}^2}{\sin^2\theta_{12}}\right), \tag{A2}$$

where $I_{di}^\dagger$ is the "diatomic" moment of inertia for the centers of mass of the two fragments. Upon transforming to the variables appearing in Eq. (11) of the text, Eq. (A2) becomes

$$T_{12}^0 = \frac{1}{2I_{di}^\dagger}\left(\mathbf{J}_T - \mathbf{k}\right)^2 = \frac{1}{2I_{di}^\dagger}\left(J_T^2 + k_x^2 + k_y^2 + k_z^2 - 2J_T k_z\right), \tag{A3}$$

since $\mathbf{J_T}$ is chosen to have only one nonzero component, J_{Tz}.

We now consider how T^0 depends on the four variables ϕ, $\bar{\phi}_1 \equiv \phi_1 - \phi_{12}$, $\bar{\phi}_2 \equiv \phi_2 - \phi_{12}$, and ϕ_{12}. An inspection of Eqs (A1) - (A3) shows that $k_x^2 + k_y^2$ is the only quantity in T^0 which depends on the above angles. Referring to Eq. (9) of the text and focussing on the dependence of k_x and k_y on these above angles, it is seen that k_x and k_y may be written in the form

$$k_x = \sum_{i=1}^{2}\left(f_i\cos\phi_i + g_i\sin\phi_i\right) \tag{A4a}$$

$$k_y = \sum_{i=1}^{2}\left(f_i\sin\phi_i - g_i\cos\phi_i\right) \tag{A4b}$$

where f_i and g_i are functions of the remaining variables $(\theta_i, \psi_i, \mathbf{p}_i)$. Thereby, after some simplification

$$\begin{aligned} k_x^2 + k_y^2 =& f_1^2 + f_2^2 + g_1^2 + g_2^2 \\ &+ 2\left(f_1 f_2 + g_1 g_2\right)\cos\left(\phi_1 - \phi_2\right) + 2\left(g_1 f_2 - f_1 g_2\right)\sin\left(\phi_1 - \phi_2\right). \end{aligned} \tag{A5}$$

We note, too, that $\phi_1 - \phi_2$ can be written as $\bar{\phi}_1 - \bar{\phi}_2$. Thus, the T^0 in Eqs. (A1) is independent of ϕ_{12}. Also, Eqs. (A1) - (A3) and (A5) show that T^0 is also independent of ϕ.

It remains to be shown that the potential energy $V(\theta_i, \phi_i, \psi_i, \phi_{12}, \theta_{12})$ is independent of ϕ_{12} and ϕ when the $\bar{\phi}_i$ are introduced. This independence can be shown by first considering the dependence of θ_{12} on the variables ϕ_i, ϕ_{12} and ϕ, and then considering the dependence of the interatomic separation distances on these same variables.

We first note that θ_{12} depends on ϕ_{12} via the expression, obtained from a consideration of Eqs. (6) and (8) with $\sin\theta$ set to zero,

$$\theta_{12} = \cot^{-1}\left(\frac{k_x \cos\phi_{12} + k_y \sin\phi_{12}}{J_T - k_z}\right). \qquad (A6)$$

Use of the definitions of k_x and k_y and use of Eq. (A4) shows that an expression occurring in Eq. (A6), as well as in the Jacobian term in Eq. (11), may be written as

$$k_x \cos\phi_{12} + k_y \sin\phi_{12} = \sum_{i=1}^{2} \left(f_i \cos\bar{\phi}_i + g_i \sin\bar{\phi}_i\right). \qquad (A7)$$

Thus, θ_{12} is independent of ϕ and ϕ_{12} when written in terms of the $\bar{\phi}_i$'s.

The space-fixed coordinates $\mathbf{x}_i$ of a specific point in fragment i relative to the space-fixed coordinates of the center of mass of fragment i are given by $\mathbf{A}_i^{-1}\mathbf{x}_i'$, where the $\mathbf{x}_i'$ are the body-fixed coordinates of the point in fragment i and $\mathbf{A}_i^{-1}$ is the inverse rotation matrix[8] (using the convention in Ref. 8). The space-fixed coordinates of the center of mass of fragment i relative to a space-fixed origin at the overall center of mass are $\mathbf{A}_{12}^{-1}\mathbf{x}_{12,i}'$ where the $\mathbf{x}_{12,i}'$ are the coordinates describing the initial location (i.e., along the space-fixed z-axis) of the center of mass of fragment i, and $\mathbf{A}_{12}^{-1}$ is the inverse rotation matrix describing the orientation of the line of centers. Thereby,

$$\mathbf{x}_i = \mathbf{A}_i^{-1}\mathbf{x}_i' + \mathbf{A}_{12}^{-1}\mathbf{x}_{12,i}'. \qquad (A8)$$

The separation distance r_{12} between a point in fragment 1 and a point in fragment 2 is given by

$$r_{12}^2 = (\mathbf{x}_1 - \mathbf{x}_2) \cdot (\mathbf{x}_1 - \mathbf{x}_2) \qquad (A9)$$

Here, the observation is made that any inverse rotation matrix for rotation through $(\theta_i, \phi_i, \psi_i)$ may be written in the form[8] $\mathbf{A}_i^{-1} = \mathbf{D}_i^{-1}\mathbf{C}_i^{-1}\mathbf{B}_i^{-1}$, where all of the dependence of $\mathbf{A}_i^{-1}$ on ϕ_i is in the matrix $\mathbf{D}_i^{-1}$, which in turn is given by[8]

$$\mathbf{D}_i^{-1} = \begin{pmatrix} -\sin\phi_i & -\cos\phi_i & 0 \\ \cos\phi_i & -\sin\phi_i & 0 \\ 0 & 0 & 1 \end{pmatrix}. \qquad (A10)$$

Also, $\mathbf{A}_{12}^{-1}$ for rotation through (θ_{12}, ϕ_{12}) may be written in the form $\mathbf{A}_{12}^{-1} = \mathbf{D}_{12}^{-1}\mathbf{C}_{12}^{-1}$, where $\mathbf{D}_{12}^{-1}$ contains all the ϕ_{12} dependence and is given by Eq. (A10) with ϕ_i replaced by ϕ_{12}. Upon substituting Eqs. (A10) and (A8) into Eq. (A9) one finds after some straightforward algebraic manipulations that the separation distance r_{12} depends on the variables ϕ_i and ϕ_{12} only through the variables $\bar{\phi}_i$ and is independent of ϕ. Thus, all the quantities in Eq. (11) have now been shown to be independent of ϕ and of ϕ_{12} when written in terms of the $\bar{\phi}_i$'s.

REFERENCES

[1] F. F. Crim, Annu. Rev. Phys. Chem. **35**, 657 (1984); T. R. Rizzo and F. F. Crim, J. Chem. Phys. **76**, 2754 (1982); T. R. Rizzo, C. C. Hayden, and F. F. Crim, Far. Disc. Chem. Soc. **75**, 223 (1983); T. R. Rizzo, C. C. Hayden, and F. F. Crim, J. Chem. Phys. **81**, 4501 (1984); H.-R. Dübal and F. F. Crim, *ibid.* **83**, 3863 (1985); E. S. McGinley and F. F. Crim, *ibid.* **85**, 5741, 5748 (1986); L. J. Butler, T. M. Ticich, M. D. Likar, and F. F. Crim, *ibid.* **85**, 2331 (1986); T. R. Ticich, T. R. Rizzo, H.-R. Dübal, and F. F. Crim, *ibid.* **84**, 1508 (1986); J. Syage, W. R. Lambert, P. M. Felker, A. H. Zewail, and R. M. Hochstrasser, *Chem. Phys. Lett.* **88**, 266 (1982); J. F. Shepanski, B. W. Keelan, and A. H. Zewail, *ibid.* **103**, 9 (1983); J. L. Knee, L. R. Khundkar, and A. H. Zewail, J. Chem. Phys. **82**, 4715 (1985); J. L. Knee, L. R. Khundkar, and A. H. Zewail, *ibid.* **83**, 1996 (1985); J. L. Knee, L. R. Khundkar, and A. H. Zewail, *J. Phys. Chem.* **89**, 4659 (1985); N. F. Scherer, J. L. Knee, D. D. Smith, and A. H. Zewail, *ibid.* **89**, 5141 (1985); N. F. Scherer, F. E. Doany, A. H. Zewail, and J. W. Perry, *J. Chem. Phys.* **84**, 1932 (1986); L. R. Khundkar, J. L. Knee, and A. H. Zewail, *ibid.* **87**, 77 (1987); N. F. Scherer and A. H. Zewail, *ibid.* **87**, 97 (1987); J. L. Knee, L. R. Khundkar, and A. H. Zewail, *ibid.* **87**, 115 (1987); I. Nadler, J. Pfab, G. Radhakrishnan, H. Reisler, and C. Wittig, *ibid.* **79**, 2088 (1983); I. Nadler, J. Pfab, H. Reisler, and C. Wittig, *ibid.* **81**, 653, (1984); I. Nadler, M. Noble, H. Reisler, and C. Wittig, *ibid.* **82**, 2608 (1985); C. Wittig, I. Nadler, H. Reisler, M. Noble, J. Catanzarite, and G. Radhakrishnan, *ibid.* **83**, 5581 (1985); C. X. W. Qian, M. Noble, I. Nadler, H. Reisler, and C. Wittig, *ibid.* **83**, 5573 (1985); N. Nakashima, N. Shimo, N. Ikeda, and K. Yoshihara, *ibid.* **81**, 3738 (1984); N. Ikeda, N. Nakashima, and K. Yoshihara, *ibid.* **82**, 5285 (1985); D. J. Bamford, S. V. Filseth, M. F. Foltz, J. W. Hepburn, and C. B. Moore, *ibid.* **82**, 3032 (1985); D. J. Nesbitt, H. Petek, M. F. Foltz, S. V. Filseth, D. J. Bamford, and C. B. Moore, *ibid.* **83**, 223 (1985); H. L.

Dai, R. W. Field, and J. L. Kinsey, *ibid.* **82**, 1606 (1985); A. Amirav and J. Jortner, Chem. Phys. Lett. **95**, 295 (1983); J. Troe, A. Amirav, and J. Jortner, *ibid.* **115**, 245 (1985); H. Hippler, K. Luther, J. Troe, and H. J. Wendelken, J. Chem. Phys. **79**, 239 (1983).

[2] R. Viswanathan, L. M. Raff, and D. L. Thompson, J. Chem. Phys. **81**, 3118 (1984); R. Viswanathan, L. M. Raff, and D. L. Thompson, *ibid.* **81**, 828 (1984); R. J. Duchovic and W. L. Hase, *ibid.* **82**, 3599 (1985); W. L. Hase and R. J. Duchovic, *ibid.* **83**, 3448 (1985); W. L. Hase, S. L. Mondro, R. J. Duchovic, and D. M. Hirst, J. Am. Chem. Soc. **109**, 2916 (1987); T. Uzer, J. T. Hynes, and W. P. Reinhardt, Chem. Phys. Lett. **117**, 600 (1985); T. Uzer, J. T. Hynes, and W. P. Reinhardt, J. Chem. Phys. **85**, 5791 (1986).

[3] M. Quack and J. Troe, Ber. Bunsenges. Phys. Chem. **78**, 240 (1974); M. Quack and J. Troe, *ibid.* **79**, 170 (1975); M. Quack and J. Troe, *ibid.* **81**, 329 (1977); J. Troe, J. Chem. Phys. **75**, 226 (1981); J. Troe, *ibid.* **79**, 6017 (1983); C. J. Cobos and J. Troe, Chem. Phys. Lett. **113**, 419 (1985); C. J. Cobos and J. Troe, J. Chem. Phys. **83**, 1010 (1985); J. Troe, J. Phys. Chem. **90**, 3485 (1986); L. Brouwer, C. J. Cobos, J. Troe, H.-R. Dübal, and F. F. Crim, J. Chem. Phys. **86**, 6171 (1987).

[4] (a) D. M. Wardlaw and R. A. Marcus, Chem. Phys. Lett. **110**, 230 (1984); (b) D. M. Wardlaw and R. A. Marcus, J. Chem. Phys. **83**, 3462 (1985); (c) D. M. Wardlaw and R. A. Marcus, J. Phys. Chem. **90**, 5383 (1986); (d) D. M. Wardlaw and R. A. Marcus, Adv. Chem. Phys. *in press.*

[5] P. J. Robinson and K. A. Holbrook, *Unimolecular Reactions* (Wiley, New York, 1972); W. Forst, *Theory of Unimolecular Reactions* (Academic, New York, 1973); R. E. Weston and H. A. Schwarz, *Chemical Kinetics* (Prentice-Hall, Englewood Cliffs, NJ, 1972); R. A. Marcus, J. Chem. Phys. **20**, 359 (1952); R. A. Marcus and O. K. Rice, J. Phys. Colloid. Chem. **55**, 894 (1951); R. A. Marcus, J. Chem. Phys. **43**, 2658 (1965); R. A. Marcus, *ibid.*

52, 1018 (1970).

[6] S. J. Klippenstein and R. A. Marcus, J. Chem. Phys. **87**, 3410 (1987).

[7] When the energies of interest are so large as to make a direct count algorithm inside a Monte Carlo routine too time consuming one may instead calculate and store an array of $N_V(E)$ values for all the energies of interest. E.g., see Appendix F of Ref. 4b.

[8] H. Goldstein, *Classical Mechanics*, 2nd ed. (Addison-Wesley, Reading, MA 1980). The "y-convention" given there in Appendix B is used here. There is a typo in the last row of the rotation matrix **A** there, namely, the ψ's should be replaced by ϕ's.

[9] I. N. Levine, *Molecular Spectroscopy*, (Wiley, New York, 1975).

[10] More precisely, one transforms to variables $\phi_{12}, \bar{\phi}_i = \phi_i - \phi_{12} (i = 1,2)$ and then, after the ϕ_{12} integration, transforms the $\bar{\phi}_i$ back to the ϕ_i with ϕ_{12} set at any preassigned value ϕ_{12}^*.

[11] J. P. Valleau and S. G. Whittington, in *Statistical Mechanics*, edited by B. J. Berne (Plenum, New York, 1977); p. 137; J. P. Valleau and G. M. Torrie, in *Statistical Mechanics*, edited by B. J. Berne (Plenum, New York, 1977); p. 169.

[12] The minor differences at higher energies corresponding to smaller $R^\dagger$'s are most likely due to the *ad hoc* 'dynamic' barrier restriction in the Monte Carlo sampling procedure which was used in Ref. 4c (see footnote (15) there) but not here. Also, the Monte Carlo errors in the present calculation are larger at these higher energies.

Table 6.1: Test of N_{EJ}. Calculation for the Reaction $2CH_3 \rightarrow C_2H_6$

$E - E_{ZP}(\infty)^a$ kcal mol^{-1}	J $\hbar$	$R^\dagger$ Å	N_{EJ}^b	N_{EJ}^c
0.13	25	5.7	1.4	1.7
0.44	25	5.6	1.4 (3)	1.4 (3)
1.18	25	5.6	4.5 (4)	4.4 (4)
	50	4.4	1.1 (4)	1.1 (4)
2.36	25	3.8	4.4 (5)	4.3 (5)
	50	4.0	2.7 (5)	2.8 (5)
4.73	25	3.6	4.3 (6)	4.2 (6)
	50	3.6	4.2 (6)	4.1 (6)
	100	3.7	1.5 (5)	1.4 (5)
9.53	25	3.3	7.5 (7)	7.1 (7)
	50	3.4	9.4 (7)	8.8 (7)
	100	3.4	1.7 (7)	1.7 (7)
19.55	25	3.1	3.1 (9)	3.4 (9)
	50	3.1	5.0 (9)	4.9 (9)
	100	3.1	1.9 (9)	1.8 (9)
	150	3.1	1.1 (8)	1.0 (8)
39.10	25	2.8	3.6 (11)	3.7 (11)
	50	2.8	6.9 (11)	6.7 (11)
	100	2.8	4.1 (11)	4.2 (11)
	150	2.8	6.4 (10)	6.7 (10)
63.52	25	2.6	1.6 (13)	2.0 (13)
	50	2.6	4.3 (13)	3.9 (13)
	100	2.6	3.5 (13)	2.8 (13)
	150	2.6	8.5 (12)	7.9 (12)

[a] $E_{ZP}(\infty)$ refers to the zero-point energy of the products (i.e., the zero point energy of two isolated CH_3 fragments.)

[b] Present calculations of N_{EJ}. The numbers in parentheses denote the power of 10. Monte Carlo errors are in all cases less than 7%, with the largest error bars arising in the highest energy calculations.

[c] N_{EJ} taken from Ref. 4c.

Chapter 7: Unimolecular Reaction Rate Theory for Highly Flexible Transition States. II. Conventional Coordinate Formulae for the Various Possible Fragment Combinations. Miscellaneous Topics

[The text of this chapter is in press and will appear in: S. J. Klippenstein and R. A. Marcus, J. Phys. Chem. (1988).]

ABSTRACT

A method for using conventional coordinates in the implementation of RRKM theory for unimolecular dissociations was described in part I of this series, for the case where both fragment molecules are nonlinear. The corresponding formalism for all possible types of fragments, atomic, linear and nonlinear fragments and their combinations, is presented here. Also discussed analytically is the tendency, in a unimolecular dissociation, for the position of the transition state to move to shorter fragment-fragment separation distances with increasing total energy E. This tendency has marked consequences, including increasing deviation of rate constants from those of phase space theory with increasing E and, in the case of fragment-fragment recombination, a corresponding tendency for high-pressure rate constants to decrease with increasing temperature. Two other topics considered in this paper are the case of two minima in the variational calculation, and the role of the repulsive potential energy curves in the unimolecular dissociations under consideration.

I. INTRODUCTION

The number of states $N_{EJ}(R)$ for a given excess energy E, total angular momentum quantum number J, and position along a reaction coordinate enters into the RRKM theory[1] of unimolecular dissociations. With a sufficiently accurate determination of this quantity and of the density of states ρ_{EJ} of the molecule itself, good agreement between theoretically and experimentally determined rate constants k_{EJ} is anticipated, as long as the statistical assumption is valid. For k_{EJ} we have

$$k_{EJ} = N_{EJ}(R^\dagger)/h\rho_{EJ}, \tag{1}$$

where $R^\dagger$ is variationally determined. (A correction for nuclear tunneling along the reaction coordinate, a rare circumstance in dissociations into two polyatomic fragments, may be found in Ref. 2.)

One facet of an accurate treatment of $N_{EJ}(R)$ is the manner in which the "transitional" modes are treated. These transitional modes are those modes which undergo a considerable change in character during the transformation from reactants to products. In particular these modes are typically the bending/hindered rotor and overall rotational modes of the reactant which change to free rotations and to translations of the products. The remaining modes (apart from the reaction coordinate) have been termed the "conserved" modes, and are typically vibrations in both the reactant and product configurations.

Recently, Wardlaw and Marcus[3] described a method for treating the transitional mode interactions within a *classical* framework, while retaining a *quantum* treatment for the conserved modes. The method of Ref. 3 for determining $N_{EJ}(R)$ was based on the approximate separation of variables into the transitional modes and conserved modes described above, with a transformation of variables to canonically conjugate action-angle variables being used for the transitional modes. That method also implicitly assumed a reaction coordinate defined by the center of mass to center of mass separation distance of the two fragments. Subsequently the present authors calculated the effect of using a

quantum mechanical treatment of the transitional modes on thermally averaged rate constants.[4] This calculation was performed via a Feynman path integration of partition function ratios. It indicated, at least for the reaction studied, the $C_2H_6 \rightarrow 2CH_3$ dissociation reaction, that the quantum mechanical correction for the transitional modes was negligible at the temperatures investigated.

The present authors have also shown in part I[5] how conventional coordinates could be used to implement RRKM theory in a formalism based on the same separation of variables as that of Ref. 3. The formalism presented in part I was for the specific case of two nonlinear fragments. In the present article expressions are given for the determination of N_{EJ} for the various other possible fragment-fragment cases which arise in practice. In section II a brief summary of the derivation of N_{EJ}'s in terms of conventional coordinates is given. In section III the definition of certain quantities needed in the evaluation of $N_{EJ}(R)$ and which are specific to the given fragment type are given. In particular the detailed formulae pertaining to the cases of an atomic fragment, a linear fragment, and a nonlinear fragment are considered. In section IV a particular phenomenon is discussed in which the position of the transition state tends to move to shorter fragment-fragment separation distance with increasing total energy. Its consequences are also described there. In section V a third topic is considered: the case of two minima in the plot of the number of states versus reaction coordinate curve, in particular the results which we have obtained in a practical case. In section VI the role (or nonrole) of repulsive potential energy curves in the type of dissociation into two fragments that is being considered is discussed, together with the corresponding question in phase space theory[6] (PST). Concluding remarks follow in section VII.

II. THEORY

Conventional coordinates were introduced in part I instead of the action-angle coordinates used earlier[3] in calculating N_{EJ}. The reaction coordinate R in part I was again taken to be the the center-of-mass to center-of-mass separation

distance between the two fragments. The approximate separation of variables into the conserved modes and the transitional modes, which was the basis of the previous method,[3] results in the number of states being given by the convolution

$$N_{EJ}(R) = \int_0^E N_V\,(E-\epsilon)\,\rho_J\,(\epsilon)\,d\epsilon, \tag{2}$$

where $N_V(E-\epsilon)$ is the number of quantum states for the conserved modes with an energy less than or equal to $E-\epsilon$, and $\rho_J(\epsilon)$ is the density of states for the transitional modes at the given energy ϵ and total angular momentum quantum number J for the given R.

The evaluation of $\rho_J(\epsilon)$ involves the choice of a coordinate system. The appropriate coordinate system depends upon whether the fragments have zero, two, or three rotational degrees of freedom. However, in all cases the rotation of the line of centers connecting the two centers of masses of the fragments is a two degree of freedom rotation and so may be described by the coordinates θ_{12} and ϕ_{12} defining the spatial orientation of this line of centers. For the other coordinates, the case of two nonlinear polyatomic fragments (i.e., each a three-dimensional rotor) was considered in part I, and the coordinates chosen were for the *absolute* orientation in space of fragment i and were the conventional Euler angles[7]. If fragment i is, instead, linear, and so is a two-dimensional rotor, the appropriate coordinates for this fragment are the angles θ_i and ϕ_i, which describe the *absolute* orientation in space of the axis of this linear species. When fragment i is an atom no orientational coordinates are needed for it. The coordinates describing the orientation of fragment i are denoted $\mathbf{\Omega}_i$ and their conjugate momenta by $\mathbf{p}_i$, regardless of which type of fragment is being referred to.

With the above choice of coordinate system for the appropriate fragment cases, $\rho_J\,(\epsilon)$ is given, as in part I, by

$$\rho_J(\epsilon) = \frac{g_e}{\sigma h^{(n_1+n_2+2)}} \int \delta\left[\epsilon - H\,(\tau)\right] \hbar\delta\left[J\hbar - J_T\,(\tau)\right] d\tau\ , \tag{3}$$

where τ denotes the orientational coordinates $\mathbf{\Omega}_i$, θ_{12}, and ϕ_{12} and their conjugate momenta, and $d\tau$ denotes the corresponding phase space volume element.

The quantity J_T in Eq. (3) is the magnitude of the total angular momentum as a function of the coordinates, whereas J in the second delta function in Eq. (3) is the total angular momentum quantum number. The quantities n_1 and n_2 are the number of rotational degrees of freedom for fragments 1 and 2; g_e is the electronic degeneracy factor, and σ is the usual degeneracy factor for the fragment pair; and σ equals $2\sigma_1\sigma_2$ or $\sigma_1\sigma_2$, according as the fragments are or are not identical; σ_i denotes the symmetry number of fragment i. The Hamiltonian H is given by $H = T^0 + V$, where V is the potential energy and T^0 the total kinetic energy for the transitional modes. T^0 in turn is given by the sum of T^0_{12}, the kinetic energy for the line of centers rotation and the kinetic energies T^0_1 and T^0_2 of the two fragments. The former is given by

$$T^0_{12} = \frac{1}{2I^\dagger_{di}} \left(p^2_{\theta_{12}} + \frac{p^2_{\phi_{12}}}{\sin\theta^2_{12}} \right), \tag{4}$$

with $I^\dagger_{di}$ being the diatomic moment of inertia for the line of centers, i.e., $I^\dagger_{di}$ equals $M_1M_2R^2/(M_1 + M_2)$, where M_1 and M_2 are the masses of fragment 1 and 2, respectively. The kinetic energy T^0_i is given in section III for each of the separate fragment cases.

Substituting the above expression for $\rho_J(\epsilon)$ into Eq. (2) and performing the integration over ϵ yields

$$N_{EJ}(R) = \frac{g_e\hbar}{\sigma h^{(n_1+n_2+2)}} \int N_V\left[E - H\left(\tau\right)\right] \delta\left[J\hbar - J_T\left(\tau\right)\right] d\tau \ . \tag{5}$$

Equation (5) provides an expression for N_{EJ}. Next, the dimension of the phase space integral in Eq. (5) is reduced as in part I.

First, the angular momentum is fixed along the z-direction by introducing a delta function in $J_T - J_{T_z}$, multiplying by the range of J_{T_z}, $(2J+1)\hbar$, and then transforming from the line of centers coordinates and conjugate momenta to the Cartesian components of the orbital angular momentum (l_x, l_y, l_z) and the line of centers coordinate ϕ_{12}. This transformation is specified by[8]

$$l_x = -p_{\theta_{12}} \sin\phi_{12} - p_{\phi_{12}} \cos\phi_{12} \cot\theta_{12},$$

$$l_y = p_{\theta_{12}} \cos\phi_{12} - p_{\phi_{12}} \sin\phi_{12} \cot\theta_{12}, \quad l_z = p_{\phi_{12}}, \tag{6}$$

with the Jacobian of the transformation being given by

$$\begin{aligned} \left|\partial\left(\theta_{12} p_{\theta_{12}} p_{\phi_{12}}\right)/\partial\left(l_x l_y l_z\right)\right| &= \left|\sin^2\theta_{12}/p_{\phi_{12}}\right| \\ &= |l_z| \Big/ \left[\left(\cos\phi_{12} l_x + \sin\phi_{12} l_y\right)^2 + l_z^2\right]. \end{aligned} \tag{7}$$

With these results the expression for $N_{EJ}(R)$ becomes

$$\begin{aligned} N_{EJ}(R) =& \frac{g_e\,(2J+1)\,\hbar^2}{\sigma h^{(n_1+n_2+2)}} \\ &\times \int N_V\left[E - H\left(\tau'\right)\right] \frac{\delta\left[J\hbar - J_T\left(\tau'\right)\right] \delta\left[J_T\left(\tau'\right) - J_{Tz}\left(\tau'\right)\right] |l_z|}{\left(\cos\phi_{12} l_x + \sin\phi_{12} l_y\right)^2 + l_z^2} d\tau' \,, \end{aligned} \tag{8}$$

where τ' now denotes the coordinates $\mathbf{\Omega}_i, \mathbf{p}_i, \phi_{12}, l_x, l_y, l_z$, and $d\tau'$ is the corresponding volume element.

Next, a transformation is made from l_x, l_y, and l_z to J_T, θ, and ϕ, where the θ and ϕ are the polar coordinates of $\mathbf{J}_T$:

$$l_x + k_x = J_T \sin\theta\cos\phi, \quad l_y + k_y = J_T \sin\theta\sin\phi, \quad l_z + k_z = J_T \cos\theta. \tag{9}$$

Here, k_x, k_y and k_z are the Cartesian components of the sum of the space-fixed rotational angular momenta of the individual fragments $\mathbf{j}_i$ (e.g., $k_x = j_{x_1} + j_{x_2}$), which in turn are specified in section III for each of the fragment types. The Jacobian of the transformation in Eq. (9) is given by $\left|\partial\left(l_x l_y l_z\right)/\partial\left(J_T \theta\phi\right)\right| = J_T^2 \sin\theta$.

Integration in Eq. (8), using the delta functions, over J_T and θ and then over ϕ_{12} and ϕ, after considering the dependence of the resulting integral on the ϕ, ϕ_i and ϕ_{12} coordinates, yields

$$\begin{aligned} N_{EJ}(R) =& \frac{g_e\,(2J+1)}{\sigma h^{(n_1+n_2)}} \int N_V\left[E - H\left(\mathbf{\Omega}_i, \mathbf{p}_i, \phi_{12}^*, J\hbar, \theta = 0\right)\right] \\ &\times \frac{|J\hbar - k_z|\, J\hbar}{\left(\cos\phi_{12}^* k_x + \sin\phi_{12}^* k_y\right)^2 + \left(J\hbar - k_z\right)^2} \prod_{i=1}^{2} d\mathbf{\Omega}_i d\mathbf{p}_i. \end{aligned} \tag{10}$$

The quantity ϕ_{12}^* defines a fixed azimuthal angle for the line of centers orientation and can be set equal to zero (i.e., $\phi_{12} = \phi_{12}^* = 0$), as was shown in part I.

The integration over the delta functions also results in expressions for the quantities l_x, l_y, and l_z in terms of the coordinates and momenta $\mathbf{\Omega}_i$ and $\mathbf{p}_i$ (or alternatively the k's). These expressions, in turn, specify the quantities θ_{12}, ϕ_{12}, $p_{\theta_{12}}$, and $p_{\phi_{12}}$ in terms of the k's, ϕ_{12}^* and J_T. More specifically, the coordinates for the orientation of the line of centers (θ_{12}, ϕ_{12}) and their conjugate momenta are specified to be

$$\theta_{12} = \cot^{-1}\left(\frac{k_x \cos\phi_{12}^* + k_y \sin\phi_{12}^*}{J_T - k_z}\right) \ , \phi_{12} = \phi_{12}^*$$
$$p_{\theta_{12}} = k_x \sin\phi_{12}^* - k_y \cos\phi_{12}^* \ , p_{\phi_{12}} = J_T - k_z \ . \tag{11}$$

The expressions given in Eq. (11) are used in all terms in the final integral involving these quantities, e.g., in T_{12}^0 and in the expressions for the determination of the potential energy given in section III.

With these definitions, Eq. (10) for N_{EJ} provides an expression which can be used for all possible fragment types. By combining Eq. (10) with the definitions of the various fragment-dependent quantities given in section III an explicit expression is obtained for N_{EJ} for each fragment case. The integral in Eq. (10) may be evaluated through Monte Carlo importance sampling by introducing the weighting function $\exp(-\beta T_1^0)\exp(-\beta T_2^0)$. The integral over this weighting function is given by the product $Q_1^0 Q_2^0$ of the free-rotation canonical partition functions for each fragment, 1 and 2. The result of the introduction of this weighting function and a transformation of momenta variables to $\mathbf{p}_i'$, defined in section III for each of the different types of fragments, yields N_{EJ} in the form

$$N_{EJ}(R) = \frac{g_e\,(2J+1)\,J\hbar}{\sigma} Q_1^0 Q_2^0 \left\langle \frac{N_V\,(E-H)\,(J\hbar - k_z)\exp\left[\beta\left(T_1^0 + T_2^0\right)\right]}{\left(\cos\phi_{12}^* k_x + \sin\phi_{12}^* k_y\right)^2 + \left(J\hbar - k_z\right)^2} \right\rangle , \tag{12}$$

where $\langle f \rangle$ denotes an average with respect to the free-rotation weight function,

$$\langle f \rangle = \frac{1}{Q_1^0 Q_2^0 h^{(n_1+n_2)}} \int f \exp\left[-\beta\left(T_1^0 + T_2^0\right)\right] \prod_{i=1}^{2} d\mathbf{\Omega}_i d\mathbf{p}_i' \left|\frac{\partial \mathbf{p}_i}{\partial \mathbf{p}_i'}\right| . \tag{13}$$

In Eq. (13) $|\partial \mathbf{p}_i/\partial \mathbf{p}'_i|$ is the Jacobian of the transformation to be given in section III. The explicit definitions of the partition functions Q_i^0 and fragment kinetic energies T_i^0 for the specific cases are also given in section III.

The β in Eqs. (12) and (13) equals $1/k_B T$, where T is a sampling temperature and k_B is Boltzmann's constant. In the calculation this T is chosen to ensure that the maximum kinetic energy sampled is about two to three times the maximum available energy.

N_{EJ} may now be straightforwardly evaluated from Eq. (12) by using, as in part I, crude sampling over all space for the orientational coordinates and importance sampling[9] for the momentum coordinates, with $\exp[-\beta(T_1^0 + T_2^0)]$ as the weighting function. In the importance sampling over the momentum coordinates, step sizes which gave a roughly 50 % acceptance ratio were typically used in the applications in part I and Ref. 10.

III. PROPERTIES OF DIFFERENT FRAGMENTS

(a) General Formulae

We consider here the calculation of the potential energy $V(\mathbf{r}_{i,j})$, where $\mathbf{r}_{i,j}$ denotes the space-fixed position of atom j in fragment i, in terms of the orientational coordinates $\mathbf{\Omega}_i$, θ_{12} and ϕ_{12}, and the reaction coordinate R. The position $\mathbf{r}_{i,j}$ of atom j in fragment i may be written in terms of its position in space relative to the center-of-mass of fragment i, and in terms of the position of the center-of-mass of fragment i in space. This latter position is determined by the orientation of the line of centers connecting the two fragments and by the center-of-mass to center-of-mass separation distance. In particular, this position may be written as $\mathbf{A}_{12}^{-1}(\theta_{12}, \phi_{12})\mathbf{r}'_i$, where[7]

$$\mathbf{A}_{12}^{-1}(\theta_{12}, \phi_{12}) = \begin{pmatrix} \cos\theta_{12}\cos\phi_{12} & -\sin\phi_{12} & \sin\theta_{12}\cos\phi_{12} \\ \cos\theta_{12}\sin\phi_{12} & \cos\phi_{12} & \sin\theta_{12}\sin\phi_{12} \\ -\sin\theta_{12} & 0 & \cos\theta_{12} \end{pmatrix}, \qquad (14)$$

and $\mathbf{r}'_i$ is the body-fixed position of the center of mass of fragment i,

$$\mathbf{r}'_1 = (0, 0, \frac{M_2}{M_1 + M_2} R), \quad \mathbf{r}'_2 = (0, 0, -\frac{M_1}{M_1 + M_2} R), \qquad (15)$$

and the axis of the body in space is defined by θ_{12} and ϕ_{12}. The position of the center-of-mass as a whole, as seen from Eq. (15), is chosen to be at the origin.

The position of atom j of fragment i in space relative to the center-of-mass of fragment i can be written as $\mathbf{A}_i^{-1}(\mathbf{\Omega}_i)\mathbf{r}'_{i,j}$, where the $\mathbf{r}'_{i,j}$ are the body-fixed coordinates which describe the initial position (prior to any rotations) of atom j in fragment i, relative to the center of mass of fragment i. The orientation of the body-fixed axes of fragment i relative to the space-fixed Cartesian axes is defined by the $\mathbf{\Omega}_i$ coordinates. The specific form of the inverse rotation matrix $\mathbf{A}_i^{-1}(\mathbf{\Omega}_i)$ describing this orientation of the body-fixed axes is discussed later for different types of the fragment.

Thus, finally we have

$$\mathbf{r}_{i,j} = \mathbf{A}_i^{-1}(\mathbf{\Omega}_i)\mathbf{r}'_{i,j} + \mathbf{A}_{12}^{-1}(\theta_{12}, \phi_{12})\mathbf{r}'_i \ . \tag{16}$$

In sections III(b) to (d) the detailed expressions involved in the determination of N_{EJ} for the different types of fragments are given.

(b) Atomic Fragment

When fragment i is an atom rather than a molecule there are no orientational coordinates or rotational momenta for this fragment and so the quantities T_i^0, j_{x_i}, j_{y_i}, j_{z_i}, and n_i are all replaced by zero. The matrix $\mathbf{A}_i^{-1}$ is replaced by the 3 by 3 identity matrix. Also, the free-rotation canonical partition function Q_i^0 is replaced by unity and the differentials $d\mathbf{\Omega}_i$, $d\mathbf{p}_i$, and $d\mathbf{p}'_i$ do not appear. The body-fixed coordinates for the atomic fragment i, $\mathbf{r}'_{i,1}$, are just the coordinates of the origin (the center of fragment i), i.e., $\mathbf{r}'_{i,1} = (0,0,0)$.

(c) Linear Fragment

When fragment i is linear, the orientational coordinates are chosen to be the spherical polar angles θ_i and ϕ_i. Their conjugate momenta are denoted by p_{θ_i} and p_{ϕ_i}, respectively. The transformed momenta are given by $\mathbf{p}'_i = (p_{a_i}, p_{b_i})$ with $p_{a_i} = -p_{\phi_i}/\sin\theta_i$ and $p_{b_i} = p_{\theta_i}$. The Jacobian $|\partial\mathbf{p}_i/\partial\mathbf{p}'_i|$ is thus equal to $\sin\theta_i$.

The kinetic energy for fragment i is given in terms of these transformed momenta by

$$T_i^0 = \left(p_{a_i}^2 + p_{b_i}^2\right)/2I_i^\dagger, \tag{17}$$

where $I_i^\dagger$ is the moment of inertia for fragment i in its transition state structure. For a diatomic fragment we have, for example, $I_i^\dagger = m_1 m_2 r_e^2(R)/(m_1 + m_2)$, where m_1 and m_2 are the masses of the two atoms in the diatomic fragment and $r_e(R)$ is the equilibrium separation distance between the two atoms for the given separation distance R between the centers of masses of the two fragments.

The Cartesian components of the space-fixed rotational angular momentum for fragment i, j_{x_i}, j_{y_i} and j_{z_i} are now given by[8]

$$\begin{aligned} j_{x_i} &= -p_{\phi_i}\cos\phi_i\cos\theta_i/\sin\theta_i - p_{\theta_i}\sin\phi_i \\ j_{y_i} &= -p_{\phi_i}\sin\phi_i\cos\theta_i/\sin\theta_i + p_{\theta_i}\cos\phi_i \\ j_{z_i} &= p_{\phi_i}. \end{aligned} \tag{18}$$

The inverse rotation matrix $\mathbf{A}_i^{-1}(\mathbf{\Omega}_i)$ used to determine the transformation from orientational coordinates to space-fixed coordinates is given by[7]

$$\mathbf{A}_i^{-1}(\mathbf{\Omega}_i) = \begin{pmatrix} \cos\theta_i\cos\phi_i & -\sin\phi_i & \sin\theta_i\cos\phi_i \\ \cos\theta_i\sin\phi_i & \cos\phi_i & \sin\theta_i\sin\phi_i \\ -\sin\theta_i & 0 & \cos\theta_i \end{pmatrix}. \tag{19}$$

The initial body-fixed coordinates $\mathbf{r}'_{i,j}$ of atom j in fragment i must be aligned in agreement with the definition of the Cartesian components of the angular momenta given in Eq. (18). For this reason the axis of the linear fragment for these initial coordinates $\mathbf{r}'_{i,j}$ is aligned along the space-fixed z-axis, and the center of mass of $\mathbf{r}'_{i,j}$ is placed at the origin. For the specific case of a diatomic fragment the body-fixed coordinates $\mathbf{r}'_{i,j}$ are thus given as

$$\begin{aligned} \mathbf{r}'_{i,1} &= \left(0, 0, \frac{m_2}{m_1 + m_2} r_e(R)\right) \\ \mathbf{r}'_{i,2} &= \left(0, 0, \frac{-m_1}{m_1 + m_2} r_e(R)\right). \end{aligned} \tag{20}$$

The free-rotation canonical partition function for use in the averaging in Eq. (12) is[11]

$$\begin{aligned} Q_i^0 &\equiv \frac{1}{h^2} \int \exp\left(-\beta T_i^0\right) \sin\theta_i d\mathbf{\Omega}_i d\mathbf{p}_i' \\ &= 2I_i^\dagger k_B T/\hbar^2, \end{aligned} \tag{21}$$

where no degeneracy factor need be included in a partition function used purely for averaging.

(d) Nonlinear Fragment

When fragment i is nonlinear, the treatment is analogous to that given previously in part I, where the dissociation into two nonlinear fragments was treated. The results are given here for completeness. The orientational coordinates are taken to be the Euler angles θ_i, ϕ_i, and ψ_i. Their conjugate momenta are then denoted by p_{θ_i}, p_{ϕ_i}, and p_{ψ_i}, respectively. The transformed momenta are given by $\mathbf{p}_i' = (p_{a_i}, p_{b_i}, p_{c_i})$ with[8]

$$\begin{aligned} p_{a_i} &= -\cos\psi_i \csc\theta_i p_{\phi_i} + \cos\psi_i \cot\theta_i p_{\psi_i} + \sin\psi_i p_{\theta_i}, \\ p_{b_i} &= \sin\psi_i \csc\theta_i p_{\phi_i} - \sin\psi_i \cot\theta_i p_{\psi_i} + \cos\psi_i p_{\theta_i}, \\ p_{c_i} &= p_{\psi_i}. \end{aligned} \tag{22}$$

The Jacobian $!\partial\mathbf{p}_i/\partial\mathbf{p}_i'|$ is then equal to $\sin\theta_i$.

For the kinetic energy of fragment i the specific expression depends on whether the fragment is an asymmetric top, a symmetric top, or a spherical top. Since all cases are included in the asymmetric top expression, we employ it. In terms of the transformed momenta $\mathbf{p}_i'$, this kinetic energy is given by[8]

$$T_i^0 = \frac{p_{a_i}^2}{2I_{A_i}^\dagger} + \frac{p_{b_i}^2}{2I_{B_i}^\dagger} + \frac{p_{c_i}^2}{2I_{C_i}^\dagger}, \tag{23}$$

where $I_{A_i}^\dagger$, $I_{B_i}^\dagger$, and $I_{C_i}^\dagger$, are the principal moments of inertia of fragment i for the transition state structure.

The Cartesian components of the space-fixed rotational angular momentum for fragment i, j_{x_i}, j_{y_i} and j_{z_i} are given in terms of the transformed momenta $\mathbf{p}'_i$ by

$$j_{x_i} = (\cos\theta_i \cos\phi_i \cos\psi_i - \sin\phi_i \sin\psi_i)\, p_{a_i} - (\cos\theta_i \cos\phi_i \sin\psi_i + \sin\phi_i \cos\psi_i)\, p_{b_i} + \sin\theta_i \cos\phi_i p_{c_i}$$

$$j_{y_i} = (\cos\theta_i \sin\phi_i \cos\psi_i + \cos\phi_i \sin\psi_i)\, p_{a_i} + (\cos\phi_i \cos\psi_i - \cos\theta_i \sin\phi_i \sin\psi_i)\, p_{b_i} + \sin\theta_i \sin\phi_i p_{c_i}$$

$$j_{z_i} = -\sin\theta_i \cos\psi_i p_{a_i} + \sin\theta_i \sin\psi_i p_{b_i} + \cos\theta_i p_{c_i} \tag{24}$$

The inverse rotation matrix $\mathbf{A}_i^{-1}(\mathbf{\Omega}_i)$ used to determine the transformation from orientational coordinates to space fixed coordinates is given by[7]

$$\mathbf{A}_i^{-1}(\mathbf{\Omega}_i) =$$

$$\begin{pmatrix} -\sin\psi_i \sin\phi_i + \cos\theta_i \cos\phi_i \cos\psi_i & -\cos\psi_i \sin\phi_i - \cos\theta_i \cos\phi_i \sin\psi_i & \sin\theta_i \cos\phi_i \\ \sin\psi_i \cos\phi_i + \cos\theta_i \sin\phi_i \cos\psi_i & \cos\psi_i \cos\phi_i - \cos\theta_i \sin\phi_i \sin\psi_i & \sin\theta_i \sin\phi_i \\ -\cos\psi_i \sin\theta_i & \sin\psi_i \sin\theta_i & \cos\theta_i \end{pmatrix}. \tag{25}$$

The initial body-fixed coordinates $\mathbf{r}'_{i,j}$ must be aligned in agreement with the definition of the Cartesian components of the angular momenta given in Eq. (24). Thus, the principal axes a, b, and c for these body-fixed coordinates $\mathbf{r}'_{i,j}$ are aligned along the space-fixed x, y, and z axes, respectively. Additionally, the center of mass of $\mathbf{r}'_{i,j}$ is at the origin.

The definition of the free-rotation canonical partition function for use in the averaging is[11]

$$\begin{aligned} Q_i^0 &\equiv \frac{1}{h^3} \int \exp\left(-\beta T_i^0\right) \sin\theta_i d\mathbf{\Omega}_i d\mathbf{p}'_i \\ &= \left(8\pi I_i^{A\dagger} I_i^{B\dagger} I_i^{C\dagger}\right)^{1/2} (k_B T)^{3/2} / \hbar^3. \end{aligned} \tag{26}$$

IV. TREND OF $R^\dagger$ WITH INCREASING ENERGY E

In several calculations[3,5,10,12,13] we and others have noticed a tendency of $R^\dagger$, the fragment-fragment separation distance in the transition state, to decrease

with increasing energy E. This effect has certain important consequences, which we describe after first considering its origin analytically.

The position $R^\dagger$ of the transition state is the solution of

$$\partial N_{EJ}(R^\dagger)/\partial R^\dagger = 0, \tag{27}$$

which yields, implicitly, $R^\dagger$ as a function of E. We may write the left hand side as a function $f(R^\dagger, E)$ and note that in the standard way the ordinary derivative $dR^\dagger/dE$ is given by

$$dR^\dagger/dE = -(\partial f/\partial E)/(\partial f/\partial R^\dagger). \tag{28}$$

But $\partial f/\partial R^\dagger$ equals $\partial^2 N_{EJ}(R^\dagger)/\partial R^{\dagger 2}$, and this quantity is positive since $N_{EJ}(R)$ is a minimum at $R = R^\dagger$. Further, upon interchanging the order of partial differentiation, $\partial f/\partial E$ can be written as $(\partial/\partial R^\dagger)(\partial N_{EJ}(R^\dagger)/\partial E)$, i.e., $(\partial/\partial R^\dagger)\rho^\dagger_{EJ}(R^\dagger)$, where $\rho^\dagger_{EJ}(R^\dagger)$ is the density of states, $\partial N_{EJ}(R)/\partial R$ of the transition state at $R = R^\dagger$ and at the energy E. It has usually been the case that since the hindered rotations at smaller R become free rotations at larger R and, hence, that the states become more closely spaced as R increases, $(\partial/\partial R^\dagger)\rho^\dagger_{EJ}(R^\dagger)$ tends to be positive. One circumstance could modify this. As R increases, there will be somewhat less energy available for distribution among the transitional modes, since the bonding potential energy of the fragments is less negative. This factor above would make $\partial\rho^\dagger_{EJ}(R^\dagger)/\partial R^\dagger$ negative, but apparently the first factor is the dominant one in the few cases we have considered thus far and for the limited energy range for which the model potential energy surfaces used are valid. At higher energies (e.g., above about 3000 cm^{-1} for the study of Ref. 10) the model potential energy surfaces are not accurate enough and so no conclusions may be drawn as to which of the above factors is the dominant one.

This result on $dR^\dagger/dE$ has some major implications: At very low energies E the $R^\dagger$ occurs at the $R \to \infty$ limit and phase space theory[6] (PST), and the variationally implemented RRKM theory become rather similar. However, with

increasing energy the overall minimum in the number of states $N_{EJ}(R^\dagger)$ occurs at R's which are less than the PST R_l's, where the latter denote the location of the orbital angular momentum (l)-dependent effective potential energy barriers. As a result, at these energies, when $dR^\dagger/dE$ is negative, there is increasing deviation between PST and variationally implemented RRKM theory. I.e., the transition state under these conditions becomes increasingly "tight." Again, in the case of fragment-fragment recombination this effect, when thermally averaged to yield a high pressure rate constant, yields an $R^\dagger$ which decreases as the temperature increases. Such an effect causes the high pressure recombination rate constant to decrease with increasing temperature.[3,4,12,13]

V. CASE OF TWO MINIMA IN THE $N_{EJ}(R)$ PLOT

From our previous calculations we have found that in a certain energy range there may be two local minima in the number of states. In particular, we have observed the following change in the plot of the number of states versus R as the energy E is increased above the dissociation limit: At low excess energies there is basically only one minimum (or smallest value) which occurs at $R^\dagger = \infty$. At slightly higher excess energies an inner minimum appears with this inner minimum being very shallow and having a much larger number of states than the $R^\dagger = \infty$ one. At still higher energies the number of states at the inner minimum begins to approach the number at the $R^\dagger = \infty$ minimum. Our potential energy surface needs improvement at smaller $R^\dagger$'s to see how the trend changes as E is increased further.

In the energy region where there are two transition states it is useful to consider the modified formalism resulting from the two transition states which act in series. In the case of the recently studied NCNO dissociation reaction,[10] N_{EJ}^{max} typically proved to be a small maximum relative to the larger value of the number of states occurring at each of the two minima, i.e., $N_{EJ}^{max} \approx max(N_{EJ}^1, N_{EJ}^2)$, where N_{EJ}^1, and N_{EJ}^2 are the number of states for the two minima. Thus, the various two-transition state theories[14,15] largely reduced almost everywhere to

Eq. (1), where $N_{EJ}(R^{\dagger})$ now denotes the smaller of N^1_{EJ} and N^2_{EJ}. In particular, we found that the rate constants calculated from the lower bound formula given below differed by at most a factor of 0.5 from those calculated with Eq. (1), using in the latter the global minimum for $N_{EJ}(R^{\dagger})$. Additionally, the rate constant obtained from the "unified statistical theory" discussed below differed by, at most, a factor of 0.8.

A treatment of the typical situation in chemical reactions when there are two values of R where the reactive flux may be reflected and/or transmitted was first given by Hirschfelder and Wigner.[16] Subsequently, Miller[14] introduced into that formalism expressions for the reflection probabilities in terms of statistical flux ratios (or equivalently in terms of the number of states) and obtained a "unified statistical theory" (UST). As noted by Chesnavich *et al.*[17] when these ideas are applied to a unimolecular dissociation reaction the rate constant is given by[17]

$$k_{EJ} = \frac{1}{h\rho_{EJ}} \frac{N^{\dagger 1}_{EJ} N^{\dagger 2}_{EJ}}{N^{\dagger 1}_{EJ} + N^{\dagger 2}_{EJ} - \frac{N^{\dagger 1}_{EJ} N^{\dagger 2}_{EJ}}{N^{max}_{EJ}}}. \tag{29}$$

Subsequently, studies by Pollak *et al.*[15] showed that the assumption embodied in Eq. (29) of having statistically determined reflection probabilities is not a good one at all energies. For simple reactions such as $H + H_2 \rightarrow H_2 + H$ and $F + H_2 \rightarrow FH + H$, UST was shown to give substantially larger reaction probabilities at high energies than those determined from classical trajectories. Pollak *et al.*[15] then presented a method for determining a lower bound for the reaction probabilities based on consideration of only those trajectories which cross the surface having the maximum flux two times or less. The dynamical results of Ref. 15 were shown to be in significantly better agreement with the lower bound probabilities than with UST for the cases examined. This result can once again be directly applied to the unimolecular dissociation case and the rate constant is then given by

$$k_{EJ} = \frac{\left(N^{\dagger 1}_{EJ} + N^{\dagger 2}_{EJ} - N^{max}_{EJ}\right)}{h\rho_{EJ}}. \tag{30}$$

However, as already noted, for the NCNO system we have studied, these formulae (29) and (30) reduce in practice to Eq. (1), with $N^{\dagger}_{EJ}$ having now the smaller of the number of states at the two local minima.

VI. ROLE OF THE REPULSIVE CURVES IN UNIMOLECULAR DISSOCIATION

Typically, in a unimolecular dissociation into two fragments there are two or more potential energy curves, for example the singlet and triplet curves in Fig. 7.1. If phase space theory is applied,[18] the l-dependent effective potential energy barriers may occur at such large separation distances that these curves are almost degenerate at the barrier maximum, and the question arises whether both the singlet and triplet levels or just the singlet one should be used in the PST calculation. In the variational RRKM method, on the other hand, the $R^{\dagger}$ moves to shorter fragment-fragment separation distances, even when the excess energy is quite small (e.g., when $E \approx 500$ cm^{-1} in both the $C_2H_6 \rightarrow 2CH_3$ and the NCNO $\rightarrow$ NC + NO cases). In particular, it moves to a value where the singlet-triplet splitting becomes fairly large relative to the excess energy. In this case the contribution of the triplet state to $N^{\dagger}_{EJ}$ becomes relatively minor. Moreover, it is also arguable whether there would be time between $R^{\dagger}$ and the PST R_l for the system to undergo an intersystem crossing from the singlet to the triplet state.

Thus, in our past and current applications we have largely confined our attention to calculating $N^{\dagger}_{EJ}$ from the singlet curve, rather than from any excited state curves. We have examined in detail in Ref. 10 the case of NCNO decomposition. Here, there is the ground state singlet S_0 and a weakly bound triplet T_1, both leading to the quadruply degerate asymptotic state ($NO_{1/2}$,CN). There are also the upper repulsive singlet S_1 and T_2 curves, leading to an asymptote ($NO_{3/2}$,CN) 120 cm^{-1} higher in energy than that of ($NO_{1/2}$,CN). The upper two curves (Ref. 10) may be disregarded in the reaction rate calculation, for the reason described in the previous paragraph. We found, using an approximate

potential energy function and assuming rapid singlet-triplet conversions, that the lower triplet T_1 state made a contribution to $N^{\dagger}_{EJ}$ only at low E's. But even the inclusion of that contribution becomes uncertain if the singlet-triplet conversion rate is not high in the transition state region.

VII. CONCLUDING REMARKS

General formulae for determining $N_{EJ}(R)$, the number of states as a function of center-of-mass to center-of-mass separation for the various possible fragment cases, have been presented. From the specific formulae given for the three different possible types of fragments the overall computational expression for any combination of two fragments is immediately obtained. In particular Eqs. (12) and (13) are used with the combinations (sum, product, etc.) of the formulae given for the two separate types of fragments. This method is a general one and may be easily applied to a large variety of unimolecular dissociation reactions. The method can also be modified to treat unimolecular isomerizations, in which case there is only one fragment. It has been applied in recent papers to experimental data on the unimolecular dissociation reactions $C_2H_6 \rightarrow 2CH_3$,[5] and $NCNO \rightarrow NC + NO$.[10]

In the application of this method the uncertain quantity is the molecular potential energy surface. In previous applications[3,5,10] model potential energy surfaces were used. At short separation distances the repulsive interactions between the nonbonded atoms are much too strong in these model potential energy functions. We found as a result that there appeared to be no local minimum in the $N_{EJ}(R)$ plot at energies above about 3000 cm^{-1} for the $NCNO \rightarrow NC + NO$ reaction. This disappearance of the local minimum in $N_{EJ}(R)$ indicates the need for more accurate potential energy surfaces. A further indication of just how strongly repulsive the model potential energy surface is at short distances is given by the comparison of $N_{EJ}(R)$ at $R = R_e$ with the number of states for the reactant (excluding the dissociation coordinate) as determined by Whitten-Rabinovitch type calculations. These two quantities are given by

0.1×10^7 and 4×10^7, respectively, for an excess energy of 2348 cm^{-1} and a total angular momentum of 5, for the parameters in Ref. 10. One hope is that studies such as those of Ref. 10 will motivate the *ab initio* calculation of potential energy surfaces for the fragment-fragment hindered rotational motions at center of mass to center of mass separation distances near $R^\dagger$ (about 3.0 to 4.5 $\AA$ for the NCNO $\rightarrow$ NC + NO reaction).

We have also presented here arguments providing some insight into the previously observed trend of $R^\dagger$ decreasing with increasing energy. This trend indicates a larger deviation with increasing energy of RRKM rates from those of PST. A discussion of the various formulae for considering the effect of two transition states in series has also been given, along with a consideration of their importance in unimolecular dissociation reactions. Finally a discussion of which potential energy surfaces should be used in unimolecular dissociation rate calculations has also been given.

ACKNOWLEDGMENTS

We are pleased to acknowledge the support of this research by a grant from the National Science Foundation.

REFERENCES

[1] P. J. Robinson and K. A. Holbrook, *Unimolecular Reactions* (Wiley, New York, 1972); W. Forst, *Theory of Unimolecular Reactions* (Academic Press, New York, 1973); R. E. Weston and H. A. Schwarz, *Chemical Kinetics* (Prentice-Hall, Englewood Cliffs, NJ, 1972); R. A. Marcus, J. Chem. Phys. **20**, 359 (1952); R. A. Marcus and O. K. Rice, J. Phys. Colloid. Chem. **55**, 894 (1951); R. A. Marcus, J. Chem. Phys. **43**, 2658 (1965); *ibid.* **52**, 1018 (1970).

[2] R. A. Marcus, J. Chem. Phys. **45**, 2138 (1966); *ibid.* **45**, 2630 (1966); W. H. Miller, J. Am. Chem. Soc. **101**, 6810 (1979).

[3] D. M. Wardlaw and R. A. Marcus, Chem. Phys. Lett. **110**, 230 (1984); D. M. Wardlaw and R. A. Marcus, J. Chem. Phys. **83**, 3462 (1985); D. M. Wardlaw and R. A. Marcus, J. Phys. Chem. **90**, 5383 (1986); D. M. Wardlaw and R. A. Marcus, Adv. Chem. Phys. **70**, 231 (1988).

[4] S. J. Klippenstein and R. A. Marcus, J. Chem. Phys. **87**, 3410 (1987).

[5] S. J. Klippenstein and R. A. Marcus, J. Phys. Chem. *in press*, hereinafter referred to as part I.

[6] P. Pechukas and J. C. Light, J. Chem. Phys. **42**, 3281 (1965); P. Pechukas, R. Rankin, and J. C. Light, J. Chem. Phys. **44**, 794 (1966); C. Klotz, J. Phys. Chem. **75**, 1526 (1971); C. Klotz, Z. Naturforsch, Teil A **27**, 553 (1972); W. Chesnavich and M. Bowers, J. Chem. Phys. **66**, 2306 (1977).

[7] H. Goldstein, *Classical Mechanics*, 2nd ed. (Addison-Wesley, Reading, MA 1980). The "y-convention" given there in Appendix B is used here. There is a typographical error in the last row of the rotation matrix **A** there, namely, the ψ's should be replaced by ϕ's.

[8] I. N. Levine, *Molecular Spectroscopy*, (Wiley, New York, 1975).

[9] J. P. Valleau and S. G. Whittington, in *Statistical Mechanics*, edited by B. J. Berne, (Plenum Press, New York, 1977), p. 137; J. P. Valleau and G. M. Torrie, in *Statistical Mechanics*, edited by B. J. Berne, (Plenum Press, New

York, 1977), p. 169.

[10] S. J. Klippenstein, L. R. Khundkar, A. H. Zewail, and R. A. Marcus, J. Chem. Phys. to be submitted.

[11] D. A. McQuarrie, *Statistical Mechanics*, (Harper and Row, New York, 1976).

[12] S. N. Rai and D. G. Truhlar, J. Chem. Phys. **79**, 6046 (1983).

[13] W. L. Hase, Chem. Phys. Lett. **139**, 389 (1987), and references cited therein; M. Quack and J. Troe, Ber. Bunsenges Phys. Chem. **81**, 329 (1977); G. P. Smith and D. M. Golden, Int. J. Chem. Kinet. **10**, 489 (1978); S. W. Benson, Can. J. Chem. **61**, 881 (1983).

[14] W. H. Miller, J. Chem. Phys. **65**, 2216 (1976).

[15] E. Pollak and P. Pechukas, J. Chem. Phys. **70**, 325 (1979); E. Pollak, M. S. Child, and P. Pechukas, J. Chem. Phys. **72**, 1669 (1980).

[16] J. O. Hirschfelder and E. Wigner, J. Chem. Phys. **7**, 616 (1939).

[17] W. J. Chesnavich, L. Bass, T. Su, and M. T. Bowers, J. Chem. Phys. **74**, 2228 (1981). Calculations using the unified statistical model are also described in Ref. 12.

[18] For other discussions of which states to include in PST calculations see, for example, E. Herbst and S. K. Knudson, Chem. Phys. **55**, 293 (1981).

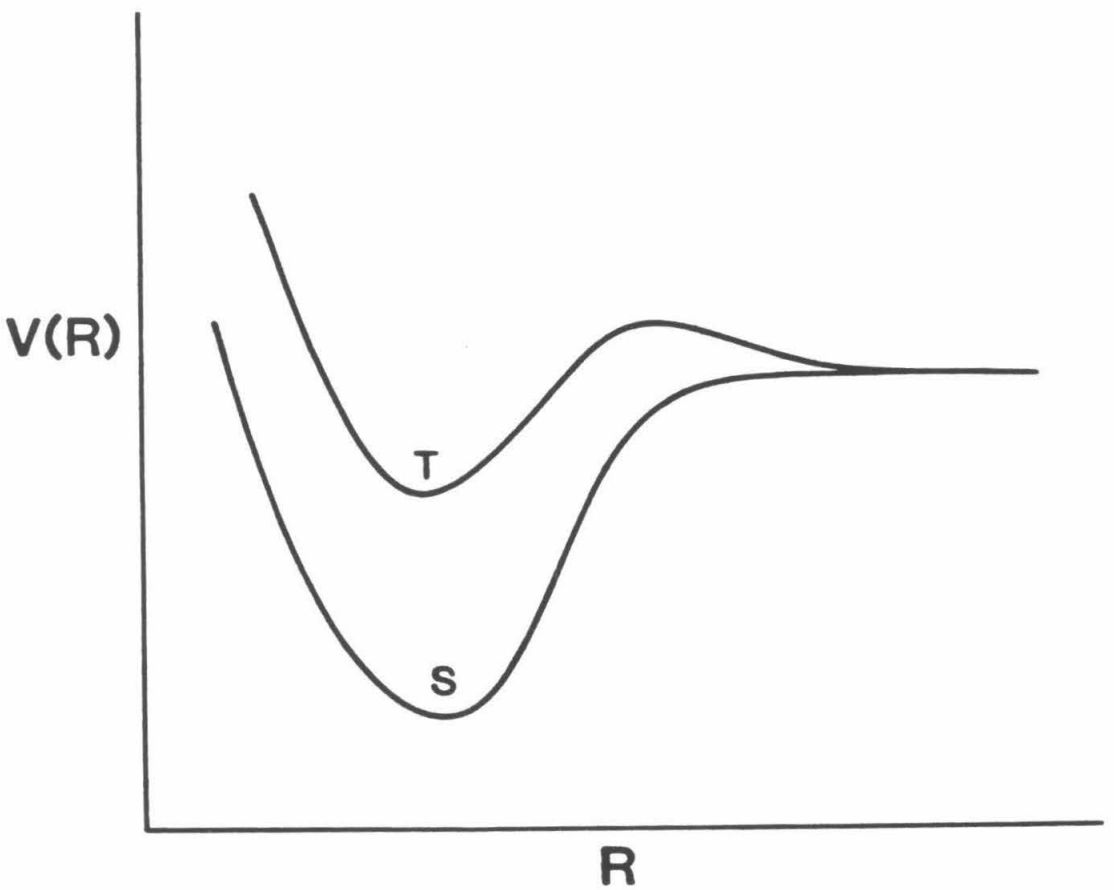

FIG. 7.1. Schematic diagram of potential energy curves for typical unimolecular dissociation into two fragments. S denotes the lower singlet level and T denotes the upper triplet level. V(R) is the minimum potential energy for a given center of mass to center of mass separation distance R.

Chapter 8: Application of Unimolecular Reaction Rate Theory for Highly Flexible Transition States to the Dissociation of NCNO into NC and NO

[A modified version of the text of this chapter is to be submitted to J. Phys. Chem. and is authored by S. J. Klippenstein, L. R. Khundkar, A. H. Zewail and R. A. Marcus]

ABSTRACT

A recently described method for implementing RRKM theory for unimolecular reactions with highly flexible transition states is applied to the calculation of energy and angular momentum resolved rate constants and rotational-vibrational energy distributions for the reaction NCNO $\xrightarrow{h\nu}$ NCNO* $\rightarrow$NCNO(vib. hot) $\rightarrow$NC + NO. The dissociation rate results are compared to the recent experimental results of Khundkar *et al.*, and the vibrational and rotational distribution results are compared to the experimental values of Nadler *et al.* Comparison is also made with phase space theory calculations. The calculated rotational distributions at energies below the vibrational threshold of the products are the same as those of PST. At energies (2348, 2875 cm^{-1}) above this threshold energy the rovibrational distributions are in better agreement with the data than are those of PST. The need for obtaining more accurate *ab initio* potential energy surfaces is noted, particularly for treating reactions at still higher energies.

I. INTRODUCTION

Recent detailed experimental results for energy-resolved reaction rates have been compared with several simplified models of the transition state. In particular, the energy and partially-angular momentum resolved reaction rate constants for the unimolecular dissociation of NCNO determined by Khundkar *et al.*[1] via picosecond photofragment spectroscopy could not be fit[1] using a tight transition state form of RRKM theory,[2] i.e., one having transition state modes that are treated as harmonic oscillators. As they noted, too, there was also uncertainty[1] in comparing the results with phase space theory[3] regarding the role played by the near-degeneracy of the various electronic states at large distances where phase space theory (PST) has its "transition state". In PST the transition state is postulated to consist of two fragments which rotate freely.

It is desirable, therefore, to explore a more detailed model of the transition state (TS), as part of a study on the suitability of statistical models for rates and product state distributions. The rotational and vibrational energy distributions of the products of the same dissociation reaction have been experimentally determined by Nadler *et al.*[4] and were in good agreement with those predicted by PST when the energy was below that needed to produce vibrationally excited fragments. Some deviations were found at somewhat higher energies. In the case of RRKM theory some added assumption regarding the dynamics in the exit channel is needed for predicting product energy distributions. One such dynamical approximation was described recently[5] in conjunction with a recent implementation of RRKM theory.[6–8] The results of this method will be compared with the experimentally determined vibrational-rotational distributions for NCNO, together with the results of RRKM theory for the rate constants themselves.

In the present treatment the transformation of the bending modes of the reactant to the hindered rotations of the transition state and then finally to the free rotations of the products is considered, using a potential energy surface. In addition, the coupling of these hindered rotational modes with the overall rota-

tions is included. Examples of this variational implementation of RRKM theory for flexible transition states of other systems are given in several recent papers[6–8] from this laboratory. In the nomenclature of Refs. 6 - 8 the modes which change their nature appreciably are termed the transitional modes and the remaining modes, excluding the reaction coordinate, the conserved modes. In this work the full coupling between the various transitional modes is considered together with conservation of total angular momentum. The method is based on Monte Carlo integration of the phase space volume for the transitional modes, convoluted with the distribution of the conserved modes, treated quantum mechanically. A given potential energy surface is used, together with an assumed separability of the conserved modes from the transitional modes. In the transition state region the conserved modes are treated as quantum mechanical oscillators while the transitional modes are treated classically but otherwise generally for any given potential energy surface.

In the present article this implementation of RRKM theory is applied to the calculation of rate constants and product state distributions for the NCNO dissociation. There are four potential energy surfaces involved in the transition state region, namely two singlet states and two triplets. Consideration is given to which states are involved in determining the transition state. At the present time, the potential energy surfaces for the transition state (TS) region of unimolecular dissociations are not well-known, and so the dependence of the results on various model potential energy surfaces is also discussed. The results obtained may then be used as a guide for the subsequent determination of an *ab initio* or improved semi-empirical potential energy surface in the TS region. In section II a brief description of the theoretical determination of the number of states for the highly flexible transition state of NCNO is given. Results for the present k_{EJ} calculations are given in section III, and discussed in section IV. In section V the corresponding results for the NC and NO rovibrational distributions are given and discussed, and are followed by concluding remarks in section VI.

II. THEORY

The specific rate constant k_{EJ} for unimolecular dissociation at a given energy E and total angular momentum quantum number J is given by[2]

$$k_{EJ} = N^{\dagger}_{EJ}/h\rho_{EJ} \ , \tag{1}$$

where ρ_{EJ} is the density of states for the reactant at the given E and J. The quantity $N^{\dagger}_{EJ}$ is the number of available quantum states of the transition state with energy less than or equal to E and with the given J.

When a tight transition state is used in RRKM theory, harmonic frequencies are usually assumed for the various vibrational modes, and some rotational constants are employed for the transition state. $N^{\dagger}_{EJ}$ is then determined through a direct count of the available vibrational-rotational states at the given energy and total angular momentum.

In phase space theory[3] (PST) the TS involves two freely rotating fragments, whose vibrational modes are those of the fragments themselves. The rotational modes are approximated as free rotations. An attractive fragment-fragment potential of the form R^{-n} is used, where n is usually 6 and R is the dissociation coordinate. In the present application the dissociation coordinate R is chosen to be the separation distance between the centers of masses of the NC and NO fragments. In PST effective barriers are calculated as a function of the orbital angular momentum quantum number of the two fragments l, and $N^{\dagger}_{EJ}$ denotes the total number of these vibrational-rotational-orbital states which satisfy the total angular momentum conservation rule and have an energy greater than that of the l-dependent effective barrier. The allowed l's are those consistent with the triangular inequality for the total angular momentum and with a radial kinetic energy sufficient to exceed the barrier's maximum. The $R^{\dagger}$ of the latter varies with l, and so there are a number of such $R^{\dagger}(l)$'s for the given J.

In Refs. 7 and 8 it has been shown how conventional coordinates may be used in an implementation of RRKM theory developed by Wardlaw and Marcus

to treat these highly flexible transition states. They used action-angle variables to facilitate the imposition of the constraint of fixed total angular momentum. In Ref. 7 a convenient way for imposing this constraint using conventional coordinates was presented. In these studies an approximate separation of variables into the conserved and transitional modes mentioned earlier is introduced. In the present article the method of Refs. 7 and 8 is used in all determinations of $N_{EJ}(R)$. In particular, a computational method based on Eqs. (12), (13) and (17) - (21) of Ref. 8 is employed.

Before proceeding with the determination of k_{EJ}'s using Eq. (1), several points are considered first: The fragments NC and NO each have a doubly degenerate ground state (spin degeneracy). In addition, NO has a doubly-degenerate excited electronic state at 120 cm^{-1} excess energy, this splitting arising from a spin-orbit interaction ($j_{el} = 1/2, 3/2$). In Fig. 8.1 a schematic correlation diagram is given for the present NCNO photodissociation. The initial photoexcitation involves excitation to the S_1 state. The latter state is calculated[9] to have a barrier height above the value at $R = \infty$ of 6674 cm^{-1}, and thus for excess energies below this amount either internal conversion to the S_0 (cf. Fig. 8.1) or intersystem crossing to the T_1 state must occur before dissociation can take place. Because of the usual rapidity of internal conversion processes the former is assumed typically to occur next in the dissociation. Following this step there may be "intersystem crossings" and "internal conversions" between the various states in the region of the transition state. However, the calculated barrier of 6674 cm^{-1} for the S_1 state indicates that the S_1 and T_2 states probably have little influence on the rates. In principle, they could play a role in a determination of the product state distributions in the case of PST, since in PST itself no detailed dynamics are postulated to restrict such usage of these states, intersystem crossing, etc., and the states may be nearly degenerate at the large $R^{\dagger}(l)$'s involved in PST.

A general discussion of the role of the triplet level in RRKM calculations has

been given in Ref. 8. The discussion there indicates that what appears to be the best current approach to the rate calculations, in the case where the intersystem crossing rates and triplet potential energy surfaces are not well-known, is to consider only the singlet state S_0. An alternative model is to consider a limiting case where the intersystem crossing rates are very rapid and calculate an $N^{\dagger}_{EJ}(R)$ as the sum of the number of states for both the S_0 and T_1 states ($N_{EJ} = N^{S_0}_{EJ} + N^{T_1}_{EJ}$, each of which contains a degeneracy factor g_e which is one for the singlet state and three for the triplet state). Then the $R^{\dagger}$ at which this $N_{EJ}(R)$ has a minimum is calculated.

In order to perform the above calculation a potential energy surface for the triplet state T_1 is needed. This triplet state is expected to be initially repulsive with a small barrier, before becoming attractive by an amount of about 11000 cm^{-1} at its equilibrium configuration. (The singlet-triplet splitting is then about 6000 cm^{-1} or about half the singlet-singlet energy difference as in other nitroso compounds.[4]) Recent *ab initio* calculations[9] of the T_1 potential surface indicate that the barrier height above the value at infinite separation is 4597 cm^{-1}. This reasonably large barrier height indicates that the T_1 triplet state is not likely to play a major role in the determination of the dissociation rates.

However, in section III we consider a simple barrierless model for the T_1 state (which overestimates the possible effect of the triplet state based on the *ab initio* results of Ref. 9) to indicate the difference between a PST and a RRKM treatment of an excited triplet state for the case in which the intersystem crossing rates are rapid. In PST one typically considers the degeneracies at $R = \infty$ (because the $R^{\dagger}(l)$'s of PST are usually quite large) in which case the T_1 contributes an extra factor of 3. For comparison with the contribution of T_1 with RRKM theory the triplet potential energy is set to zero throughout the transition state region (the dashed line in Fig. 8.1.)

Another point discussed elsewhere[8] is that in the expression for k_{EJ} given in Eq. (1) it is assumed that there is one dominant minimum in the number of

states N_{EJ} as a function of the dissociation coordinate R. For highly flexible transition states there may, in fact, be two local minima in the plot of N_{EJ} versus R. In section IV, results are given which indicate that although there are two local minima in the $N_{EJ}(R)$ plot for a certain energy range, the rate is still well-described by merely using the principal minimum in $N_{EJ}(R)$ for $N^{\dagger}_{EJ}$.

One final consideration involves the determination of the density of states for the reactant molecule. For the present NCNO dissociation reaction, the number of vibrational modes for the reactant is small enough that a direct count of the number of states is easily performed. Diagonal anharmonicities were included in the direct count used here. These diagonal anharmonicities were estimated through consideration of the frequencies and dissociation energies of the respective bonds. Their inclusion increased the density of states by a factor of only 1.25 at energies near the dissociation threshold of 17085 cm^{-1}. Off-diagonal anharmonicites are expected to increase the density of states further, perhaps by a factor of similar magnitude. These off-diagonal anharmonicities were not included in the present density of states calculation, their values not being known. However, the correction due to these anharmonicities should be reasonably constant over the experimentally-considered energy range of only 700 cm^{-1} for the rates.

III. REACTION RATE CONSTANT RESULTS

In this section the results of the present k_{EJ} calculations are compared with the experimental results of Ref. 1. Unless otherwise specified the results given here are for the case of reaction on only the singlet state S_0. Also, all reaction rate calculations were performed for a total angular momentum quantum number J of 3, which is the estimate of its average value given in Refs. 1 and 4.

Before presenting these results we first consider properties of the conserved and the transitional modes used here. In the absence of a detailed potential energy surface the conserved modes were treated as harmonic oscillators with an exponential interpolation between the reactant and product frequencies and

reactant and product bond distances being used.

$$\lambda_i(R) = \lambda_i^p + (\lambda_i^r - \lambda_i^p)g(R), \tag{2}$$

where $g(R) = \exp[-\alpha(R - R_e)]$,[6,10] R_e is the equilibrium value of R for the reactants, and λ denotes ν or r_e, i denotes NC or NO, ν_{NC} and $r_{e,NC}$ are the terminal NC stretch frequency and separation distance, and ν_{NO} and $r_{e,NO}$ denote those of NO. The r and p superscripts denote the reactant (NCNO) and products (NC + NO), respectively. A value of 1.0 Å^{-1} for the parameter α, which has been commonly found to provide agreement with experiment in the adiabatic channel model,[10] was used. The properties for the conserved modes are given in Table 8.1, together with the frequencies and anharmonicities for the transitional modes of the reactant.

In the model of the potential energy surface assumed here for the transitional modes, the sum of a bonding potential for the central NC—NO bond and a nonbonding potential for the other interactions within the transitional modes was used. The nonbonding potential was chosen to be a sum of 6-12 Lennard-Jones potentials for the van der Waals interactions between the nonbonded atoms of the two separate fragments, as in Eq. (3) below.[11] The bonding potential was approximated by a Varshni potential,[12,13] multiplied by the factor $\cos^2(\theta_{NCN} - \theta_{e,NCN})\cos^2(\theta_{CNO} - \theta_{e,CNO})$ to allow for the loss of bonding which occurs when the fragments are improperly oriented. Here, θ_{NCN} and θ_{CNO} are the NCN and CNO bending angles, respectively, while $\theta_{e,NCN}$ and $\theta_{e,CNO}$ denote their equilibrium values, as given in Table 8.1. The Varshni potential rather than a Morse potential was employed since the latter is known[10,13] to decay to zero too slowly at large separation distances, whereas the former is believed to provide a better representation for this region.[13]

Assuming this representation of the nonbonding potential V_{LJ} in terms of van der Waals interactions we have

$$V_{LJ} = {}'\sum_{i,j=1}^{2}{}' 4\epsilon_{ij}\left[(\sigma_{ij}/r_{ij})^{12} - (\sigma_{ij}/r_{ij})^{6}\right], \tag{3}$$

where i and j label atoms in the NC and NO fragments, respectively, and the prime indicates that the central NC—NO bond is not included in the sum. The parameters σ_{ij} and ϵ_{ij} denote the usual Lennard-Jones parameters for the interaction between atoms i and j; r_{ij} is then the separation distance between atoms i and j. The Varshni potential V_V for the NC-NO bond, denoted by CN in Eq. (4), is given by the standard form[12,13]

$$V_V = D_{CN}\left\{1 - \left(\frac{r_{e,CN}}{r_{CN}}\right)\exp\left[-\beta_{CN}\left(r_{CN}^2 - r_{e,CN}^2\right)\right]\right\}^2 - D_{CN}. \qquad (4)$$

The parameters for this model potential energy surface for the transitional modes are given in Tables 8.2 and 8.3. The parameters for the Lennard-Jones potential V_{LJ} (Table 8.2) were taken for convenience to be the same as those which gave good results in Monte Carlo simulations of amides and peptides.[14] The parameters D_{CN} and β_{CN} of the Varshni potential were chosen to fit the *total* potential energy function to an assumed Varshni potential surface for the NC—NO separation distance in the range of 3.3 Å. The parameters for this assumed Varshni potential surface are given in Table 8.3 and were determined here from a consideration of the spectroscopic constants and the force constants determined by Wilson G-matrix analysis of the harmonic frequencies in Ref. 15. The parameter $r_{e,CN}$ for the fitted potential was held fixed at 1.2 Å. The results depended relatively little on this parameter.

Results for k_{EJ} calculations for the above model of the potential energy surface are given in Fig. 8.2, where the dissociation rates are plotted versus energy. Also given for comparison in Fig. 8.2 are results for the case in which T_1 is included (but with no barrier) and in which the intersystem crossing rate in the transition state region is assumed to be much larger than the dissociation rates. Recent *ab initio* calculations show that the triplet state T_1 is even more repulsive than this simplified model. The result of this is that the contribution from the T_1 state will be even less than that shown in Fig. 8.2, and it will also disappear at lower excess energies. Results are given in Fig. 8.3 for a potential

energy surface for which the dissociative singlet state (S_0) potential has been fit to an assumed β parameter of 0.7Å^{-2} rather than 0.48Å^{-2}. The resulting parameters for this surface are also given in Table 8.3 and labelled as potential surface (ii).

Results of three types of PST calculations are given in Fig. 8.4. They involve a classical PST, a quantum PST, and a calculation in which $N_{EJ}(\infty)$ is used for $N_{EJ}^{\dagger}$ in Eq. (1). (The latter calculation corresponds to a PST calculation in which the l-dependent barriers are all at "infinite" separation. While the effective barriers can never be at infinity, they can be at such a large separation distance that the effective barrier energy, a centrifugal potential plus an attractive potential, is negligible.) The PST calculations have all been performed as described in Refs. 1 and 4 with a C_6 potential parameter of 1.6×10^5 cm $^{-1}\text{Å}^6$.

IV. REACTION RATE DISCUSSION

The results in Fig. 8.2 corresponding to the singlet plus triplet deviate significantly from the singlet state calculation only in the low energy region, namely, for E less than about 400 cm^{-1}. This disappearing contribution of the triplet state occurs as the rate changes from being determined mainly by the number of states at $R = \infty$ to being determined mainly by the the number of states at the inner minimum in N_{EJ}. Also, this effect reflects the R of the inner minimum in the number of states being small enough that the singlet-triplet gap for the present model surfaces is comparable to or larger than the excess energy. That is, when this inner minimum in N_{EJ} is less than about 4 Å the difference between the minimum potential energy for a given R on the singlet and triplet states becomes quite large, while at the same time the orbital kinetic energy of the two fragments is becoming relatively large, resulting in a much lower number of states for the triplet potential surface. In PST the R-value of the purely l-dependent barrier of PST does not become this small until much higher energies are reached and so the contribution from the triplet remains considerable until much higher energies.

The results given for the low energies E in Fig. 8.2 for dissociation on the singlet state only are quite similar to the PST results for the singlet state shown in Fig. 8.4. This similarity arises because at these energies the inner minimum in the number of states N_{EJ} is about the same or more than the number of PST states (and because the triplet state is being neglected). At higher energies this value of this minimum of N_{EJ} actually becomes less than that for PST and so, within the framework of the present potential energy surface this new minimum represents a better transition state. This effect can be seen in Figs. 8.5 - 8.7, where plots of $N_{EJ}(R)$ versus R are given for the $\beta = 0.7\text{Å}^{-2}$ potential energy surface at the the three energies, 50 cm^{-1}, 700 cm^{-1} and 2000 cm^{-1}. The results in Figs. 8.5 - 8.7 indicate that with increasing energy the inner minimum becomes more and more the dominant minimum.

There are two parts of the potential energy surface function which can significantly affect the calculated rates: the dissociative and the hindered rotational potentials. If the dissociative (bonding) potential actually approaches zero more rapidly than that given by the Varshni potential energy surface considered in Fig. 8.2 the results start to deviate from PST results at lower energies. This effect can be seen in Fig. 8.3, where results are given for the different values of the β parameter. In this case for a $\beta = 0.70$ Å^{-2} the RRKM results already differ from those of PST by a factor of 0.69 at an $E = 700$ cm^{-1}. The calculated rates also depend on the strength and location of the attractive wells of the Lennard-Jones potentials describing the hindered rotation of the fragments. While results for this case are not presented here, when one simply increases σ_{ij} by about 0.3Å, the results are analogous to those obtained for the larger β parameter study.

The results in Fig. 8.4 indicate that classical PST and the $N_{EJ}(\infty)$ treatments of the transitional modes are very similar for these energies, with the differences being only about one to two percent. This similarity occurs because for the energies employed in the experimental work in Ref. 1 the assumed attractive potential in PST is essentially such a long range potential that $R^{\dagger}(l)$ is so

large that the effective barrier is negligible for even the largest l's present. If these l-dependent barriers were completely negligible then the $N_{EJ}(\infty)$ and PST calculations would give identical results. Similarly, the classical and quantum phase space theory results are in good agreement, with the classical calculation being typically 10 to 15 percent below the quantum one. Finally, it also interesting to note that when only the singlet surface S_0 is considered as here, the present results using the different types of PST or using RRKM theory are in better agreement with the experimental results than the PST calculations given in Fig. 14 of Ref. 1, where the electronic degeneracy was treated simply as some constant over the energy range with a second contribution arising from the upper singlet and triplet states shifted by 120 cm^{-1}.

In Fig. 8.8 the results from three methods for taking into account the presence of two minima in the $N_{EJ}(R)$ plot are given. The simplest method is to take $N_{EJ}^{\dagger}$ as the overall minimum in $N_{EJ}(R)$, and this is what has been done in Figs. 8.2 and 8.3 here. In another method, termed unified statistical theory,[16] statistical reflection and transmission probabilities are introduced to obtain $N_{EJ}^{\dagger}$. In a third method[17] a lower bound is determined (within certain dynamical assumptions) to $N_{EJ}^{\dagger}$. Formulae for these different treatments are summarized in Ref. 8. The results plotted in Fig. 8.8 for potential surface (i) indicate that in the present case the effect of there being two minima was never larger than a factor of 1.4. Similar results for potential surface (ii) indicate that the effect was never larger than a factor of 2.0.

In Figs. 8.9 - 8.12 the dependence of the present potential energy surfaces on certain bending angles are presented for typical $R^{\dagger}$'s. These figures are given for a range of R where an *ab initio* determination of the potential surface for the transitional modes would be particularly useful for obtaining improved bending and hindered rotational potential energy surfaces. In particular, from this figure it is seen that in the TS region the absolute minimum in the potential for a given R is negative and has a magnitude of a few thousand cm^{-1} while the rotational

barriers are positive and have a much larger magnitude.

V. PRODUCT STATE DISTRIBUTIONS

In order to calculate vibrational and rotational distributions of the products using RRKM theory, some dynamical assumption needs to be introduced regarding the motion in the exit channel. In particular, it was assumed in Ref. 5 that the conserved modes are adiabatic from $R^\dagger$ to $R = \infty$, and that the transitional modes, which are usually of low frequency in the TS region, behave quite differently. Namely, it was assumed that they may freely interchange energy from $R^\dagger$ to R_l, the position of the loose (PST) transition state. In implementing such a theory, the number of states $N_{EJi}(R)$ for a state of excitation i of the conserved modes is calculated and its minimum found, at $R = R_i^\dagger$, say, as in Eq. (6) of Ref. 5. (The corresponding rate expression is given by Eq. (7) there.) This procedure is followed in obtaining the results in Table 8.4. A more approximate procedure is to remove from $N_{EJ}(R^\dagger)$ any states i whose channels are "closed" at $R = \infty$, as discussed in Ref. 5. We have used this procedure also. It entails less calculation, particularly at large E's, since only one $R^\dagger$ is required instead of an $R_i^\dagger$ for each i. In each case, using this vibrational distribution the rotational distribution is then calculated from the statistics at $R^\dagger(l)$.[5]

Results for energies below the vibrational excitation threshold for the products are not presented here, since the distributions predicted by the theory described in Ref. 5 at those energies are the same as the PST distributions. The latter have been described in detail in Ref. 4. For energies above the vibrational excitation thresholds calculations have been performed as described in sections III and IV except that the conserved modes were treated as Morse rather than harmonic oscillators and now the total angular momentum quantum number J was taken to be 5 so as to compare with the previous calculations of Nadler *et al.*[4] Potential surface (i) was used.

Plots of the NO and NC rotational distributions, determined by the above method are given in Figs. 8.13 - 8.15. Also given there are the corresponding

plots determined experimentally and by PST. These results indicate that the theory of Ref. 5 provides an improvement over PST in describing the rotational distributions at excitation energies above the vibrational threshold.

In Table 8.4 the vibrational distributions calculated from the present implementation of RRKM theory are compared with those determined both experimentally and from PST by Nadler *et al.*[4] It is seen from Table 8.4 that the RRKM distributions for the excess energies of 2348 cm^{-1} and 2875 cm^{-1} are in better agreement with the experimental distributions than are the PST distributions. The RRKM theory distributions could not be determined for excess energies higher than 3000 cm^{-1} because the assumed Lennard-Jones potentials were so strongly repulsive in this region that there was no local minimum in the $N_{EJ}(R)$ plot. Indeed, by calculating this $N_{EJ}(R)$ at the equilibrium value of R in the NCNO molecule, where $N_{EJ}(R)$ is known, it is clear that the Lennard-Jones/Varshni combination does not yield a good result for $N_{EJ}(R_e)$, at such small R's. There is no reason why it should. Instead, the Lennard-Jones potentials might only be accurate at low excess energies. Thus, the need for accurate *ab initio* potentials for the transitional modes is once again emphasized.

Nadler *et al.* have obtained similar improved agreement with the experimental vibrational-rotational distributions at excess energies above the vibrational threshold. Their modifaction of PST labelled SSE in effect calculated the vibrational distribution for a constant l in the exit channel and neglected the centrifugal and radial potentials. The resulting vibrational distribution was then used to determine the full rotational-vibrational distribution from PST.

VI. CONCLUDING REMARKS

An implementation of RRKM theory for highly flexible transition states has been applied to the NCNO dissociation reaction. The ground singlet state S_0 is most likely the only state contributing to the determination of the rate constants. The results also indicate that the rate constants determined from RRKM theory are similar to the PST results for the S_0 state only with minor differences

at the highest energies studied. The results for the rotational-vibrational distributions indicate that the RRKM-theory-based method of Ref. 5 may explain the difference between the experimental and the PST rotational-vibrational distributions at energies above the vibrational excitation threshold. One common point of the results presented here is the dependence on the values used for the potential surface parameters. Also, the product state distributions could not be determined for excess energies above about 3000 cm^{-1} due to the inaccuracies of the repulsive Lennard-Jones surface at these high energies. Thus, an accurate *ab initio* potential energy surface for the transition state region is highly desirable.

ACKNOWLEDGMENTS

It is a pleasure to acknowledge the support of this research by the National Science Foundation.

REFERENCES

[1] L. R. Khundkar, J. L. Knee, and A. H. Zewail, J. Chem. Phys. **87**, 77 (1987).

[2] P. J. Robinson and K. A. Holbrook, *Unimolecular Reactions* (Wiley, New York, 1972); W. Forst, *Theory of Unimolecular Reactions* (Academic, New York, 1973); R. E. Weston and H. A. Schwarz, *Chemical Kinetics* (Prentice-Hall, Englewood Cliffs, NJ, 1972); R. A. Marcus, J. Chem. Phys. **20**, 359 (1952); R. A. Marcus and O. K. Rice, J. Phys. Colloid. Chem. **55**, 894 (1951); R. A. Marcus, J. Chem. Phys. **43**, 2658 (1965); R. A. Marcus, *ibid.* **52** 1018 (1970).

[3] P. Pechukas and J. C. Light, J. Chem. Phys. **42**, 3281 (1965); P. Pechukas, R. Rankin, and J. C. Light, J. Chem. Phys. **44**, 794 (1966); C. Klotz, J. Phys. Chem. **75**, 1526 (1971); C. Klotz, Z. Naturforsch, Teil A **27**, 553 (1972); W. Chesnavich and M. Bowers, J. Chem. Phys. **66**, 2306 (1977).

[4] I. Nadler, J. Pfab, G. Radhakrishnan, H. Reisler, C. Wittig J. Chem. Phys. **79**, 2088 (1983); I. Nadler, J. Pfab, H. Reisler, C. Wittig, *ibid.* **81**, 653 (1984); M. Noble, I. Nadler, H. Reisler, C. Wittig, *ibid.* **81**, 4333 (1984); I. Nadler, M. Noble, H. Reisler, C. Wittig,*ibid.* **82**, 2608 (1985); C. Wittig; I. Nadler, H. Reisler, M. Noble, J. Catanzarite, G. Radhakrishnan, *ibid.* **83** 5581 (1985); C. X. W. Qian, M. Noble, I. Nadler, H. Reisler, C. Wittig, *ibid.* **83**, 5573 (1985);

[5] R. A. Marcus, Chem. Phys. Lett. **144**, 208 (1988).

[6] D. M. Wardlaw and R. A. Marcus, Chem. Phys. Lett. **110**, 230 (1984); D. M. Wardlaw and R. A. Marcus, J. Chem. Phys. **83**, 3462 (1985); D. M. Wardlaw and R. A. Marcus, J. Phys. Chem. **90**, 5383 (1986); D. M. Wardlaw and R. A. Marcus, Adv. Chem. Phys. **70**, 231 (1988).

[7] S. J. Klippenstein and R. A. Marcus, J. Phys. Chem. *in press*, 1988.

[8] S. J. Klippenstein and R. A. Marcus, J. Phys. Chem. *in press*, 1988.

[9] Y. Y. Bai and G. A. Segal, *to be published* (1988).

[10] M. Quack and J. Troe, Ber. Bunsenges. Phys. Chem. **78**, 240 (1974); J. Troe, J. Phys. Chem. **88**, 4375 (1984).

[11] The effect of the Coulombic potentials between the partial charges on the different atoms which are typically included in molecular dynamics simulations were also considered here. They were found to have a negligible effect on the number of states and so were neglected in the calculations presented here.

[12] Y. P. Varshni, Rev. Mod. Phys. **29**, 664 (1957).

[13] R. J. Duchovic, W. L. Hase, B. Schlegel, M. J. Frisch, and K. Raghavachari, Chem. Phys. Lett. **89**, 120 (1982); R. J. Duchovic and W. L. Hase, Chem. Phys. Lett. **110**, 474 (1984); D. Steele, E. R. Lippincott, and J. T. Vanderslice, Rev. Mod. Phys. **34**, 239 (1962).

[14] W. L. Jorgensen and C. J. Swenson, J. Am. Chem. Soc. **107** 569 (1985).

[15] B. Bak, F. M. Nicolaisen, O. J. Nielsen, and S. Skaarup, J. Mol. Struct. **51**, 17 (1979).

[16] J. O. Hirschfelder and E. Wigner, J. Chem. Phys. **7**, 616 (1939); W. H. Miller, J. Chem. Phys. **65**, 2216 (1976); W. J. Chesnavich, L. Bass, T. Su, and M. T Bowers, J. Chem. Phys. **74**, 2228 (1981); S. N. Rai and D. G. Truhlar, J. Chem. Phys. **79**, 6046 (1983).

[17] E. Pollak and P. Pechukas, J. Chem. Phys. **70**, 325 (1979); E. Pollak, M. S. Child, and P. Pechukas, J. Chem. Phys. **72**, 1669 (1980).

Table 8.1: Spectroscopic Parameters for NCNO

Parameter		Reactants Value[a]	Products Value[a]
(i) Frequencies	NC stretch	2170	2068.7
(cm^{-1})	NO stretch	1501	1904.03
	CN stretch	820	
	CNO bend	216.5	
	NCN bend	588.5	
(ii) Anharmonicities[b]	NC stretch	13.1	13.1
(cm^{-1})	NO stretch	14.1	14.1
	CN stretch	9.4	
	CNO bend	0.2	
	NCN bend	0.5	
Coordinates	R_e	2.4Å	
	$r_{e,NC}$	1.163 Å	1.1718 Å
	$r_{e,NO}$	1.217 Å	1.1508 Å
	$\theta_{e,CNO}$ [c]	120°	
	$\theta_{e,NCN}$ [c]	180°	

[a] Unless stated otherwise, all values are as specified in Ref. 4.

[b] Anharmonicities have been obtained from Ref. 4 or estimated from the dissociation energy.

[c] The values used correspond to *sp* and sp^2 bonding geometries rather than to the equilibrium bending angles.

Table 8.2: Lennard-Jones Potential Parameters for NCNO

Parameter	Value[a]	Units
σ_{CO}	3.36	Å
σ_{NN}	3.25	Å
σ_{NO}	3.11	Å
ϵ_{CO}	51.9	cm^{-1}
ϵ_{NN}	59.5	cm^{-1}
ϵ_{NO}	46.7	cm^{-1}

[a] All values have been obtained from Ref. 14 making use of the combination rules $\epsilon_{ij} = (\epsilon_{ii}\epsilon_{jj})^{1/2}$ and $\sigma_{ij} = \frac{1}{2}(\sigma_{ii} + \sigma_{jj})$.

Table 8.3: Varshni Potential Parameters for NCNO

Surface	Parameter	Assumed potential[a]	Effective potential
(i)	$r_{e,CN}$	1.418 Å	1.2 Å
	β_{CN}	0.48 Å^{-2}	0.517 Å^{-2}
	D_{CN}	17880 cm^{-1}	32110 cm^{-1}
(ii)	$r_{e,CN}$	1.418 Å	1.2 Å
	β_{CN}	0.70 Å^{-2}	0.7725 Å^{-2}
	D_{CN}	17880 cm^{-1}	42600 cm^{-1}

[a] The parameter β_{CN} was obtained by setting $\partial^2 V_{varsh}/\partial r_{CN}^2 = k$ where k is the force constant for the central CN stretch given in Ref. 15. For surface (ii) β_{CN} was arbitrarily set to 0.70 Å^{-2}. All other parameters of the assumed potential are as determined spectroscopically in Ref. 4.

Table 8.4: Vibrational Distributions for NCNO at Different Excess Energies

Vibrational level	Excess energy (cm^{-1})	Vibrational distributions Exptl.	$R_i^{\dagger}$ [a]	$R^{\dagger}$ [b]	PST
$v_{CN} = 1$	2348	0.07 ± 0.02	0.06	0.07	0.034
$v_{NO} = 1$	2348	0.12 ± 0.03	0.13	0.13	0.07
$v_{CN} = 1$	2875	0.16 ± 0.02	[c]	0.13	0.11
$v_{CN} = 1$	3514	0.20 ± 0.03	[c]	[c]	0.17
$v_{CN} = 1$	4050	0.24 ± 0.03	[c]	[c]	0.20
$v_{CN} = 1$	4269	0.27 ± 0.04	[c]	[c]	0.21

[a] $R_i^{\dagger}$ corresponds to the use of the minimum of $N_{EJ,i}(R)$ for each vibrational level i.

[b] $R^{\dagger}$ corresponds to the use of the minimum of $N_{EJ}(R)$.

[c] $R^{\dagger}$ not known. If $R^{\dagger}$ or $R_i^{\dagger} \approx \infty$, the results are similar to those of PST. If instead $R^{\dagger} = 3.3$Å, the value at $E = 2875$ cm^{-1}, the values for $E = 3514, 4050$, and 4269 cm^{-1} are 0.15, 0.20 and 0.23, respectively.

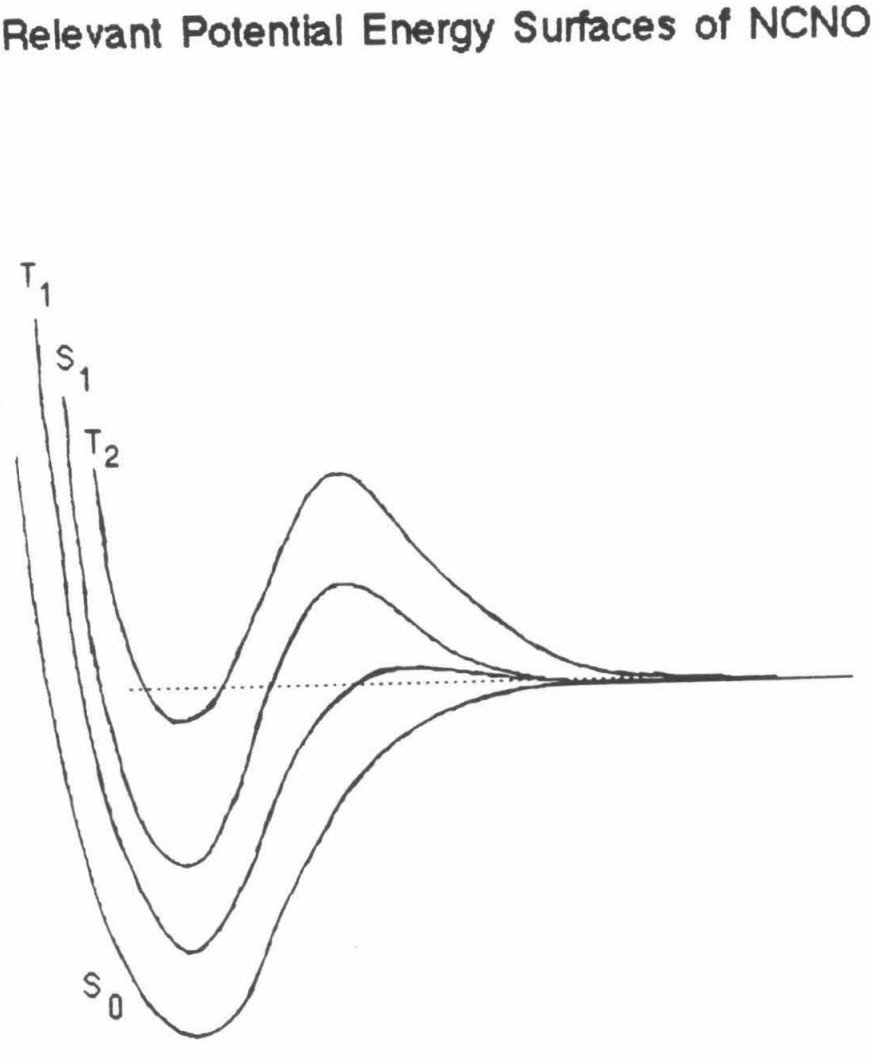

FIG. 8.1. Schematic potential energy diagram for the dissociation of NCNO into NC and NO, indicating singlet and triplet states.

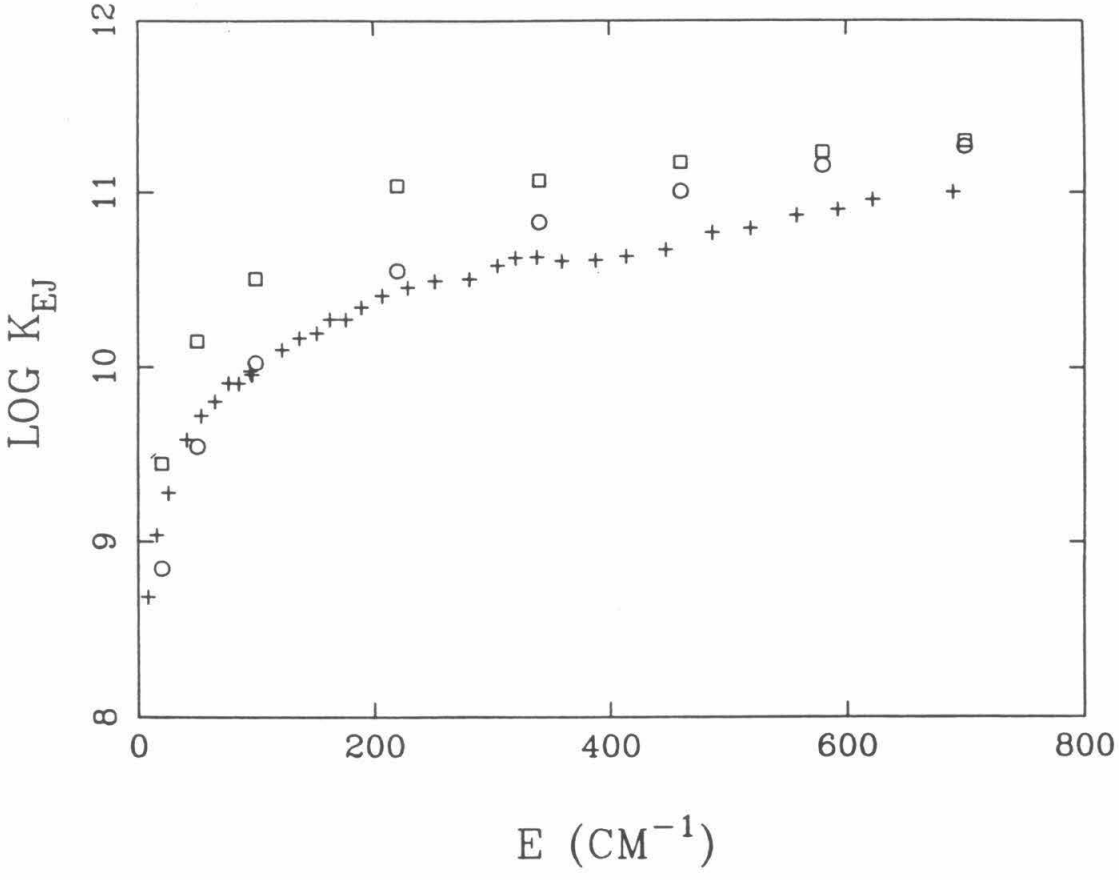

FIG. 8.2. Plot of theoretically determined rate constants log k_{EJ} vs. energy for a variety of treatments of the T_1 triplet surface, and plot of the experimentally determined rate constants (plus signs). The circles denote RRKM calculations on the singlet surface only; boxes denote RRKM calculations including singlet and triplet surfaces with a degeneracy of three for the triplet.

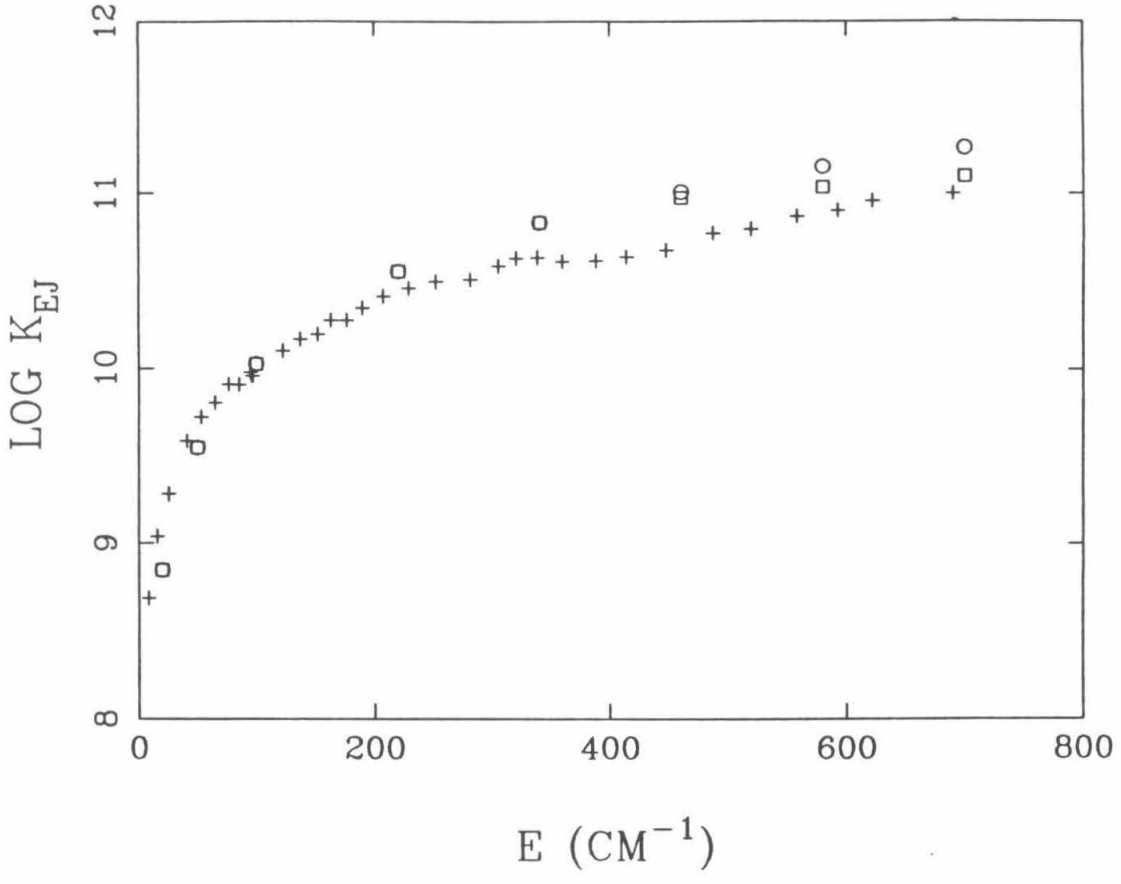

FIG. 8.3. Plot of theoretically determined rate constants log k_{EJ} vs. energy for two different assumed parameters for the Varshni bonding potential, and a plot of the experimentally determined rate constants (plus signs). Also included is a calculation which uses $N_{EJ}(\infty)$. The circles denote RRKM calculations for an assumed potential with a β parameter of 0.48 Å^{-2}; boxes denote RRKM calculations for an assumed potential with a β parameter of 0.70 Å^{-2}.

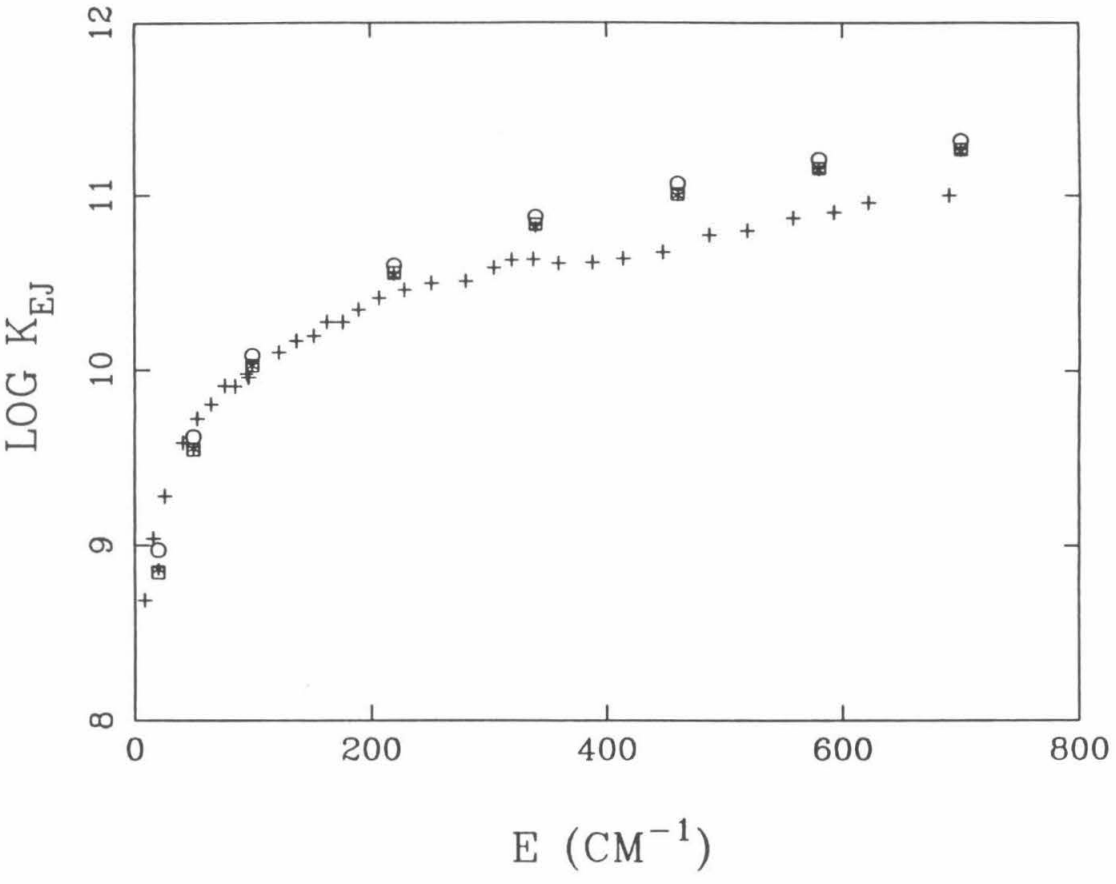

FIG. 8.4. Plot of rate constants log k_{EJ} vs. energy as determined via quantum PST, classical PST and $N_{EJ}(\infty)$ and a plot of the experimentally determined rate constants (plus signs). Circles denote quantum PST calculations, asterisks the classical PST calculations, and boxes the $N_{EJ}(\infty)$ calculation.

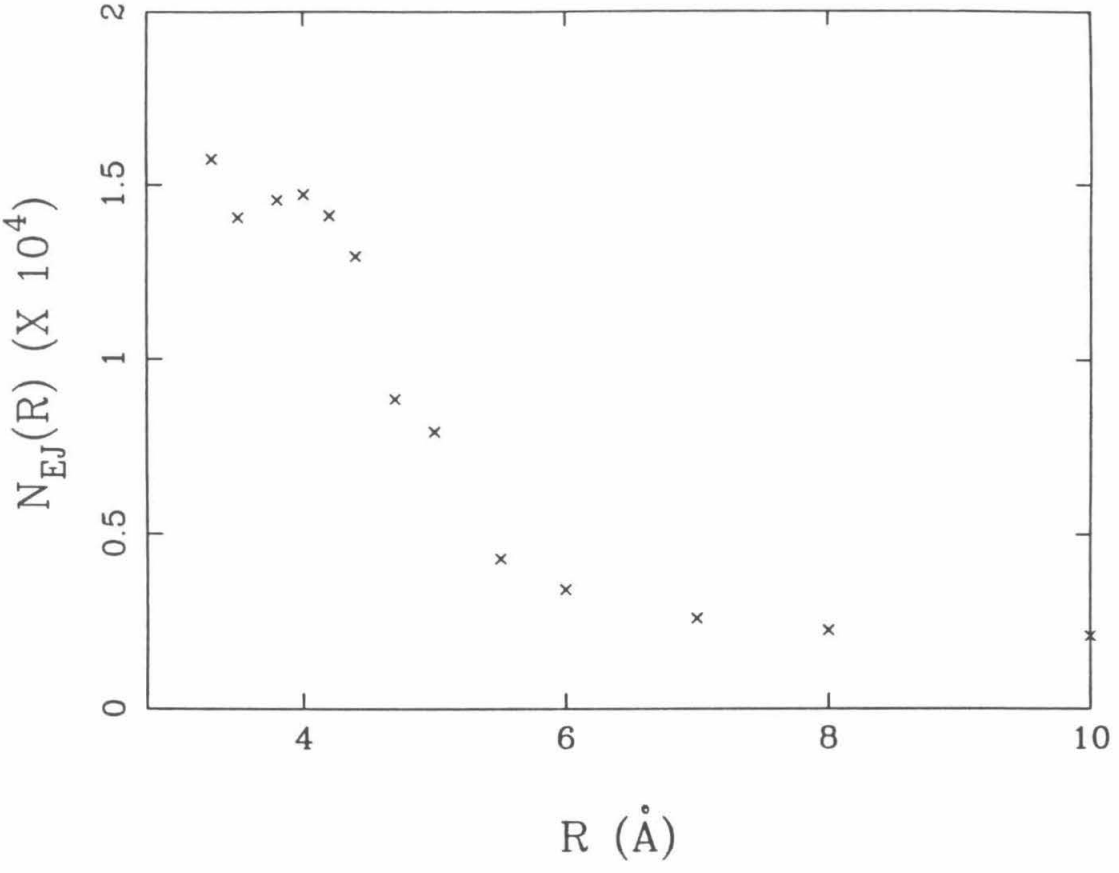

FIG. 8.5. Plot of number of states $N_{EJ}(R)$ vs. separation distance R for potential energy surface (ii) for an excess energy of 50 cm^{-1}.

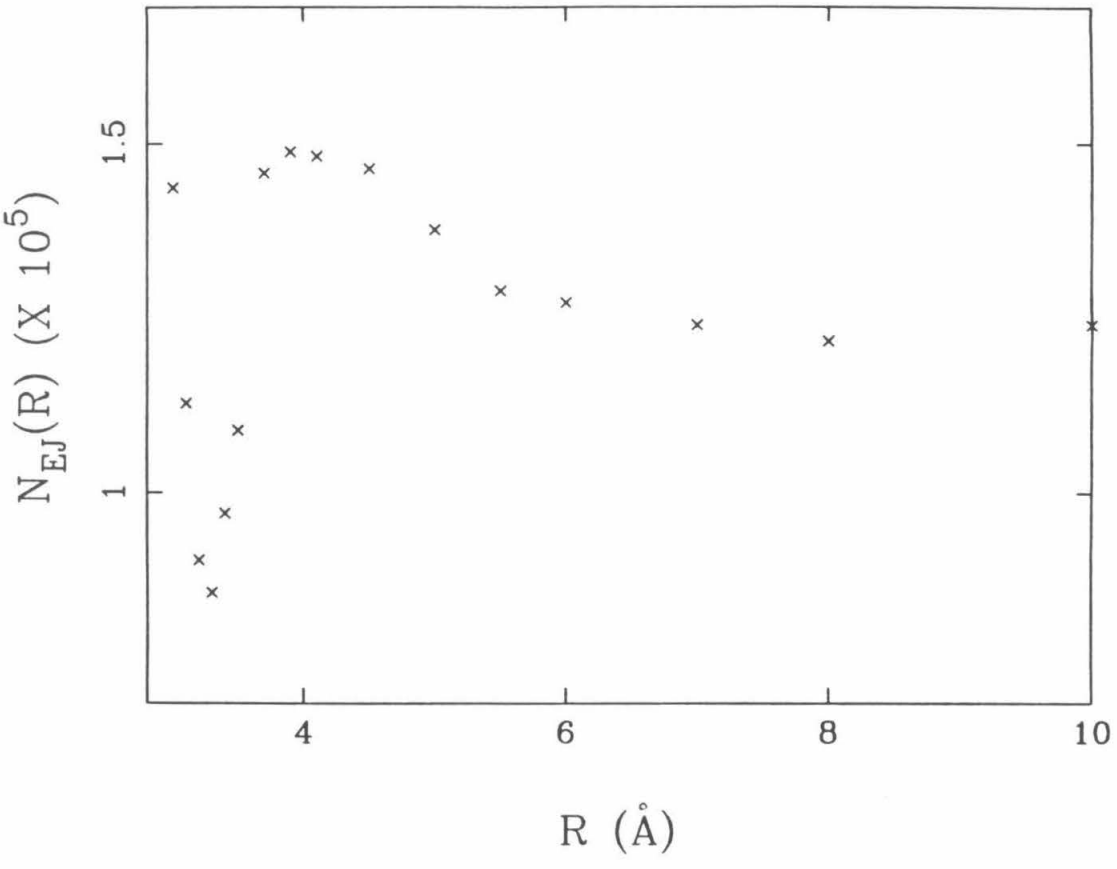

FIG. 8.6. As in Fig. 8.5 but for an excess energy of 700 cm^{-1}.

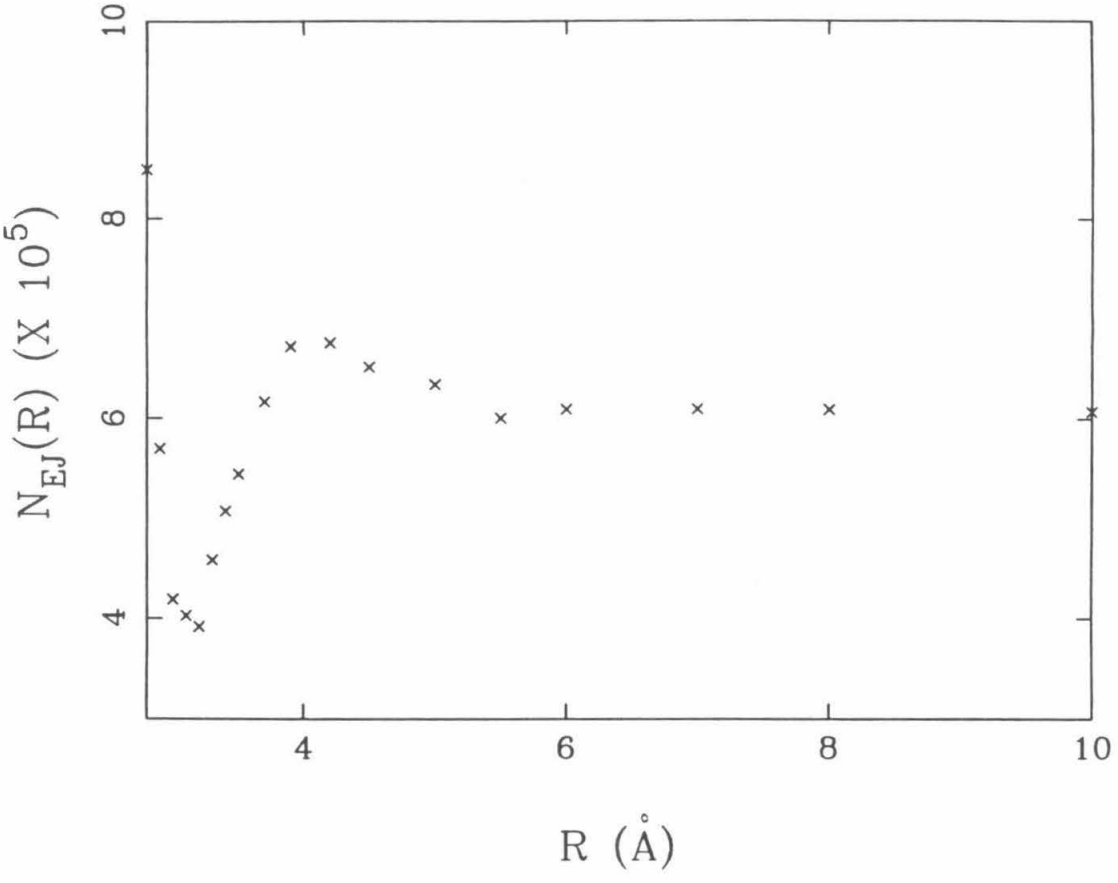

FIG. 8.7. As in Fig. 8.5 but for an excess energy of 2000 cm^{-1}.

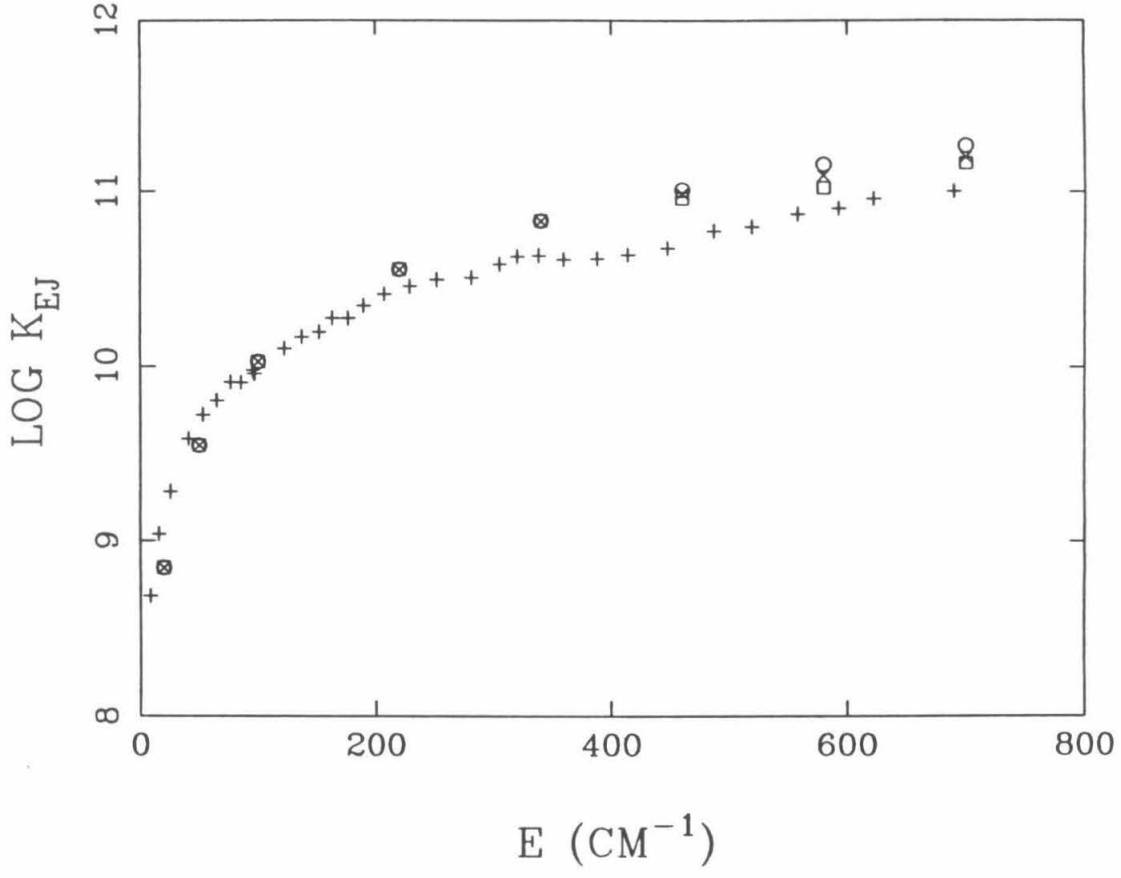

FIG. 8.8. Plot of rate constants log k_{EJ} vs. energy when the two minima in the $N_{EJ}(R)$ plot are taken into account, and a plot of the experimentally determined rate constants (plus signs). Crosses denote the use of the unified statistical theory of Ref. 16, boxes refer to the use of the lower bound of Ref. 17, and circles are for the use of the overall minimum.

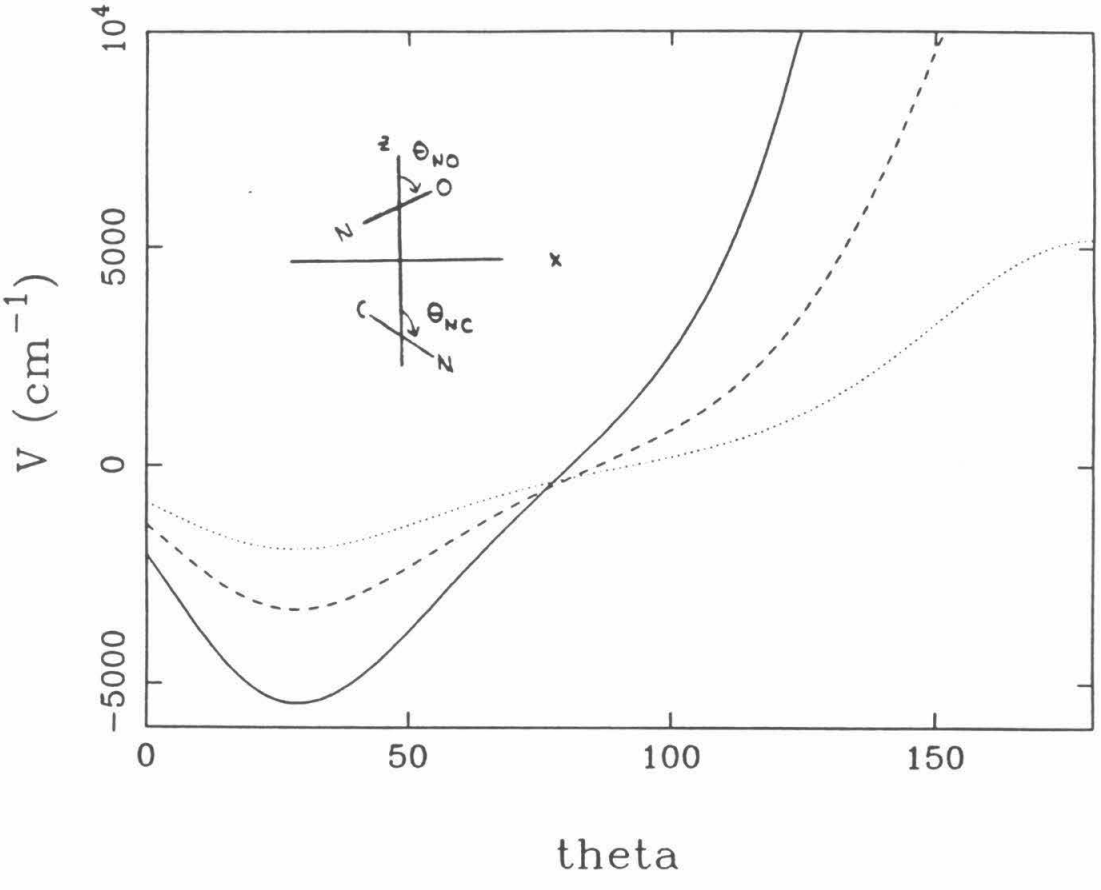

FIG. 8.9. Plot of potential energy surface (i), as a function of θ_{NC}, and θ_{NO} for a variety of R's in the transition state region. θ_{NO} and θ_{NC} are the angles defining the orientation of the fragments NC and NO for a planar NCNO molecule and are illustrated in the inset. The equilibrium orientation is for $\theta_{NO} \approx 30°$ and $\theta_{NC} \approx 180°$. The dependence of the potential energy on θ_{NO} for $\theta_{NC} = 180°$ and R = 3.3, 3.5, and 3.7 Å is given by the solid, dashed, and dotted lines, respectively.

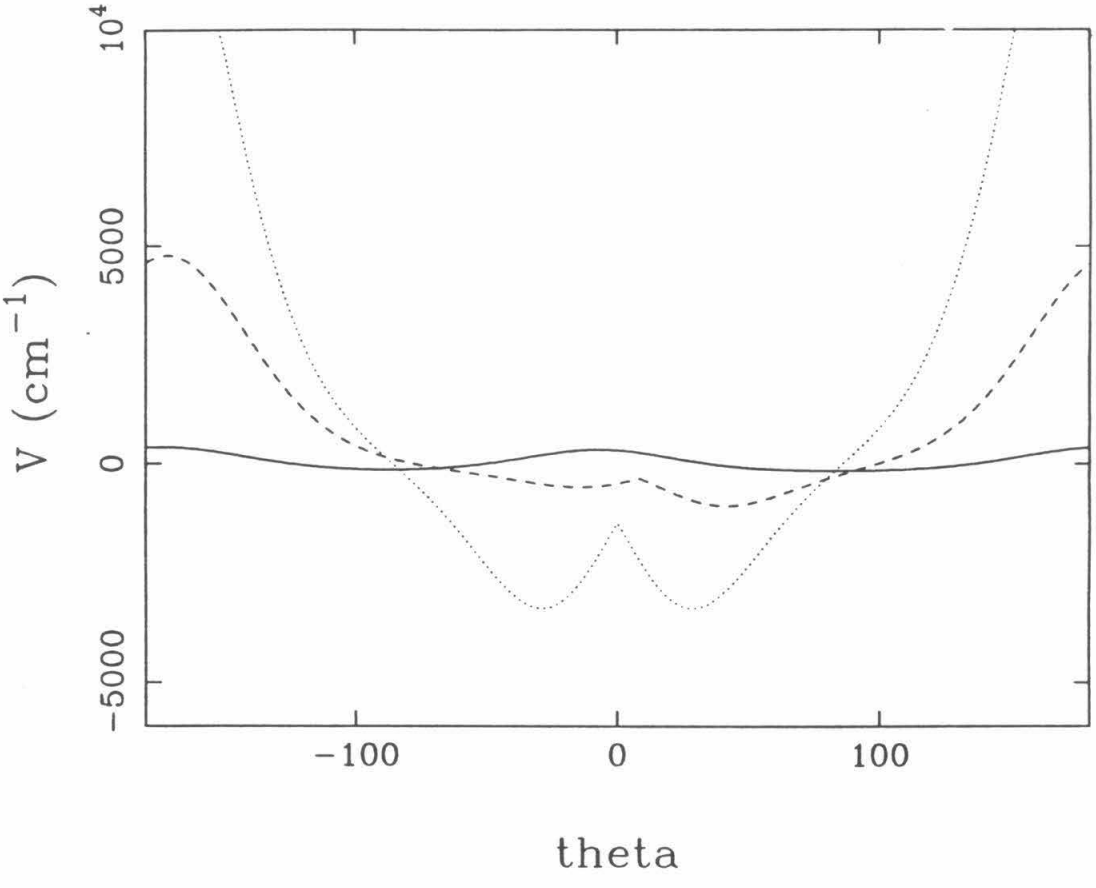

FIG. 8.10. The dependence of potential energy surface (i) on θ_{NO} for $R = 3.5$ Å and $\theta_{NC} = 90°$, 135°, and 180° is given by the solid, dashed, and dotted lines, respectively.

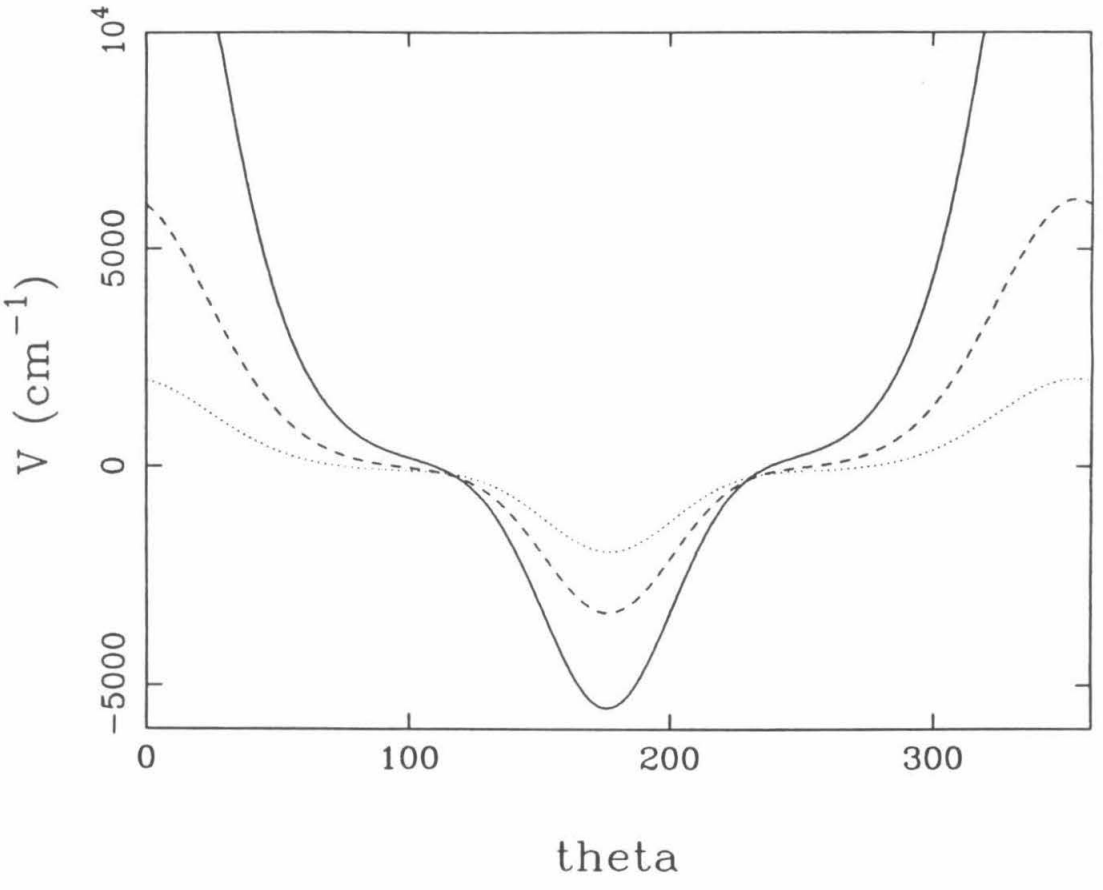

FIG. 8.11. The dependence of potential energy surface (i) on θ_{NC} for θ_{NO} = 30 and R = 3.3, 3.5, and 3.7 Å is given by the solid, dashed, and dotted lines, respectively.

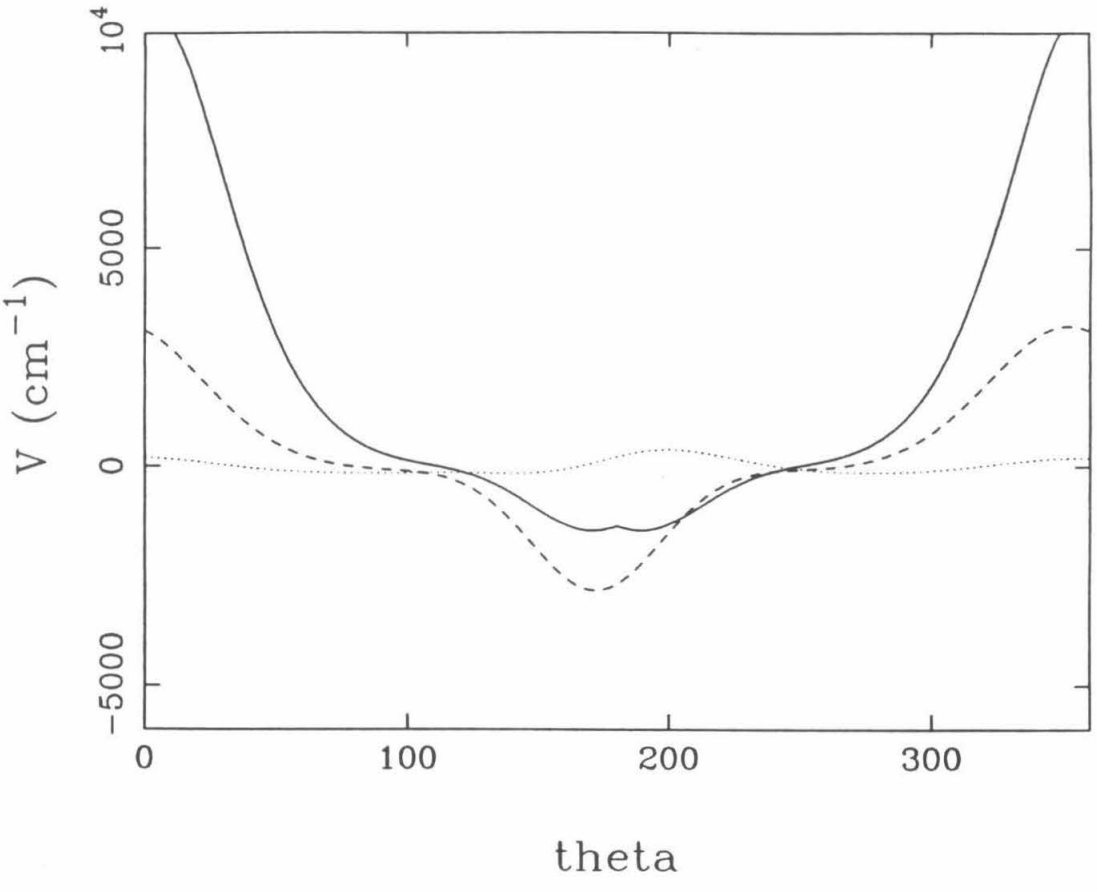

FIG. 8.12. The dependence of potential energy surface (i) on θ_{NC} for $R = 3.5$ Å and $\theta_{NO} = 0°$, 45°, and 90° is given by the solid, dashed, and dotted lines, respectively.

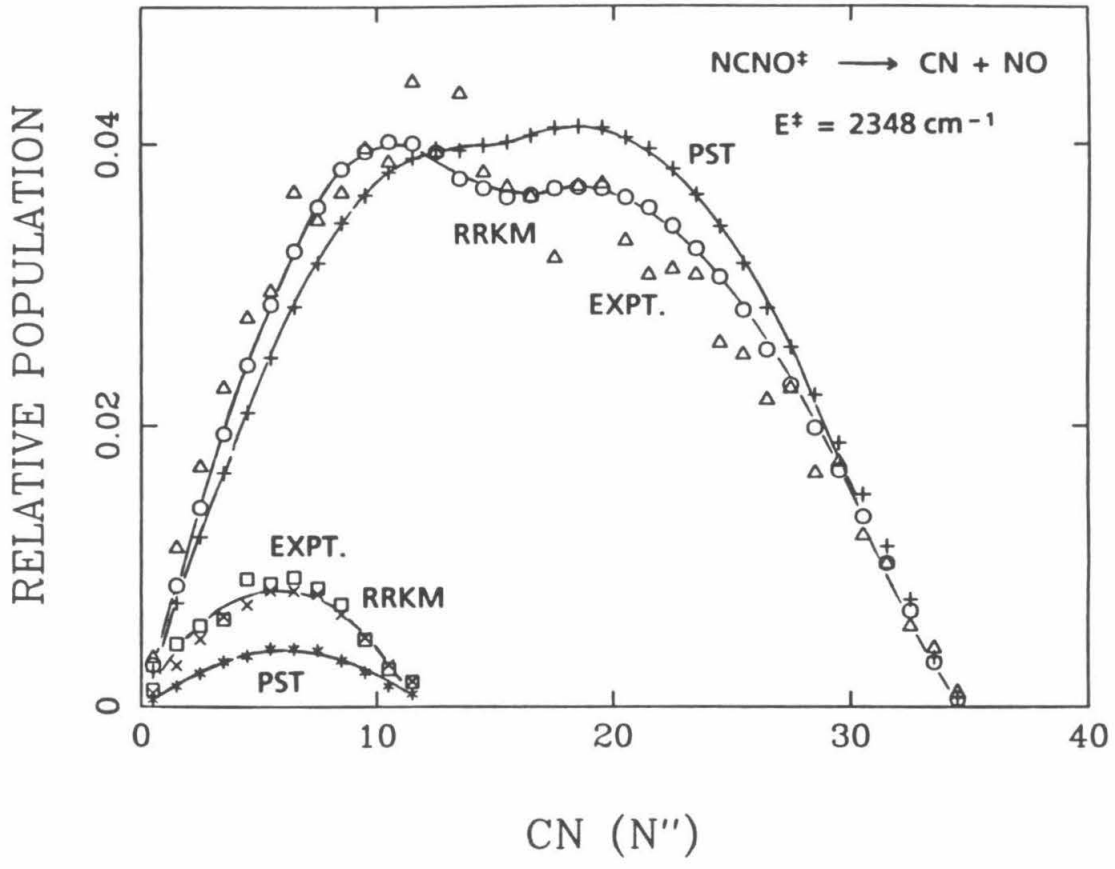

FIG. 8.13. Plot of CN rotational distribution for both the v=0 and the v=1 CN vibrational states at an excess energy of 2348 cm^{-1}. For v=0 the triangles denote the experimental results, the circles the present RRKM results, and the pluses the PST results. For v=1 the boxes denote the experimental results, the x's the present RRKM results, and the asterisks the PST results.

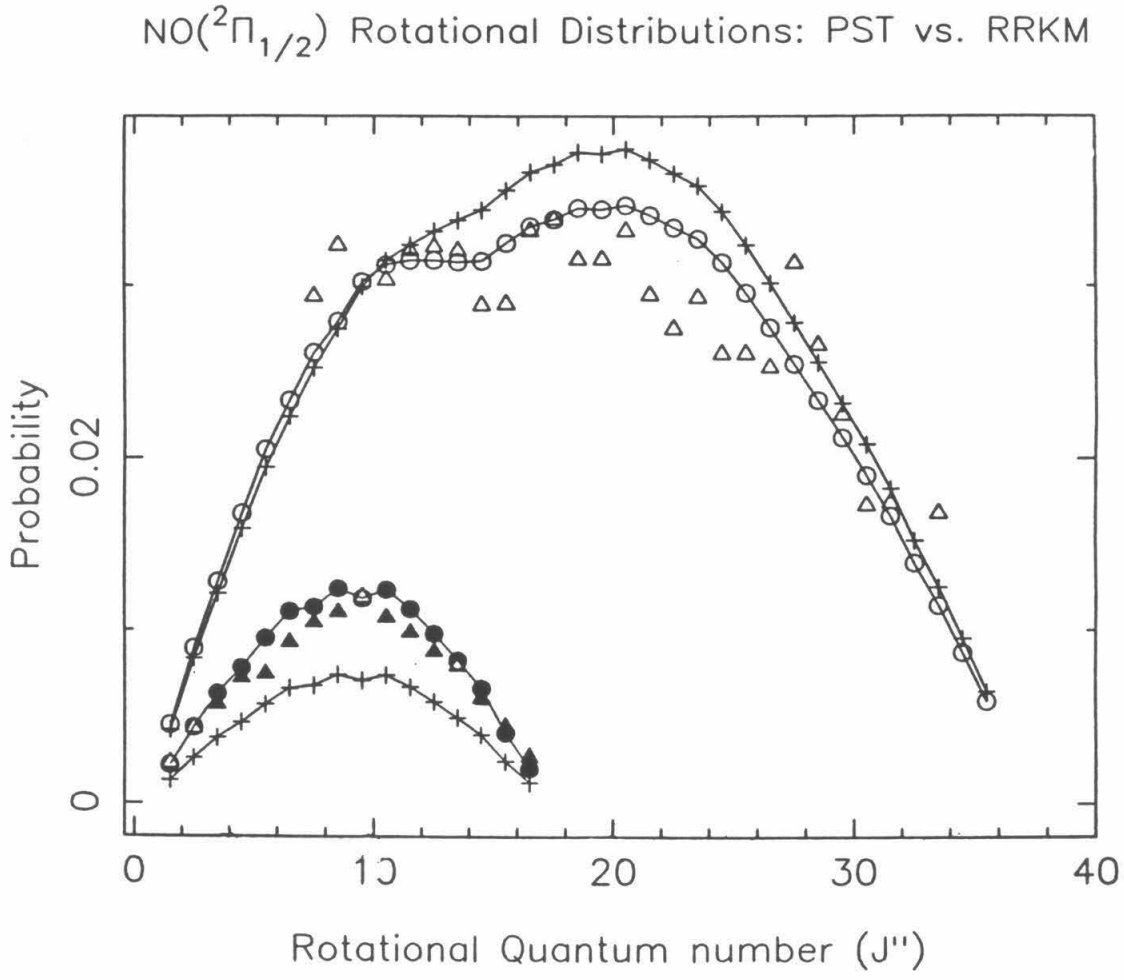

FIG. 8.14. Plot of NO($^2\Pi_{1/2}$) rotational distribution for both the v=0 and v=1 NO vibrational states at an excess energy of 2348 cm^{-1}. The triangles denote the experimental results, the circles the present results, and the pluses the PST results. The v=1 results are the ones with the lower populations.

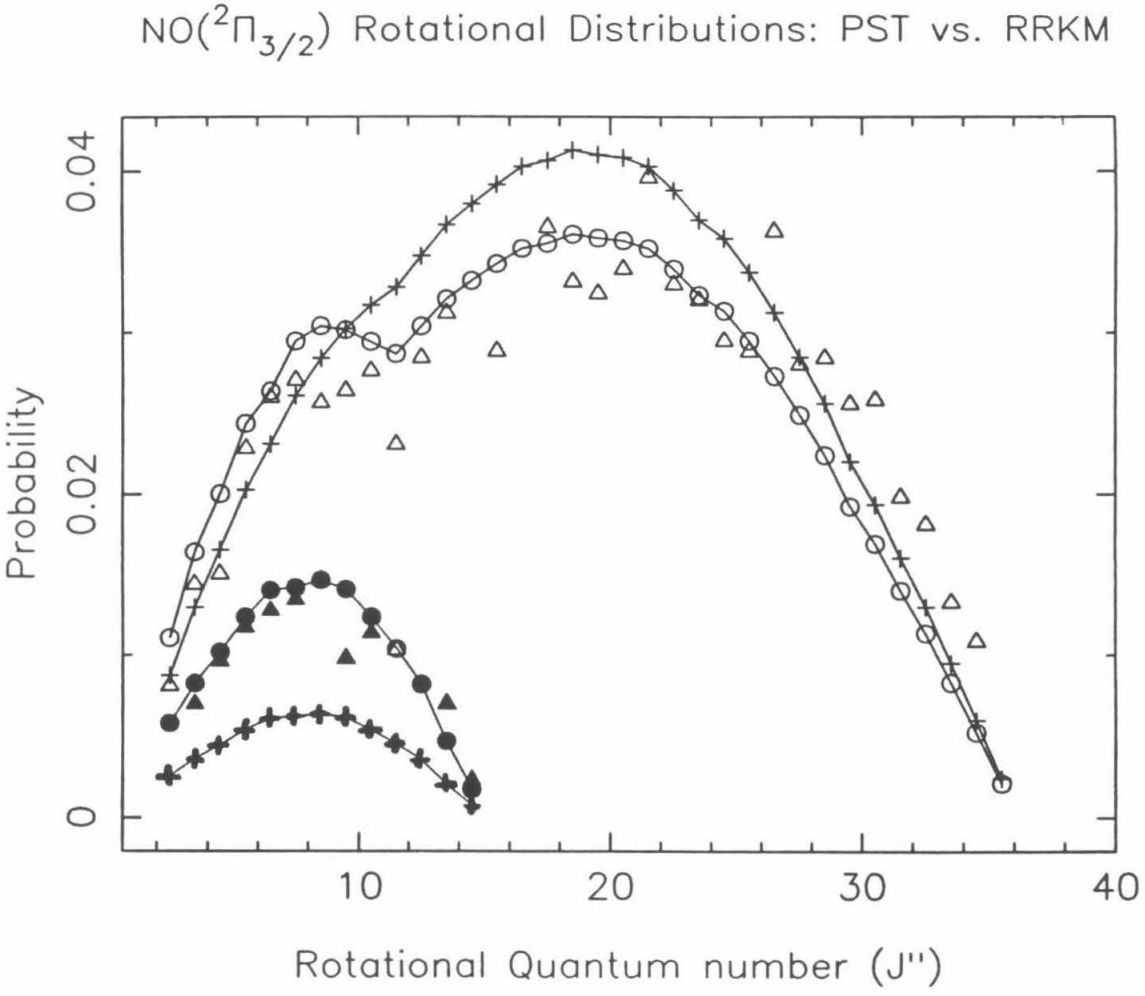

FIG. 8.15. As in Fig. 8.14 but for the NO($^2\Pi_{3/2}$) state.

Chapter 9: Application of Unimolecular Reaction Rate Theory for Highly Flexible Transition States to the Dissociation of CH_2CO into CH_2 and CO

I. INTRODUCTION

Detailed experimental results on the energy dependence of unimolecular dissociation reactions are just beginning to be obtained. In particular, energy and partially angular momentum resolved rate constants and/or energy resolved rovibrational product state distributions have recently been obtained for a variety of unimolecular dissociations reactions including those of NCNO,[1,2] H_2O_2,[3,4] CH_2CO,[5–9] and $C_6H_6^+$.[10] A recent series of experiments by Moore *et al.*[5–8] has examined particularly the nascent product state distributions of the $CH_2CO \longrightarrow CH_2 + CO$ dissociation reaction. In these latter experiments ketene molecules have been photoexcited from both cold molecular beams[7,8] and room temperature samples[5,6] at a variety of wavelengths. Also, picosecond photofragment spectroscopy experiments are currently in progress in the Zewail group[9] to determine the unimolecular dissociation rate constant for this CH_2CO dissociation reaction.

As in NCNO (e.g., see chapter 8 of the present thesis), the ketene photofragmentation occurs through first a photoexcitation to the S_1 state followed by either an internal conversion to the S_0 state or an intersystem crossing to the T_1 state. Dissociation can then occur on either the S_0 or T_1 state with the possiblity of intersystem crossing occurring between these two states.

For a given energy there are basically five different rates which must be considered when assessing the relative contributions of the singlet and triplet states to the overall dissociation process:

(i) The rate of internal conversion from S_1 to S_0.

(ii) The rate of intersystem crossing from S_1 to T_1.

(iii) The rate of dissociation on the S_0 state.

(iv) The rate of dissociation on the T_1 state.

(v) The rate of intersystem crossing from the S_0 to T_1 states.

The question of the role of the first triplet state for ketene is slightly more

complicated than it is for NCNO (e.g., see chapter 8 of the present thesis). In the case of NCNO the singlet and triplet states correlate to product states of the same energy, while the triplet state is postulated to have a barrier with a height of approximately 4500 cm^{-1} above the value of the potential at infinite separation. This relatively large barrier height indicates that the first triplet state has a negligible contribution to the dissociation process for excess energies below about 5000 cm^{-1}. The schematic diagram of the low-lying electronic states for ketene, given in Fig. 9.1, indicates that the situation is quite different in this case. In particular, the triplet state correlates to a product $^3CH_2$ + CO state which is 3556 cm^{-1} below the product $^1CH_2$ + CO state to which the singlet state correlates. The ketene triplet state does have a barrier; however, experiments suggest[8] that this barrier is less than about 1500 cm^{-1}. The above two differences from the NCNO dissociation process suggest that the triplet state may make a large contribution to the overall dissociation rate. At low enough excess energies (e.g., at and below the threshold for the singlet) the dissociation must of course occur only on the triplet potential energy surface. At slightly higher energies the situation is not so clear, while at energies of about 2500 cm^{-1} or more above the singlet threshold the singlet state appears to have the only nonnegligible contribution to the dissociation.

A discussion of a few possible limiting cases for these rates has been given in Ref. 8. In the photofragment excitation spectroscopy experiment of Ref. 8, Chen *et al.* found that the singlet/triplet branching ratio increases from 0 to 2 in the first 125 cm^{-1} above threshold. The absence of observation of a triplet product at an excess energy of 2350 cm^{-1} in both the molecular beam study of Hayden *et al.*[11] and the VUV LIF study Nesbitt *et al.*[5] indicates that for this higher excess energy the singlet/triplet branching ratio is at least 10. Therefore, the triplet state has little effect on the dissociation process at this dissociation energy, and only the singlet state needs to be considered when calculating the unimolecular dissociation rate constant for this energy region. Actually, the rapid rise from 0

to 2 in the singlet/triplet branching ratio suggests that the triplet level may be of negligible importance to the dissociation even at excess energies considerably lower than 2350 cm^{-1}.

These results can be understood if one assumes that the rate of internal conversion from the S_1 state to the S_0 state is considerably greater than the rate of intersystem crossing from the S_1 state to the T_1 state. Then, as the number of singlet states rapidly increases with energy, the singlet dissociation rate also rapidly increases until the dissociation occurs so rapidly that there is no time for an intersystem crossing from the S_0 to the T_1 surface to occur. Additionally, the presence of a barrier in the triplet surface may cause the number of states for the triplet state to increase much more slowly than the number for the singlet state. As a result, the dissociation rate constant for the singlet state may become considerably larger than that for the triplet state, giving rise to only singlet products regardless of the rate of intersystem crossing from S_0 to T_1.

The results of the photofragment excitation spectroscopy experiments of Refs. 7 and 8 for the rotational state distribution at low excess energies are well modelled by phase space theory[12] (PST). However, PST is not expected to give a particularly good description of the dissociation rate constant and the vibrational-rotational distribution at higher excess energy. For this reason, the theoretical method presented in chapters 6 and 7 is applied here to the calculation of rate constants and vibrational state distribution for the dissociation of ketene. The rate constant and vibrational distribution for a dissociation process occurring on only the singlet state will be studied. The model potential surface used is similar to that of chapter 8 and is briefly described in Sec. II. The results are presented and discussed in Sec. III. The calculational method used here is as described in chapters 6 through 8 of the present thesis and so is not discussed here.

II. POTENTIAL ENERGY SURFACES

The potential surface for the transitional modes is taken as the sum of a

bonding potential for the breaking CC bond and a nonbonding potential for the interfragment interactions for the remaining atoms. The intrafragment interactions correspond to the conserved modes and were not represented by a potential surface but rather by interpolation formulae.

The bonding potential was given by a modified effective Varshni potential written as

$$\begin{aligned} V_{bond} =& V_V^{eff} \cos^2\left(\theta_{CCO} - \theta^e_{CCO}\right) \\ & \times \left[\cos^2\left(\theta_{HCC_1} - \theta^e_{HCC_1}\right) + \cos^2\left(\theta_{HCC_2} - \theta^e_{HCC_2}\right)\right]/2 \end{aligned} \tag{1}$$

Here, θ_{CCO}, θ_{HCC_1} and θ_{HCC_2} denote the CCO, and two HCC bending angles, while the e superscripts here and elsewhere denote equilibrium values. These equilibrium values along with the other spectroscopic parameters used here may be found in Table 9.1.

In Eq. (1) V_V^{eff} denotes an effective Varshni potential[18] given by the standard form

$$V_V^{eff} = D_{CC}^{eff}\left\{1 - \left(\frac{r_{CC}^{e,eff}}{r_{CC}}\right)\exp\left[-\beta_{CC}^{eff}\left(r_{CC}^2 - r_{CC}^{e,eff\,2}\right)\right]\right\}^2 - D_{CC}^{eff}. \tag{2}$$

The quantities D_{CC}^{eff}, and $r_{CC}^{e,eff}$ correspond to the C–C dissociation energy and separation distance, respectively, while β_{CC}^{eff} is the standard Varshni β constant and is related to the C–C force constant. The parameters for this surface are given in Table 9.2 and were determined through a fit of the total potential surface (including the nonbonding interactions) to the Varshni parameters, which correspond to the spectroscopically determined force constant, dissociation energy and separation distance. This fit was performed for a center-of-mass to center-of-mass separation R of 2.8 to 3.0 Å.

The nonbonding potential was taken as the sum of the van der Waals interactions between the nonbonded atoms, with the Van der Waals interactions represented by Lennard-Jones 6-12 potentials:

$$V_{LJ} = \sum_{i=1}^{3}{}' \sum_{j=1}^{2}{}' 4\epsilon_{ij}\left[\left(\sigma_{ij}/r_{ij}\right)^{12} - \left(\sigma_{ij}/r_{ij}\right)^{6}\right], \tag{3}$$

where i and j label atoms in the CH_2 and CO fragments, respectively, and the prime indicates that the C–C bond is not included in the sum. The parameters σ_{ij} and ϵ_{ij} denote the usual Lennard-Jones parameters for the interaction between atoms i and j while r_{ij} is the separation distance between atoms i and j. The Lennard-Jones parameters used here were taken from Ref. 19 and are given in Table 9.3.

The conserved modes were treated with an exponential interpolation[20,21] between their reactant and product values given by

$$\lambda_i(R) = \lambda_i^p + (\lambda_i^r - \lambda_i^p)g(R), \tag{4}$$

where $g(R) = \exp[-\alpha(R - R^e)]$.[20,21] The quantity λ denotes ν, r^e, or θ^e, the frequency, separation distance and bending angle, respectively, for the given atoms, and i denotes CH, CO, or HCH. The r and p superscripts denote the reactant (CH_2CO) and products ($^1CH_2$ + CO), respectively. The parameters for the conserved modes are given along with the other spectroscopic parameters in Table 9.1.

III. RESULTS AND DISCUSSION

The calculations presented here are all for a total angular momentum J of 3. The overall statistical factor for the dissociation on the singlet state only is given by 1. The density of states was calculated from the harmonic frequencies given in Table 9.1. The contribution of the anharmonicities to the density of states should be small (i.e., less than about 2) and also it should be the same for both of the calculations to be presented. Thus the qualitative findings would be unchanged.

In Fig. 9.2 results are presented for the rate constant for the dissociation on S_0 in the energy range from 100 to 5000 cm^{-1} above the singlet threshold. Given there are results from both a variational treatment of the transition state and from an alternative calculation where the transition state location ($R^\dagger$) is fixed at ∞. This latter calculation corresponds to a classical PST[12] calculation on a very

strongly attractive potential, because in the case of a strongly attractive potential the orbital angular-momentum-dependent effective barriers are negligible. Chen *et al.*[8] have found that in the PST model a very strongly attractive potential gives the best agreement with the experimental results. From the results given in Fig. 9.2 it is seen that the deviation between the variational RRKM calculation and the $R^{\dagger} = \infty$ calculation rapidly increases as the energy increases. The ratio of the result at $R^{\dagger} = \infty$ to the variational result increases from 1.5 to 7.5 as the excess energy increases from 100 to 5000 cm^{-1}.

It is interesting to note that this deviation of the variationally determined rate constant from the $R^{\dagger} = \infty$ rate constant is considerably larger than that observed in the previous applications of this method. One reason for this can be seen when making a comparison of the Varshni β parameter for the previous applications with that for CH_2CO. For NCNO, C_2H_6, and H_2O_2 the β parameter is given by 0.48, 0.37 and 0.61 $Å^{-2}$, whereas for CH_2CO the β parameter is given by 0.73 $Å^{-2}$. As a result, the fragments come in closer contact before feeling any strong bonding attraction, thereby allowing the repulsions between them (i.e., the Van der Waals repulsions and the orbital angular momentum repulsion) to be of larger magnitude, leading to a smaller value for the phase space integral at the transition state, which enters the variational RRKM rate constant.

Preliminary calculations on the distribution of vibrational states have also been performed. These calculations are based on the method presented in Ref. 22 and are similar to those described in chapter 8 of the present thesis for NCNO. In particular, the vibrational distribution is postulated to be determined by the number of states at $R_i^{\dagger}$, i.e., the location of the minimum in the number of states for vibrational state i. The rotations, however, are postulated to be determined by the statistical PST[12] distribution at the location of the PST orbital angular momentum-l-dependent transition state R_l. In Table 9.4 results of calculations for the vibrational distribution are presented for three different energies. These three energies correspond to typical energies of the photoexcited ketene molecules

in the experimental work of Ref. 5 (taking into account both the initial thermal energy of the ketene molecules and the laser excitation energy). The laser wavelength used in Ref. 5 corresponds to an excess energy of 2350 cm^{-1} while the thermal distribution resulted in populations of initial ketene of greater than 0.01 for energies in excess of 1000 cm^{-1} (e.g., see Fig. 4 of Ref. 5). For a direct comparison of the present results with those of Ref. 5 the vibrational distributions should be averaged over the thermal distribution given there. However, for purposes of illustration the calculated vibrational distribution is given for an energy which corresponds to the laser excitation energy and also for two other energies which correspond to the sum of the laser excitation and 500 and 1000 cm^{-1}.

The experimental result[5] for the $v_{CO} = 1$ vibrational distribution was 0.09 ± 0.05 at an excess energy of 2350 cm^{-1}. Taking into account the initial thermal distribution of the ketene molecules, the PST result[5] was given by 0.013. The results given in Table 9.4 suggest that with the proper thermal averaging, the RRKM theory result would increase the PST result by roughly the amount necessary to accommodate the experimental data.

Perhaps it should be mentioned here that a difficulty arises in the calculation of the vibrational distributions in the case where an overall $R^\dagger$ is used rather than individual $R_i^\dagger$'s. This difficulty occurs for the following reason: The total number of states is at its minimum at $R = R^\dagger$ and thus slowly varies with R for R near $R^\dagger$. The number of states for the particular vibrational state of interest is instead far from its minimum at $R = R^\dagger$ and thus rapidly varies with R in this region. Thus, a small error in $R^\dagger$ can result in a large error in the number of states for the particular vibrational state of interest. Correspondingly, the value obtained for the particular vibrational distribution depends strongly on the exact location of $R^\dagger$.

In summary, the CH_2CO dissociation process presents a good example of a dissociation process where the hindered rotor nature of a loose transition state

causes considerable differences from PST to occur. The present implementation of RRKM theory predicts a decrease by a factor of about 7 from the PST result for the singlet state rate constant at an excess energy of 5000 cm^{-1}. Such a difference could well be distinguished experimentally. Also, the present implementation predicts an increased vibrational excitation over PST in accord with the experimental observations of Ref. 5.

ACKNOWLEDGMENTS

It is a pleasure to acknowledge the support of this research by the National Science Foundation.

REFERENCES

[1] C. X. W. Qian, M. Noble, I. Nadler, H. Reisler, and C. Wittig, J. Chem. Phys. **83**, 5573 (1985), and references cited therein.

[2] L. R. Khundkar, J. L. Knee and A. H. Zewail, J. Chem. Phys. **87**, 77 (1987).

[3] L. J. Butler, T. M. Ticich, M. D. Likar, and F. F. Crim, J. Chem. Phys. **85**, 2331 (1986); T. M. Ticich, T. R. Rizzo, H. R. Dübal, and F. F. Crim, J. Chem. Phys. **84**, 1508 (1986), and references cited therein.

[4] N. F. Scherer and A. H. Zewail, J. Chem. Phys. **87**, 97 (1987), and references cited therein.

[5] D. J. Nesbitt, H. Petek, M. F. Foltz, S. V. Filseth, D. J. Bamford, and C. B. Moore, J. Chem. Phys. **83**, 223 (1985).

[6] H. Bitto, I.-C. Chen, and C. B. Moore, J. Chem. Phys. **85**, 5101 (1986).

[7] H. Bitto, D. R. Gwyer, W. F. Polik and C. B. Moore, Far. Disc. Chem. Soc. **81**, 149 (1986).

[8] I.-C. Chen, W. H. Green, Jr., and C. B. Moore, preprint.

[9] A. J. Hoffman, L. R. Khundkar, and A. H. Zewail, work in progress.

[10] A. Kiermeier, H. J. Neusser, and E. W. Schlag, Z. Naturforsch. **42a**, 1399 (1987).

[11] C. C. Hayden, D. M. Neumark, K. Shobatake, R. Sparks, and Y. T. Lee, J. Chem. Phys. **76**, 3607 (1982).

[12] P. Pechukas and J. C. Light, J. Chem. Phys. **42**, 3281 (1965); P. Pechukas, R. Rankin, and J. C. Light, J. Chem. Phys. **44**, 794 (1966); C. Klotz, J. Phys. Chem. **75**, 1526 (1971).

[13] C. B. Moore and G. C. Pimentel, J. Chem. Phys. **38**, 2816 (1963).

[14] P. D. Mallinson and L. Nemes, J. Mol. Spect. **59**, 470 (1976).

[15] G. Herzberg, F. R. S., and J. W. C. Johns, Proc. R. Soc. London, Ser. A, **295**, 107 (1966).

[16] K. P. Huber and G. Herzberg, *Constants of Diatomic Molecules* (Van Nostrand-Reinhold, New York, 1979).

[17] H. Petek, D. J. Nesbitt, P. R. Ogilby, and C. B. Moore, J. Phys. Chem. **87**, 5367 (1983).

[18] Y. P. Varshni, Rev. Mod. Phys. **29**, 664 (1957); D. Steele, E. R. Lippincott, and J. T. Vanderslice, Rev. Mod. Phys. **34**, 239 (1962).

[19] W. L. Jorgensen and C. J. Swenson, J. Am. Chem. Soc. **107**, 569 (1985).

[20] M. Quack and J. Troe, Ber. Bunsenges. Phys. Chem. **78**, 240 (1974); J. Troe J. Phys. Chem. **88**, 4375 (1984).

[21] D. M. Wardlaw and R. A. Marcus, J. Chem. Phys. **83**, 3462 (1985).

[22] R. A. Marcus, Chem. Phys. Lett. **144**, 208 (1988).

Table 9.1: Spectroscopic Parameters for CH_2CO

Parameter		Reactants[a] Value	Products[b] Value
Frequencies	CH stretch	3166	2864
(cm^{-1})	CH stretch	3070	2806
	CO stretch	2152	2156
	HCH bend	1388	
	CC stretch	1118	
	CH_2 rock	977	1352
	CH_2 wag	591	
	CCO bend	525	
	CCO bend	438	
Coordinates	R_e	2.054 Å	
	$r_{e,CH}$	1.077 Å	1.11 Å
	$r_{e,CO}$	1.161 Å	1.128 Å
	θ^e_{HCH}	122.0°	102.0°
	θ^e_{CCO}	180°	

[a] The parameters for the reactants have been obtained from Refs. 13 and 14.

[b] The parameters for the products have been obtained from Refs. 15 - 17.

Table 9.2: Lennard-Jones Potential Parameters for CH_2CO

Parameter	Value[a]	Units
σ_{CO}	3.36	Å
σ_{CH}	3.40	Å
σ_{OH}	3.00	Å
ϵ_{CO}	56.	cm^{-1}
ϵ_{CH}	11.	cm^{-1}
ϵ_{OH}	13.	cm^{-1}

[a] All values have been obtained from Ref. 19 making use of the combination rules $\epsilon_{ij} = (\epsilon_{ii}\epsilon_{jj})^{1/2}$ and $\sigma_{ij} = \frac{1}{2}(\sigma_{ii} + \sigma_{jj})$.

Table 9.3: Varshni Potential Parameters for CH_2CO

Parameter	Assumed potential[a]	Effective potential
$r_{e,CC}$	1.316 Å	1.15 Å
β_{CC}	0.73 $Å^{-2}$	0.7765 $Å^{-2}$
D_{CC}	32304 cm^{-1}	65750 cm^{-1}

[a] The parameter β_{CC} was obtained by setting $\partial^2 V_{varsh}/\partial r_{CC}^2 = k$ where k is the force constant for the central CC stretch given in Ref. 14.

Table 9.4: Vibrational Distributions for CH_2CO at Different Excess Energies

Vibrational level	Excess energy (cm^{-1})	Vibrational distributions $R_i^{\dagger}$ [a]	$R^{\dagger}$ [b]
$v_{CO} = 1$	2350	0.016	0.06
$v_{CO} = 1$	2850	0.07	0.11
$v_{CO} = 1$	3350	0.10	0.09

[a] $R_i^{\dagger}$ corresponds to the use of the minimum of $N_{EJ,i}(R)$ for each vibrational level i.

[b] $R^{\dagger}$ corresponds to the use of the minimum of $N_{EJ}(R)$.

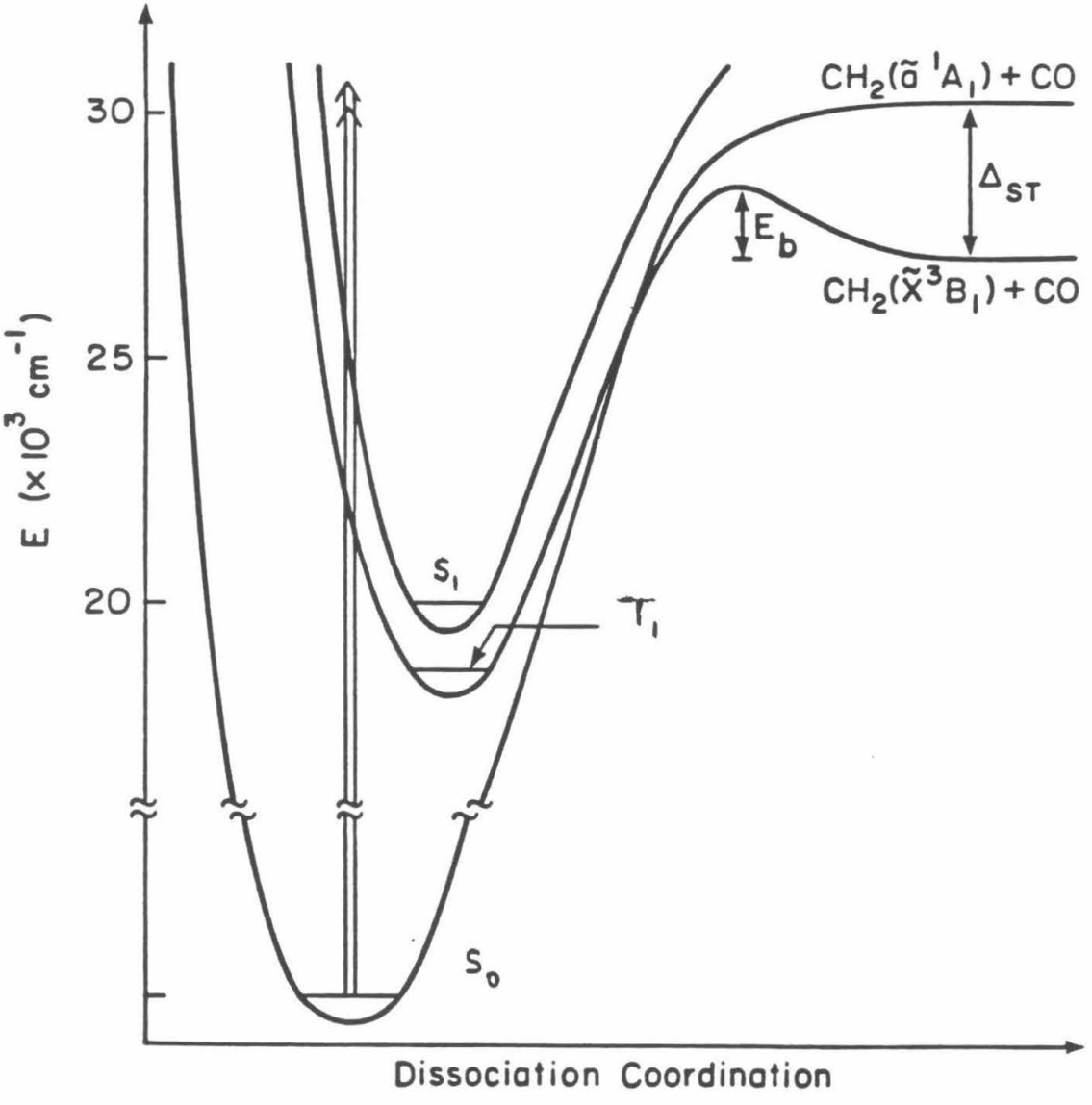

FIG. 9.1. Schematic potential energy diagram for the dissociation of CH_2CO into CH_2 and CO. (Taken from Ref. 8.)

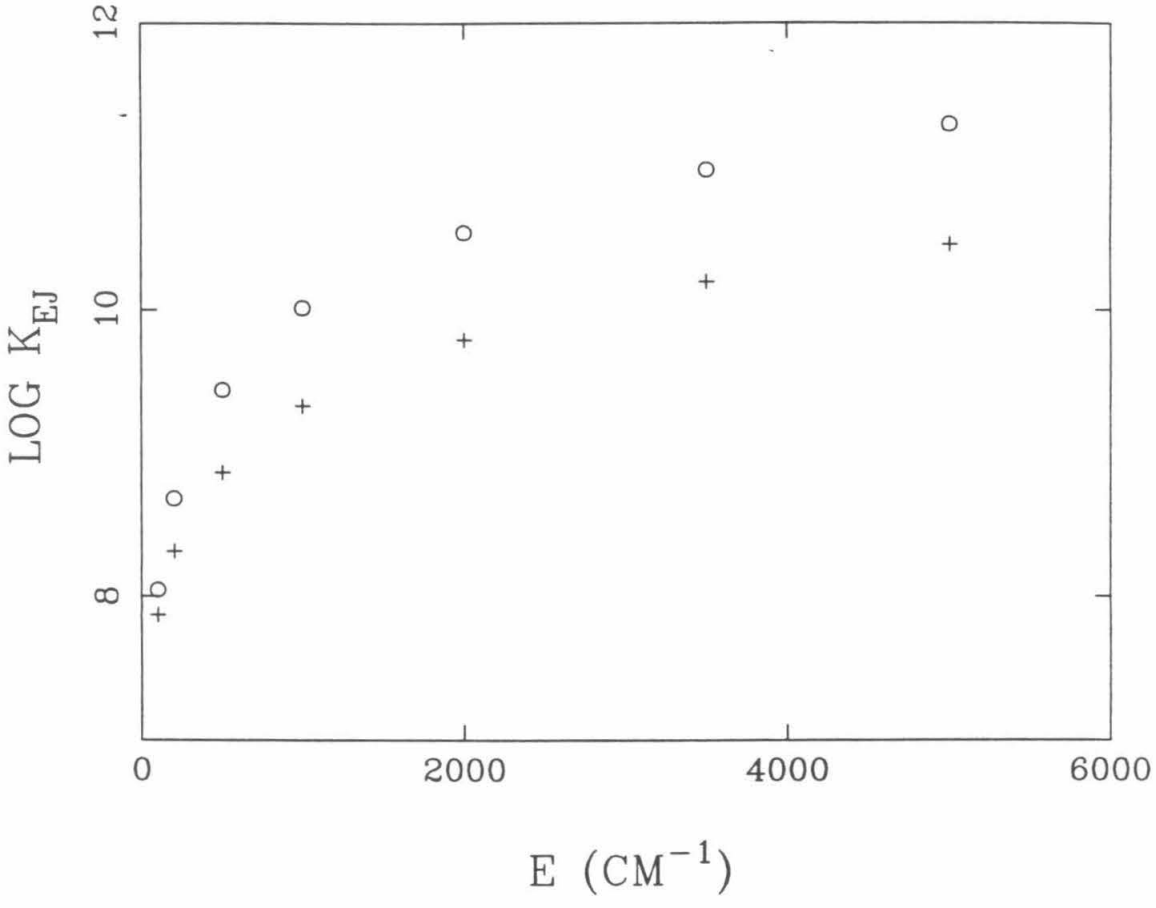

FIG. 9.2. Plot of calculated rate constant log k_{EJ} versus energy. The circles denote the $N_{EJ}(\infty)$ calculation, while the pluses denote the variational RRKM calculation.

Appendix: Comparison of RRKM Theory with the Statistical Adiabatic Channel Model and with Phase Space Theory for the H_2O_2 Dissociation

An alternative method for determining the transition state number of states for dissociation reactions containing highly flexible transition states was developed by Quack and Troe[1] and has been termed the statistical adiabatic channel model (SACM). This method is based on an adiabatic approximation for the motion from the reactants to the product. Interpolation formulae are then used to calculate the energy levels as a function of separation distance R. The number of states for a given energy E and angular momentum J is then given by the sum over all the different rotational vibrational states whose total angular momentum is J and whose maximum energy as a function of R is less than the energy E.

In this appendix the results of a variational RRKM theory calculation are given and compared with the corresponding results of a SACM calculation. Also given, for comparison, are results of calculations based on classical phase space theory[2] and calculations based on the number of states when the fragments are at infinite separation. The SACM calculations are taken from Ref. 3, while the variational RRKM calculations are based on the formalism presented in chapters 6 through 9 of the present thesis.

The calculations presented are for the photodissociation of H_2O_2. This photodissociation reaction has been of considerable interest recently.[3–9] Scherer *et al.*[6] used picosecond photofragment spectroscopy to determine the dissociation rate constant for the $v_{CH} = 5$ overtone. The energy of this overtone state is just below the threshold for dissociation, and so the dissociating molecules must have an initial thermal excitation of either a vibrational mode or, alternatively, their rotational state. Other experiments have been performed by Crim *et al.*[4] in which the product state distribution is determined for both the $v_{CH} = 5$ and $v_{CH} = 6$ overtones. They also used linewidth measurements in Ref. 5 to estimate the lifetimes for these same overtone states.

The potential energy surface used is identical to that discussed in Ref. 9. For completeness the spectroscopic parameters and the parameters for the potential energy surface are given here in Table A.1. The potential surface used is based on

a sum of exponentially interpolated bending potentials for the HOO bends and an exponentially interpolated torsional potential. Also, the bonding interaction is treated as a Morse potential. More detail of the potential surface used is given in Ref. 9. The density of states was not calculated here, but rather the values listed in Table I of Ref. 3 were used.

The results of the present RRKM theory calculations are given in Tables A.2 and A.3, along with the results from the SACM calculation of Ref. 3, a classical phase space theory[2] (PST) calculation and a calculation based on infinite separation of the fragments. Quantum PST calculations are very similar to the classical PST calculations, differing by at most 10%, and so are not presented. The C_6 parameter used in the PST calculations is 1×10^6 cm^{-1}Å^6.

Considering first the $J = 10$ results of Table A.2 we observe that the results of all four calculations are quite similar. The $N_{EJ}(\infty)$ and the PST results are within 3% for all energies listed, indicating that the orbital angular momentum effective barriers play little role. The variational RRKM results are a factor of 0.61 below the $N_{EJ}(\infty)$ results at $E = 200$ cm^{-1} and rapidly increase to a factor of 0.88 at energies of 1200 cm^{-1}. It appears that the reason for the greater difference at lower energies is due to the torsional potential which rapidly loses its importance as the energy increases. Also, the torsional potential is interpolated with the exponential interpolation $g(R)$ rather than its square as in the bending potential and for this reason may be dominant at large separation distance. The ratio of the SACM calculations to the $N_{EJ}(\infty)$ on the other hand is more constant ranging from 0.62 to 0.75.

In the $J = 40$ calculations much larger differences are observed between the four calculations. For this large value of the total angular momentum quantum number J, the orbital angular momentum (l) dependent effective barriers now become a dominant factor at the lower energies. The importance of the l-dependent effective barriers can be easily seen by comparing the $N_{EJ}(\infty)$ calculation, for which the l-dependent barriers are neglected, with the PST calculation. Here,

the PST results obtained are quite strongly dependent on the value of C_6 potential parameter. For example, a C_6 parameter of 5×10^5 gives PST results of 1.4×10^9 and 1.0×10^{10} for excess energies of 200 and 400 cm^{-1}.

Once again the exponentially interpolated torsional potential causes the RRKM calculation results to be below those of the SACM calculation at the lowest energies. However, at higher energies the RRKM calculation gives results which more closely approach the PST and $N_{EJ}(\infty)$ results than do the SACM results. A possible explanation for this effect lies in the fact that the SACM calculation assumes harmonic oscillator bending energy levels in its interpolation formulae regardless of the excess energy. In fact these bending motions are hindered rotational motions, and so at high enough energies the energy levels will deviate quite strongly from the equivalent harmonic oscillator levels. The energy levels are actually more closely spaced than the harmonic oscillator energy levels and as result the number of states is closer to that of PST.

In summary, for the parameters used here to model the H_2O_2 dissociation reaction there is little difference, in the results for the rate constant, between the PST calculations and the more detailed RRKM and SACM calculations. The differences that do arise between the results of the different calculations are largest in the case of low energy for $J = 40$. In particular, the importance of the orbital angular momentum effective barriers is evident in the latter case.

REFERENCES

[1] M. Quack and J. Troe, Ber. Bunsenges. Phys. Chem. **78**, 240 (1974); M. Quack and J. Troe, Ber. Bunsenges. Phys. Chem. **79**, 170 (1975); J. Troe, J. Chem. Phys. **75**, 226 (1981).

[2] P. Pechukas and J. C. Light, J. Chem. Phys. **42**, 3281 (1965); P. Pechukas, R. Rankin, and J. C. Light, J. Chem. Phys. **44**, 794 (1966); C. Klotz, J. Phys. Chem. **75**, 1526 (1971).

[3] L. Brouwer, C. J. Cobos, J. Troe, H.-R. Dubal, and F. F. Crim, J. Chem. Phys. **86**, 6171 (1987).

[4] T. R. Rizzo and F. F. Crim, J. Chem. Phys. **76**, 2754 (1982); T. R. Rizzo, C. C. Hayden, and F. F. Crim, Far. Disc. Chem. Soc. **75**, 223 (1983); T. R. Rizzo, C. C. Hayden, and F. F. Crim, J. Chem. Phys. **81**, 4501 (1984); H. R. Dübal and F. F. Crim, J. Chem. Phys. **83**, 3863 (1985); T. M. Ticich, T. R. Rizzo, H. R. Dübal, and F. F. Crim, J. Chem. Phys. **84**, 1508 (1986).

[5] L. J. Butler, T. M. Ticich, M. D. Likar, and F. F. Crim, J. Chem. Phys. **85**, 2331 (1986).

[6] N. F. Scherer, F. E. Doany, A. H. Zewail, and J. W. Perry, J. Chem. Phys. **84**, 1932 (1986); N. F. Scherer and A. H. Zewail, J. Chem. Phys. **87**, 97 (1987).

[7] T. Uzer, J. T. Hynes, W. P. Reinhardt, Chem. Phys. Lett. **117**, 600 (1985); T. Uzer, J. T. Hynes, W. P. Reinhardt, J. Chem. Phys. **85**, 5791 (1986).

[8] B. G. Sumpter and D. L. Thompson, J. Chem. Phys. **82**, 4557 (1985).

[9] D. M. Wardlaw and R. A. Marcus, Chem. Phys. Lett. **110**, 230 (1984); D. M. Wardlaw and R. A. Marcus, J. Chem. Phys. **83**, 3462 (1985).

Table A.1: Potential and Spectroscopic Parameters for H_2O_2.[a]

Parameter	Value	Parameter	Value
		Reactants	
θ_1^e	100°	f_{θ_1}	6.34×10^4 cm^{-1}
θ_2^e	100°	f_{θ_2}	6.34×10^4 cm^{-1}
r^e_{HO-OH}	1.462 Å	D_{HO-OH}	19097 cm^{-1}
r^e_{OH}	0.965 Å	β_{HO-OH}	2.45 Å^{-1}
R^e	1.485 Å	τ^e	120°
ν_{OH} stretch	3608 cm^{-1}	V_0	876.3 cm^{-1}
ν_{OH} stretch	3599 cm^{-1}	V_1	1093.4 cm^{-1}
ν_{HOO} bend	1402 cm^{-1}	V_2	546.7 cm^{-1}
ν_{HOO} bend	1266 cm^{-1}	V_3	-56.4 cm^{-1}
ν_{OO} stretch	877 cm^{-1}		
ν_τ torsion	243 cm^{-1}		
		Products	
ν_{OH} stretch	3735 cm^{-1}	r^e_{OH}	0.9710 cm^{-1}
		Interpolation	
α	1.08 Å^{-1}		

[a] All parameters except for β_{HO-OH} and α are as described in Ref. 3. The latter two parameters are as described in Ref. 9.

Table A.2: Comparison of RRKM, SACM, $N_{EJ}(\infty)$, and PST Calculations of $k(E,J)$ for the Unimolecular Dissociation of H_2O_2. $J = 10$

E^a	k_{RRKM} $(s^{-1})^b$	k_{SACM} $(s^{-1})^c$	$k_{N_{EJ}(\infty)}$ $(s^{-1})^d$	k_{PST} $(s^{-1})^e$
		J = 10		
200	3.7 (9)[f]	4.2 (9)	6.1 (9)	5.9 (9)
400	1.8 (10)	1.8 (10)	2.4 (10)	2.3 (10)
800	7.0 (10)	6.0 (10)	8.5 (10)	8.4 (10)
1200	1.6 (11)	1.2 (11)	1.8 (11)	1.8 (11)
1600	2.5 (11)	1.8 (11)	2.9 (11)	2.9 (11)
2000	3.5 (11)	2.7 (11)	4.0 (11)	4.0 (11)
2400	4.6 (11)	3.6 (11)	5.2 (11)	5.2 (11)
2800	5.7 (11)	4.3 (11)	6.4 (11)	6.3 (11)

[a] Energy above the zero-point energy level of the products.

[b] RRKM calculations of k_{EJ}.

[c] SACM result from Ref. 3.

[d] Calculation using the number of states at infinite separation of the two OH fragments.

[e] Classical PST calculation.

[f] The numbers in parentheses denote the power of 10. Monte Carlo errors are in all cases less than 5%.

Table A.3: Comparison of RRKM, SACM, $N_{EJ}(\infty)$, and PST Calculations of $k(E,J)$ for the Unimolecular Dissociation of H_2O_2. $J = 40$

E^a	k_{RRKM} $(s^{-1})^b$	k_{SACM} $(s^{-1})^c$	$k_{N_{EJ}(\infty)}$ $(s^{-1})^d$	k_{PST} $(s^{-1})^e$
		J = 40		
200	5.7 (7)[f]	4.6 (8)	4.3 (9)	0
400	2.7 (9)	4.5 (9)	1.7 (10)	3.6 (9)
800	2.4 (10)	2.5 (10)	6.1 (10)	3.2 (10)
1200	6.5 (10)	6.0 (10)	1.2 (11)	8.0 (10)
1600	1.2 (11)	1.0 (11)	2.0 (11)	1.4 (11)
2000	1.9 (11)	1.5 (11)	2.8 (11)	2.2 (11)
2400	2.6 (11)	2.1 (11)	3.7 (11)	3.0 (11)
2800	3.4 (11)	2.7 (11)	4.5 (11)	3.8 (11)

[a] Energy above the zero-point energy level of the products.

[b] RRKM calculations of k_{EJ}.

[c] SACM result from Ref. 3.

[d] Calculation using the number of states at infinite separation of the two OH fragments.

[e] Classical PST calculation.

[f] The numbers in parentheses denote the power of 10. Monte Carlo errors are in all cases less than 5%.